

NEURAL PLASTICITY OF EARLY SENSORY PATHWAYS IN THE ADULT
MOUSE OLFACTORY SYSTEM

by

MARLEY DEENA KASS

A dissertation submitted to the
Graduate School-New Brunswick
Rutgers, The State University of New Jersey

In partial fulfillment of the requirements

For the degree of

Doctor of Philosophy

Graduate Program in Psychology

Written under the direction of

John P. McGann

And approved by

New Brunswick, New Jersey

October 2017

ABSTRACT OF THE DISSERTATION

Neural plasticity of early sensory pathways in the adult mouse olfactory system

by MARLEY DEENA KASS

Dissertation Director:

Professor John P. McGann

Conventional wisdom suggests that the body's sensory systems should be consistent, so that a given sensory stimulus always produces more-or-less the same signal to the brain, which can then retrieve related memories or information. However, using optical neurophysiological tools to observe the earliest parts of the mouse olfactory system, we have found that actually these signals are highly flexible, such that different sensory experiences and previously learned information radically affect the way sensory stimuli are processed in the brain. The first stage of sensory processing in the olfactory system takes place in the olfactory bulb, where axons from olfactory sensory neurons (OSNs) in the nose segregate by receptor type and converge into one or two glomeruli on the surface of the bulb. The brain's initial (primary) neural code for the identity of an odor in the nose is thus the spatiotemporal pattern of olfactory bulb glomeruli receiving synaptic input from OSNs, which can be modulated by local circuits in the glomerular layer of the bulb. Here, we demonstrate that these primary odor representations are changed *in vivo* through simple environmental manipulations, such as olfactory sensory deprivation or odor exposure. Subsequent experiments show that passive odor exposure leads to changes in temporal patterns of OSN synaptic output that are correlated with perceptual changes in odor quality.

We move on from simple environmental manipulations to explore how emotional learning can influence early sensory processing, and surprisingly find that discriminative olfactory fear conditioning can selectively enhance the synaptic output of OSNs during the presentation of threat-predictive odorants. By contrast, when conditioned fear generalizes across olfactory stimuli that are quite different from a threat-predictive odor, there is a corresponding facilitation of odor-evoked activity in inhibitory interneurons in the olfactory bulb that generalizes across threatening and non-threatening odors. These experience-dependent effects may be further modulated by individual differences in endogenous factors such as the expression of certain transduction proteins or circulating levels of sex hormones that can independently shape primary sensory odor representations. Collectively, the results from these experiments demonstrate that early neural representations of odors are highly malleable on the basis of prior sensory experience and learning, even as early as the primary sensory input to the brain. Such plasticity presumably maximizes the detection and discrimination of meaningful sensory stimuli in a constantly changing olfactory environment, and is of broad importance for downstream brain regions that receive input from the bulb.

ACKNOWLEDGEMENTS

I thank my advisor, Dr. John McGann, for everything. I am truly grateful that he trusted me to ask the research questions that I found most interesting, and that he helped me tackle them with rigorous scientific inquiry. This was an exciting topic to chip away at, and I am fortunate to have had the opportunity to do so with his continuous guidance and support. Throughout this entire process he has challenged me in many ways and taught me a great deal about being a neuroscientist as well as a mentor to others.

I would like to thank my committee members, Drs. Tracey Shors, Tim Otto, and Don Wilson, for all of their time and advice. I have benefitted from stimulating discussions with them during this dissertation project and also during seminars and conferences that helped refine my research and better my graduate experience.

Endless thanks to my entire lab family. This experience would not have been the same without you all. I am especially indebted to Lindsey Czarnecki and Michelle Rosenthal for intellectually rich discussions and, more importantly, years of friendship. It has been a privilege to collaborate with such a hard-working and supportive group of scientists throughout the years, and I sincerely thank Michelle Rosenthal, Andrew Moberly, Joe Pottackal, Lindsey Czarnecki, Dan Turkel, and Stephanie Guang for their direct contributions to various aspects of my dissertation project.

Last, but certainly not least, I thank my family as this achievement would not have been possible without them. Mom and Dad, thank you for your infinite love and for giving me a lifetime of encouragement and support. Sam, words cannot express how lucky I am

to share my life with you. Thank you for standing by my side throughout this entire journey, and being my source of inspiration to aim for the stars.

This work was supported by The National Institute on Deafness and Other Communication Disorders [R00 DC009442 and R01 DC013090 to JPM and F31 DC013719 to MDK] and The National Institute of Mental Health [R01 MH101293 to JPM]. I also thank The Graduate School-New Brunswick for awarding me with a University and Louis Bevier Dissertation Fellowship to complete this project.

TABLE OF CONTENTS

ABSTRACT OF THE DISSERTATION	ii
ACKNOWLEDGEMENTS	iv
TABLE OF CONTENTS	vi
INTRODUCTION	1
<i>Overview of the olfactory system.</i>	2
<i>Overview of dissertation experiments.</i>	4
Introduction Figures	8
<i>Figure 0.1</i>	8
<i>Figure 0.2</i>	9
GENERAL METHODS ACROSS EXPERIMENTS	11
Olfactory stimuli	11
<i>Vapor dilution olfactometry.</i>	11
<i>Liquid dilution olfactometry.</i>	12
<i>Manual delivery of olfactory stimuli.</i>	13
Subjects	13
<i>Olfactory marker protein (OMP)- synaptopHluorin (spH) mice.</i>	14
<i>GCaMPs expressed in olfactory bulb interneurons.</i>	14
Surgical implantation of cranial windows	15
Optical recordings and analyses	16
<i>In vivo optical neurophysiology recordings.</i>	16
<i>Quantification and analysis of odorant-evoked optical signals.</i>	18
CHAPTER 1	20
Abstract	21
Introduction	22
Methods	23
<i>Subjects</i>	23
<i>Reversible unilateral naris occlusion.</i>	23
<i>Histological procedures and analyses.</i>	25
<i>Olfactory stimuli used during in vivo optical imaging.</i>	26
<i>Statistical analysis.</i>	26
Results	27

<i>Unilateral sensory deprivation reduces the magnitude of odorant-evoked synaptic input from OSNs to olfactory bulb glomeruli on both plugged and open sides equally.</i>	27
<i>Unilateral sensory deprivation increases the number of olfactory bulb glomeruli receiving odorant-evoked synaptic input from OSNs contralateral to the noseplug.</i>	28
<i>Unilateral deprivation increases the odorant response selectivity of OSN populations contralateral to the noseplug.</i>	31
Discussion	32
Acknowledgements	38
Chapter 1 Figures	39
<i>Figure 1.1</i>	39
<i>Figure 1.2</i>	40
<i>Figure 1.3</i>	41
<i>Figure 1.4</i>	42
<i>Figure 1.5</i>	43
<i>Figure 1.6</i>	44
CHAPTER 2	46
Abstract	47
Introduction	48
Methods	49
<i>Subjects</i>	49
<i>Acquisition and analysis of odorant-evoked spH signals.</i>	50
<i>Cross-habituation/dishabituation behavioral testing and analysis.</i>	51
Results	53
<i>The number of odorant-evoked glomerular responses is increased in OMP^{-/-} mice.</i>	53
<i>OSN odorant-selectivity is decreased in OMP^{-/-} mice.</i>	55
<i>Total odorant-evoked nerve output is unaltered in OMP^{-/-} mice.</i>	56
<i>Odor maps develop on a longer time scale in OMP^{-/-} mice than in OMP^{+/+} mice.</i>	57
<i>OMP^{-/-} mice exhibit attenuated odor habituation and delayed odor investigation.</i>	58
Discussion	60
Acknowledgements	64
Chapter 2 Figures	65
<i>Figure 2.1</i>	65
<i>Figure 2.2</i>	67
<i>Figure 2.3</i>	68

<i>Figure 2.4</i>	70
<i>Figure 2.5</i>	72
CHAPTER 3	73
Abstract	74
Introduction	75
Methods	76
<i>Subjects</i>	76
<i>Chronic odorant exposure</i>	77
<i>Acquisition and analysis of imaging data sets</i>	80
Results	83
<i>Experience-dependent changes in the number and size of OSN inputs to olfactory bulb glomeruli in heterozygous OMP-spH mice</i>	83
<i>A different pattern of experience-dependent changes in OSN inputs to olfactory bulb glomeruli in OMP knockout mice</i>	86
<i>Exposure-induced changes in glomerular inputs reflect changes in odorant selectivity</i>	89
Discussion	90
Acknowledgements	95
Chapter 3 Figures	96
<i>Figure 3.1</i>	96
<i>Figure 3.2</i>	98
<i>Figure 3.3</i>	100
<i>Figure 3.4</i>	102
<i>Figure 3.5</i>	104
<i>Figure 3.6</i>	106
CHAPTER 4	108
Abstract	109
Introduction	110
Methods	113
<i>Subjects</i>	113
<i>Olfactory stimuli</i>	114
<i>Odorant exposure</i>	114
<i>Habituation/dishabituation behavioral assessment and analysis</i>	115
<i>Quantification and analysis of odorant-evoked optical signals</i>	117
Results	120

<i>A perceptually indiscriminable odorant pair becomes discriminable after one week of exposure to a single, chemically-different odorant.</i>	120
<i>A week-long ester-odorant exposure does not alter the peak response amplitudes or overall spatial representations of two unexposed aldehydes.</i>	121
<i>Exposure to a single ester odorant can modify temporal properties of OSN responses to unexposed, aldehyde homologues and consequently enhance contrast between shared representational features.</i>	123
Discussion	125
Acknowledgements	128
Chapter 4 Figures	129
<i>Figure 4.1</i>	129
<i>Figure 4.2</i>	131
<i>Figure 4.3</i>	133
<i>Figure 4.4</i>	135
<i>Figure 4.5</i>	136
CHAPTER 5	137
Abstract	138
Introduction	139
Methods	139
<i>Subjects</i>	139
<i>Discriminative olfactory fear conditioning.</i>	140
<i>In vivo optical imaging procedures and analyses.</i>	142
<i>Respiration recordings and analysis.</i>	147
Results and Discussion	149
Acknowledgements	154
Chapter 5 Figures	155
<i>Figure 5.1</i>	155
<i>Figure 5.2</i>	156
<i>Figure 5.3</i>	158
<i>Figure 5.4</i>	159
<i>Figure 5.5</i>	161
<i>Figure 5.6</i>	163
<i>Figure 5.7</i>	165
<i>Figure 5.8</i>	167

<i>Figure 5.9</i>	169
<i>Figure 5.10</i>	171
<i>Figure 5.11</i>	172
<i>Figure 5.12</i>	174
<i>Figure 5.13</i>	175
<i>Figure 5.14</i>	177
CHAPTER 6	179
Abstract	180
Introduction	181
Methods	183
<i>Subjects</i>	183
<i>Olfactory fear conditioning</i>	184
<i>In vivo optical recordings and analyses</i>	185
Results	188
<i>Long-lasting generalization of conditioned fear to odors</i>	188
<i>Long-lasting enhancement of CS-evoked PG interneuron activity after conditioning</i> ...	189
<i>Neural generalization to non-threatening odors and correlation with freezing behavior</i>	191
<i>Broader odor tuning and increased similarity of odor representations after fear generalization</i>	192
<i>Fear conditioning preferentially boosts CS-evoked activity in weakly-responsive glomeruli</i>	193
<i>Olfactory fear conditioning increases odor sensitivity in PG interneurons</i>	194
Discussion	195
Chapter 6 Figures	200
<i>Figure 6.1</i>	200
<i>Figure 6.2</i>	202
<i>Figure 6.3</i>	204
<i>Figure 6.4</i>	205
<i>Figure 6.5</i>	207
<i>Figure 6.6</i>	209
Chapter 6 Supplementary Information	210
<i>Supplementary Figure S6.1</i>	210
<i>Supplementary Figure S6.2</i>	212

<i>Supplementary Figure S6.3</i>	214
<i>Supplementary Figure S6.4</i>	217
<i>Supplementary Figure S6.5</i>	219
<i>Supplementary Table S6.1</i>	222
<i>Supplementary Figure S6.6</i>	224
<i>Supplementary Table S6.2</i>	226
<i>Supplementary Figure S6.7</i>	227
<i>Supplementary Figure S6.8</i>	229
<i>Supplementary Table S6.3</i>	230
<i>Supplementary Figure S6.9</i>	231
<i>Supplementary Table S6.4</i>	232
<i>Supplementary Figure S6.10</i>	233
<i>Supplementary Figure S6.11</i>	235
<i>Supplementary Figure S6.12</i>	237
<i>Supplementary Figure S6.13</i>	239
<i>Supplementary Table S6.5</i>	240
<i>Supplementary Table S6.6</i>	241
<i>Supplementary Figure S6.14</i>	242
<i>Supplementary Figure S6.15</i>	244
CHAPTER 7	246
Abstract	247
Introduction	248
Methods	250
<i>Subjects</i>	250
<i>Gonadectomy surgical procedures</i>	250
<i>In vivo optical neurophysiology recordings</i>	251
<i>Quantification and analysis of odorant-evoked optical signals</i>	253
Results	256
<i>Odors evoke OSN input to more olfactory bulb glomeruli in females than in males</i>	256
<i>Odor-evoked OSN output is faster in females than in males</i>	259
<i>Higher contrast between odorants in the primary sensory odor representations of females than males</i>	261
<i>The number of glomeruli receiving odorant-evoked OSN input is influenced by circulating gonadal hormones in males and females</i>	263

<i>Gonadal hormones modulate the timing and discriminability of odorant-evoked OSN activity</i>	267
Discussion	270
Acknowledgements	276
Chapter 7 Figures	277
<i>Figure 7.1</i>	277
<i>Figure 7.2</i>	279
<i>Figure 7.3</i>	281
<i>Figure 7.4</i>	282
<i>Figure 7.5</i>	284
<i>Figure 7.6</i>	285
Chapter 7 Supplementary Information	286
<i>Supplementary Figure S7.1</i>	286
<i>Supplementary Figure S7.2</i>	287
<i>Supplementary Figure S7.3</i>	290
<i>Supplementary Figure S7.4</i>	292
<i>Supplementary Figure S7.5</i>	293
<i>Supplementary Figure S7.6</i>	295
<i>Supplementary Figure S7.7</i>	297
REFERENCES	300

INTRODUCTION

Sensory systems have traditionally been presumed to be simple “stimulus analyzers”, capable only of selecting modality-specific environmental cues that are then synthesized by higher-order structures with superior analyzing capabilities (Pavlov and Anrep, 1927). This early framework presumes that sensory transduction is a fixed process in which a given sensory stimulus always results in the same neural signal that is passed along to other brain regions that initiate an appropriate behavioral response. However, outside of the laboratory, a given stimulus is rarely experienced in the exact same form every time that it is encountered. For example, when we hear a friend talking over the phone, shouting during a concert, or whispering during class we are still able to identify that friend’s voice, even though the initial sensory responses during each of those encounters are quite different. Alternatively, there might be instances in which the overall features of a given stimulus are more-or-less the same each time that it is encountered, but to respond appropriately that stimulus may need to be interpreted in different contexts comprised of vastly different sensory environments. For instance, seeing a bear at the zoo will result in a very different behavioral response than seeing a bear during a morning run through the park. Thus, contrary to traditional views, environmental cues must be flexibly interpreted by the brain’s sensory systems.

Across sensory modalities, sensory circuits have indeed been found to be quite flexible, being shaped by passive sensory experiences (Wiesel and Hubel, 1965; Hubel and Wiesel, 1970; Finnerty et al., 1999; Lendvai et al., 2000; Chang and Merzenich, 2003; Karmarkar and Dan, 2006; Goel and Lee, 2007; Zhou and Merzenich, 2007; Gilbert et al., 2009; Pienkowski and Eggermont, 2011) and even by previously learned information

(Weinberger, 2007; McGann, 2015). However, most studies addressing experience-dependent sensory plasticity have focused on effects in sensory cortex or thalamus. Until relatively recently, it has been technically challenging to assess *in vivo* plasticity in primary sensory inputs and “low-level” processing in most sensory systems. Using *in vivo* optical neurophysiology this dissertation will explore plasticity in early sensory pathways in the adult mouse olfactory system.

Overview of the olfactory system.

In the olfactory system, odors are initially processed in the olfactory bulb, where there is a high convergence of “bottom-up” input from the nose with “top-down” projections from cortical and neuromodulatory centers (Figures 0.1 and 0.2). This organization implies that low-level sensory coding in the olfactory bulb can integrate higher-order cognition and previous sensory experiences with the initial stages of odor processing. In mice, the olfactory bulbs are anterior to the prefrontal cortex and directly below the skull (Figure 0.1), making them optically accessible *in vivo*. Thus, the tractability of the mouse olfactory system provides a unique model to study how different experiences can shape early sensory representations.

Olfactory transduction occurs in the olfactory epithelium (Figure 0.1), where odorant molecules stimulate neural activity by binding to G protein-coupled odor receptors in the cilia of olfactory sensory neurons (OSNs). Each OSN expresses only one of a large repertoire of odor receptor types (Buck and Axel, 1991), and as OSN axons project ipsilaterally to the olfactory bulb, they segregate by receptor type (Figure 0.2, color-coded axons) so that each glomerulus receives projections exclusively from OSNs expressing a specific odor receptor (Mombaerts et al., 1996). An odorant in the nose will bind to a

subset of olfactory receptor types in the epithelium and thus drive OSN synaptic output into a corresponding subset of olfactory bulb glomeruli. Consequently, the global configuration of odorant-evoked OSN synaptic input to glomeruli across the surface of the bulb represents the chemical identity of that odorant (Malnic et al., 1999; Youngentob et al., 2006). This dissertation will include the visualization of patterns of odorant-evoked neurotransmitter release from OSN axon terminals in the olfactory bulb in a line of gene-targeted mice that express the fluorescent exocytosis indicator synaptopHluorin (spH) under the control of the olfactory marker protein (OMP) promoter (Bozza et al., 2004).

The glomerular layer of the olfactory bulb contains distinct populations of interneurons, with the largest population being comprised of GABAergic cells that express different forms of glutamic acid decarboxylase (GAD, the rate-limiting enzyme for GABA synthesis) that can be further divided into populations that express GAD65, GAD67, or both forms of the enzyme (Parrish-Aungst et al., 2007). Periglomerular (PG) interneurons (Figure 0.2, red cells) predominantly express GAD65 (Kiyokage et al., 2010) and have processes that are confined to a single glomerulus (Shao et al., 2009; McGann, 2013), whereas short axon cells (SACs; Figure 0.2, orange cell) either express GAD67 or coexpress GAD67 and tyrosine hydroxylase (TH, the rate-limiting enzyme for dopamine synthesis) and have processes with extensive multiglomerular connections (Aungst et al., 2003; Parrish-Aungst et al., 2007; Kosaka and Kosaka, 2008; Kiyokage et al., 2010). PG interneurons and SACs thus form two local bulbar circuits, with the former cell population supporting an intra/uniglomerular circuit and the latter forming an inter/multiglomerular circuit. While it is important to consider the manner in which these two glomerular networks can interact to shape odor representations in the bulb, the intraglomerular circuit

is organized such that it suppresses neurotransmitter release from OSNs expressing the same odorant receptor (McGann et al., 2005; McGann, 2013), and could thus provide a local circuit mechanism for plasticity in primary sensory odor representations. As such, this dissertation will visualize odorant-evoked activity in populations of PG interneurons in mice expressing a genetically encoded calcium indicator (Zariwala et al., 2012; Chen et al., 2013) via cre recombinase-mediated recombination in cells expressing the *gad2* gene (Taniguchi et al., 2011), which includes PG interneurons in the olfactory bulb (Wachowiak et al., 2013; Fast and McGann, 2017b).

On top of the complex circuit interactions that occur locally in the bulb, activity in forebrain and brainstem transmitter systems can modulate bulbar circuitry (Figure 0.2, example neuromodulatory afferents shown in grey). Because these systems are diffusely modulatory they can serve as coincident signals in regions of the bulb that are activated during olfactory-guided behaviors, and could thus tune bulbar circuitry to differentially filter odorant stimuli based on sensory experience. The olfactory bulb also receives substantial top-down input from sensory and higher-order association areas that undergo experience-dependent plasticity and that are involved in learning and perceptual processes. Thus, it is possible for these regions to adjust their own sensory inputs via modulation of bulbar processing based on previously learned information and current task demands.

Overview of dissertation experiments.

As intimated above, the olfactory system is a dynamic sensory system that can adapt to maximize the detection and discrimination of different statistical distributions of sensory stimuli in a constantly changing olfactory environment. Odors are initially

processed in the brain's olfactory bulb, where neural representations are shaped by complex and highly plastic circuitry before being communicated to other brain regions.

This dissertation will first evaluate how the physiology of OSNs is changed by passive experiences, such as olfactory sensory deprivation (Chapter 1) or mere exposure to odor stimuli in the surrounding environment (Chapter 3). Based in part on these results, this project will also explore how olfactory marker protein (OMP, a transduction protein) can influence OSN physiology and odor perception in naïve, adult animals (Chapter 2), as well as its role in odor exposure-induced sensory plasticity (Chapter 3). Olfactory sensory enrichment can modulate bulbar signal processing in a manner that correlates with perceptual plasticity. Consequently, this dissertation will also evaluate odor exposure-induced physiological and perceptual changes in odor processing, and show that experience-dependent changes in temporal patterns of OSN input to olfactory bulb glomeruli correlate with perceptual changes in odor quality (Chapter 4).

Next, this dissertation will assess learning-dependent changes in early sensory representations of odors. Fear learning, in which the subject learns that a sensory stimulus predicts an unpleasant outcome, seems to be particularly effective at altering the sensory processing of threat-predictive stimuli (Barrett and Bar, 2009; Headley and Weinberger, 2013; Krusemark and Li, 2013). Indeed, in the olfactory system associative fear conditioning can enhance difficult olfactory discriminations (Li et al., 2008) and alter odor-evoked activity in the piriform cortex (Li et al., 2008; Barnes et al., 2011; Chen et al., 2011) and olfactory bulb (Fletcher, 2012). Chapter 5 will present evidence that discriminative olfactory fear conditioning selectively enhances the output of OSNs during the presentation of threat-predictive odorants, suggesting that sensory representations can incorporate

learned affective information as early as the input to the brain. We extend these findings in Chapter 6 by showing that fear generalization is accompanied by a robust facilitation of odor-evoked activity in inhibitory interneurons in the olfactory bulb that generalizes across threatening and non-threatening odors.

The results from Chapters 5 and 6 showing that fear learning can alter early sensory processing of threat-predictive odors and harmless (though categorically-similar) odors may have important implications for the etiology and treatment of anxiety disorders with sensory sequelae. There is a notable difference between men and women in the prevalence of anxiety disorders, as well as in general olfactory abilities. Thus, in Chapter 7 we begin to explore differences between sexes in odor processing in the olfactory bulb.

Six of the chapters in this dissertation have already been published (Chapters 1 through 5 and 7), while one chapter was submitted for review (Chapter 6). The citations for these publications are listed below and noted at the beginning of each chapter.

Publication history.

Chapter 1: †Kass MD, Pottackal J, Turkel DJ, McGann JP (2013c) Changes in the neural representation of odorants after olfactory deprivation in the adult mouse olfactory bulb. *Chem Senses* 38:77-89. ‡*featured on cover and highlighted in in an accompanying editorial commentary.*

Chapter 2: Kass MD, Moberly AH, McGann JP (2013a) Spatiotemporal alterations in primary odorant representations in olfactory marker protein knockout mice. *PLoS One* 8:e61431.

Chapter 3: Kass MD, Moberly AH, Rosenthal MC, Guang SA, McGann JP (2013d) Odor-specific, olfactory marker protein-mediated sparsening of primary olfactory input to the brain after odor exposure. *J Neurosci* 33:6594-6602.

Chapter 4: †Kass MD, Guang SA, Moberly AH, McGann JP (2016) Changes in Olfactory Sensory Neuron Physiology and Olfactory Perceptual Learning After Odorant Exposure in Adult Mice. *Chem Senses* 41:123-133. †*featured on cover and highlighted in in an accompanying editorial commentary.*

Chapter 5: Kass MD*, Rosenthal MC*, Pottackal J, McGann JP (2013b) Fear learning enhances neural responses to threat-predictive sensory stimuli. *Science* 342:1389-1392. **co-first authors*

Chapter 6: Kass MD, McGann JP (Submitted) Persistent, generalized hypersensitivity of olfactory bulb interneurons after olfactory fear generalization.

Chapter 7: Kass MD, Czarnecki LA, Moberly AH, McGann JP (2017) Differences in peripheral sensory input to the olfactory bulb between male and female mice. *Sci Rep* 7:45851.

Introduction Figures

Figure 0.1

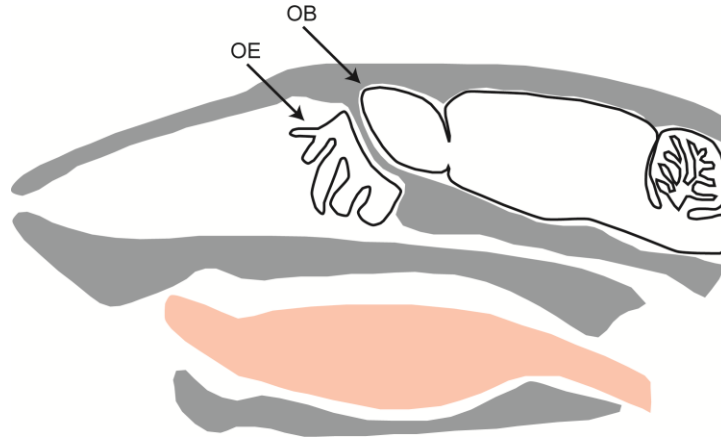
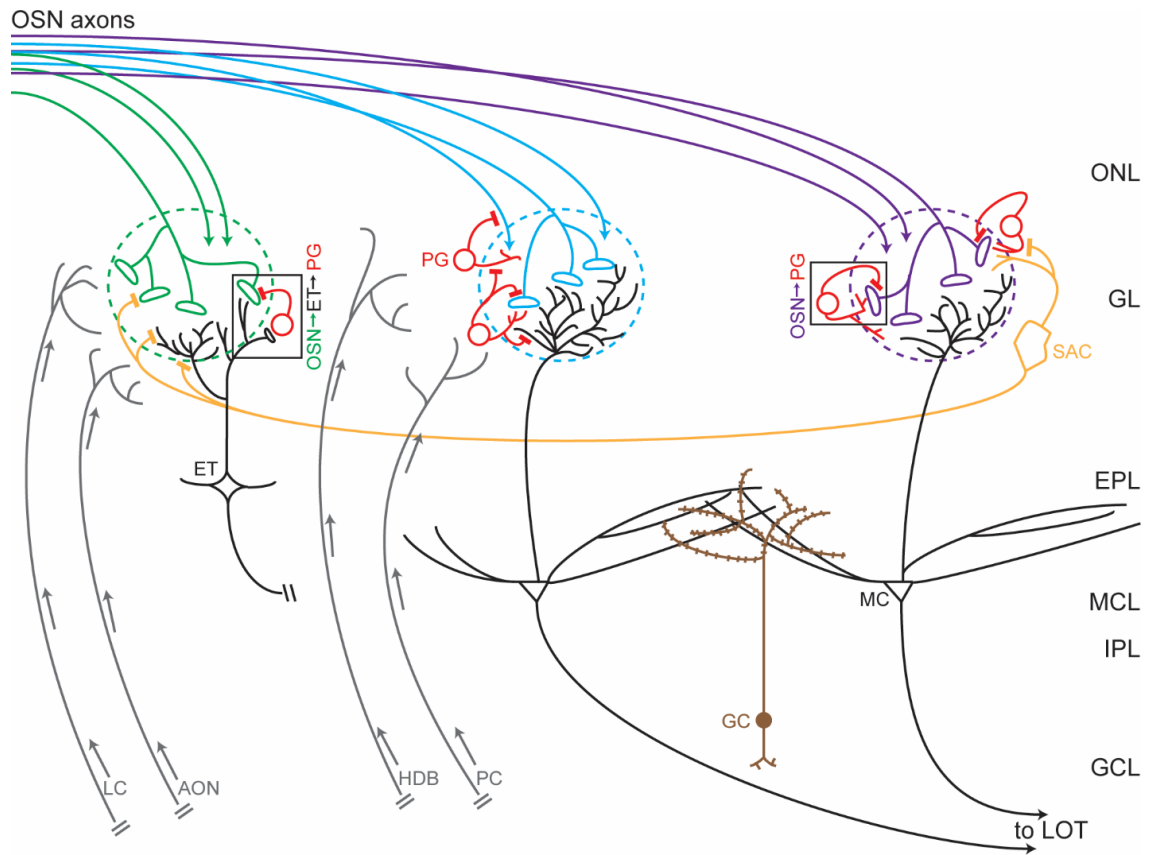


Figure 0.1. Gross anatomy of the olfactory system. This simplified cartoon shows a sagittal view of a mouse hemi-head, which highlights the experimental accessibility of the olfactory system. OSNs located in the olfactory epithelium (OE) in the nose project their axons to the ipsilateral olfactory bulb (OB). A cranial window can be surgically implanted above the dorsal surface of the olfactory bulbs, permitting repeated *in vivo* visualization of odor representations in the olfactory bulbs of the same mouse before and after experimental manipulations that can include passive sensory experiences or associative learning.

Figure 0.2**Figure 0.2. Simplified schematic showing the gross organization of the olfactory bulb.**

The orderly mapping of odor receptor type on the surface of the bulb is represented here by color-coded axons that are mixed together in the epithelium and that segregate by color (receptor type) as they project to the glomerular layer of the bulb. In the glomerular layer, OSNs form glutamatergic synapses with principal output neurons (mitral/tufted cells) and local interneurons. Examples of the monosynaptic (OSN → PG) and disynaptic (OSN → ET → PG) components of intraglomerular circuitry are shown in boxed regions. The dopaminergic interglomerular circuitry is exemplified by a SAC (orange) making contact with more than one glomerulus. For simplicity, only a few synaptic contacts are indicated in the local bulbar circuitry, and top-down input from a few cortical and neuromodulatory centers are only shown as projecting to the glomerular layer. Acronym key for olfactory bulb lamina indicated at far right: ONL, olfactory nerve layer; GL, glomerular layer; EPL, external plexiform layer; MCL, mitral cell layer; IPL, internal plexiform layer; GCL, granule cell layer. Acronym key for cell types: ET, external tufted cell; GC, granule cell;

MC, mitral cell; OSN, olfactory sensory neuron; PG, periglomerular cell; SAC, short axon cell. Acronym key for efferent and afferent projections: LOT, lateral olfactory tract; AON, anterior olfactory nucleus; HDB, horizontal limb of the diagonal band; LC, locus coeruleus; PC, piriform cortex.

GENERAL METHODS ACROSS EXPERIMENTS

Olfactory stimuli

We selected stimuli that are known to drive input to glomeruli on the dorsal surface of the olfactory bulb (Bozza et al., 2004; McGann et al., 2005; Soucy et al., 2009), and would thus permit *in vivo* visualization of odorant-evoked optical signals in early olfactory bulb circuitry. All stimuli were monomolecular odorants obtained at 95-99% purity (Sigma-Aldrich), and were comprised of several different chemical classes, mostly including esters, ketones, and aldehydes. A photoionization detector (PID; either a ppbRAE Plus or a ppbRAE 3000, depending on the experiment; RAE Systems) was used to standardize odorant concentrations across multiple imaging sessions for a given subject, as well as between different subjects. The same stimulus calibration procedure was also used to match concentrations across methods in experiments that included imaging and behavioral components. Details on the specific odorants and concentrations that were used for each experiment are noted accordingly in the subsequent chapters. Concentration is reported as percent dilution of saturated vapor or as arbitrary units (a.u., as measured by a PID).

Vapor dilution olfactometry.

As previously reported (Czarnecki et al., 2011; Moberly et al., 2012; Kass et al., 2013a; Kass et al., 2013c), a custom-built, 8-channel vapor dilution olfactometer using nitrogen as the carrier was used to present olfactory stimuli to subjects on the imaging rig. Separate lines were used to avoid cross-contamination between odorants. Compressed gases were filtered with hydrocarbon moisture purifiers (Chromatography Research

Supplies). To achieve desired concentrations, odorants were diluted relative to a constant flow (500 mL/min) of ultrazero air by adjusting the flow rate of a nitrogen stream being passed through a vial containing a single odorant. User-defined odorant dilutions were made using a mass flow controller (Aalborg) operating through custom software written in Matlab, and were adjusted based on measurements from the PID calibrations that were performed immediately prior to all imaging sessions. During imaging, the odorant delivery manifold was positioned ~1-2 cm in front of the mouse's nose.

Liquid dilution olfactometry.

We used liquid dilution olfactometry to deliver discrete olfactory stimuli during behavioral tasks that were carried out in operant/fear conditioning chambers, as detailed in (Czarnecki et al., 2012; Kass et al., 2013b). Briefly, each conditioning chamber was equipped with its own olfactometer and was modified to contain a port for odorant delivery (2.5 cm above the floor at approximately the mouse's nose height) and a vacuum exhaust for odorant removal. Room air was passed through a vial containing an odorant diluted in mineral oil and then to the odor port. In later experiments, the apparatus was modified into a double-valved system where room air was passed through an odorant vial, then through a second valve, and finally to the odor port. Depending on the specific odorant being used and the desired target concentration being measured inside the chamber, odorant dilutions in the vials ranged from 1:50 to 1:250 and air flow rates ranged from 0.8-1.2 sL/min. As described above, a PID was used to measure and calibrate actual odorant concentrations in the chamber.

Manual delivery of olfactory stimuli.

Odorant stimuli were freshly prepared prior to each day of testing in the cross-habituation/dishabituation behavioral experiments. After the manner of (Mandairon et al., 2006b; Mandairon et al., 2006a), individual odorants were diluted in mineral oil in proportion to their respective vapor pressures to yield pairs of stimuli that had approximately equivalent vapor concentrations. The experimenter manually presented odorant stimuli during testing by dispensing 0.6 mL of an odorant dilution onto a filter paper that was placed in a weigh boat. To match concentrations between this behavioral paradigm and the imaging experiments, a PID was used to measure the a.u. concentrations of the vapor-equivalent dilutions, and the resulting measurements were used as target values for stimulus calibrations on the imaging rig.

Subjects

All subjects were adults (ranging from 3-11 months of age) at the onset of experimentation, and were comprised of mixed sexes. Specific age and sex details are noted for each experiment reported in the chapters below. Animals were group-housed up until 3-7 days prior to experimentation, at which point they were singly-housed for the duration of the study. The subjects were housed in a colony room that was maintained on a 12:12-hr light/dark cycle with food and water provided *ad libitum*. All experiments were performed in accordance with protocols approved by the Rutgers University Institutional Animal Care and Use Committee (Prot. #09-022).

To visualize early olfactory sensory coding *in vivo*, we used mice expressing genetically-encoded activity indicators that were targeted to OSNs or to GAD65-

expressing periglomerular (PG) interneurons (detailed below). For behavioral experiments that were run in parallel to optical imaging experiments we used either littermates that did not inherit the GCaMP indicator from the GAD2×GCaMP6f and GAD2×GCaMP3 crosses (detailed below) or wild-type C57BL/6J mice that were obtained from either Charles River Laboratories (strain code #027) or Jackson Laboratory (strain code #000664).

Olfactory marker protein (OMP)- synaptopHluorin (spH) mice.

To study how different sensory experiences can modulate primary neural representations of odors *in vivo*, we used mice expressing the synaptopHluorin (spH) exocytosis indicator under the control of the olfactory marker protein (OMP) promoter (Bozza et al., 2004). In these mice, spH is expressed in all mature OSNs, and odorant-evoked spH signals linearly indicate neurotransmitter release from OSN terminals into olfactory bulb glomeruli (Bozza et al., 2004; Wachowiak et al., 2005). Homozygous and heterozygous OMP-spH mice were generated as previously reported (Czarnecki et al., 2011). The homozygous OMP-spH mice were on an albino C57BL/6 background, and were OMP-null (OMP^{-/-}) because they had both copies of the OMP coding region replaced with spH. Mice that were heterozygous for spH and OMP were bred by crossing the OMP^{-/-}-spH^{+/+} mice described above with either wild-type 129SvJ mice (analogous to those used by (Lee et al., 2011)) or with albino C57BL/6 mice.

GCaMPs expressed in olfactory bulb interneurons.

The olfactory bulb glomerular circuitry contributes to shaping primary olfactory sensory information (McGann et al., 2005; Murphy et al., 2005; Shao et al., 2009; McGann, 2013). One element of this circuit is a GABA_B-receptor-mediated presynaptic inhibition onto OSN terminals arising from GAD65-expressing PG cells, which modulates glutamate

release from OSNs by suppressing presynaptic N-type calcium conductances (Wachowiak et al., 2005). To permit the visualization of odorant-evoked activity in olfactory bulb PG interneurons, we crossed mice from the GAD2-IRES-Cre driver line (Taniguchi et al., 2011) (Jackson Laboratory, stock #010802) with mice from either the Ai95D reporter line (Chen et al., 2013) (Jackson Laboratory, stock #024105) or the Ai38(RCL-GCaMP3) reporter line (Zariwala et al., 2012) (Jackson Laboratory, stock # 014538), as previously reported (Wachowiak et al., 2013; Fast and McGann, 2017b). The resulting offspring conditionally expressed either the genetically-encoded calcium indicator GCaMP6f or GCaMP3 in all GAD65-expressing neurons in the brain (including PG interneurons in the glomerular layer of the olfactory bulb (Wachowiak et al., 2013; Fast and McGann, 2017b)) via a lox/cre recombinase expression system where cre-mediated recombination removes a STOP codon upstream of the GCaMP coding region in neurons that express cre under the gad2 promoter.

Surgical implantation of cranial windows

Acute (Czarnecki et al., 2011; Moberly et al., 2012; Kass et al., 2013c) and chronic (Czarnecki et al., 2012; Kass et al., 2013d) bilateral windows were implanted as previously reported. Mice were anesthetized via i.p. administration of 100 mg/kg pentobarbital, and additional boosters were administered as needed to maintain deep anesthesia throughout the duration of the surgical and imaging procedures. While subjects were anesthetized, body temperature was maintained at $38.0^{\circ}\text{C} \pm 0.5^{\circ}\text{C}$ via rectal probe thermometry and a feedback-regulated heating pad. A 0.1% atropine solution was administered (s.c.) to reduce intranasal mucous secretion, and a 0.25% bupivacaine solution was administered

(s.c.) along the scalp to provide local anesthesia surrounding the incision. The scalp was shaved, wiped down with a topical antiseptic bactericide, and then surgically removed. The periosteal membrane was peeled back and the skull was then cleaned and dried with a 70% ethanol solution before being mounted to a custom head holder. The skull was directly fixed to a head bar with dental acrylic for acute imaging preparations, and for chronic preparations the skull was fitted with a dental acrylic head cap designed to permit replicable positioning across repeated imaging sessions. The bone overlying the dorsal surface of both olfactory bulbs was thinned until transparent with a hand-held dental drill, and for chronic preparations, the window was then coated with a thin layer of clear-drying cyanoacrylate adhesive. During imaging sessions, cranial windows were topped with Ringer's solution and a glass cover slip. Between imaging sessions (for chronic preparations), the cranial window was protected by a metal cover. After the implantation of a chronic window, carprofen (5 mg/mL) was administered (s.c.) for post-operative analgesia and subjects were given an overnight recovery period on a heating pad.

Optical recordings and analyses

In vivo optical neurophysiology recordings.

All imaging was performed on freely-breathing, anesthetized mice. A custom imaging apparatus using fluorescence epi-illumination on an Olympus BX51 microscope was used for optical neurophysiology recordings, and is detailed in (Czarnecki et al., 2011; Czarnecki et al., 2012; Kass et al., 2013a; Kass et al., 2013c). Briefly, illumination was provided by either a 150W Xenon arc lamp (Optosource lamphouse; Cairn Research, Ltd) or a 470 nm bright light-emitting diode (LED, Thorlabs), and a filter set containing

HQ480/40 excitation, Q505LP dichroic, and HQ535/50 emission filters was used to visualize spH and calcium signals. Optical signals were acquired at a pixel resolution of 256×256 via a back-illuminated, monochrome CCD camera (NeuroCCD, SM-256; RedShirtImaging) that was mounted onto the microscope with either a $0.38\times$ or $0.5\times$ coupler. A $4\times$ (0.28 NA) objective was used for standard widefield imaging. spH and GCaMP signals were acquired at frame acquisition rates of 7 Hz and 25 Hz, respectively. Data acquisition and shutter control were performed using either Neuroplex or Turbo-SM software (RedShirtImaging).

Odorant-evoked spH signals were most typically collected in blocks of 4-8 individual trials that were averaged together offline. Individual trials consisted of a 4-sec pre-odorant baseline, a 6-sec odorant presentation, and a 6-sec post-odorant recovery period, and were each separated by 60-sec inter-trial intervals (ITIs). While odorant-evoked GCaMP signals were also collected in blocks of 4-8 individual trials, the odorant presentations were triggered relative to the mouse's respiratory cycle, so the pre- and post-odorant trial phases varied from trial to trial. Each 6-sec odorant presentation was triggered during the rising portion of the exhalation phase of the respiratory cycle to ensure that the beginning of each odorant presentation was immediately followed by the onset of an inhalation. This permitted equal comparison of inhalation 1-evoked calcium transients across trials, subjects, and repeated imaging sessions. Blank (no-odorant) trials were given throughout each imaging preparation and were later averaged together off-line and subtracted from odorant trials to correct for photobleaching.

Quantification and analysis of odorant-evoked optical signals.

Imaging data were extracted and analyzed as reported in (Czarnecki et al., 2011; Czarnecki et al., 2012; Kass et al., 2013a; Kass et al., 2013d; Kass et al., 2013c; Kass et al., 2013b; Kato et al., 2013). Data were processed and analyzed in Neuroplex, Matlab, and SPSS, and were subsequently graphed in SigmaPlot, Matlab, and Origin.

To generate odorant-evoked difference maps for OMP-spH mice, the average fluorescence during 1-2 sec immediately prior to stimulus onset was subtracted from the average fluorescence during the most typical peak odorant-evoked response, which is approximately around the time of stimulus offset. Difference maps were then spatially filtered with a low-pass median filter to correct for shot noise, and a high-pass Gaussian filter to separate discrete odorant-evoked spH signals (corresponding to individual glomeruli) from broad changes in tissue reflectance (presumably corresponding to diffuse metabolic activity). Putative glomerular regions of interest (ROIs) were hand-selected from spatially high-pass-filtered difference maps and were then confirmed with a statistical criterion (McGann et al., 2005; Czarnecki et al., 2011). Specifically, if the mean odorant-evoked change in fluorescence (ΔF) across repeated trials was more than 3 standard errors greater than 0 for a glomerular ROI, then it was considered to be a response. To quantify odorant-evoked spH signals for traces from each pixel overlying a glomerular ROI, we subtracted the average pre-odorant (baseline) fluorescence from the average of 1-2 sec of frames centered on the most typical peak inflection across the traces. Peak odorant-evoked ΔF values were quantified in most experiments and were normalized to permit averaging across mice. Specific details on normalizations for peak ΔF values, as well as for pre-peak analyses, are indicated appropriately for each experiment reported below. For most

experiments with OMP-spH mice, we also quantified the number of glomerular responses contributing to each odor representation, as well as the odorant response selectivity of individual glomeruli. These quantified parameters were analyzed with a combination of parametric and non-parametric statistical tests that are described for each experiment in the chapters below.

Inhalation-evoked odor maps were generated for the imaging data that was collected from GAD2×GCaMP mice. The average of 25-50 frames (equivalent to 1-2 sec) immediately prior to odorant onset was subtracted from the average of 5 frames occurring ~1/5 of a sec after the onset of an inhalation during the odorant presentation. Subjects were freely-breathing and thus the number of inhalations during each 6-sec odorant presentation was not fixed and ranged from 8-12. Each inhalation-evoked change in fluorescence (ΔF) that occurred during an odorant presentation was then divided by baseline fluorescence ($\Delta F/F$) and used for all subsequent analyses. Procedures for map extraction and ROI selection were identical to those described above.

CHAPTER 1

Changes in the neural representation of odorants after olfactory deprivation in the adult mouse olfactory bulb

The results from this chapter are reported in Kass MD, Pottackal J, Turkel DJ, McGann JP (2013b) Changes in the neural representation of odorants after olfactory deprivation in the adult mouse olfactory bulb. *Chem Senses* 38:77-89.

Abstract

Olfactory sensory deprivation during development has been shown to induce significant alterations in the neurophysiology of olfactory receptor neurons (ORNs), the primary sensory inputs to the brain's olfactory bulb. Deprivation has also been shown to alter the neurochemistry of the *adult* olfactory system, but the physiological consequences of these changes are poorly understood. Here we used *in vivo* synaptopHluorin (spH) imaging to visualize odorant-evoked neurotransmitter release from ORNs in adult transgenic mice that underwent 4 weeks of unilateral olfactory deprivation. Deprivation reduced odorant-evoked spH signals compared to sham-occluded mice. Unexpectedly, this reduction was equivalent between ORNs on the open and plugged sides. Changes in odorant selectivity of glomerular subpopulations of ORNs were also observed, but only in ORNs on the open side of deprived mice. These results suggest that naris occlusion in adult mice produces substantial changes in primary olfactory processing that may reflect not only the decrease in olfactory stimulation on the occluded side but also the alteration of response properties on the intact side. We also observed a modest effect of true sham occlusions that included noseplug insertion and removal, suggesting that conventional noseplug techniques may have physiological effects independent of deprivation *per se* and thus require more careful controls than has been previously appreciated.

Introduction

Experimentally-induced sensory deprivation has been an essential tool to study how overall levels of sensory input shape the structure and function of brain regions in the olfactory (Brunjes, 1985; Brunjes et al., 1985; Franks and Isaacson, 2005; Kim et al., 2006), visual (Wiesel and Hubel, 1965; Kirkwood et al., 1996), auditory (Chang and Merzenich, 2003; Zhou and Merzenich, 2007; de Villers-Sidani et al., 2008), and somatosensory (Finnerty et al., 1999; Lendvai et al., 2000) systems. However, only a few studies have investigated the effects of deprivation on the behavior of primary sensory neurons, including in photoreceptors during development (Tian and Copenhagen, 2001) and in olfactory sensory neurons (OSNs) both during development and after brief deprivations in adults (Tyler et al., 2007; He et al., 2012). To date, this work has been mostly restricted to *in vitro* assessment of synaptic transmission, leaving open the possibility of deprivation-induced changes in transduction of natural stimuli, neuronal firing properties, or other factors. Characterizing any deprivation-induced alterations in the neural response to a stimulus at the level of the primary receptor neurons is a critical step in understanding the observed plasticity of the downstream brain regions working to interpret this modified sensory signal.

Here, we evaluated the effects of olfactory sensory deprivation on primary neural representations of odors in the adult brain. Adult OMP-spH mice underwent unilateral naris occlusion (or a sham occlusion procedure) for 4 weeks using a removable noseplug. After the deprivation period, odorant-evoked neural activity in the olfactory bulb ipsilateral to the occlusion was compared to that of the contralateral bulb and to that in the olfactory bulbs of sham-occluded mice.

Methods

Subjects.

Imaging experiments used 17 heterozygous olfactory marker protein-synaptobHluorin (OMP-spH) mice that were on a mixed C57BL/6×129 background and were of mixed sexes. Additional wild-type C57BL/6 mice (Charles River Laboratories) were used in immunohistochemistry experiments to confirm deprivation efficacy. Respiration measurements from reversibly-occluded mice were compared to that taken from additional naïve wild-type 129 mice.

Reversible unilateral naris occlusion.

Removable noseplugs were constructed after the manner of (Cummings and Brunjes, 1997; Cummings et al., 1997). The plugs were constructed out of polyethylene (PE) tubing (PE10; Becton Dickinson), chromic gut suture (5-0; MYCO Medical), and braided silk suture (6-0; Surgical Specialties Corp), and were varied in length (5 or 7 mm) to account for differences in animal size.

For deprivation (DEP group; $N = 6$ in experiment 1a & $N = 6$ in experiment 1b), adult mice were lightly anesthetized with isoflurane and a noseplug was gently inserted into the left or right external naris with curved forceps. Plugged (PLUG) and open (OPEN) sides were counterbalanced across animals. This design permitted within-subjects comparisons between the PLUG and OPEN sides because the nasal septum separates the left and right nares and OSNs project exclusively to the ipsilateral olfactory bulb. After a brief recovery (between 10 and 20 minutes on a heating pad) mice were returned to the colony room in standard cages that were lined with white paper towels. The paper towel

lining was checked twice (at 24 and 48 hours) to determine if the plug had fallen out, and then the animals were switched back to standard bedding.

After 4 weeks of unilateral naris occlusion, mice were lightly anesthetized with isoflurane and noseplugs were removed with curved forceps. In pilot experiments, we observed no response to odorants in bulbs ipsilateral to the noseplug immediately after plug removal. Consequently, mice were given a 24-hour recovery period after plug removal prior to imaging to ensure the restoration of airflow. As shown in Figure 1.1, the restoration of airflow was confirmed in a subset of mice via intranasal thermocouple measurements. Respiration was recorded on the PLUG (re-opened) side in a subset of DEP mice ($n = 2$) and also on a single side in naïve control mice ($N = 2$). A thermocouple (emtss-010g-12; Omega Engineering) was acutely implanted into the nasal bone after the manner of (Wesson et al., 2008a). Briefly, the sensor was lowered into the naris approximately 3 mm anterior to the frontal-nasal fissure and 1 mm lateral to the septal bone along the midline. The thermocouple signal was amplified 1000 \times , low-pass filtered at 1 Hz (model BMA-931; CWE, Inc), digitized at 100 Hz, and saved to a hard drive via Neuroplex software. Respiration was recorded from each deeply anesthetized subject during 4 consecutive 16-sec trials (examples shown in Figure 1.1A) and the frequency of inhalations was quantified. As shown in Figure 1.1B, respiration frequency did not differ ($p = 0.655$) between deprived nares and unmanipulated control nares.

Additional wild-type mice that were not imaged but were included in the histological procedures were perfused either immediately or 24 hours after the plug removal procedure. Sham-occluded mice (SHAM group; $N = 5$ in experiment 1a) received identical treatment to occluded mice, including isoflurane anesthesia and insertion of a

plug, but the plug was removed immediately after insertion. Sham-occluded mice later received a sham plug removal in which the mice were anesthetized and forceps inserted into the naris as if a plug had been present.

Histological procedures and analyses.

Adult olfactory deprivation causes a reduction in juxtaglomerular tyrosine hydroxylase (TH) expression (Baker et al., 1993). To validate the deprivation technique used here, TH expression was assessed via immunohistochemistry in juxtaglomerular interneurons of PLUG and OPEN bulbs from DEP mice. Olfactory bulb histology and immunohistochemistry was performed as previously reported (Moberly et al., 2012). Briefly, mice were intracardially perfused with 0.1 M phosphate-buffered saline (PBS) solution followed by 4% paraformaldehyde either immediately following imaging procedures or following plug removal procedures (no differences were observed between these time points). Brains were removed, postfixed in 4% paraformaldehyde, and then transferred to PBS for a minimum of 24 hours prior to sectioning. Both olfactory bulbs were sectioned horizontally on a Vibratome at 50 μ m. Sections were incubated in solutions containing primary antibody against TH (a 1:1000 dilution of rabbit anti-mouse TH; Millipore, #AB152) and 10 μ g/mL of fluorophore-tagged secondary antibody (goat anti-rabbit IgG H + L conjugated to AlexaFluor568; Invitrogen, #A-11011). Sections were mounted on glass slides in a ProLong Gold antifade reagent (Invitrogen) containing 4',6-diamidino-2-phenylindole (DAPI, nuclear counterstain).

Images were acquired at 4 \times magnification via an Olympus BX series fluorescence microscope with a Jenoptik MFcool CCD camera, and were then analyzed with ImageJ software obtained through NIH. DAPI fluorescence was first used to identify regions of

interest. The optical density of identified regions was then quantified in the corresponding AlexaFluor fluorescent image. Experimenters were blind while performing all histological procedures and quantifications.

Juxtaglomerular TH immunoreactivity was reduced by reversible, unilateral naris occlusion (Figure 1.2), consistent with earlier studies using the same (Cummings et al., 1997) or alternative (Baker et al., 1993; Cho et al., 1996) methods of occlusion. Relative to contralateral (OPEN) bulbs, there was a 31% ($\pm 7\%$) reduction in TH expression in ipsilateral (PLUG) bulbs (Figure 1.2B; one-sample t test, $t_{df=4} = -4.554$, $p = 0.01$). Thus, the efficacy of the occlusion method used here is comparable to that of methods used in earlier research (Baker et al., 1993; Cummings et al., 1997).

Olfactory stimuli used during in vivo optical imaging.

In experiment 1a (shown in Figures 1.3, 1.4, & 1.6), a panel of up to 4 odorants, including *n*-butyl acetate (BA), methyl valerate (MV), 2-hexanone (2HEX), and *trans*-2-methyl-2-butanal (2M2B), was delivered, with each odorant being presented at up to 3 concentrations. In experiment 1b (shown in Figure 1.5), BA was delivered at 9 concentrations spanning an almost 300-fold range. In experiments 1a and 1b concentration is expressed as percent dilution of saturated vapor and in arbitrary units (a.u.), respectively.

Statistical analysis.

Data from experiment 1a (shown in Figures 1.3, 1.4, & 1.6) were pooled across odorants and concentrations. These data were then analyzed via mixed-model ANOVAs (with side as a within-subjects factor and group as a between subjects factor) and appropriate *post-hoc* tests to evaluate measures of central tendency. These data were also analyzed with Kolmogorov-Smirnov (K-S) and Mann-Whitney (M-W) U tests to evaluate

overall distributions. Data from experiment 1b (shown in Figure 1.5) were analyzed via 2-way repeated-measures ANOVAs (with side and concentration as within-subjects factors) and *t* tests for planned *post hoc* comparisons.

Results

Unilateral sensory deprivation reduces the magnitude of odorant-evoked synaptic input from OSNs to olfactory bulb glomeruli on both plugged and open sides equally.

To evaluate the physiological consequences of olfactory sensory deprivation, 11 OMP-spH mice were randomly assigned to undergo either a reversible unilateral deprivation via a noseplug inserted into the external naris (DEP group, $N = 6$) or a sham procedure in which the plug was inserted but then immediately removed (SHAM group, $N = 5$). After 4 weeks of deprivation, noseplug removal was performed (DEP group) or simulated (SHAM group). The following day, each mouse was anesthetized and neurotransmitter release from OSNs into olfactory bulb glomeruli was visualized via optical imaging of spH signals bilaterally through an implanted cranial window (for example cranial windows see Figure 1.3A-B, top). For each mouse, the odorant-evoked change in fluorescence (ΔF) was calculated for each glomerulus based on difference maps of the baseline fluorescence subtracted from the fluorescence following odorant presentation (Figure 1.3A-B, bottom).

As shown in Figure 1.3C, there was a main effect of group, such that the observed spH signals were about half as big in DEP mice as in SHAM mice (Figure 3C, inset; $F_{1,9} = 78.30$, $p < 0.001$, $\eta_p^2 = 0.897$). Surprisingly, there was no main effect of side ($F_{1,9} = 2.28$, $p = 0.165$, $\eta_p^2 = 0.202$) and no significant side by group interaction ($F_{1,9} = 0.86$, $p = 0.087$,

$\eta_p^2 = 0.087$). Following up on this analysis, the overall distributions of response amplitudes in each group were compared using cumulative frequency histograms and non-parametric tests (Figure 1.3D). For both PLUG and OPEN olfactory bulbs, glomerular responses observed in SHAM mice were larger than those in corresponding bulbs of DEP mice across the full range of response amplitudes (Figure 1.3D; PLUG sides, K-S, $Z = 9.15$, $p < 0.001$ and M-W U, $Z = 19.543$, $p < 0.001$; OPEN sides, K-S $Z = 10.795$, $p < 0.001$ and M-W U, $Z = 23.599$, $p < 0.001$). Within the DEP group, the distribution of response amplitudes was not different between the PLUG and OPEN sides (Figure 1.3D; K-S, $Z = 1.593$, $p = 0.013$ and M-W U, $Z = 0.826$, $p = 0.409$). Within the SHAM group, the distribution of responses on the PLUG side was slightly but significantly shifted toward smaller responses across the distribution (Figure 1.3D; K-S, $Z = 2.101$, $p < 0.001$ and M-W U, $Z = 3.697$, $p < 0.001$). This difference presumably shows an effect of the sham plug removal, which includes brief anesthesia and the insertion of forceps deep into the nasal passages on the PLUG side.

Unilateral sensory deprivation increases the number of olfactory bulb glomeruli receiving odorant-evoked synaptic input from OSNs contralateral to the noseplug.

For each olfactory bulb (examples shown in Figure 1.4A-B), the number of glomeruli receiving detectable synaptic input from the olfactory nerve was quantified for each odorant presented in the experiment described above. As shown in Figure 1.4C, there was no effect of group (inset; $F_{1,9} = 0.31$, $p = 0.589$, $\eta_p^2 = 0.034$) nor a group by side interaction ($F_{1,9} = 0.975$, $p = 0.349$, $\eta_p^2 = 0.098$), but there was a significant main effect of side ($F_{1,9} = 7.24$, $p = 0.025$, $\eta_p^2 = 0.446$). To follow up on this analysis, we compared the distributions of the numbers of glomeruli receiving odorant-evoked OSN input across groups, pooling across odorants and concentrations (Figure 1.4D). The number of

glomeruli receiving measurable input during our odorant panel on the PLUG side of DEP mice was identical to that on the PLUG side of SHAM mice (Figure 1.4D, black vs. red; K-S, $Z = 0.88$, $p = 0.417$ and M-W U, $Z = 0.44$, $p = 0.663$), suggesting that deprivation did not affect the number of responsive glomeruli on the PLUG side. Comparing between sides in DEP mice, the number of glomeruli receiving measurable input during our odorant panel was clearly greater on the OPEN side than the PLUG side (Figures 1.4B & 1.4D; K-S, $Z = 2.25$, $p < 0.001$ and M-W U, $Z = 3.92$, $p < 0.001$). Comparing the distribution of responses between the OPEN bulbs in DEP and SHAM mice (Figure 1.4D, orange vs. gray), the OPEN bulbs in DEP mice consistently exhibit more glomeruli receiving input in the top half of the distribution, which corresponds to trials on which larger numbers of glomerular responses were evoked (for overall distribution: K-S, $Z = 1.37$, $p = 0.046$; M-W U, $Z = 1.97$, $p = 0.049$). These data suggested that a) deprivation does not affect the number of glomeruli receiving odorant-evoked synaptic input from OSNs in olfactory-deprived or sham-deprived olfactory bulbs, b) deprivation could cause an increase in the number of responsive glomeruli in olfactory bulbs on the OPEN side, and c) that rather than being an increase of fixed size (which would have shifted the entire distribution towards larger numbers of responses) the increase could be proportional to the number of glomeruli responding.

To test the hypothesis that deprivation induces a proportional increase in the number of glomeruli that respond to an odorant in the OPEN side, we repeated the experiment using a single odorant over a broad range of concentrations. Because additional glomeruli are recruited into the odor representation at higher concentrations (Malnic et al., 1999; Rubin and Katz, 1999; Meister and Bonhoeffer, 2001; Spors and Grinvald, 2002),

this experiment permitted the comparison of the effects of deprivation on the number of activated glomeruli across a range of total response numbers.

Six additional OMP-spH mice were nares occluded for 4 weeks and then (24 hours after plug removal) underwent a bilateral imaging session in which OSN inputs to the bulb were evoked by 9 different concentrations of BA over an almost 300-fold range (Figure 1.5). The magnitudes of glomerular responses were measured in this experiment and were comparable between OPEN and PLUG bulbs at all concentrations tested (Figure 1.5B-C), consistent with the previous results (Figure 1.3). There was no main effect of side (Figure 1.5B-C; $F_{1,5} = 0.241$, $p = 0.644$, $\eta_p^2 = 0.046$) nor a significant interaction of deprivation state with concentration (Figure 1.5B-C; $F_{8,40} = 0.586$, $p = 0.783$, $\eta_p^2 = 0.105$). The main effect of concentration was of course significant (Figure 1.5C; $F_{8,40} = 12.318$, $p < 0.001$, $\eta_p^2 = 0.711$).

As expected, the absolute number of BA-evoked glomerular responses also increased across concentrations (Figure 1.5A & 1.5D; main effect of concentration, $F_{8,40} = 22.12$, $p < 0.001$, $\eta_p^2 = 0.816$). There was no main effect of side ($F_{1,5} = 3.306$, $p = 0.129$, $\eta_p^2 = 0.398$). Importantly, there was a significant concentration \times side interaction ($F_{8,40} = 3.45$, $p = 0.004$, $\eta_p^2 = 0.408$). This confirms the previous finding that the difference in number of evoked responses between OPEN and PLUG sides is greatest when larger numbers of glomeruli are responding.

Notably, the size of the increase seemed proportional to the absolute number of responses across concentrations (Figure 1.5D). To test this proportionality statistically, data were normalized to the maximum number of glomeruli to respond to any odorant concentration within each olfactory bulb (Figure 1.5E). If the increase is indeed

proportional, this normalization should equalize the number of responses between OPEN and PLUG bulbs. As shown in Figure 1.5E, the normalized concentration-response curves overlap almost perfectly. Normalization eliminates the statistical interaction between side and concentration ($F_{8,40} = 0.818$, $p = 0.592$, $\eta_p^2 = 0.141$), while preserving the main effect of concentration ($F_{8,40} = 69.135$, $p < 0.001$, $\eta_p^2 = 0.933$), as predicted. Side continues to have no significant main effect ($F_{1,5} = 0.468$, $p = 0.524$, $\eta_p^2 = 0.086$).

Unilateral deprivation increases the odorant response selectivity of OSN populations contralateral to the noseplug.

The population of OSNs expressing a given odorant receptor (and projecting to an individual glomerulus in the olfactory bulb) typically responds to a range of odorants determined by the receptor identity (Zhao et al., 1998; Malnic et al., 1999; Bozza et al., 2004; Grosmaitre et al., 2006). Conversely, a given odorant typically activates a range of OSN populations and drives input to multiple olfactory bulb glomeruli in a concentration-dependent manner (see Figure 1.5 for example). The change in the number of glomeruli responding to a given odorant in olfactory bulbs on the OPEN side thus raises the question of whether the OSNs in these bulbs might have an altered odorant-response profile. To test this hypothesis we examined the odorant-selectivity of individual glomeruli in the olfactory bulbs of SHAM and DEP mice (examples shown in Figure 1.6A-B) across the 4 odorants presented in experiment 1a and summarized in Figures 1.3-1.4.

Each individual responding glomerulus was categorized as responding to 1, 2, 3, or 4 odorants in the panel. Then, the values (ranging from 1 to 4) from individual glomeruli were averaged together for each olfactory bulb ($N = 20$) of each mouse ($N = 10$). As shown in Figure 1.6C, this measure of selectivity (number of odorants evoking a response in each

glomerulus) was then analyzed with a 2-way mixed ANOVA, with group (DEP or SHAM) and side (PLUG or OPEN) as factors, which revealed a significant group by side interaction ($F_{1,8} = 7.325, p = 0.027, \eta_p^2 = 0.478$). *Post-hoc* comparison revealed that glomeruli in the olfactory bulb on the OPEN side of deprived mice responded to significantly fewer odorants than glomeruli on the DEP side of the same animals (paired *t*-test, $t_{df=5} = -3.046, p = 0.029$) and also responded to significantly fewer odorants than glomeruli on the OPEN side of SHAM mice (independent-groups *t*-test, $t_{df=8} = 3.327, p = 0.01$). Interestingly, response-selectivity of glomeruli on the PLUG side of SHAM control mice did not differ from that of the PLUG sides of the DEP group (independent-groups *t*-test, $t_{df=8} = 0.51, p = 0.624$), or from the OPEN sides in the same (SHAM) mice (paired *t*-test, $t_{df=3} = 0.342, p = 0.418$).

To more richly display these results, the distributions of glomerular selectivities are plotted in Figure 1.6D, such that for each side by group population the percentage of glomeruli that responded to 1, 2, 3, or 4 odorants is depicted as the distance from a common origin. The areas of the resulting plots are a constant 100%, but their shapes reflect their distributions of odorant selectivities. Note that the plot for the DEP-OPEN bulbs is notably skewed towards fewer odorants, reflecting an increase in selectivity.

Discussion

In this study, we found that 4 weeks of unilateral olfactory deprivation during adulthood altered the primary neural responses to odorants after naris reopening in mice. The magnitude of total odorant-evoked OSN synaptic input to olfactory bulb glomeruli was greatly reduced by deprivation, but surprisingly this reduction was comparable

between the olfactory bulb on the plugged side and on the open side across odorants and concentrations. Despite the smaller response magnitudes, the number of glomeruli receiving detectable OSN synaptic input was not different between sensory-deprived and sham-deprived olfactory bulbs. However, in mice that underwent deprivation, the olfactory bulb contralateral to the plug exhibited a proportional increase in the number of glomeruli receiving detectable odorant-evoked synaptic input from OSNs across a broad range of concentrations. These glomeruli also exhibited a change in their odorant-response profile such that they were more odorant-selective than their counterparts on the plugged side.

The present *in vivo* results provide important physiological context to the wealth of literature on the neurochemical, morphological, behavioral, and *in vitro* consequences of olfactory sensory deprivation. Previous reports have revealed a cascade of seemingly compensatory responses observed in adult OSNs following *early postnatal* naris occlusion. Adenylate cyclase type III and phosphodiesterase type IV are upregulated in OSNs ipsilateral to the occlusion (Coppola et al., 2006) in a manner that suggests a compensatory increase in the gain of olfactory transduction, while epithelial electroolfactograms (Waggener and Coppola, 2007) and recordings from individual OSNs reveal an increase in the amplitude of population-level neural responses to odorants ipsilateral to deprivation (He et al., 2012). OSN terminals exhibit an increase in both the probability of release and quantal content in an olfactory bulb slice preparation from both neonatally occluded and briefly deprived adults rats (Tyler et al., 2007), and odorant-evoked uptake of 2-deoxyglucose (2-DG) is enhanced in the olfactory bulb glomeruli of neonatally-occluded rats (Guthrie et al., 1990). These results have been interpreted as evidence of homeostatic plasticity, such that neural responses are enhanced to compensate for the reduction in

primary sensory input (Coppola, 2012; Coppola and Waggner, 2012). However, the present results indicate that in *adult* mice a period of deprivation substantially reduces the amplitude of odorant-evoked OSN synaptic input to the brain (Figure 1.3). This suggests that the compensatory responses observed in neonatally occluded mice may be unique to early development and not indicative of adult function. That said, previous reports have shown decreases in the odorant selectivity of mitral and tufted cells that might reflect changes in intrabulbar circuitry after 60 days of naris occlusion in young adult rats (Wilson and Sullivan, 1995), suggesting that compensatory responses may still occur downstream of the OSNs (Saghatelian et al., 2005).

Naris occlusion is often viewed as the olfactory analog of visual deprivation via eyelid suture (Wiesel and Hubel, 1965). However, the two techniques are not strictly equivalent because naris occlusion forces all nasal airflow to pass through the contralateral nasal passage, while closing one eyelid does not change the light levels in the contralateral eye. In light of the relatively recent discovery that some OSNs are mechanosensitive (Grosmaître et al., 2007), naris occlusion is potentially confounded *a priori* by the elimination of airflow (in addition to olfactory stimuli) on the occluded side and by the presumed increase in airflow on the contralateral side. The present results demonstrate that unilateral naris occlusion via noseplug had large effects on *both* olfactory bulbs. This confirms that the bulb on the open side can be affected by occlusion just as much as the bulb on the plugged side.

With neonatal deprivation, the expression of OMP and transduction proteins like adenylyl cyclase III in OSNs increases on the closed side and decreases on the open side (Coppola, 2012), which would likely lead to an increase in OSN sensitivity to odorants

(Lee et al., 2011). However, the present data do not exhibit corresponding changes in the OSN response to odorants, and instead show a comparable decrease in odorant-evoked OSN response amplitudes on both sides (Figure 1.3). As noted above, it is possible that mice deprived in adulthood do not exhibit the same changes in protein expression, or perhaps that these effects are counteracted *in vivo* by changes in other aspects of the system like energy metabolism or mucus composition. It is intriguing but unexpected that we observed a large decrease in spH response amplitude in DEP-OPEN bulbs. The constant airflow through the nasal passages on the opened side may have caused this reduction through either an adaptive downregulation of OSN responsivity in reaction to the chronic odorant exposure or possibly through adaptation of mechanosensitive OSNs (Grosmaître et al., 2007) in reaction to the chronic stimulation. Alternatively, because the spH signals reflect total OSN neurotransmitter release throughout the entire 6 sec odorant presentation, it is possible that this reduction reflected a more rapid or more complete adaptation to the odorant rather than a decrease in peak spike rate.

The reduction in odorant-evoked response amplitude and modest increase in odorant selectivity in OSNs in DEP-OPEN bulbs is consistent with the effects of odorant exposure (Buonviso and Chaput, 2000; Mandairon and Linster, 2009). Brief odorant exposures can increase the selectivity of mitral cells (Fletcher and Wilson, 2003) or shift the pattern of some mitral cell responses from increases in firing rate to decreases in firing rate (Buonviso and Chaput, 2000). The present results thus suggest that the effects observed in DEP-OPEN bulbs may reflect increased exposure to odors caused by forcing all airflow through that side.

The proportional increase in the number of glomeruli responding to an odorant observed in olfactory bulbs contralateral to the noseplug (Figure 1.5) is unexpected and in contrast to the increased odorant selectivity of responsive glomeruli (Figure 1.6). This seeming contradiction can potentially be explained by differential effects across subpopulations of OSNs (Cavallin et al., 2010; Cadiou et al., 2014), some of which become more selective (presumably as a result of increased odorant exposure (Buonviso and Chaput, 2000)) and others of which begin to respond broadly across odorants. One model for the latter effect would be the presence of some number of broadly tuned OSN populations (such as SR1-expressing OSNs, see (Grosmaître et al., 2009)) in DEP-OPEN sides that begin responding to odorants after the 1-month deprivation period. Such an effect could occur through activity-dependent alterations in inhibitory bulbar circuitry (Parrish-Aungst et al., 2011; Lau and Murthy, 2012) or through the relief of tonic presynaptic inhibition that unmasks previously subthreshold responses in some glomeruli but not others (McGann et al., 2005; Pirez and Wachowiak, 2008). Alternatively, the endogenous turnover of OSNs over the one month occlusion period could permit changes in odorant receptor expression. For instance, olfactory deprivation can cause individual OSNs to express more than one odorant receptor (Tian and Ma, 2008), which would be expected to increase the range of odorants a given OSN population responds to, especially if different OSNs within a given glomerulus select different secondary receptors. Second, olfactory deprivation has been shown to reduce the pruning of OSN projections to “incorrect” glomeruli during development (Zou et al., 2004). On the timescale assessed here, it is thus possible that the increase in the number of glomerular responses reflects the addition of “miswired” adult-born OSNs that are not pruned away during the deprivation

period. Finally, it is possible that the increase in the number of glomeruli receiving odorant-evoked OSN input that we observed in DEP-OPEN bulbs is caused by the interactive effects of odorant deprivation and exposure. Specifically, deprivation increases proliferation in the olfactory epithelium on the open side (Suh et al., 2006) and long-term odorant exposure can increase the number of supernumerary glomeruli (Valle-Leija et al., 2012). An increase in adult-born OSNs on the open side coupled with the increased odorant exposure on that side may give rise to glomerular maps that integrate additional odorant specific-glomeruli.

OMP expression is developmentally regulated such that it is expressed only in mature OSNs (Graziadei et al., 1980), at which point it can convey an increase in odorant-selectivity (Lee et al., 2011). After neonatal olfactory deprivation, OMP expression is reduced in the olfactory epithelium on the side opposite the occlusion (Coppola et al., 2006), though it is not clear if this represents a downregulation of OMP expression within mature OSNs or the addition of a population of immature, potentially less odorant-selective OSNs. If such a decrease occurred in our adult-deprived mice, it could potentially explain the increase in the number of glomeruli (OSN populations) stimulated by a given odorant in DEP-OPEN bulbs (Figures 1.4 & 1.5).

The results in Figure 1.3 demonstrate the importance of careful sham controls in naris occlusion studies. The majority of naris occlusion studies use control animals that are either unmanipulated (for example, (Cummings and Belluscio, 2010)) or have received sham occlusions on the outside of the snout (for example, (Wilson and Sullivan, 1995)) that do not actually affect the nasal passages. Such designs do not control for potential irritation or inflammation associated with the occlusion itself, independent of olfactory

deprivation *per se*. However, here we find modest but significant effects of the nose plug insertion and removal in our sham mice, which had a noseplug actually inserted and then immediately removed during the initial “occlusion” and then experienced a simulated removal in which forceps were inserted into the nasal passages in a manner comparable to the occluded mice. This difference suggests that conventional techniques for the mechanical occlusion of the olfactory system may have confounding effects besides mere removal of sensory stimuli.

The present results illustrate that experience-dependent plasticity can produce substantial changes in sensory codes as early as the synaptic output of the receptor neurons themselves. In other sensory systems the primary sensory neurons are less experimentally accessible *in vivo*, and investigations of experience-dependent plasticity have been largely confined to downstream processing, especially in sensory cortices. The current findings suggest that primary sensory neurons can change in complex and stimulus-selective ways (beyond just stronger-weaker) that could be essential to interpreting subsequent sensory information processing.

Acknowledgements

I thank Joseph Pottackal and Daniel J. Turkel for performing the immunohistochemistry experiments, which were used to confirm the efficacy of the deprivation method employed in this project. I also thank Daniel Wesson for sharing his protocols for noseplug construction and intranasal thermocouple implantation.

Chapter 1 Figures

Figure 1.1

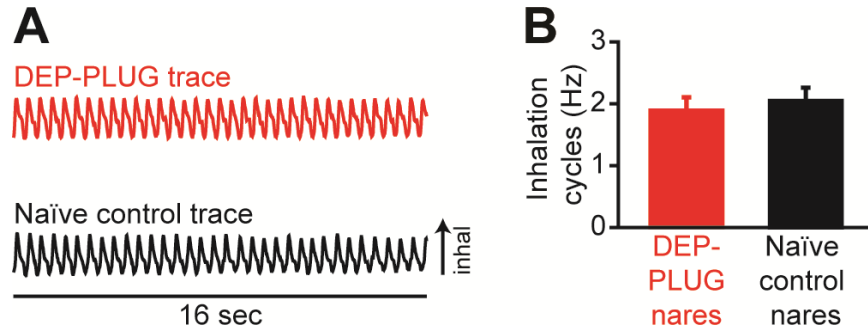


Figure 1.1. Demonstration of the patency of the re-opened airway 24 hours after plug removal. (A) Representative thermocouple traces recorded from a DEP-PLUG airway (top, red) and from an airway of a naïve control mouse (bottom, black). Inflections correspond with inhalations (inhal) and deflections correspond with exhalations. (B) No difference was observed in the mean \pm SEM inhalation cycles that were recorded from DEP-PLUG nares (red) and naïve control nares (black).

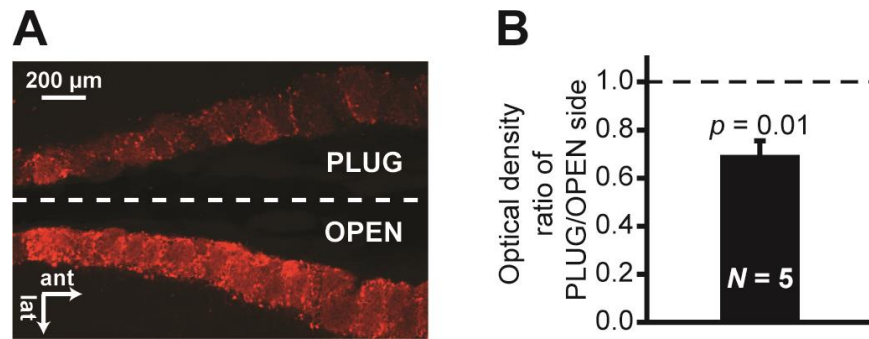
Figure 1.2

Figure 1.2. Four weeks of unilateral naris occlusion causes a relative reduction in periglomerular TH expression in the olfactory bulb ipsilateral to the occluded naris. (A) Representative horizontal section showing the posterior-medial edges of the OPEN and PLUG bulbs. Note that data quantification was performed across the entire bulb and only a portion of this section is displayed. **(B)** Mean \pm SEM ratio of TH expression on the PLUG side relative to that on the OPEN side.

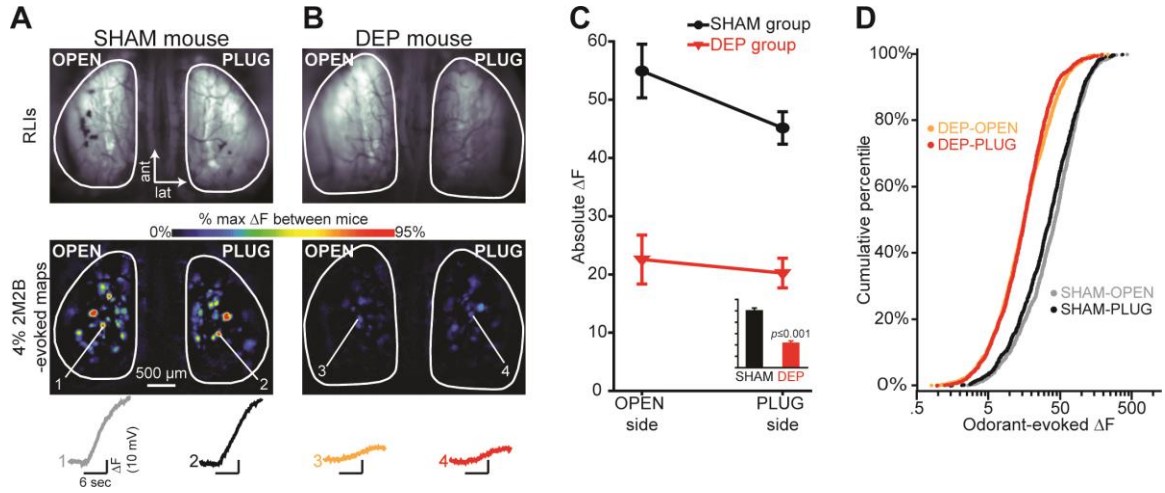
Figure 1.3

Figure 1.3. The magnitude of odorant-evoked nerve output is suppressed equally in both the OPEN and PLUG sides of DEP mice, as compared with the OPEN and PLUG sides of SHAM controls. (A-B) Resting light images (RLIs) of the dorsal olfactory bulbs through the cranial window (top) and pseudocolored difference maps (bottom) from a representative SHAM mouse (**A**) and a representative DEP mouse (**B**). RLIs are scaled individually to control for differences in windows. Numbered callouts indicate traces showing the change in fluorescence (ΔF) that was evoked by a 6-sec presentation of 4% 2M2B in the corresponding glomeruli. (**C**) Mean \pm SEM odorant-evoked ΔF plotted as a function of side for SHAM and DEP groups. The inset displays the main effect of group and is scaled to the same y-axis. (**D**) The four distributions (separated by group and side) of observed ΔF values are shown as cumulative probability plots.

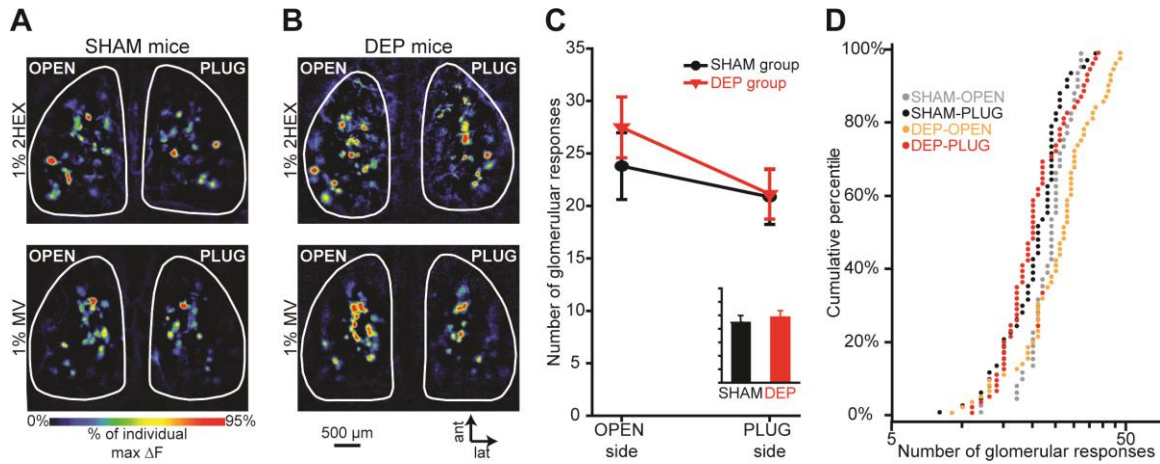
Figure 1.4

Figure 1.4. The number of glomeruli receiving measurable OSN input increases in the OPEN side of DEP mice. (A-B) Pseudocolored difference maps evoked by 1% 2HEX (top) and 1% MV (bottom) in SHAM mice (A) and DEP mice (B). (C) Mean \pm SEM number of odorant-evoked responses plotted as a function of side for SHAM and DEP groups. The inset displays the main effect of group ($p > 0.05$, n.s.) and is scaled to the same y-axis. (D) The 4 distributions (separated by group and side) of observed response numbers are shown as cumulative probability plots.

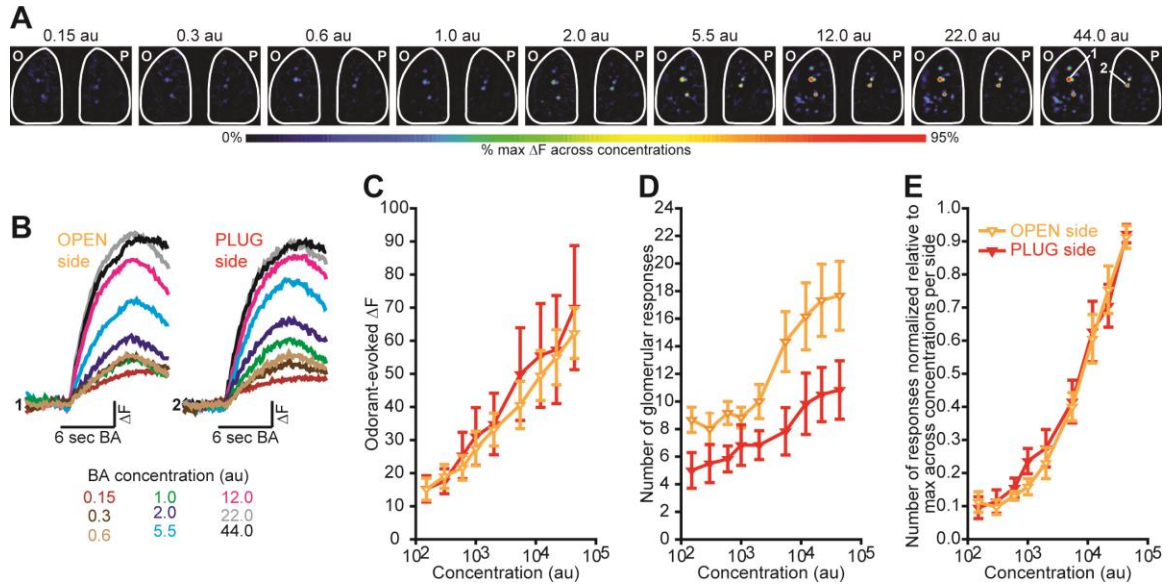
Figure 1.5

Figure 1.5. The increased number of evoked glomerular responses on the OPEN side relative to the PLUG side is proportional to the number of responses evoked across concentrations. (A) Pseudocolored difference maps evoked by an almost 300-fold range of BA concentrations (shown in arbitrary units, au) in a DEP mouse. O, OPEN side; P, PLUG side. (B) Sets of traces corresponding to 2 glomeruli shown across 9 concentrations in (A) with the callouts indicated in the 44.0au-evoked map. Response amplitudes from both glomeruli are scaled to the same maximum. (C) Odorant-evoked change in fluorescence (ΔF) plotted as a function of concentration for the OPEN and PLUG sides of DEP mice. (D) Absolute number of BA-evoked responses plotted as a function of concentration for the OPEN and PLUG sides of DEP mice. (E) Normalized number of responses plotted as a function concentration. Data are normalized relative to the maximum number of BA-evoked responses across all 9 concentrations within each olfactory bulb of each mouse. Data in C-E are displayed as the mean \pm SEM.

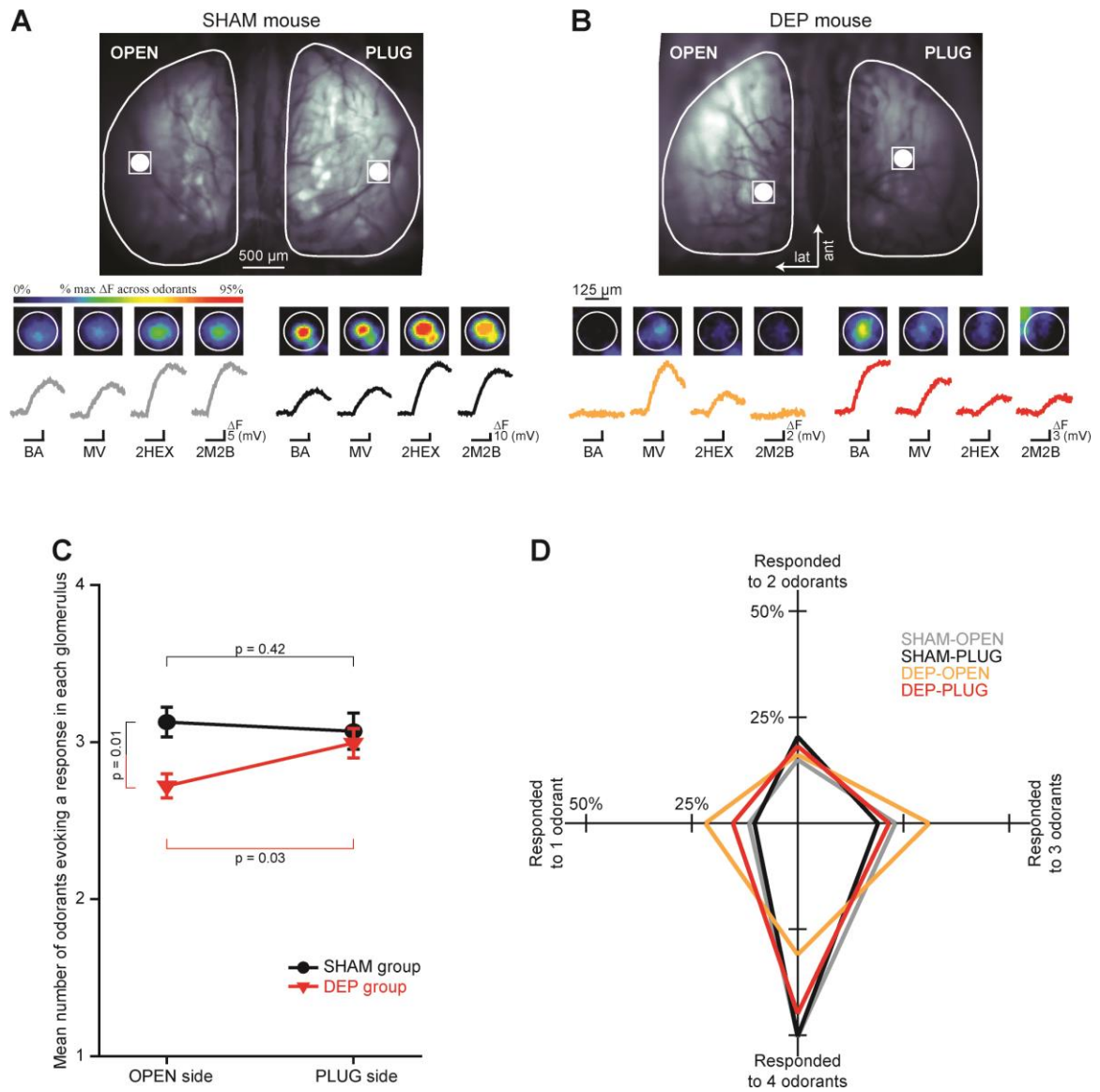
Figure 1.6

Figure 1.6. Glomerular response selectivity is increased in the OPEN side of DEP mice. (A-B) Resting light images (RLIs) from a SHAM mouse (A) and a DEP mouse (B) are used to indicate the location of a single glomerulus on the OPEN and PLUG sides. The responses of each of the 4 indicated glomeruli to BA, MV, 2HEX, and 2M2B are shown immediately below the RLIs in the magnified pseudocolored images. Black scale bars indicate the 6 sec odorant presentation corresponding to each trace. Each set of 4 traces is scaled relative to the maximum evoked amplitude across odorants. (C) Mean \pm SEM number of odorants responded to (min = 1, max = 4) plotted as a function of side for SHAM

and DEP groups. **(D)** The percent of glomeruli from OPEN and PLUG sides of SHAM and DEP groups that responded to 1, 2, 3, or 4 odorants. The surface area of each polygon totals 100% and represents the overall response selectivity of each population of responding glomeruli.

CHAPTER 2

Spatiotemporal alterations in primary odorant representations in olfactory marker protein knockout mice

The results from this chapter are reported in Kass MD, Moberly AH, McGann JP (2013a) Spatiotemporal alterations in primary odorant representations in olfactory marker protein knockout mice. *PLoS One* 8:e61431.

Abstract

Olfactory marker protein (OMP) is highly and selectively expressed in primary olfactory sensory neurons (OSNs) across species, but its physiological function remains unclear. Previous studies in the olfactory epithelium suggest that it accelerates the neural response to odorants and may modulate the odorant-selectivity of OSNs. Here we used a line of gene-targeted mice that express the fluorescent exocytosis indicator synaptopHluorin in place of OMP to compare spatiotemporal patterns of odorant-evoked neurotransmitter release from OSNs in adult mice that were heterozygous for OMP or OMP-null. We found that these patterns, which constitute the primary neural representation of each odorant, developed more slowly during the odorant presentation in OMP knockout mice but eventually reached the same magnitude as in heterozygous mice. In the olfactory bulb, each glomerulus receives synaptic input from a subpopulation of OSNs that all express the same odor receptor and thus typically respond to a specific subset of odorants. We observed that in OMP knockout mice, OSNs innervating a given glomerulus typically responded to a broader range of odorants than in OMP heterozygous mice and thus each odorant evoked synaptic input to a larger number of glomeruli. In an olfactory habituation task, OMP knockout mice behaved differently than wild-type mice, exhibiting a delay in their onset to investigate an odor stimulus during its first presentation and less habituation to that stimulus over repeated presentations. These results suggest that the actions of OMP in olfactory transduction carry through to the primary sensory representations of olfactory stimuli in adult mice *in vivo*.

Introduction

Olfactory marker protein (OMP) is a 19 kDa intracellular protein expressed at high levels in olfactory sensory neurons (OSNs) in many vertebrate species (Krishna et al., 1992; Buiakova et al., 1994) with very limited expression elsewhere in the nervous system (Baker et al., 1989). The molecular genetics (Sydor et al., 1986; Danciger et al., 1989) and structure (Baldisseri et al., 2002; Smith et al., 2002; Wright et al., 2005) of OMP are now well understood. OMP is expressed only late in cellular development and is widely used as a marker of mature OSNs (Monti-Graziadei et al., 1977; Farbman and Margolis, 1980). Perhaps in concert with this expression pattern, OMP may also play a role in epithelial neurogenesis (Farbman et al., 1998) and axon guidance (perhaps indirectly through changes in neuronal activity; (St John and Key, 2005)).

The physiological role of OMP is increasingly well understood. It is an olfactory transduction protein whose deletion in OMP knockout mice produces smaller and slower OSN responses to odorants when recorded via electroolfactogram (Buiakova et al., 1996) or in individual OSNs (Lee et al., 2011) as well as significant perceptual effects, including elevated odor response thresholds (Youngentob and Margolis, 1999). No overall odor discrimination deficit has been observed in psychophysical tasks (Youngentob et al., 2001), but OMP-knockout mice do fail to exhibit a preference for their own mother over another lactating female (Lee et al., 2011). Some of these neurophysiological and perceptual deficits can be rescued by viral vector-mediated gene replacement (Ivic et al., 2000; Youngentob et al., 2004), proving that these effects are directly caused by the lack of OMP. OMP's action is early in the olfactory transduction cascade, upstream of both cAMP and chloride channel activation (Reisert et al., 2007), and it can modulate calcium extrusion

from OSNs by the sodium/calcium exchanger (Kwon et al., 2009), but despite this body of research, the precise function of OMP in olfactory physiology remains unknown.

Interestingly, OMP-knockout mice exhibit changes in the spatiotemporal pattern of odorant-evoked epithelial voltage responses *in vitro* and presumably corresponding changes in perceived odor quality (Youngentob et al., 2001; Youngentob et al., 2003). In identified OSNs expressing the MOR23 receptor, immature (pre-OMP expression) OSNs and mature OSNs from OMP-knockout mice both exhibited smaller and slower responses to odorant stimulation compared to mature, OMP- and MOR23-expressing OSNs (Lee et al., 2011). Remarkably, this study also demonstrated an increase in odorant selectivity with OMP expression, such that OMP-null OSNs responded to a broader range of odorants than mature, OMP-expressing OSNs expressing the same receptor. However, it remains unclear how these differences in OSN response dynamics in the epithelium translate into corresponding alterations of OSN synaptic signaling to the brain. In the present study, we compare spatiotemporal patterns of odorant-evoked OSN synaptic output *in vivo* and odorant-guided behavior in OMP-null and OMP-expressing mice to investigate the functional role of OMP in the olfactory system. Because these patterns indicate the output of the first neurons in the circuit, they are considered the primary neural representations of olfactory stimuli.

Methods

Subjects.

Fifteen mice were used as subjects in the imaging experiments. These subjects were adult (8-9 months) females, and were either homozygous OMP-spH mice (OMP^{-/-})

on an albino C57BL/6 background (Czarnecki et al., 2011) or heterozygous OMP-spH mice (OMP^{+/-}) on a mixed C57BL/6×129 background, analogous to those used by (Lee et al., 2011).

An additional 25 mice were used for behavioral testing. Specifically, we compared the behavior of 11 homozygous OMP-spH mice (OMP^{-/-}) on a C57BL/6 background with that of 14 wild-type C57BL/6 mice obtained from Charles River Laboratories (strain code #027). Subjects used for behavioral experimentation were adults of mixed sexes.

Acquisition and analysis of odorant-evoked spH signals.

Odorant-evoked synaptic input to glomeruli on the dorsal surface of the olfactory bulbs was imaged *in vivo*, as described above under General Methods. A panel of 4 odorants (including BA, MV, 2HEX, and 2M2B) was presented to deeply-anesthetized subjects via an 8-channel, air dilution olfactometer with each odorant being delivered at 3 concentrations (including 7.5 a.u., 15 a.u., and 30 a.u.). Peak odorant-evoked changes in fluorescence were analyzed as described above. Because spH provides an integrative signal of exocytosis over time, this peak typically occurred near the end of the odorant presentation and was considered a “late” response signal. Late (peak) responses were used to evaluate overall differences between groups in odor maps (Figures 2.1-2.3). To evaluate differences in odor maps that may occur earlier in the response, a second analysis (shown in Figure 2.4) was performed, whereby the average of 7 frames (1 sec) immediately prior to odorant onset were subtracted from the average of 7 frames beginning 2 sec after odor onset. Early frame subtractions are shown in the stimulus diagram in Figure 2.4C and late frame subtractions are shown in Figure 2.3B and Figure 2.4C.

Data used to perform the late response signal analyses (results shown in Figures 2.1-2.3) came from 654 responsive glomeruli in 22 olfactory bulbs from 11 OMP^{-/+} mice and 249 responsive glomeruli in 8 olfactory bulbs from 4 OMP^{-/-} mice. The early response signal analyses (results shown in Figure 2.4) were performed on a subset of the data that was collected from 264 early-responsive glomeruli in 10 olfactory bulbs from 5 OMP^{-/+} mice and 190 early-responsive glomeruli in 8 olfactory bulbs from 4 OMP^{-/-} mice.

The number of evoked glomerular responses and the magnitude of those responses were first analyzed with omnibus mixed-model ANOVAs, with odorant (BA; MV; 2HEX; 2M2B) and concentration (7.5 a.u.; 15 a.u.; 30 a.u.) as within-subjects factors and OMP expression (OMP^{-/-}; OMP^{-/+}) as a between-subjects factor. These overall analyses were followed up with *post hoc* tests (including additional ANOVAs and *t* tests) to perform planned comparisons and further evaluate interactions of interest. To investigate odorant response selectivity, each observed glomerular ROI was categorized based on 3 parameters: 1) OMP expression (OMP^{-/-} or OMP^{-/+}), 2) odorant selectivity (highly selective, responding to only 1 or 2 odorants in the panel; non-selective, responding to 3 or 4 odorants in the panel), and 3) concentration sensitivity (responding to 1-2 or 3-4 odorants at 7.5 a.u., 15 a.u., or 30 a.u.). The cross-tabulated frequency data were then analyzed via log-linear regression to determine if the odorant selectivity that we observed in responsive glomeruli could be best accounted for by a model including all 3 categorical variables. Additional χ^2 tests were performed for *post hoc* comparisons.

Cross-habituation/dishabituation behavioral testing and analysis.

Investigation of a novel odor stimulus and subsequent odor habituation and cross-habituation/dishabituation were assessed in 25 mice that were single-housed in standard

open shoebox cages (15 cm x 12 cm x 25 cm, WxHxL). During testing, the home cage was transferred from the colony room to the behavioral testing room and all procedures were then carried out in the home cage. During each trial a hexagonal weigh boat (6.4cm top; 4.7cm base) containing filter paper treated with 0.6 mL of solution was placed on the wire cage top. As shown in the procedure summary in Figure 2.5A, the first trial of a behavioral testing session was a mineral oil only (no odor) trial that was used to acclimate subjects to the procedures and assess baseline levels of activity. The second through fifth trials were odor habituation trials, where the filter paper was treated with hexaldehyde (HEX; Sigma-Aldrich, St. Louis), and the sixth trial was a test trial in which the odor was switched and the filter paper was treated with heptaldehyde (HEPT; Sigma-Aldrich). Both odorants were diluted in mineral oil to produce equivalent vapor concentrations (HEX diluted to 0.01%; HEPT diluted to ~0.26%). We selected HEX and HEPT as the testing pair for this behavioral assessment because the 2 odorants are aliphatic homologues (differing only in carbon chain length) and potentially difficult to discriminate. We reasoned that using a difficult cross-habituation/dishabituation task could reveal subtle perceptual differences in the discrimination abilities of individual OMP^{-/-} and OMP^{+/+} mice. As shown in Figure 2.5A, all trials were 50 sec in duration and given at 5 min ITIs. The experimenter manually scored investigation time (in sec) in the “odor zone” (a clearly demarcated 15 cm x 12 cm x 10 cm, WxHxL region underlying the stimulus) during all trials. All behavioral sessions were recorded, and a random sample of trials were then scored by a second experimenter to confirm inter-observer reliability.

To assess odor habituation, a non-associative form of learning, investigation during the second through fifth trials (i.e., HEX-presented trials 1-4) was analyzed with an overall

OMP expression ($OMP^{-/-}$; $OMP^{+/+}$) \times trial (HEX₁; HEX₂; HEX₃; HEX₄) mixed ANOVA. Planned *post hoc* ANOVAs and *t* tests were also used to evaluate habituation rates per group and group differences per trial. Detection of an odor stimulus was also assessed by comparing the total investigation time during the first (no odor) and second (HEX₁) trials (see procedure summary in Figure 2.5A). The latency to begin stimulus investigation during these 2 trials was used as an additional measure of initial odor detection abilities. Note that we expected the animals to reduce (or potentially stop) their investigation of the odor stimulus across trials. Consequently, we restricted our analysis on investigation latency to the mineral oil only and HEX₁ trials. Both behavioral parameters, which were 1) the total stimulus investigation time during each 50 sec trial and 2) the latency to begin stimulus investigation, were analyzed with 2-way ANOVAs and planned *post hoc t* tests. Cross-habituation/dishabituation to a different, highly similar test odorant was determined by comparing investigation time during the fourth odor habituation trial to investigation time during the test odor trial (Figure 2.5A; HEX₄ versus HEPT).

Results

The number of odorant-evoked glomerular responses is increased in $OMP^{-/-}$ mice.

To determine if there were differences between $OMP^{-/-}$ and $OMP^{+/+}$ mice in the number of odorant-evoked glomerular responses, the number of responses evoked by a panel of 4 odorants presented at 3 concentrations each was quantified per olfactory bulb in each mouse and then analyzed via a factorial ANOVA, as described above. As shown in Figure 2.1A and 2.1B, the number of glomeruli receiving odorant-evoked nerve output tended to be greater in $OMP^{-/-}$ mice than in $OMP^{+/+}$ mice, and this increase became more

robust as the concentration of the odor stimulus was increased (significant genotype \times concentration interaction, $F_{2,56} = 6.455$, $p = 0.003$, $\eta_p^2 = 0.187$). However, there was no main effect of OMP expression on the overall number of evoked responses (Figure 2.1B, inset; $F_{1,28} = 1.625$, $p = 0.213$). This suggests that OMP may play a role in the rate of glomerular recruitment, a phenomenon that is observed when odor stimuli are presented at increasing concentrations (Stewart et al., 1979; Johnson and Leon, 2000; Bozza et al., 2004).

To test this hypothesis we normalized the number of evoked glomerular responses at each concentration relative to the maximum number of evoked responses across the 3 odorant concentrations that were presented. This normalization was performed within each test odorant per olfactory bulb. The normalized values were then analyzed via a genotype (OMP^{-/-}; OMP^{+/-}) \times odorant (BA; MV; 2HEX; 2M2B) \times concentration (7.5 a.u.; 15 a.u.; 30 a.u.) mixed ANOVA. If OMP is not involved in concentration-dependent glomerular recruitment, then the normalized concentration response curve for OMP^{-/-} mice should be identical to that of OMP^{+/-} mice. However, if OMP does play a role in this phenomenon, then the normalized concentration response functions should differ, and the slope corresponding to the rate of glomerular recruitment in OMP^{-/-} mice should be steeper. Consistent with our hypothesis, this normalization identifies significantly differing rates of recruitment based on OMP expression (Figure 2.1C), including a significant genotype \times concentration interaction ($F_{2,56} = 4.467$, $p = 0.016$, $\eta_p^2 = 0.138$; *post hoc* group comparisons shown in Figure 2.1C). Specifically, the effect of concentration is greater in OMP^{-/-} mice (*post hoc* odorant \times concentration ANOVA, $F_{2,14} = 49.854$, $p < 0.001$, $\eta_p^2 = 0.877$) than in OMP^{+/-} mice (*post hoc* odorant \times concentration ANOVA, $F_{2,42} = 17.395$, $p < 0.001$, $\eta_p^2 =$

0.453), demonstrating that the number of evoked responses in OMP^{+/-} mice saturates more quickly than in OMP^{-/-} mice. These data thus implicate a role for OMP in normal glomerular recruitment.

OSN odorant-selectivity is decreased in OMP^{-/-} mice.

OMP is necessary for the development of mature odorant response specificity in OSNs (Lee et al., 2011). Thus, it is possible that the increased number of glomerular responses evoked by our 4-odorant panel that we observed in OMP^{-/-} mice (Figure 2.1) is caused not by the appearance of “new” glomeruli in OMP^{-/-} mice but by each glomerulus responding to more than one odorant (i.e., a difference in odorant response selectivity). Accordingly, we tested the hypothesis that odorant-responsive glomeruli in OMP^{-/-} mice were more likely to respond to multiple odorants in our panel than those in OMP^{+/-} mice.

To test this we first quantified the number of odorants evoking a response in each individual glomerulus (ranging from 1–4). Next, we collapsed the glomeruli responding to 1 or 2 odorants into a single “higher selectivity” category and the glomeruli responding to 3 or 4 odorants into another “lower selectivity” category. For example, in Figure 2.2A the sets of traces corresponding to glomeruli 4 and 5 are categorized as having higher selectivity, whereas the sets of traces corresponding to glomeruli 1–3 and 6 are characterized as having lower selectivity. Note that collapsing into the two higher/lower categories greatly simplifies analysis and presentation, but a parallel analysis using all four original values produced equivalent results. We then used log-linear regression to analyze glomerular response selectivity across odorant concentrations. Individual glomerular responses were categorized best by a model that included all 3 variables (i.e., genotype, odorant response selectivity, and concentration). Specifically, a larger percentage of the

OMP^{-/-} glomerular population was categorized as having lower response selectivity (see sample traces 1-3 relative to sample traces 4-6 shown in Figure 2.2A) than that of the OMP^{+/-} glomerular population (Figure 2.2B; partial $\chi^2_{df=1} = 36.698$, $p < 0.001$). The difference in the selectivity of glomerular populations was also enhanced at higher odorant concentrations (3-way association, $\chi^2_{df=2} = 7.295$, $p = 0.026$). For example, when the imaging odor panel was presented at a concentration of 30 a.u. (the highest concentration presented), 45% of OMP^{-/-} glomeruli were categorized as having low response selectivity, whereas only 26% of OMP^{+/-} glomeruli were placed in the same category.

Total odorant-evoked nerve output in unaltered in OMP^{-/-} mice.

The magnitude of odorant-evoked OSN synaptic output into each responsive olfactory bulb glomerulus was calculated by subtracting the average of ~2 sec of baseline frames from the average of ~2 sec of frames collected at the peak of the spH signal, normally at or about the odor stimulus offset (see Figure 2.3B). This difference, representing the odorant-evoked change in fluorescence (ΔF , response magnitude), was quantified for each responding glomerulus. The average of all evoked glomerular responses was then separately calculated for the 4 odors (and 3 concentrations) presented to each mouse. The overall average response magnitudes were analyzed via mixed model ANOVA, as described above.

On average, peak odorant-evoked ΔF did not differ between OMP-null and heterozygous mice (Figure 2.3C, inset; $F_{1, 28} = 0.224$, $p = 0.64$, $\eta_p^2 = 0.008$), and this was true across all 3 odorant concentrations that were presented (Figure 2.3B & 2.3C; group \times concentration interaction, $F_{2, 56} = 1.179$, $p = 0.315$, $\eta_p^2 = 0.04$). In addition to our parametric analysis using the averages (representing the overall magnitude of evoked

responses), we assessed the distributions of response magnitudes (Figure 2.3D). Individual ΔF values for glomeruli in $OMP^{-/-}$ mice and $OMP^{+/+}$ mice were ranked evenly (Mann-Whitney U , M-W U , $Z = -0.732$, $p = 0.71$), and the overall distributions of ΔF values in $OMP^{-/-}$ and $OMP^{+/+}$ glomerular populations were indistinguishable (Figure 2.3D; Kolmogorov-Smirnov, K-S, $Z = 0.805$, $p = 0.535$). These data demonstrate that the total synaptic output from OSNs across a 6 sec odorant presentation is not reduced in OMP knockout mice.

Odor maps develop on a longer time scale in $OMP^{-/-}$ mice than in $OMP^{+/+}$ mice.

OSN response kinetics are slowed without OMP expression (Buiakova et al., 1996; Lee et al., 2011). Thus, while the peak amplitudes of the odorant-evoked spH signals do not differ between $OMP^{-/-}$ mice and $OMP^{+/+}$ mice (Figure 2.3), it is possible that there may be a difference in the time course of these responses. To address this, we generated early response maps from a subset of mice in both groups by subtracting the average of 1 sec of frames collected immediately prior to odorant onset from the average of 1 sec of frames beginning 2 sec after odor onset (shown in Figure 2.4C). This allowed us to examine early differences in the evolution of odor maps with higher resolution (i.e., the initial subtraction is generated from 2 sec averages).

As shown in Figure 2.4A-B, the early MV-evoked response map in an $OMP^{-/-}$ mouse (Figure 2.4A) exhibits smaller responses and is less spatially distinct than that seen in an $OMP^{+/+}$ mouse (Figure 2.4B). However, in these same subjects, no difference is observed between MV-evoked response magnitudes during the late (peak) response phase. There is also a larger difference between the early and late MV-evoked responses in the $OMP^{-/-}$ subject (Figure 2.4A) than in the $OMP^{+/+}$ subject (Figure 2.4B). On average, the

odorant-evoked ΔF values were significantly smaller in OMP^{-/-} mice than in OMP^{+/-} mice when measured early in the odorant presentation (Figure 2.4D, inset; $F_{1, 16} = 5.287$, $p = 0.035$, $\eta_p^2 = 0.248$). This difference was most pronounced when odorants were presented at concentrations of 7.5 and 15 a.u. (Figure 2.4D; significant genotype \times concentration interaction, $F_{2, 32} = 3.915$, $p = 0.03$, $\eta_p^2 = 0.197$). Additionally, when we took each individual response into account the ΔF values that were observed in OMP^{-/-} mice were ranked consistently lower than that in OMP^{+/-} mice (Figure 2.4E; M-W U , $Z = -5.882$, $p < 0.001$), and the overall distributions differed as well (Figure 2.4E; K-S, $Z = 2.696$, $p < 0.001$). These results are consistent with previous reports from the epithelium (Buiakova et al., 1996; Ivic et al., 2000; Lee et al., 2011) and suggest that primary sensory representations of odor stimuli develop more slowly in OMP-null mice than in OMP-expressing mice.

OMP^{-/-} mice exhibit attenuated odor habituation and delayed odor investigation.

We hypothesized that if the altered physiological responses to odor stimuli (Figures 2.1, 2.2, and 2.4) are meaningful to the mouse, then we should see a difference in behavioral responses to olfactory stimuli. To test this, we used a non-associative cross-habituation/dishabituation odor investigation paradigm (Figure 2.5A) in which investigation time was observed during a 50 sec presentation of a mineral oil vehicle followed by 4 successive presentations of HEX and then 1 presentation of HEPT at 5 min ITIs.

Both groups of mice investigated the mineral oil vehicle stimulus for comparable durations (Figure 2.5B; $t_{28} = 0.216$, $p = 0.831$) and also exhibited comparable investigation latencies (Figure 2.5C, compare open bars; $t_{23} = 0.556$, $p = 0.584$), suggesting that there

were no inherent differences in locomotion or propensity to investigate novel stimuli. As shown in Figure 2.5B, there was also no change in average investigation time on the first odorant presentation compared to the mineral oil only trial (main effect of trial: $F_{1, 28} = 0.002$, $p = 0.962$, $\eta_p^2 = 0.00$), and no significant 2-way interaction of trial type and genotype ($F_{1, 28} = 0.197$, $p = 0.661$, $\eta_p^2 = 0.007$), demonstrating that OMP expression did not prevent the initial detection of a novel odorant. However, when we compared the latency to initiate stimulus investigation during these 2 trial types between groups we found an OMP expression ($OMP^{-/-}$; $OMP^{+/+}$) \times trial type (mineral oil only; HEX₁) interaction (Figure 2.5C; $F_{1, 23} = 6.247$, $p = 0.020$, $\eta_p^2 = 0.214$). $OMP^{+/+}$ subjects exhibited a significant decrease in their latency to investigate the first presentation of HEX compared with their latency to investigate the mineral oil vehicle stimulus (within-subjects comparison, $t_{13} = 2.484$, $p = 0.027$), whereas $OMP^{-/-}$ subjects exhibited no difference in their latency to investigate the mineral oil and HEX stimuli (within-subjects comparison, $t_{10} = 1.189$, $p = 0.262$). Moreover, the $OMP^{-/-}$ group tended to take longer to begin investigating HEX during its first presentation than the $OMP^{+/+}$ subjects ($t_{23} = 2.065$, $p = 0.050$). Thus, while $OMP^{-/-}$ mice perceived the odor stimulus during its first presentation (Figure 2.5B), their behavioral responses were slightly delayed (Figure 2.5C).

To evaluate differences in habituation to HEX over successive presentations, total investigation time (sec) was analyzed via a 2-way mixed ANOVA, as described above. This analysis yielded a significant genotype \times trial interaction (Figure 2.5B; $F_{3, 84} = 5.702$, $p = 0.001$, $\eta_p^2 = 0.169$). Specifically, $OMP^{+/+}$ mice exhibited a significant reduction in the amount of time spent investigating HEX across 4 consecutive presentations (*post hoc* ANOVA, main effect of trial, $F_{3, 54} = 36.267$, $p < 0.001$, $\eta_p^2 = 0.668$), whereas $OMP^{-/-}$ mice

did not exhibit a significant reduction in their investigation times (*post hoc* ANOVA, main effect of trial, $F_{3,30} = 0.87$, $p = 0.468$, $\eta_p^2 = 0.08$), suggesting that only OMP^{+/+} mice fully habituated to the odor stimulus. We switched the odor stimulus to HEPT after the fourth habituation trial and observed a very modest and non-significant increase in the investigation time of the OMP^{+/+} group (Figure 2.5B; $t_{18} = 1.846$, $p = 0.081$), suggesting that, on average, cross-habituation occurred in these mice. Similarly, there was no change in average investigation time in the OMP^{-/-} group (Figure 2.5B; $t_{10} = 0.183$, $p = 0.859$). However, unlike the OMP^{+/+} group, it is unclear if this is indicative of cross-habituation because OMP^{-/-} mice did not exhibit complete behavioral habituation to HEX (Figure 2.5B).

Discussion

In the present work we expanded on previous reports showing changes in OSN response dynamics, magnitudes, and odorant selectivity in OMP knockout mice (Buiakova et al., 1996; Lee et al., 2011). In our OMP-spH model that visualizes total odorant-evoked neurotransmitter release from OSNs *in vivo*, we found that odorant presentation evoked synaptic input to more olfactory bulb glomeruli in OMP^{-/-} mice than in OMP^{+/+} mice (Figure 2.1), and that this was at least partially due to a decrease in odorant selectivity across glomerular populations (Figure 2.2). Surprisingly, the total neurotransmitter release evoked by a 6 sec odorant presentation was found to be comparable between OMP heterozygous and knockout mice (Figure 2.3), though the responses in OMP^{-/-} were significantly smaller early in the odorant presentation (Figure 2.4). OMP^{-/-} mice were found to behave very differently than wild-type mice in an olfactory habituation task

(Figure 2.5), where OMP^{-/-} mice exhibited a delayed onset in their initial investigation of a novel odor (although the total duration of this investigation was comparable between groups) and much less evidence of habituation across odorant presentations.

The decreased odorant selectivity of OSNs in OMP knockout mice is consistent with a previous report showing similar effects during patch-clamp experiments in single OSNs that express the MOR23 receptor (Lee et al., 2011). The present findings demonstrate that OMP knockouts also exhibit reduced OSN odorant selectivity during natural odorant presentations *in vivo* and across OSN populations. It remains unclear whether this selectivity is conveyed by a direct action of OMP on the olfactory receptor or by some thresholding function that gates out nonspecific responses to suboptimal odorants prior to signal amplification in the OSN cilium.

Interestingly, OSNs in OMP knockout mice exhibited less total odorant-evoked neurotransmitter release (smaller spH signals) than those from heterozygous mice when assessed within the first two seconds of an odorant presentation (Figure 2.4) but “caught up” later in the odorant presentation such that the total neurotransmitter release was comparable towards the end of the trial (Figure 2.3). The delayed initial response is consistent with many reports from recordings of both single OSNs and populations of OSNs in the epithelium (Buiakova et al., 1996; Youngentob et al., 2003; Lee et al., 2011). These reports indicated that the offset of the odorant-evoked response was delayed as well in OMP-null OSNs, potentially explaining how these OSNs could release more neurotransmitter than controls in the later part of the odorant presentation. Here we demonstrate that the primary odorant representations evoked in OMP^{-/-} mice indeed take longer to fully develop, but eventually become comparable in magnitude to those of mice

that do express OMP. This delayed response may explain why OMP knockout mice can perform comparably to controls on olfactory guided tasks that provide plenty of time for odor sampling (Figure 2.5, first HEX trial; see also (Youngentob and Margolis, 1999; Youngentob et al., 2001)), though they may exhibit different patterns of errors (Youngentob et al., 2001). It also explains why our earlier reports using the OMP-spH mouse line failed to observe differences in peak response magnitudes between homozygous and heterozygous mice (Bozza et al., 2004).

Though it is difficult to causally link the changes in OSN neurophysiology to the differences in odorant-guided behavior, the delayed onset of initial odor investigation and the reduced behavioral habituation in OMP-null mice may reflect the underlying difference in the timing of OSN synaptic output, whereby the delayed synaptic output from OSNs results in a corresponding delay in investigative behavior and somehow impedes the normal process of habituation. We did not observe any differences between OMP-null and OMP-expressing mice in their ability to discriminate between two highly similar odorants; neither group showed dis-habituation from HEX to HEPT. However, it is difficult to interpret the behavior of OMP-null mice as being indicative of cross-habituation between the two odorants because these subjects showed little evidence of habituation to the first odorant.

Because the spH data provide an aggregate signal of neurotransmitter release from the population of OSNs innervating each glomerulus, we cannot in principle distinguish between increased exocytosis at each synapse and an increased total number of synapses in the population. In the present study, we found that total odorant-evoked neurotransmitter release was no different between OMP-null and OMP-heterozygous mice, despite a

previous report that glomeruli in OMP-null mice include significantly more axodendritic synapses (which may arise from OSNs) than wild-type mice (Griff et al., 2000). However, we cannot rule out the possibility that the OSNs in our OMP-null mice made more synapses than the OMP-expressing mice but compensated for this increase by somehow reducing their odorant-evoked neurotransmitter release per synapse. Similarly, we cannot entirely exclude the possibility that the slower response kinetics between our OMP-null and OMP-heterozygous mice somehow reflected an increased expression of spH in the OMP-null mice, which were homozygous for spH. However, previous experiments in olfactory bulb slices from homozygous spH mice showed an excellent correspondence between electrically-evoked presynaptic spH signals and postsynaptic currents in wild-type mice (Wachowiak et al., 2005). Highly synchronous, electrically-evoked neurotransmitter release can evoke a transient change in synaptic pH that partially masks the rise of the spH signal (McGann et al., 2005), but this transient occurs on the scale of milliseconds (not seconds) and has not been observed with odorant presentations *in vivo*. An actual change in OSN response kinetics thus seems the most parsimonious explanation of the present results.

Because of its high levels of selective expression, the OMP promoter is frequently used for gene-targeted expression of scientifically useful constructs, including fluorescent markers (Potter et al., 2001), physiological indicators like synaptopHluorin (Bozza et al., 2004), and optogenetic stimulation tools like channelrhodopsin (Dhawale et al., 2010). However, this application in gene-targeted models potentially disrupts the normal function of OMP in olfactory physiology. The present results indicate the need for caution in

interpreting data from mice with altered OMP expression, particularly with regard to odorant selectivity and habituation assays.

Acknowledgements

I thank Andrew Moberly for his contributions to the cross-habituation/dishabituation behavioral experiment and the surgical procedures prior to imaging.

Chapter 2 Figures

Figure 2.1

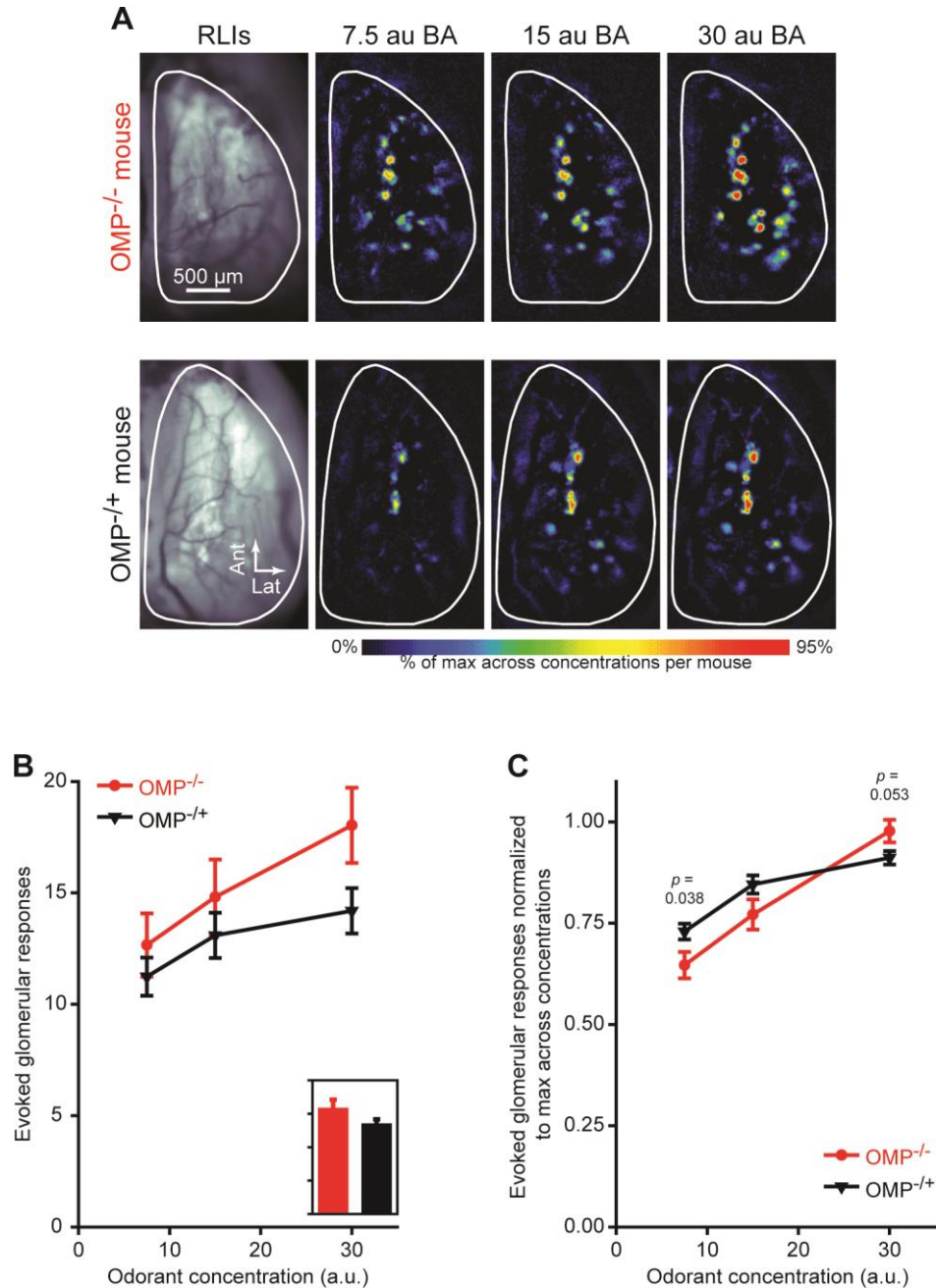


Figure 2.1. The number of glomeruli receiving odorant-evoked OSN input is enhanced in OMP^{-/-} mice. (A) Resting light images (RLIs) of the dorsal surface of the olfactory bulb through the cranial window (first column) and pseudocolored response maps

evoked by 3 concentrations of butyl acetate (BA; second-fourth columns). The top row is an example from an $OMP^{-/-}$ mouse and the bottom row is an example from an $OMP^{-/+}$ mouse. **(B)** Mean \pm SEM number of odorant-evoked glomerular responses plotted as a function of odorant concentration. The overall group means (pooled across all odorants and concentrations) are shown in the inset, which is scaled to the main y-axis of **B**. **(C)** Mean \pm SEM number of glomerular responses normalized to the maximum number of evoked responses across 3 odorant concentrations. In **B** and **C** $OMP^{-/-}$ mice and $OMP^{-/+}$ mice are shown in red and black, respectively.

Figure 2.2

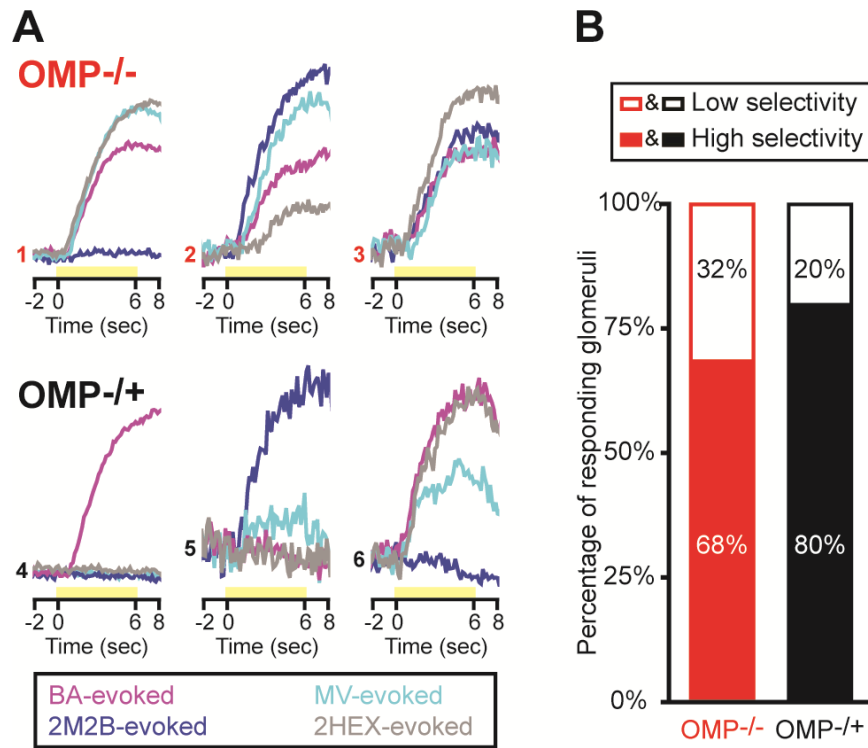


Figure 2.2. Odorant response selectivity is reduced in glomeruli from OMP^{-/-} mice. (A) Example odorant response selectivity patterns in 6 individual glomeruli; 3 OMP^{-/-} glomeruli (top row, traces #1-3) and 3 OMP^{+/-} glomeruli (bottom row, traces #4-6). Each set of 4 traces corresponds to a single glomerulus' responsivity to 4 test odorants that were all presented at a concentration of 30 a.u.: BA, magenta; MV, cyan; 2M2B, blue; and 2HEX, grey. Each set of traces is scaled relative to the maximum evoked response across all 4 odorants per glomerulus. Yellow bars indicate the time when odorant stimuli were presented. (B) Percentage of OMP^{-/-} (red) and OMP^{+/-} (black) glomerular populations that were categorized as having higher (closed bars) or lower (open bars) odorant response selectivity.

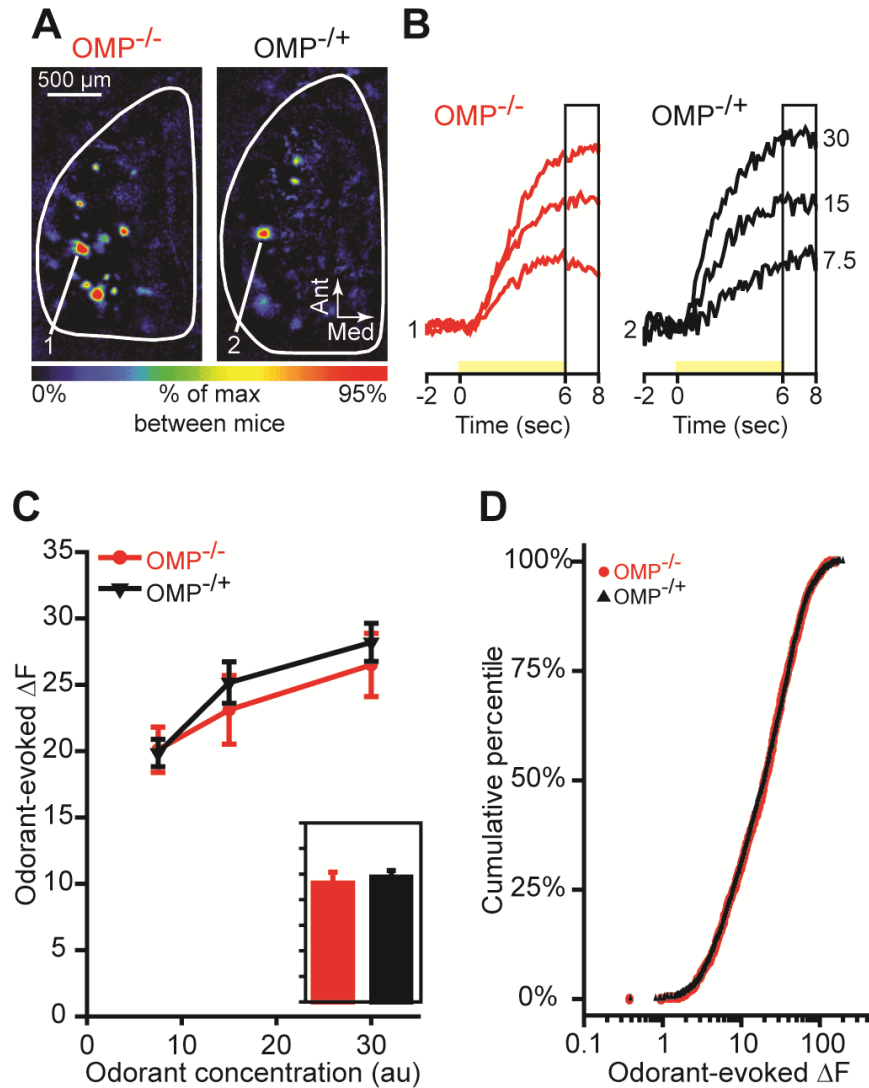
Figure 2.3

Figure 2.3. The magnitude of peak spH responses is unaltered in $OMP^{-/-}$ mice. (A) Pseudocolored difference maps from an $OMP^{-/-}$ mouse (left) and an $OMP^{+/+}$ mouse (right). These maps were evoked by presentation of 2HEX at a concentration of 30 au. (B) Sets of traces from an $OMP^{-/-}$ mouse (left) and an $OMP^{+/+}$ mouse (right) corresponding to the numbered callouts in A. Traces were evoked by 3 concentrations of 2HEX (labeled on the right in a.u.) and are all scaled relative to the maximum response across concentrations and between the 2 glomeruli. Yellow bars indicate time of 2HEX presentation. Boxed regions of the traces indicate the frames that were used to generate the peak response maps shown in A, and also to perform the analyses summarized in Figures 7-9. (C) Mean \pm SEM

odorant-evoked change in fluorescence (ΔF) plotted as a function of odorant concentration. The overall group means shown in the inset, which is scaled to the main y-axis of **C**, are averaged across all odors and concentrations. **(D)** Cumulative probability plot showing the distributions of odorant-evoked ΔF values for populations of glomerular responses in OMP^{-/-} mice and OMP^{+/+} mice. ΔF distributions for each group are pooled across 3 concentrations of 4 test odorants. In **B-D** OMP^{-/-} mice and OMP^{+/+} mice are shown in red and black, respectively.

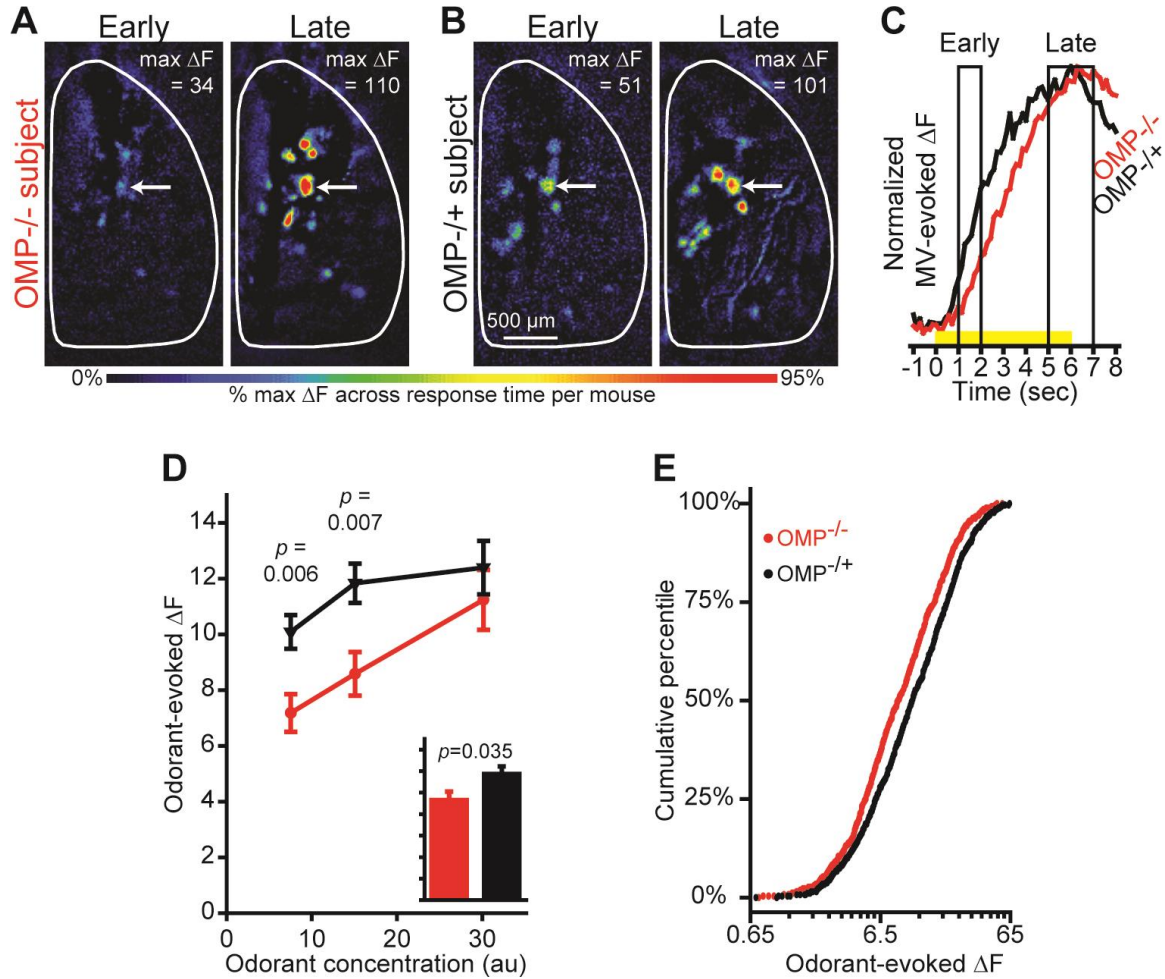
Figure 2.4

Figure 2.4. The evolution of odorant-evoked maps is slowed in *OMP*^{-/-} mice. (A-B) 7.5 a.u. MV-evoked difference maps from an *OMP*^{-/-} mouse (A) and an *OMP*^{+/-} mouse (B) showing early (left) and late (right) response phases. (C) Response amplitudes corresponding to the example *OMP*^{-/-} glomerulus and the example *OMP*^{+/-} glomerulus indicated in A and B, respectively. Boxed regions of the traces indicate the frames used to generate the early- and late-phase response maps shown in A-B. Yellow stimulus bar notes the time of odorant presentations. (D) Mean \pm SEM odorant-evoked change in fluorescence (ΔF) during the early response phase (see subtraction shown in C) plotted as a function of odorant concentration. The overall group means shown in the inset, which is scaled to the main y-axis of D, are averaged across all odors and concentrations. (E) Cumulative probability plot showing the distributions of early odorant-evoked ΔF values

for populations of glomerular responses in $OMP^{-/-}$ mice and $OMP^{-/+}$ mice. ΔF distributions for each group are pooled across 3 concentrations of 4 test odorants. In **C-E** $OMP^{-/-}$ mice and $OMP^{+/+}$ mice are shown in red and black, respectively.

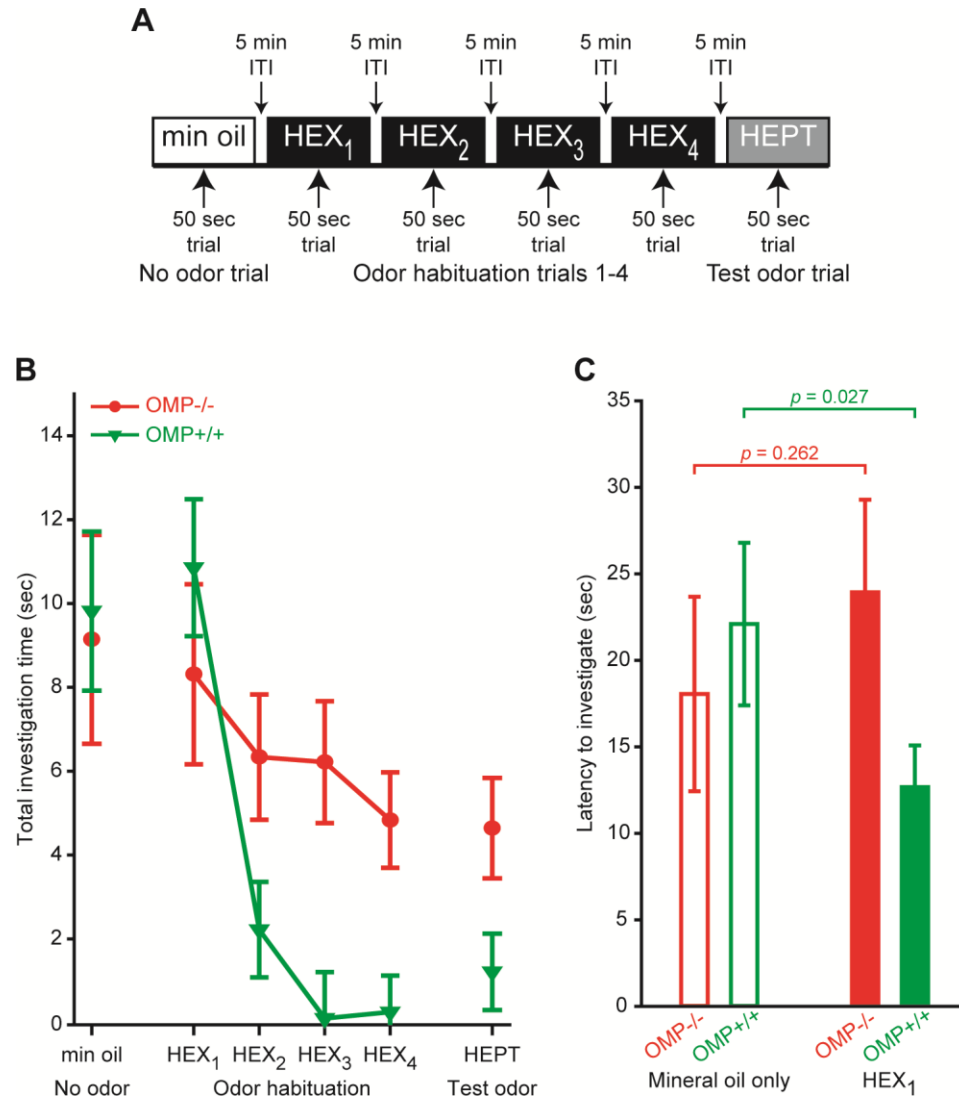
Figure 2.5

Figure 2.5. Non-associative odor-induced behaviors are altered in OMP^{-/-} mice. (A) Procedure summary of the cross-habituation/dishabituation behavioral testing protocol. (B) Mean \pm SEM duration of stimulus investigation (sec) plotted as a function of trial type. (C) Mean \pm SEM latency (sec) to begin investigating the mineral oil (no odor) stimulus (open bars) and the HEX stimulus (solid bars) during the first and second trials, respectively, of the paradigm shown in A. In B and C OMP^{-/-} mice and OMP^{+/+} mice are shown in red and green, respectively.

CHAPTER 3

Odor-specific, olfactory marker protein-mediated sparsening of primary olfactory input to the brain after odor exposure

The results from this chapter are reported in Kass MD, Moberly AH, Rosenthal MC, Guang SA, McGann JP (2013d) Odor-specific, olfactory marker protein mediated sparsening of primary olfactory input to the brain after odor exposure. *J Neurosci* 33:6594-602.

Abstract

Long-term plasticity in sensory systems is usually conceptualized as changing the brain's interpretation of sensory information, not an alteration of how the sensor itself responds to external stimuli. However, here we demonstrate that in the adult mouse olfactory system a week-long exposure to an artificially odorized environment narrows the range of odorants that can induce neurotransmitter release from olfactory sensory neurons (OSNs) and reduces the total transmitter release from responsive neurons. In animals heterozygous for the olfactory marker protein (OMP), this adaptive plasticity was strongest in the populations of OSNs that originally responded to the exposure odorant (an ester) and also observed in the responses to a similar odorant (another ester), but had no effect on the responses to odorants dissimilar to the exposure odorant (a ketone and an aldehyde). By contrast, in OMP-knockout mice odorant exposure reduced the number and amplitude of OSN responses evoked by all four types of odorants equally. The effect of this plasticity is to preferentially sparsen the primary neural representations of common olfactory stimuli, which has the computational benefit of increasing the number of distinct sensory patterns that could be represented in the circuit and might thus underlie the improvements in olfactory discrimination often observed after odorant exposure (Mandairon et al. 2006). The absence of odorant specificity in this adaptive plasticity in OMP-knockout mice suggests a potential role for this protein in adaptively reshaping OSN responses to function in different environments.

Introduction

Adaptive plasticity can permit dynamic optimization of sensory systems for different statistical distributions of sensory stimuli in a changing environment (Kaas, 1991; Dahmen and King, 2007; Schwarzkopf et al., 2009; Pienkowski and Eggermont, 2011). In sensory areas of the mammalian cerebral cortex, the sensory environment during development has long been understood to determine the circuit architecture (Hubel and Wiesel, 1970; Katz and Shatz, 1996; Cohen-Cory, 2002), and it is increasingly clear that experience-dependent neuroplasticity can continue throughout adulthood (Weinberger, 2004; Karmarkar and Dan, 2006; Goel and Lee, 2007; de Villers-Sidani et al., 2008; Li et al., 2008; Gilbert et al., 2009; Wilbrecht et al., 2010; Mendez and Bacci, 2011). In contrast to these higher brain regions, primary sensory neurons (e.g., photoreceptors in the retina, inner hair cells in the cochlea, etc.) are generally presumed to be plastic only early in life (Tian and Copenhagen, 2001; Tyler et al., 2007) and then to provide stable sensory inputs to the brain thereafter. However, this presumption has proved difficult to test because of the difficulty in performing longitudinal experiments in primary sensory neurons in most sensory modalities, particularly *in vivo*.

Olfactory sensory neurons (OSNs), the primary sensory neurons in the olfactory system, bind odorants in the nasal cavity and project their axons through the olfactory nerve to the brain's olfactory bulbs. Each OSN in the nasal epithelium expresses one out of a repertoire of about 1000 olfactory receptors in the mouse, and as the axons reach the bulb they segregate by receptor type such that all of the OSNs expressing a given receptor project to one or two specific glomeruli (spherical structures where OSN axons converge and synapse onto postsynaptic neurons) on the surface of the olfactory bulb (Mombaerts,

2006). An odorant binding to a subset of odorant receptor types in the epithelium stimulates those OSNs to fire action potentials and thus evokes neurotransmitter release from OSN synaptic terminals into a corresponding subset of olfactory bulb glomeruli. Patterns of odorant-evoked synaptic output from OSNs can be visualized optically *in vivo* in olfactory marker protein-synaptopHluorin (OMP-spH) mice. These patterns have been shown to be odorant-specific, stable across time (Bozza et al., 2004), and similar across mice (Soucy et al., 2009), thus providing a model system in which experience-dependent plasticity in the primary sensory input to the central nervous system can be observed in the same individual over time.

Here, we used optical imaging techniques in OMP-spH mice to visualize patterns of primary sensory input to the brain's olfactory bulb and how those patterns are changed when adult mice live in an artificially odorized environment for a week. Because the odorant-selectivity of mature OSNs is determined in part by OMP expression (Lee et al., 2011; Kass et al., 2013a), we then compared the effects of odorant exposure between OMP-heterozygous (OMP^{+/-}) and OMP-knockout (OMP^{-/-}) mice.

Methods

Subjects.

Adult (4–9 months) male and female OMP-spH mice that were either OMP-heterozygous or OMP-null were used as subjects in the imaging experiments. OMP is highly and selectively expressed in mature OSNs. Because OMP has been implicated in olfactory transduction (although its specific function remains elusive) we hypothesized that it may play a role in adaptively shaping OSN physiology in response to environmental

stimuli. Thus, the rationale for including OMP^{+/-} mice and OMP^{-/-} mice in the present study was to determine if OMP plays a role in activity-dependent plasticity in primary olfactory representations.

The results shown in Figures 3.2, 3.3, and 3.6D came from a total of 36 olfactory bulbs in 18 OMP^{+/-}-spH mice, and the results shown in Figures 3.4, 3.5, and 3.6E came from a total of 48 olfactory bulbs in 24 OMP^{-/-}-spH mice. The number of OMP^{+/-} subjects assigned to each exposure group is indicated in the procedure summary shown in Figure 3.2A, and the exposure group assignment for OMP^{-/-} subjects is indicated in Figure 3.4A.

Chronic odorant exposure.

A perennial challenge in olfactory research is the difference in air exchange between a typical open shoebox home cage and any kind of odorant exposure system, which must be enclosed to contain the odorant. In the present study, we used both a home cage control (HCC) group and what we call a “self-exposure” (SE) control group, which lived in the same exposure chamber as the “ester exposure” (EE) group and breathed air that was sham-odorized on the same schedule with mineral oil vehicle. We refer to this group as “self-exposure” because over the course of a week the chamber inevitably became substantially odorized with the odor of the mouse itself and its waste products, regardless of the sham-odor (i.e., mineral oil only) cycle (Figure 3.1B). This experience by itself induced a form of olfactory plasticity (see Results below), and thus provides a useful comparison for both the home cage and ester exposure groups.

Imaging experiments were performed both before and after each mouse spent 7 days in 1 of 3 randomly-assigned exposure environments (as shown in Figures 3.2A and 3.4A). In 2 of the environments, EE and SE, mice were housed in a plexiglass exposure

chamber (10cm x 20cm x 15cm, WxHxL) containing bedding, rodent chow, and a water bottle. The third environment was the mouse's wire-topped shoebox style home cage, which served as a standard laboratory environment control group (home cage control, HCC). To minimize perturbations in the airflow throughout the odorant exposure system, as well as disturbances to the actual odorant exposure (see below), the chambers were only opened for animal entry and exit. Thus, even before explicitly adding a monomolecular odorant to an exposure chamber there were differences between housing in a standard mouse cage and housing in an exposure chamber, including differences in the air exchange, the size of the housing environment, the size-appropriate amount of bedding filling each environment (a larger cage necessitates a larger quantity of bedding), the bedding changing schedule, etc. Such differences may produce distinct olfactory environments (Oliva et al., 2008), necessitating the use of a sham control group (the SE group) and a standard laboratory housing control group (the HCC group). All subjects were single-housed during the 1 week exposure period.

In the EE and SE environments, room air was constantly pulled through the chambers by a vacuum (13 L/min). With a continuous 4 hour duty cycle (Figure 3.1A), a solenoid valve shunted the airflow source between clean room air and the headspace of a bottle containing an ester odorant (BA or MV) diluted in mineral oil, or mineral oil alone for the SE group. In the EE group, the ester odorant that was added to the chamber was evenly counterbalanced across mice. Specifically, 10 of the subjects in the EE group ($OMP^{+/+}$, $N = 4$; $OMP^{-/-}$, $N = 6$) spent the week individually housed in chambers that were odorized with BA during the 4 hour ON cycles, while the other 10 ester-exposed subjects ($OMP^{+/+}$, $N = 4$; $OMP^{-/-}$, $N = 6$) spent the week individually housed in chambers odorized

with MV during ON cycles. This design permitted a comparison of the effects of ester exposure on primary sensory representations evoked by the exposed ester, the unexposed ester, and two other classes of odorants (a ketone, 2HEX, and an aldehyde, 2M2B). A photoionization detector was used to standardize the ester odorant concentrations inside the chambers daily (as well as between the 2 counterbalanced esters). Additionally, ester odorant concentrations were measured to confirm that during the ON cycles the esters were delivered at a relatively constant concentration and were then successfully cleared from the chambers during the OFF cycles, as shown in Figure 3.1A. Peak ester odorant concentrations in the exposure chambers during ON cycles varied somewhat across days, ranging from ~30 a.u. (immediately after the odorant vial was replaced) to ~15 a.u. (at which point the odorant vial was replaced). Because the mouse's own endogenously produced odorants gradually permeate the chamber (Figure 3.1B), ester odorant concentrations (and solution preparations) were calibrated based on measurements taken from vacant EE chambers arranged in parallel with occupied chambers.

Mice had a ~24 hour recovery period between baseline imaging (imaging session I in Figures 3.2A and 3.4A) and the onset of the week-long exposure period. To reduce short-term adaptation effects prior to undergoing the post-exposure imaging session (shown as imaging session II in Figures 3.2A and 3.4A), all mice were removed from the exposure chamber (or home cage) during non-odor periods and individually transferred to temporary holding cages in the imaging facility a minimum of ~1 hour prior to experimentation.

Acquisition and analysis of imaging data sets.

Chronic cranial windows were implanted bilaterally and *in vivo* optical imaging was performed as described above under General Methods. Four odorants (including, BA, MV, 2HEX, and 2M2B) were presented at a concentration of 15 a.u. to deeply, anesthetized mice both before and after the week-long exposure period (Figures 3.2A & 3.4A).

Imaging data were analyzed as described above under General Methods. The raw dataset for the experiments in Figures 3.2, 3.3, and 3.6D (data collected from OMP^{-/+} subjects) included 293 responsive glomeruli at baseline and 276 after exposure (from 10 bulbs in 5 mice) for the HCC group, 217 responsive glomeruli at baseline and 270 post-exposure (from 10 bulbs in 5 mice) for the SE group, and 459 responsive glomeruli at baseline and 345 post-exposure (from 16 bulbs in 8 mice) for the EE group. The raw dataset for the experiments in Figures 3.4, 3.5, and 3.6E (data collected from OMP^{-/-} subjects) included 473 responsive glomeruli at baseline and 485 responsive glomeruli post-exposure (from 14 bulbs in 7 mice) for the HCC group, 356 responsive glomeruli at baseline and 260 post-exposure (from 10 bulbs in 5 mice) for the SE group, and 849 responsive glomeruli at baseline and 475 post-exposure (from 24 bulbs in 12 mice) for the EE group

To determine if there were exposure-dependent changes in the overall average number of responses contributing to each odor representation, we quantified the number of glomerular responses evoked by each of 4 imaging test odorants per olfactory bulb during both imaging sessions. These data were analyzed via 3-way ANOVAs that were calculated separately for each group of subjects, as well as with planned *post hoc* ANOVAs and *t* tests to make pairwise comparisons and assess interactions of main interest. The omnibus

ANOVAs that were calculated for HCC and SE groups each included 3 within-subjects variables: imaging session (pre-exposure; post-exposure), imaging test odorant (BA; MV; 2HEX; 2M2B), and side (left olfactory bulb; right olfactory bulb). A similar ANOVA was calculated to analyze the differential effects of the exposure odorant in the EE group, except that imaging test odorants were classified as exposed (for the odorant that was added to the exposure chamber) or unexposed. There was no main effect of side in any of these 3-way factorials, demonstrating that for each mouse the average number of odorant-evoked responses in the left and right olfactory bulbs was approximately symmetric. Because bulbar maps were symmetrical, the results reported here (unless otherwise noted) consist of the main effects and interaction effects of imaging session and imaging test odorant which average across bulbs. Additionally, to evaluate potential changes in individual odorant-evoked glomerular response maps, we analyzed the distributions of the number of glomerular responses per odor map. Note that all 4 odorants were unexposed in the HCC and SE groups. Accordingly, distributions of the number of odorant-evoked glomerular responses were pooled across odorants for the HCC and SE groups. All response distributions were analyzed with non-parametric Mann-Whitney (M-W) and Kolmogorov-Smirnov (K-S) tests.

The total number of observed responses in an olfactory bulb does not equate to the total number of responsive glomeruli in that bulb because some glomeruli responded to 2 or more odors in the panel. To evaluate how the mouse's odor environment affected glomerular responsivity, we thus also quantified the total number of individual glomeruli that responded to any number of odorants during pre- and post-exposure imaging preparations and analyzed these frequency data via Pearson's χ^2 tests.

To investigate any changes in the magnitude of odorant-evoked OSN synaptic output we analyzed both the central tendencies and full distributions of response amplitudes (odorant-evoked change in fluorescence, ΔF). Odorant-evoked ΔF values were normalized to permit averaging across mice. This normalization was performed within each test odorant and used to generate an average (test odor-specific) ΔF value per olfactory bulb per mouse; that is, all ΔF values evoked by a given odorant (during both imaging sessions) were normalized relative to the maximum ΔF value evoked by that odorant across both olfactory bulbs during baseline imaging. The normalized ΔF values (representing an olfactory bulb's average ΔF in response to each test odorant) were then analyzed via ANOVAs and *t* tests, like the analyses described above for the number of odorant-evoked responses. The distributions of individual odorant-evoked response amplitudes were pooled across glomeruli and odorants for the HCC and SE groups and are displayed as cumulative frequency histograms. For the EE groups, distributions of odorant-evoked ΔF values were pooled across glomeruli per odor category (i.e., exposed ester, unexposed ester, or unexposed ketone and aldehyde). These data were analyzed with M-W and K-S tests to investigate potential changes in the full distributions of response magnitudes.

We also assessed odorant selectivity in populations of responding glomeruli. Contingency tables were first generated by characterizing individual responding glomeruli according to 3 parameters: exposure group, imaging session, and the number of test odorants that evoked a measurable response (ranging from 1-4) using the standard error-based criterion described above. This 3-way contingency table was analyzed using backwards elimination loglinear regression. Based on this preliminary analysis (which yielded the same results as those reported below) we then collapsed the selectivity category

down from 4 levels (i.e., responded to 1, 2, 3, or 4 of the test odorants) into 2 levels to simplify the summary of results, as in (Kass et al., 2013a). Thus, each individual responsive glomerulus was categorized as having either “higher” selectivity (if it responded to 1–2 odorants, as in the pre-exposure traces shown for glomeruli 1, 3, and 5 in Figures 3.6A-C) or “lower” selectivity (if it responded to 3–4 odorants, as in the pre-exposure traces shown for glomeruli 2, 4, and 6 in Figures 3.6A-C). The categorical frequency data were analyzed via loglinear regression to evaluate the 3-way association (as in our preliminary analysis), and followed with *post hoc* χ^2 tests.

Results

Experience-dependent changes in the number and size of OSN inputs to olfactory bulb glomeruli in heterozygous OMP^{+/-}-spH mice.

To longitudinally evaluate experience-dependent plasticity, the neurotransmitter release from OSNs into olfactory bulb glomeruli evoked by a panel of 4 odorants (composed of 2 esters, a ketone, and an aldehyde) was visualized in 2 optical imaging sessions 1 week apart in each of 18 heterozygous OMP^{+/-}-spH mice that were randomly assigned to 1 of 3 exposure groups (Figure 3.2A). Mice were anesthetized throughout both imaging preparations. Figure 3.2B shows resting fluorescence images of the dorsal olfactory bulb through the cranial window and pseudocolored difference maps showing the pattern of OSN synaptic input to olfactory bulb glomeruli evoked by the odorant 2M2B before and after 1 week in the HCC and SE exposure conditions.

For the HCC group, both the average number of glomeruli receiving measurable synaptic input during an odorant presentation (Figure 3.2E, inset; $F_{(1,4)} = 0.001$, $p = 0.976$)

and the mean normalized amplitude of those responses (Figure 3.2H, inset; $F_{(1, 4)} = 1.817$, $p = 0.249$) were comparable before and after the exposure period across the 4 imaging test odorants and both olfactory bulbs (glomerular responses, non-significant 3-way interaction, $F_{(3, 12)} = 1.137$, $p = 0.374$, $\eta_p^2 = 0.221$: normalized response magnitudes, non-significant 3-way interaction, $F_{(3, 12)} = 1.683$, $p = 0.223$, $\eta_p^2 = 0.296$). Because there were no test odorant-specific changes in OSN activity or bulbar symmetry, we pooled across imaging test odorants and olfactory bulbs (and thus also across mice). We then evaluated the entire population of glomerular responses (Figure 3.2E) and ΔF values (Figure 3.2H) during pre- and post-HCC exposure, and observed no changes in these distributions. Additionally, the total number of glomeruli that responded to any odorant pooled across olfactory bulbs and mice was the same during both imaging sessions (Figure 3.2G, black bar; $\chi^2_{(1)} = 0.508$, $p = 0.576$). Together, the results in HCC heterozygous OMP-spH mice demonstrate the stability of these measurements across 1 week in normal laboratory conditions (see examples in Figures 3.2B (left) and 13C).

Self exposure and ester exposure altered the pattern of odorant-evoked glomerular input, but in opposite directions. As depicted by the pre- (top) and post-exposure (bottom) pseudocolored difference maps in Figure 3.2B (right), mice in the SE group (which were not explicitly exposed to any of the odorants in the panel but were exposed to rising concentrations of their own endogenously-produced odors; see Figure 3.1B) exhibited an increase in the average number of glomeruli receiving measurable odorant-evoked OSN synaptic input during an odorant presentation compared to their own pre-exposure baseline (Figure 3.2F, inset). On average, this increase was equal across the 4 odorants tested and both sides of individual mice (non-significant imaging session \times test odorant \times side

interaction; $F_{(3, 12)} = 1.852$, $p = 0.192$). Accordingly, we pooled across test odorants and olfactory bulbs in subsequent analyses considering the entire distribution of glomerular responses. As shown in Figure 3.2F, the number of glomerular responses that represented a given odorant after 1 week of SE tended to be ranked higher than at baseline (M-W, $Z = -3.673$, $p < 0.001$) and the distribution of these augmented odor representations also differed from baseline (K-S, $Z = 1.789$, $p = 0.003$). Moreover, the total number of glomeruli that responded to any odorant pooled across mice increased after self exposure compared to the pre-exposure baseline (Figure 3.2G, blue bar; $\chi^2_{(1)} = 6.0$, $p = 0.014$).

In contrast to the SE group of OMP^{-/+} subjects, OMP^{-/+} mice in the EE group exhibited an ester-selective decrease in the number of glomeruli receiving odorant-evoked OSN input (Figures 3.3A & 3.3B; imaging session \times test odorant interaction, $F_{(3, 21)} = 14.753$, $p < 0.001$, $\eta_p^2 = 0.678$), as well as a reduction in the total number of odorant-responsive glomeruli pooled across mice ($N_{\text{PRE}} = 459$, $N_{\text{POST}} = 345$; $\chi^2_{(1)} = 16.164$, $p < 0.001$). While the number of glomerular responses evoked by both the exposed and unexposed esters decreased after 1 week of EE, the reduction in responses evoked by the exposed ester (Figure 3.3B, first pair of bars; $F_{(1, 7)} = 45.0$, $p < 0.001$, $\eta_p^2 = 0.865$) was greater than the reduction in unexposed ester-evoked responses (Figure 3.3B, second pair of bars; $F_{(1, 7)} = 9.590$, $p = 0.017$, $\eta_p^2 = 0.578$). Unlike the increase in responses to all 4 odors that occurred in the SE group, the EE group exhibited no change in the average number of (unexposed) 2HEX-evoked responses ($F_{(1, 7)} = 0.101$, $p = 0.760$, $\eta_p^2 = 0.014$) or in the average number of (unexposed) 2M2B-evoked responses ($F_{(15)} = 0.063$, $p = 0.$, $\eta_p^2 = 0.009$), as shown in Figure 3.3B (third and fourth pairs of bars).

The magnitude of the spH signals evoked in olfactory bulb glomeruli was also differentially affected by self exposure (Figures 3.2D & 3.2I) and ester exposure (Figures 3.3C-G). Self exposure significantly increased the size of these signals (Figure 3.2I, cum plot; M-W $Z = -2.061$, $p = 0.039$; Figure 3.2I, inset; main effect of imaging session, $F_{(1, 4)} = 10.159$, $p = 0.033$, $\eta_p^2 = 0.717$). By contrast, ester exposure selectively and greatly reduced the amplitude of spH signals evoked by only the exposed ester (Figures 3.3C [$F_{(1, 7)} = 9.195$, $p = 0.019$, $\eta_p^2 = 0.568$] and 3.3D [K-S, $Z = 2.823$, $p < 0.001$]), but not by the unexposed ester (Figures 3.3C [$F_{(1, 7)} = 0.298$, $p = 0.602$, $\eta_p^2 = 0.041$] and 3.3E [K-S, $Z = 0.8$, $p = 0.544$]). A careful examination revealed that while the mean response amplitudes remained unchanged for the non-exposed ketone (2HEX) and aldehyde (2M2B) odorants (Figure 3.3C), the distribution of their response amplitudes (Figures 3.3F & 3.3G) became slightly but significantly narrower (less variance) after 1 week of ester exposure (K-S, $Z = 1.533$, $p = 0.018$).

A different pattern of experience-dependent changes in OSN inputs to olfactory bulb glomeruli in OMP knockout mice.

OMP is an olfactory transduction protein that has been shown to confer odorant selectivity in individual OSNs during development (Lee et al., 2011) and in adult OMP-spH mice (Kass et al., 2013a). Because the decreased number of olfactory bulb glomeruli after odorant exposure could reflect an increase in odorant selectivity (see below), we hypothesized that OMP could play a role in this exposure-induced plasticity. To test the role of OMP in exposure-induced OSN plasticity, we replicated the above experiment in 24 mice (Figure 3.4A) that were homozygous for spH at the OMP locus and were thus OMP-null after the manner of Lee et al (2011) and Kass et al (2013b). For the HCC group,

the average number of glomeruli receiving measurable synaptic input during an odorant presentation (Figure 3.4E, inset; $F_{(1, 6)} = 0.006$, $p = 0.943$, $\eta_p^2 = 0.001$) and the amplitude of those inputs (Figure 3.4H, inset; $F_{(1, 6)} = 2.361$, $p = 0.175$, $\eta_p^2 = 0.282$) were again comparable before and after the exposure period (examples shown in Figures 3.4B (left) and 15C), and this was true across all 4 test odorants and both sides of the window (glomerular responses, non-significant session \times odor \times side interaction, $F_{(3, 18)} = 0.777$, $p = 0.522$, $\eta_p^2 = 0.115$; normalized response magnitudes, non-significant session \times odor \times side interaction, $F_{(3, 18)} = 0.761$, $p = 0.531$, $\eta_p^2 = 0.112$). Further, there was no change in the total number of odor-responsive glomeruli (Figure 3.4G, black bar; $\chi^2_{(1)} = 0.126$, $p = 0.722$). These results demonstrate that odorant-evoked responses are stable under normal laboratory conditions in adult OMP^{-/-}-spH mice, similar to the stability of odorant-evoked OSN responses in OMP^{+/-} subjects (Figure 3.2).

Unlike the self-exposed OMP^{+/-} mice that exhibited an enhancement in odorant-evoked glomerular responses after 1 week of self exposure (Figure 3.2), OMP^{-/-} mice in the SE group exhibited a non-significant reduction in the average number of glomeruli receiving measurable synaptic input during an odorant presentation (Figure 3.4F, inset; main effect of imaging session, $F_{(1, 4)} = 1.397$, $p = 0.303$, $\eta_p^2 = 0.259$) compared to their own pre-exposure baseline. Interestingly, there was a significant reduction in the total number of OMP^{-/-} glomeruli that responded to any odorant in the panel, pooled across mice (Figure 3.4G, blue bar; $\chi^2_{(1)} = 14.961$, $p < 0.001$). The decrease in the total number of responding glomeruli without a change in the average number of responses evoked by an odorant suggested that each odorant-responsive glomerulus may respond to more odorants after 1 week of SE in OMP^{-/-} mice (see selectivity analysis below).

Like the ester-exposed OMP^{+/-} mice above (Figure 3.3), OMP^{-/-} mice in the EE group exhibited a large decrease in the number of glomeruli receiving evoked OSN input (Figures 3.5A & 3.5B; main effect of imaging session, $F_{(1, 11)} = 62.108$, $p < 0.001$, $\eta_p^2 = 0.850$), but unlike OMP^{-/+} mice this decrease occurred equally for all 4 odorants in the test panel (Figure 3.5B; non-significant imaging session \times odorant interaction, $F_{(3, 33)} = 0.951$, $p = 0.427$, $\eta_p^2 = 0.080$). Further, the total number of odor-responsive glomeruli was greatly reduced after ester exposure ($N_{\text{PRE}} = 849$, $N_{\text{POST}} = 475$; $\chi^2_{(1)} = 105.647$, $p < 0.001$), more so than in ester-exposed OMP^{-/+} mice; after 1 week of ester exposure the frequency of odorant-responsive glomeruli was 75% and 56% of baseline in OMP^{-/+} mice and OMP^{-/-} mice, respectively.

The pattern of exposure-induced changes in the magnitude of spH signals evoked in olfactory bulb glomeruli were also different in OMP^{-/-} mice compared with that in OMP^{-/+} mice. Whereas 1 week of self exposure scaled the distribution of response magnitudes up in the heterozygous mice (Figure 3.2I), individual odorant-evoked ΔF values in OMP^{-/-} mice were smaller (M-W, $Z = -4.37$, $p < 0.001$) and distributed differently (K-S, $Z = 2.812$, $p < 0.001$) after 1 week of self exposure, as shown in Figure 3.4I. Moreover, ester exposure greatly reduced the amplitude of spH signals evoked by the exposed ester (Figures 3.5C & 3.5D), but this reduction was not odorant specific (Figure 3.5C; non-significant imaging session \times odorant interaction, $F_{(3, 33)} = 1.489$, $p = 0.236$, $\eta_p^2 = 0.119$), with significant reductions also observed in the magnitudes of responses to the unexposed ester (Figure 3.5E; M-W, $Z = -6.372$, $p < 0.001$; K-S, $Z = 2.85$, $p < 0.001$) and the other unexposed odors (Figures 3.5F & 3.5G; M-W, $Z = -11.025$, $p < 0.001$; K-S, $Z = 5.125$, $p < 0.001$).

Exposure-induced changes in glomerular inputs reflect changes in odorant selectivity.

Based on the pattern of results observed above, it was possible that odorant exposure caused changes in the selectivity of odor-responsive glomeruli (Figure 3.6). To assess this we categorized odorant-responsive glomeruli in each exposure group as having high odorant-selectivity or low selectivity, and then tested whether there were changes in the relative frequency of glomeruli within each category between imaging sessions. This analysis demonstrated that the distributions of odor-responsive glomeruli within each selectivity category were best accounted for in OMP^{+/-} glomerular populations (Figure 3.6D; 3-way association, $\chi^2_{(2)} = 23.171$, $p < 0.001$) and OMP^{-/-} glomerular populations (Figure 3.6E; 3-way association, $\chi^2_{(2)} = 22.678$, $p < 0.001$) when all 3 variables (exposure group, imaging session, and odorant selectivity) were included in the models. In the HCC group there was no change in the selectivity of odor-responsive glomeruli (Figures 3.6A, 3.6D [black bars], and 3.6E [black bars]) for mice of either genotype. Interestingly, there was a differential effect of self exposure and ester exposure on glomerular response selectivity. In OMP^{+/-} mice, selectivity significantly decreased in odorant-responsive glomeruli in the SE group (Figures 3.6B and 3.6D, blue bars; $\chi^2 = 19.605$, $p < 0.001$), whereas it significantly increased in odorant-responsive glomeruli in the EE group (Figures 3.6C and 3.6D, red bars; $\chi^2 = 4.224$, $p = 0.04$). In OMP^{-/-} mice the SE group showed no significant change in selectivity (Figure 3.6E; blue bars; $\chi^2 = 2.576$, $p = 0.109$), while the EE group showed a significant increase in selectivity (Figure 3.6E, red bars; $\chi^2 = 30.73$, $p < 0.001$).

Discussion

These results indicate that the primary sensory inputs to the brain's olfactory system exhibit robust experience-dependent plasticity in adult mice and that this plasticity can be specific to the environmental stimuli experienced. Such plasticity in primary sensory afferents is of broad importance for models of downstream sensory processing, which must interpret changing neural signals in response to the same physical stimulus. OSNs in OMP-null mice showed similar plasticity to OMP-heterozygous mice but seemingly without stimulus specificity, suggesting a potential role for this protein in adaptively reshaping OSN responses to different circumstances.

Interestingly, odorant exposure both sparsened the spatial representations of odorants (by reducing the number of glomeruli receiving synaptic input from OSNs) and reduced the magnitude of those inputs. The sparsening of representations is potentially valuable for increasing the number of separate representations that can be encoded and thus the system's ability to recognize and discriminate among odorants (Willmore and Tolhurst, 2001; Perez-Orive et al., 2002). Such changes in coding may contribute to the improvement in odor discrimination observed after olfactory enrichment (Mandairon et al., 2006b; Mandairon et al., 2006a). The selective sparsening of representations for the frequently-encountered ester exposure odorant and, to a lesser extent, the non-encountered ester odorant but not for the other unexposed odorants suggests an adaptive coding strategy, where the codes representing common odorants in the local environment are somehow specialized or optimized. The smaller spH signals after odorant exposure indicates a reduction in total neurotransmitter release, but does not provide enough temporal resolution to readily discriminate between a reduction in the overall rate of odorant-evoked exocytosis

throughout the odorant presentation (smaller responses) and a more rapid adaptation of odorant-evoked responses during the odorant (briefer responses). If briefer, this result would be consistent with a refinement of the temporal aspects of the odorant representation, which has been observed elsewhere in the olfactory system (Blumhagen et al., 2011) but never in primary sensory afferents or selectively in response to sensory experience.

In OMP-heterozygous mice, the effects of ester exposure seemed confined to ester-responsive OSNs, with the largest effect on the population directly activated by the exposed ester. By contrast, in OMP-null mice ester exposure produced comparable plasticity in all the OSN populations tested. One might expect this pattern of results if the plasticity were a direct consequence of OSN stimulation because OSNs lacking OMP exhibit decreased odorant-selectivity at baseline (compare pre-exposure data in Figures 3.6D & 3.6E; (Lee et al., 2011; Kass et al., 2013a)). Despite the reduced odorant-selectivity in OMP-null mice, the populations of glomeruli stimulated by the ketone and aldehyde were very different from the population stimulated by the exposure ester (Figure 3.5A). Therefore, the non-selective plasticity exhibited by OMP-null mice could not have been caused by non-selective stimulation with the exposure ester. Instead, we conclude that OMP somehow restricts the process of adaptive plasticity to the OSN populations that are stimulated by the exposure odorant.

The differential effects in OMP-null and OMP-heterozygous mice enable us to rule out certain technical explanations for these results. The reduction in evoked OSN activity cannot be a consequence of some global change in intranasal airflow induced by the ester exposure (e.g., irritation or inflammation) because it was specific to ester-responsive glomeruli in OMP-heterozygous subjects. Similarly, the ester-exposure-induced plasticity

does not result from fast adaptation of the olfactory transduction pathway (Boccaccio et al., 2006; Lecoq et al., 2009), which would be expected to yield effects only in ester-responsive OSN populations, because OSNs in OMP-null mice exhibited non-selective plasticity across three odor classes.

The reduction in the number of glomeruli receiving OSN synaptic input after ester exposure reflects an increase in odorant-selectivity, whereby the OSNs innervating some glomeruli ceased responding to one or more odorants in the panel. This is surprising because odorant selectivity is thought to be conferred by the selective expression of a single odorant receptor (Bozza et al., 2004) in all OSNs innervating a given glomerulus (Mombaerts, 2006). One possibility is that at baseline each glomerulus contained some mistargeted OSN projections expressing other receptors and that the exposure paradigm induced a pruning of these mistargeted projections, as observed during development (Zou et al., 2004; Kerr and Belluscio, 2006). It is also possible that the observed plasticity results from a refinement in receptor expression within individual OSNs (Tian and Ma, 2008), or from changes in pre-receptor enzymatic events (Nagashima and Touhara, 2010). Notably, the expression of OMP has also been shown to increase the odorant-selectivity of OSNs (Lee et al., 2011; Kass et al., 2013a) through some unknown action seemingly downstream of the odor receptor but upstream of the cAMP signaling cascade (Reisert et al., 2007). However, the increase in odorant-selectivity reported here was more pronounced in OMP-null mice than in OMP-heterozygous mice, suggesting that while OMP clearly plays a role in determining *which* OSNs undergo plasticity, it is not itself conferring the increased odorant selectivity.

While odorant exposure can alter the number and lifespan of OSNs its effects are variable, sometimes increasing the likelihood of OSN survival (Watt et al., 2004) and other times causing a decrease (Cavallin et al., 2010) or even no change (Kerr and Belluscio, 2006) in the number of OSNs expressing the cognate receptor for the exposed odorant in the epithelium. In the present experiment, we cannot discriminate between changes in the response per OSN and a change in the number of OSNs targeting each glomerulus because we imaged odorant-evoked neurotransmitter release from the entire population of OSNs innervating each glomerulus. Nonetheless, these results demonstrate that the net effect of our chronic, intermittent odorant exposure paradigm across OSNs is a selective reduction in the overall input to the olfactory bulb from the subpopulations of OSNs that normally respond to the exposure odorant and related odorants.

Neurotransmitter release from OSN presynaptic terminals is strongly modulated by presynaptic inhibition arising from GABAergic and dopaminergic juxtaglomerular circuitry (Nickell et al., 1994; McGann et al., 2005; Murphy et al., 2005; McGann, 2013). This circuit includes both a population of uniglomerular, GABAergic interneurons that express glutamic acid decarboxylase-65 (GAD65) and a separate population of multiglomerular GABAergic and dopaminergic interneurons that jointly express the transmitter synthesis enzymes GAD67 and tyrosine hydroxylase (Kiyokage et al., 2010). In the latter population the expression of both tyrosine hydroxylase and GAD67 is activity-dependent and can be strongly downregulated when the activity of OSN afferents is suppressed in adult animals (Cho et al., 1996; Parrish-Aungst et al., 2011; Kass et al., 2013c). These GABAergic/dopaminergic interneurons also exhibit substantial activity-dependent turnover via adult neurogenesis (Sawada et al., 2011), which can play a role in

olfactory perceptual learning (Bovetti et al., 2009; Moreno et al., 2009; Moreno et al., 2012). However, the plasticity that we observed was odorant-specific in ester-exposed OMP-expressing mice, which seems incompatible with a broad change in presynaptic inhibition across the many glomeruli innervated by joint GABAergic/dopaminergic interneurons (Kiyokage et al., 2010). While we cannot rule out the possibility that the observed plasticity reflected changes in inhibition, the observation that the effects of exposure on OSN physiology is both odorant-specific and dependent on OMP (which is selectively expressed in OSNs) suggests that the locus of the change is most likely within the OSNs themselves.

One unexpected result of this study was that self exposure, where mice lived in a sham-odorized exposure chamber, produced an increase in the total number of odorant-responsive glomeruli and the size of their synaptic inputs from OSNs in OMP-heterozygous mice, which is in the opposite direction from the effect of ester exposure (and also olfactory deprivation; (Kass et al., 2013c)) in these mice. It is perhaps surprising that simply exposing the mouse to more of its own odors would induce plasticity. However, previous studies have shown that simply changing a mouse's home cage can cause robust neuroanatomical changes (Oliva et al., 2010) to olfactory bulb glomeruli that are affected by exposure to naturally-produced rodent cage odors (Oliva et al., 2008). Other laboratories have also reported notable changes in olfactory discrimination by simply enriching the olfactory environment with scent-containing mesh spheres (Mandairon et al., 2006b; Mandairon et al., 2006a), suggesting that the sensory experience of a laboratory rodent may be so impoverished that modest environmental changes are sufficient to cause substantial alterations in neural function (Krech et al., 1962; Baroncelli et al., 2010). OMP-

null mice did not show this enhancement in the SE group, and in fact showed a decrease in odorant-responsive glomeruli and the size of their OSN synaptic inputs. However, naïve OMP-null subjects exhibit a much larger number of odorant-evoked glomerular responses than naïve mice heterozygous for OMP (Kass et al., 2013a) which suggests that a ceiling effect may have occurred in these mice.

Efficient coding models suggest that neural representations of the sensory world can be optimized by adapting their coding scheme to reflect the changing natural statistics of the animals' sensory world (Brenner et al., 2000; Simoncelli and Olshausen, 2001; Schwarzkopf et al., 2009). The present results indicate that such plasticity can occur as early as the primary sensory afferents in the olfactory system.

Acknowledgements

I thank Andrew Moberly for his contributions to this project. Andrew surgically implanted cranial windows in some subjects prior to the imaging procedures, and also collected imaging data from a subset of mice.

Chapter 3 Figures

Figure 3.1

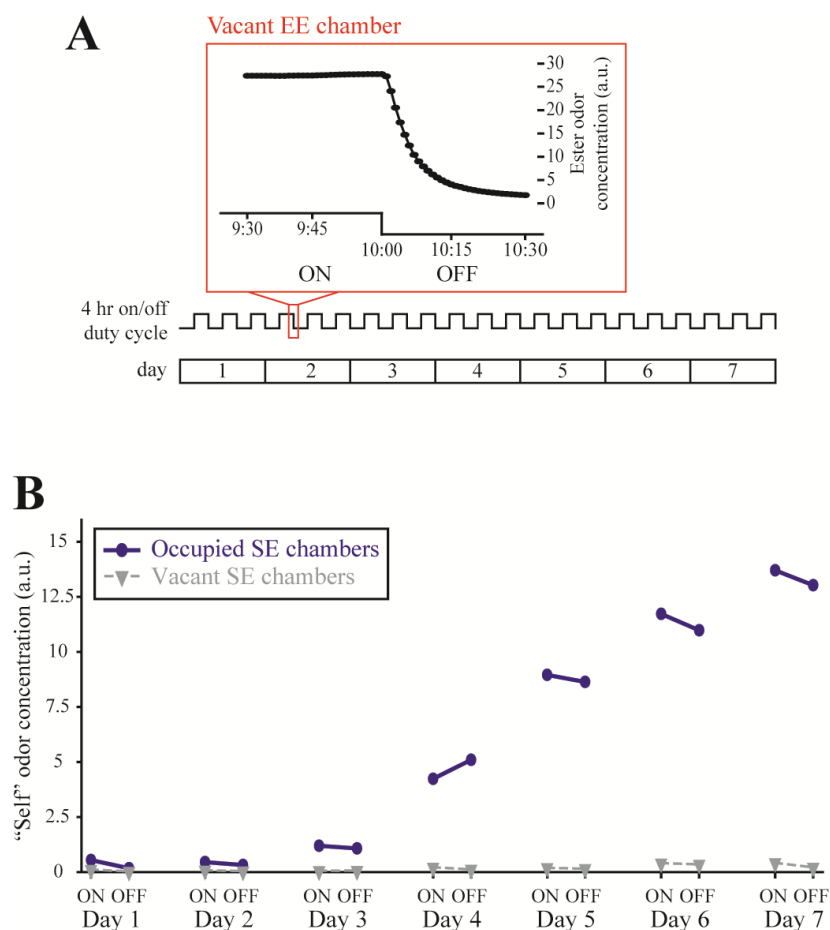


Figure 3.1. Ester odorants are reliably added and removed from the chambers on a 4 hour duty cycle, while self odors accumulate evenly during ON and OFF cycles throughout the week-long exposure period. (A) Timeline of the exposure period showing the full 7 day duration (bottom) with a trace (middle) indicating the 4 hour duty cycling in the exposure chambers. The outlined portion of the duty cycle is expanded immediately above the timeline (top) and shows photoionization detection (PID) measurements that were sampled once/minute from a butyl acetate ester exposure (EE) chamber during the last 30 minutes of an ON cycle and the first 30 minutes of an OFF cycle. (B) Mean “self” odor concentration from 12 occupied (circles, solid lines) and 6

vacant (triangles, dashed lines) self exposure (SE) chambers. PID measurements were recorded during ON and OFF cycles across 7 consecutive days.

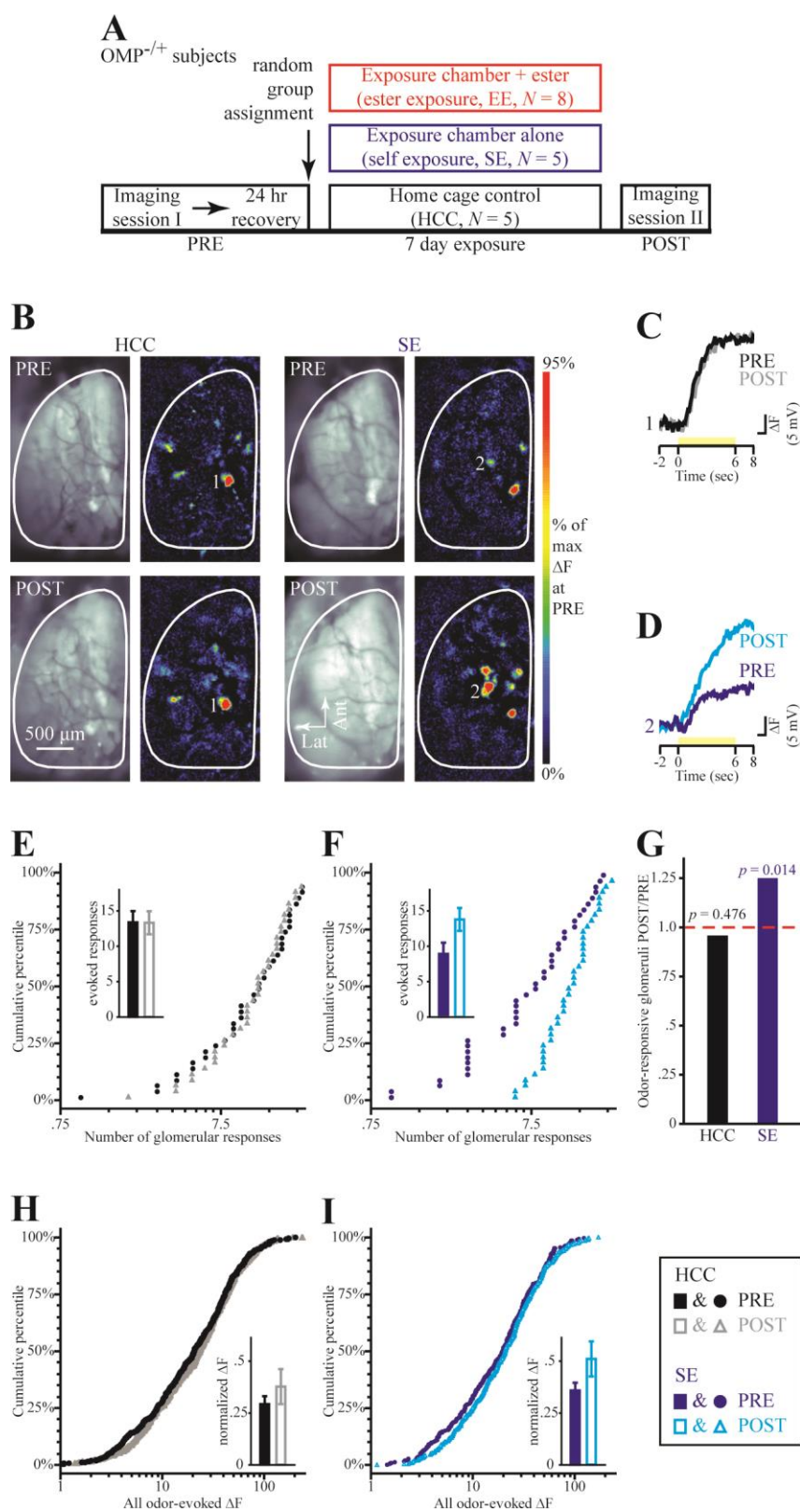
Figure 3.2

Figure 3.2. Physiological responses to test odorants in OMP-heterozygous mice are stable over time in home cage controls, but *enhanced* by one week of self control exposure. (A) Timeline of the optical imaging study showing home cage control (HCC), self exposure (SE), and ester exposure (EE) group assignments of OMP^{-/+} mice. (B) Example resting fluorescence images and 2M2B-evoked pseudocolored difference maps from a HCC mouse (left) and a SE mouse (right) during PRE (top) and POST (bottom) imaging sessions. (C-D) Sets of traces (scaled relative to each max) evoked by 2M2B (yellow stimulus bar) from HCC (C) and SE (D) subjects corresponding to the numbered callouts in (B). (E-F) Cumulative probability plots showing the distributions of odorant-evoked responses in olfactory bulbs from HCC (E) and SE (F) groups both before (closed circles) and after (open triangles) the week-long exposure period. The mean \pm SEM number of odorant-evoked glomerular responses during PRE (closed bars) and POST (open bars) imaging sessions is shown in the inset for HCC (E) and SE (F) groups. (G) Ratios for the total frequency of odorant-responsive glomeruli during POST imaging relative to that of PRE per group. P values indicate PRE versus POST comparisons within each group. (H-I) Cumulative probability plots showing distributions of response magnitudes (ΔF s) from PRE versus POST imaging sessions in HCC (H) and SE (I) groups. Individual ΔF values were normalized relative to the maximum ΔF evoked at PRE and are shown in the insets as the mean \pm SEM normalized ΔF . The legend displayed in the bottom right of the figure corresponds to panels E, F, H, & I.

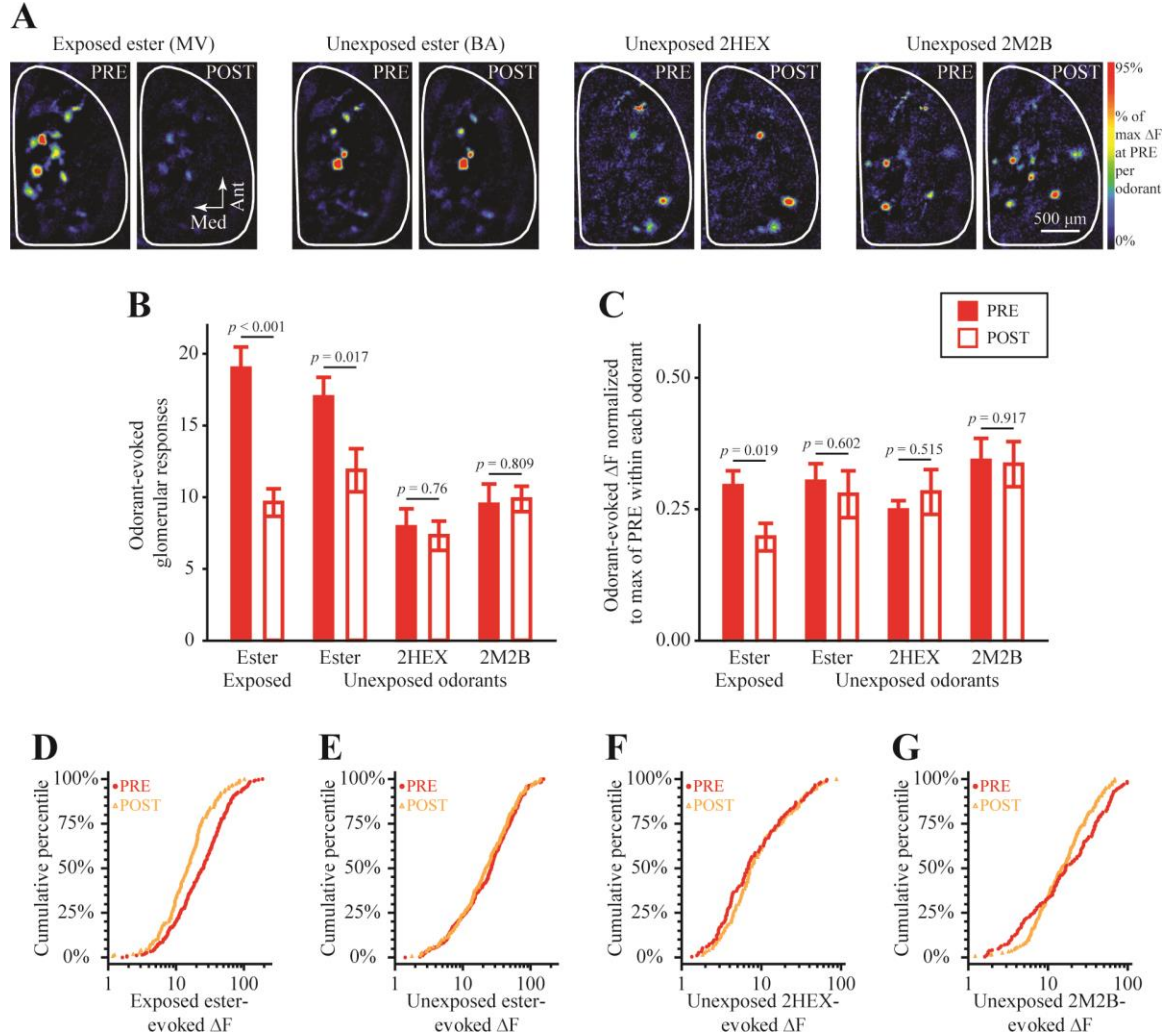
Figure 3.3

Figure 3.3. Ester exposure *selectively* alters OSN physiology in OMP-heterozygous mice. (A) Pseudocolored difference maps evoked by the exposed ester (MV, first set), unexposed ester (BA, second set), unexposed ketone (2HEX, third set) and unexposed aldehyde (2M2B, fourth set) during PRE and POST imaging in the same ester-exposed OMP^{+/-} subject. (B-C) Mean \pm SEM number of odorant-evoked glomerular responses (B) and normalized odorant-evoked change in fluorescence (ΔF , C) from PRE (solid bars) and POST (open bars) imaging sessions plotted as a function of imaging odorant stimulus. (D-G) Cumulative probability plots showing the distributions of ΔF values evoked by the exposed ester (D) and the unexposed ester (E), ketone (2HEX, F), and aldehyde (2M2B, G) during PRE (closed, red circles) and POST (open, orange triangles) imaging sessions.

Data from the exposed and unexposed esters are counterbalanced across subjects in the EE group.

Figure 3.4

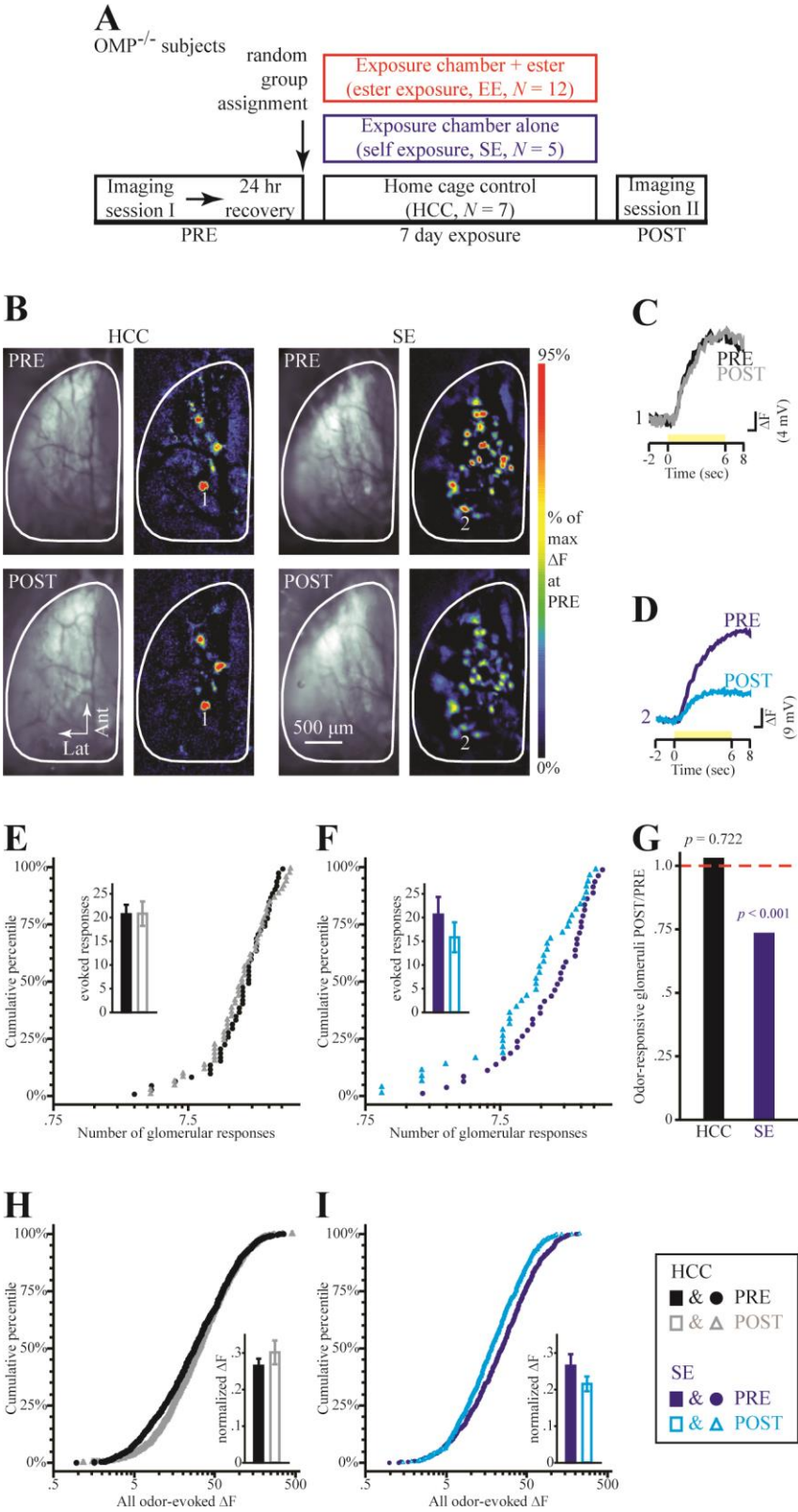


Figure 3.4. Physiological responses to test odorants in OMP-null mice are stable over time in home cage controls, but *attenuated* by one week of self control exposure. (A) Timeline of the optical imaging study showing home cage control (HCC), self exposure (SE), and ester exposure (EE) group assignments of OMP^{-/-} mice. (B) Example resting fluorescence images and 2M2B-evoked pseudocolored difference maps from HCC (left) and SE (right) subjects during PRE (top) and POST (bottom) imaging sessions. (C-D) Sets of traces (scaled relative to each max) evoked by 2M2B (yellow stimulus bar) from HCC (C) and SE (D) subjects corresponding to the numbered callouts in (B). (E-F) Cumulative probability plots showing the distributions of odorant-evoked responses in olfactory bulbs from HCC (E) and SE (F) groups both before (closed circles) and after (open triangles) the week-long exposure period. The mean \pm SEM number of odorant-evoked glomerular responses during PRE (closed bars) and POST (open bars) imaging sessions is shown in the inset for HCC (E) and SE (F) groups. (G) Ratios for the total frequency of odor-responsive glomeruli during POST imaging relative to that of PRE per group. P values indicate PRE versus POST comparisons within each group. (H-I) Cumulative probability plots showing distributions of response magnitudes (ΔF s) from PRE versus POST imaging sessions in HCC (H) and SE (I) groups. Individual ΔF values were normalized relative to the maximum ΔF evoked at PRE and are shown in the insets as the mean \pm SEM normalized ΔF . The legend displayed in the bottom right of the figure corresponds to panels E, F, H, & I.

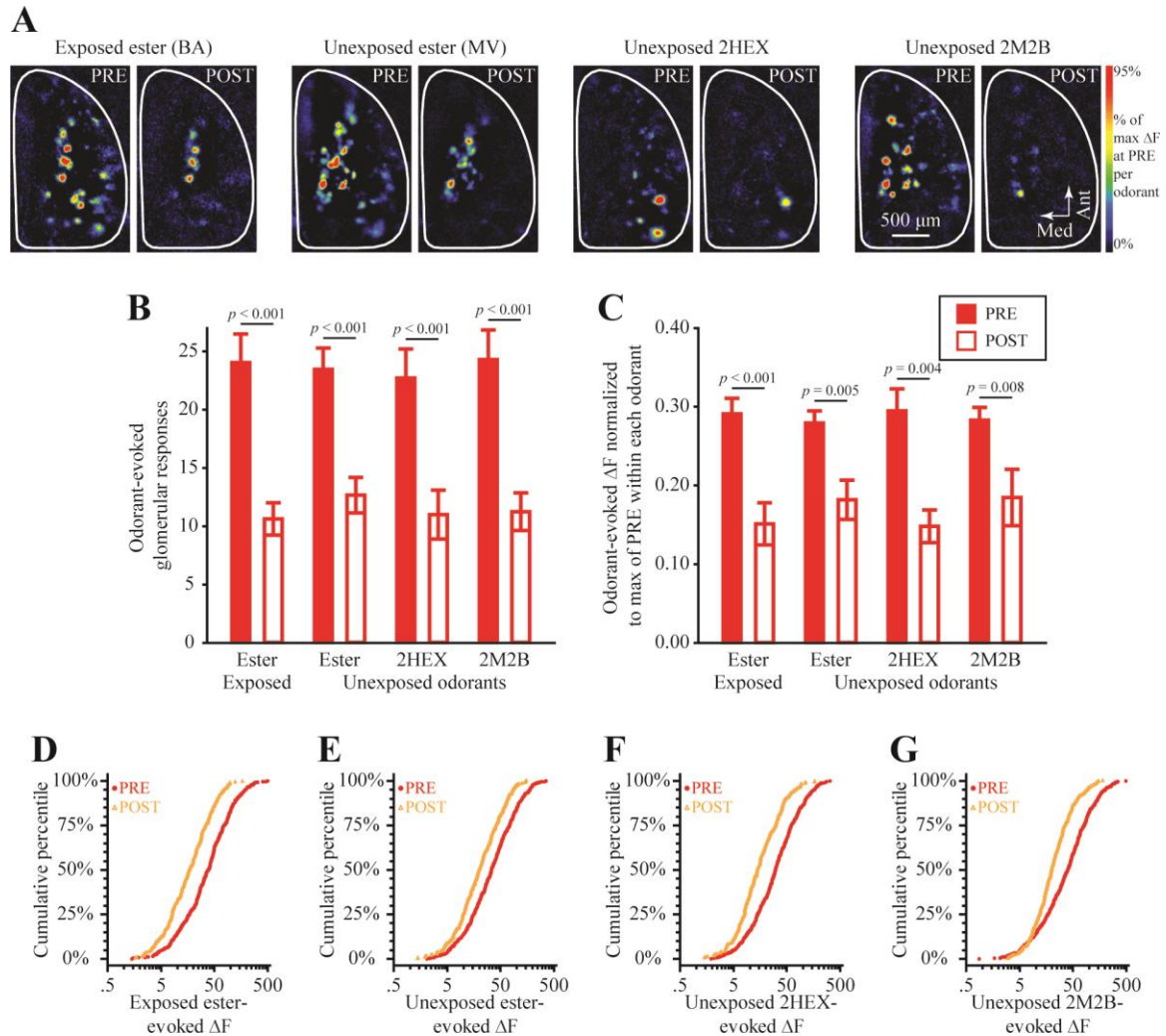
Figure 3.5

Figure 3.5. The effects of ester exposure on OSN physiology in OMP-null mice do not exhibit stimulus specificity. (A) Pseudocolored difference maps evoked by the exposed ester (BA, first set), unexposed ester (MV, second set), unexposed ketone (2HEX, third set), and unexposed aldehyde (2M2B, fourth set) during PRE and POST imaging in the same ester-exposed OMP^{-/-} subject. (B-C) Mean \pm SEM number of odorant-evoked glomerular responses (B) and normalized odorant-evoked change in fluorescence (ΔF , C) from PRE (solid bars) and POST (open bars) imaging sessions plotted as a function of imaging odor stimulus. (D-G) Cumulative probability plots showing the distributions of ΔF values evoked by the exposed ester (D) and the unexposed ester (E), ketone (2HEX, F), and aldehyde (2M2B, G) during PRE (closed, red circles) and POST (open, orange

triangles) imaging sessions. Data from the exposed and unexposed esters are counterbalanced across subjects in the EE group.

Figure 3.6

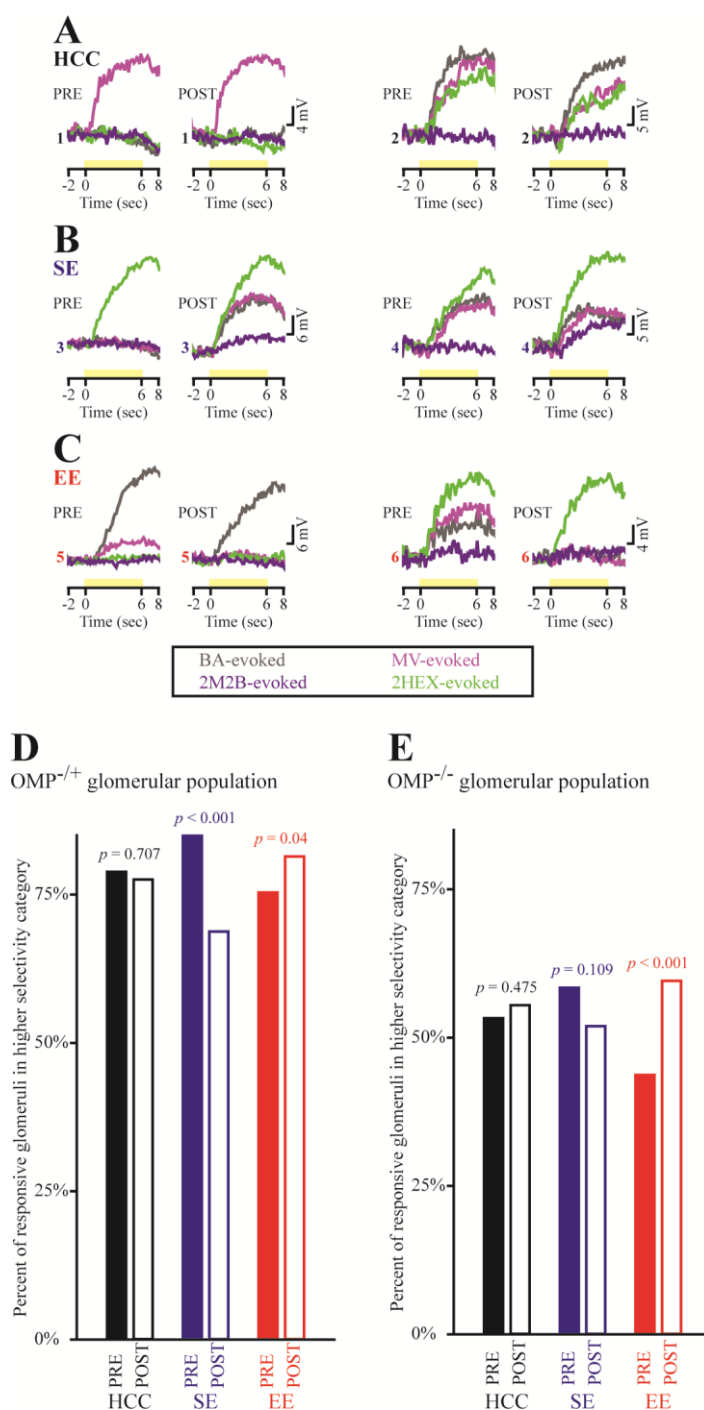


Figure 3.6. Odorant selectivity of responsive glomeruli is altered by olfactory experience. (A-C) Example selectivity patterns during PRE and POST imaging sessions in 6 individual glomeruli (numbered 1-6) from home cage control (HCC, **A**), self exposure (SE, **B**), and ester exposure (EE, **C**) subjects that were OMP^{+/+}. Each numbered set of 4

traces corresponds to that glomerulus' responsivity to presentations (shown as yellow stimulus bars) of 4 test odorants (BA, MV, 2HEX, and 2M2B) before and after the exposure manipulation. Traces are color-coded by odorant, as shown in the legend below panels **A**, **B**, and **C**. Each set of PRE and POST traces is scaled relative to the max evoked response across the 4 odorants. Glomeruli 1, 3, and 5 exhibited "higher" response selectivity at baseline, whereas glomeruli 2, 4, and 6 exhibited "lower" response selectivity at baseline. **(D-E)** Percentage of OMP-heterozygous (OMP^{-/+}, **D**) and OMP-null (OMP^{-/-}, **E**) glomerular populations within each exposure group that were categorized as having higher odorant response selectivity both before (PRE) and after (POST) the 1 week exposure period.

CHAPTER 4

Changes in olfactory sensory neuron physiology and olfactory perceptual learning after odorant exposure in adult mice

The results from this chapter are reported in Kass MD, Guang SA, Moberly AH, McGann JP (2016) Changes in olfactory sensory neuron physiology and olfactory perceptual learning after odorant exposure in adult mice. *Chem Senses* 41:123-133.

Abstract

The adult olfactory system undergoes experience-dependent plasticity to adapt to the olfactory environment. This plasticity may be accompanied by perceptual changes, including improved olfactory discrimination. Here, we assessed experience-dependent changes in the perception of a homologous aldehyde pair by testing mice in a cross-habituation/dishabituation behavioral paradigm before and after a week-long ester-odorant exposure protocol. In a parallel experiment, we used optical neurophysiology to observe neurotransmitter release from olfactory sensory neuron (OSN) terminals *in vivo*, and thus compared primary sensory representations of the aldehydes before and after the week-long ester-odorant exposure in individual animals. Mice could not discriminate between the aldehydes during pre-exposure testing, but ester-exposed subjects spontaneously discriminated between the homologous pair after exposure, whereas home cage control mice cross-habituated. Ester exposure did not alter the spatial pattern, peak magnitude, or odorant-selectivity of aldehyde-evoked OSN input to olfactory bulb glomeruli, but did alter the temporal dynamics of that input to make the time course of OSN input more dissimilar between odorants. Together, these findings demonstrate that odor exposure can induce both physiological and perceptual changes in odor processing, and suggest that changes in the temporal patterns of OSN input to olfactory bulb glomeruli could induce differences in odor quality.

Introduction

The olfactory system can adapt to a constantly changing olfactory environment to maximize the detection and discrimination of frequently encountered or novel odor stimuli. In this dynamic sensory system, the first stage of stimulus processing takes place in the olfactory bulb, where neural representations of odor stimuli are shaped by complex and highly plastic circuitry before being communicated to other brain regions. Odor codes in the olfactory bulb correlate with the perception of odor quality (Malnic et al., 1999; Linster et al., 2001; Youngentob et al., 2006; Mandaïron and Linster, 2009), and both odor perception (Dalton and Wysocki, 1996; Mandaïron et al., 2006a) and olfactory bulb signal processing (Buonviso et al., 1998; Buonviso and Chaput, 2000; Fletcher and Wilson, 2003; Mandaïron et al., 2008a) are easily modified by olfactory experience. Consequently, an extensive series of studies have sought to correlate experience-dependent changes in odor perception with corresponding changes in early olfactory circuitry.

Previous work has shown that initially indiscriminable odorant pairs can become discriminable after a period of exposure to a chemically- and perceptually-different odorant (Mandaïron et al., 2006b). This effect is robust and has motivated recent clinical trials using odor exposure as a therapy for anosmia (Damm et al., 2014; Altundag et al., 2015). The neural mechanisms underlying these perceptual effects are increasingly understood, and likely caused by experience-dependent alterations within the inhibitory circuitry of the olfactory bulb (Mandaïron et al., 2008a; Mandaïron and Linster, 2009). Passive exposure to olfactory stimuli promotes survival of inhibitory, adult-born interneurons in the glomerular and granule cell layers of the olfactory bulb and reduces cell death (Woo et al., 2006; Bovetti et al., 2009; Bonzano et al., 2014). Exposure-induced perceptual learning

requires neurogenesis of olfactory bulb granule cells (Moreno et al., 2009), as well as norepinephrine-modulated fine-tuning of sensory processing in the inhibitory bulbar circuitry (Moreno et al., 2012; Vinera et al., 2015). Olfactory sensory enrichment also enhances GAD67 (Bovetti et al., 2009) and tyrosine hydroxylase (Bonzano et al., 2014) expression in periglomerular (PG) cells involved in multiglomerular communication. The changes in bulbar neurogenesis and neurochemistry that are observed after a period of exposure are accompanied by an enhancement of odorant-evoked activity in PG (Woo et al., 2007) and granule (Mandairon et al., 2008a) cell populations. However, these data do not exclude the possibility of plasticity in the odor-response properties of the olfactory epithelium, which would result in experience-dependent changes in the sensory input to all olfactory processing regions.

Olfactory transduction occurs in the olfactory epithelium, where olfactory sensory neurons (OSNs) physically contact olfactory stimuli in the external environment. Their axons travel back to the brain through the cribriform plate and thus constitute the primary sensory input to the olfactory bulb. The survival and density of OSNs in the epithelium can be influenced by olfactory experience (Watt et al., 2004; Cavallin et al., 2010). Moreover, OSN projections to their target glomeruli in the olfactory bulb are highly dependent on experience and can be altered through enriched (Kerr and Belluscio, 2006; Valle-Leija et al., 2012) and deprived (Zou et al., 2004; Kass et al., 2013c) olfactory environments, both in the developing and the adult olfactory system. Odorant exposure alters the number of OSNs expressing a given odor receptor and can increase expression of odor receptor mRNA and associated transduction proteins like CNGA2 and

phosphodiesterase 1C, which can result in increased sensitivity to odors and faster odor transduction kinetics (Cadiou et al., 2014).

Testing the role of OSN plasticity in exposure-induced perceptual change has proved challenging. Unlike the exposure-induced changes in the bulbar inhibitory networks, exposure-induced plasticity in OSNs is usually exclusive to OSNs expressing the cognate odorant receptor for the exposure odorant. After long-term exposure, OSN population-level electro-olfactogram (EOG) responses exhibit enhanced sensitivity to an exposed odorant, but not to an unexposed odorant (Wang et al., 1993). Lyrar exposure induces dramatic molecular and physiological changes in OSNs expressing its cognate MOR23 receptor, but acetophenone exposure has no effect on these neurons (Cadiou et al., 2014). Seven days of exposure to an ester odorant selectively reduces transmitter release from the olfactory nerve evoked by the same ester and also enhances odorant-response-selectivity of OSNs, but has little or no effect on responses to non-esters (Kass et al., 2013d). It is thus unclear whether OSN plasticity could influence discrimination of odorants chemically different than the exposure odorant, though it is likely related to the spatial overlap between bulbar representations of unexposed odorants with an exposed odorant (Mandairon et al., 2008a; Mandairon and Linster, 2009). Complicating matters further, relatively few odorants have actually been employed in odorant exposure paradigms, and the limited data from genetically-identified OSN populations suggests that not all such populations are equally plastic (Cavallin et al., 2010; Cadiou et al., 2014). These challenges motivated a combined study of olfactory perceptual plasticity and OSN neurophysiological plasticity to observe any changes in OSN responses to the test odors when the perceptual change is induced.

We used optical neurophysiology to observe the neurotransmitter release from populations of OSN synaptic terminals in the dorsal olfactory bulbs of adult mice during the presentation of each of two homologous aldehydes. These odor-evoked responses, which constitute the primary olfactory input to the brain, were assessed both before and after seven days of exposure to a chemically-different odorant (an ester), or a home-cage control period, in each mouse. To assess exposure-induced changes in odor perception, we tested whether a parallel group of mice spontaneously discriminated between these homologous aldehydes both before and after the same week-long exposure protocol that was used in the imaging experiment. We hypothesized that long-term ester odorant exposure (but not home cage control exposure) would enhance discrimination between the unexposed aldehyde pair. We also predicted that we would observe enhanced contrast between the primary sensory representations of the unexposed aldehydes after ester exposure.

Methods

Subjects.

Wild-type C57BL/6 mice (Charles River Laboratories, strain code #027) were used for the habituation/dishabituation behavioral experiment, and heterozygous OMP-spH mice were used for the optical imaging experiment. In sum, 22 mice were used in the behavioral experiment (data shown in Figure 4.2), and 8 OMP-spH mice of mixed sexes were used in the imaging experiment (data shown in Figures 4.3-4.5). All subjects were adults (3-9 months) at the onset of experimentation. During experimentation, subjects were

singly-housed in either standard shoebox cages or custom odorant exposure chambers, which both contained the same bedding, food, and light/dark cycle.

Olfactory stimuli.

Based on previous experiments, an ester (BA (Kass et al., 2013d)) was selected as the exposure odorant and 2 aldehydes (HEPT and HEX (Kass et al., 2013a)) were selected as discrimination stimuli for the optical imaging and behavioral experiments. These odorants were selected because they all drive input to glomeruli on the dorsal surface of the olfactory bulbs (Xu et al., 2003; Kass et al., 2013b), permitting *in vivo* visualization of odor-evoked neural activity. Further, HEPT and HEX are aliphatic homologues that are difficult for naïve, adult mice to discriminate (Kass et al., 2013a), and thus provide an opportunity to evaluate improvement in discrimination abilities.

For the behavioral experiment, both odorants were diluted in mineral oil in proportion to their respective vapor pressures, yielding approximately equivalent vapor concentrations (HEPT diluted to ~0.26%; HEX diluted to ~0.01%). After preparing fresh, vapor-equivalent dilutions, a photoionization detector was used to measure the concentrations of the 2 stimuli in arbitrary units (au) so that the equivalent concentrations could be calibrated on the vapor dilution olfactometer that was used during imaging. Odorant dilutions were freshly prepared each morning prior to behavioral experiments, and stimuli were calibrated from the olfactometer on the imaging rig prior to all imaging sessions via photoionization detection measurements.

Odorant exposure.

As outlined in Figure 4.1A and Figure 4.1B, behavioral assessments and imaging preparations were performed both before and after each mouse spent 7 days in 1 of 2

randomly-assigned exposure environments. In one environment, mice were housed in odorant exposure chambers, and in the other, mice were housed in their (standard) home cages. Mice assigned to the latter housing environment served as the control group (home cage control, HCC). The exposure chambers are described in detail in Chapter 3 (Kass et al., 2013d). Briefly, room air was pulled through the chambers by a vacuum (13 L/min), and the airflow source was shunted on a continuous 4-hr duty cycle between an empty bottle (clean room air) and a bottle containing BA diluted in mineral oil. A photoionization detector was used to measure odorant concentration in the BA exposure chambers from day to day. As shown by the example measurements in Figure 4.1C, the sensor was also used to verify that no odor was present in the chambers during the OFF cycles, and that BA was delivered at a relatively constant concentration of ~30 a.u. during the ON cycles.

Habituation/dishabituation behavioral assessment and analysis.

To assess the perceptual similarity of HEPT and HEX both before and after the week-long exposure period (Figure 4.1A), we used a non-associative, habituation/dishabituation task (Mandairon et al., 2006b; Mandairon et al., 2006a) that we have previously utilized in our laboratory (see Chapter 2; (Kass et al., 2013a)). In this task, after mice are behaviorally habituated to one odorant through successive presentations, they are then presented with a second odorant during a single test trial and their investigation of that second odorant is quantified and used as an index of their spontaneous discrimination between the 2 stimuli (Mandairon et al., 2006b; Mandairon et al., 2006a). If there is no perceptual difference between the 2 odorants, the mouse will continue to habituate on the test trial (as evidenced by a further reduction in investigation time).

Conversely, if the odorants are perceived differently, the subject will not continue to habituate and may exhibit an increase in investigatory behavior.

Animals were housed in standard laboratory cages both before and after the exposure period, regardless of which group that they were assigned to during the week-long exposure. On testing days, the home cage was transferred from the colony room to the behavioral testing room for ~1 hour prior to experimentation to allow the animals to acclimate to the transfer, and then testing was carried out in the home cage. As described in Chapter 2 and shown here in Figure 4.2A, each testing session consisted of 1 trial of mineral oil (min oil) only, followed by 4 trials of HEX, and finally 1 trial of HEPT.

To ensure that the exposure manipulation did not lead to changes in general motor activity, baseline levels of activity were assessed by analyzing stimulus investigation during the mineral oil trial both before and after the exposure period (Figure 4.2C). Behavioral habituation to HEX was quantified across the 4 HEX trials in both test sessions for each subject (Figure 4.2B). Cross-habituation/dishabituation in each session was analyzed by comparing investigation during the last HEX trial with investigation during the HEPT (test) trial (Figure 4.2E-F). All analyses shown in Figure 4.2B-E were performed on raw investigation time (sec). The analyses shown in Figure 4.2F were performed on difference scores that were calculated from normalized investigation time. To evaluate relative changes in cross-habituation (or dishabituation) between the 2 odorants, we normalized investigation time for each subject within each testing session relative to the maximum time across the 4 HEX trials and the 1 HEPT (test) trial. Difference scores were then calculated for both tests from each subject by subtracting the normalized HEPT investigation from the normalized HEX4 investigation. All data (raw and normalized)

were analyzed with a combination of mixed-model ANOVAs (with testing session and trial as within-subjects factors, and group as a between-subjects factor) and planned *t* tests.

Quantification and analysis of odorant-evoked optical signals.

Chronic cranial windows were implanted bilaterally as reported under General Methods, and can be seen in the RLI examples shown in Figures 4.3A and 4.3B. Imaging data were processed, extracted, and analyzed in Neuroplex, Matlab, and SPSS, and were subsequently graphed in SigmaPlot, Matlab, and Origin, as detailed under General Methods.

To generate HEPT- and HEX-evoked difference maps, the average fluorescence during 1 sec immediately prior to stimulus onset was subtracted from the average fluorescence during the most typical peak odorant-evoked response. The raw dataset for the results that are summarized by Figures 4.3-4.5 included 133 glomerular ROIs from the HCC subjects and 138 glomerular ROIs from the BA-exposed subjects. Putative glomerular ROIs were first hand-selected from the spatially high-pass-filtered difference maps (examples shown in Figure 4.3A-B) and matched across imaging sessions for each individual subject.

To determine if there were BA-exposure-dependent changes in peak HEPT- or HEX-evoked response amplitudes, we calculated peak odorant-evoked ΔF s for all glomerular ROIs from spatially high-pass-filtered difference maps from each subject during each imaging session. To permit averaging across mice within each group, HEPT- and HEX-evoked ΔF values were then normalized within odorants across imaging sessions for each mouse, such that all evoked ΔF s per stimulus during PRE and POST were divided by the maximum evoked ΔF of PRE. The normalized ΔF values were then averaged within

odorants and preps for each mouse. These data (shown in Figure 4.3E) were first analyzed via mixed-model ANOVA, with imaging session (pre-exposure, PRE; post-exposure; POST) and odorant (HEPT; HEX) as within-subjects factors and group (HCC; BA) as a between-subjects factor. This analysis was then followed by planned *post hoc t* tests. Additionally, the normalized distributions of ΔF values were pooled across glomeruli (shown in Figure 4.3F-G) and analyzed with Wilcoxon signed rank tests.

We next evaluated potential BA-exposure-dependent changes in the average number of glomerular responses contributing to each odor representation. As such, we quantified the number of HEPT- and HEX-evoked responses in the spatially high-pass-filtered odor maps from each subject during each imaging session. These data (shown in Figure 4.4A) were first tested with a mixed-model ANOVA, and then with planned *post hoc t* tests. The number of responses per odor representation does not equate to the actual frequency of odorant-responsive glomeruli because some glomeruli received OSN input that was evoked by both HEPT and HEX. To evaluate how the mouse's odor environment affected glomerular responsivity, we thus also quantified the observed frequency of glomeruli that received odorant-evoked input during PRE and POST imaging sessions. Contingency tables were generated for populations of individual glomeruli, and those contingency tables were then analyzed via χ^2 tests. Odorant selectivity (shown in Figure 4.4B) was also analyzed for the same populations of glomeruli by further categorizing each glomerulus as HEPT-selective, HEX-selective, or non-selective (dual, receives input evoked by both odorants), and then analyzing the resulting contingency table with log-linear regression and post hoc χ^2 tests.

Heat maps showing the patterns of spatially high-passed HEPT- and HEX-evoked activity across all glomerular ROIs from each subject were generated for both imaging sessions (examples shown in Figure 4.4C-D). Heat maps from each subject were normalized relative to the maximum across both odorants within each imaging preparation to visualize spatial similarity between the 2 odorants both before and after the 7-day exposure period. For further analyses on glomerular spatial representations, Pearson's correlation coefficients were calculated between peak HEPT- and HEX-evoked ΔF values that were normalized relative to the max across odorants within imaging preps (examples shown in Figure 4.4E-F). Correlations were performed across all individual glomerular ROIs for each subject during each imaging session.

Odorant exposure could potentially alter the temporal dynamics of OSN output to shared spatial features of the HEPT- and HEX-evoked glomerular response maps. However, because spH provides an integrative signal of exocytosis over time, the peak response amplitudes (which were used in all of the analyses described above) most frequently occur around the time of stimulus offset, and cannot inform on potential changes in temporal aspects of the nerve's output. To determine if BA exposure caused more subtle changes in the time course of HEPT- and HEX-evoked spH signals, particularly during the (relatively) early, pre-peak part of the responses, all traces from glomerular ROIs were exported through custom software written in Matlab. For both PRE and POST sessions, each individual trace, which represented a single glomerulus' fluorescence throughout the length of an entire trial, was then normalized relative to the minimum and maximum across all traces within each odorant during each imaging session. To directly compare differences between the timing of HEPT- and HEX-evoked OSN responses, the normalized

traces were then pooled separately for each odorant across individual glomeruli from each mouse, and were plotted relative to the individual minimum and maximum within each odorant during each preparation (examples shown in Figure 4.5A-B).

Results

A perceptually indiscriminable odorant pair becomes discriminable after one week of exposure to a single, chemically-different odorant.

To determine if perceptual learning occurs following our ester-odorant-exposure paradigm, we tested individual mice in the cross-habituation/dishabituation paradigm shown in Figure 4.2A both before and after 7 days of HCC or BA exposure (Figure 4.1A). All data between groups and across testing sessions are summarized in Figure 4.2B.

There was no difference in general activity levels (as indicated by investigation during the min oil trial) between the HCC and BA groups before (Figure 4.2C, PRE; independent t test, $t_{df=20} = -0.041$, $p = 0.968$) or after (Figure 4.2C, POST; independent t test, $t_{df=20} = 0.812$, $p = 0.426$) the 7-day exposure period, nor was there a change in general activity within each group between test sessions (Figure 4.2C: HCC, paired t test, $t_{df=11} = -1.645$, $p = 0.128$; BA, paired t test, $t_{df=9} = -1.012$, $p = 0.338$).

Overall, across both groups and testing sessions, mean \pm SEM investigation time was significantly higher ($F_{1,20} = 10.894$, $p = 0.004$, $\eta_p^2 = 0.353$) during the first HEX trial (HEX1) than during the mineral oil trial (min oil, 9.741 ± 0.990 ; HEX1, 13.317 ± 0.765). This increase in investigation time (Figure 4.2B) suggests that subjects were able to detect HEX on its first presentation. Importantly, the lack of a significant testing time (PRE; POST) \times trial type (min oil; HEX1) \times group (HCC; BA) interaction (Figure 4.2B; $F_{1,20} =$

0.261, $p = 0.615$, $\eta_p^2 = 0.013$) and the lack of a between-groups difference during the first HEX trial alone (Figure 4.2D; $F_{1,20} = 0.000$, $p = 0.995$, $\eta_p^2 = 0.000$) confirms that the propensity to investigate an odor stimulus on its first presentation was comparable between groups and across testing sessions.

All subjects exhibited behavioral habituation across 4 presentations of HEX (Figure 4.2B; main effect of trial, $F_{3,60} = 177.410$, $p \leq 0.001$, $\eta_p^2 = 0.889$), and the rate of habituation did not differ between groups or across testing sessions (non-significant testing session \times trial \times group interaction, $F_{3,60} = 0.343$, $p = 0.794$, $\eta_p^2 = 0.017$).

During PRE-exposure testing, there was no evidence of discrimination between the 2 odorants, as all mice cross-habituated by significantly reducing their investigation time during the test trial (Figure 4.2E, left; effect of trial, $F_{1,20} = 7.548$, $p = 0.012$, $\eta_p^2 = 0.274$), regardless of group assignments (Figure 4.2E, left; non-significant trial \times group interaction, $F_{1,20} = 0.154$, $p = 0.699$, $\eta_p^2 = 0.008$). Overall, across both groups during PRE-exposure testing, cross-habituation was thus characterized by a $\sim 6.9 \pm 2.7\%$ decrease in odor investigation (Figure 4.2F, left). When subjects were tested a second time after the week-long exposure period, animals in the HCC group continued to cross-habituate, whereas the BA-exposed animals exhibited dishabituation and tended to increase their investigation times during the test (HEPT) trial (Figures 4.2E, right; trial \times group interaction, $F_{1,20} = 8.458$, $p = 0.009$, $\eta_p^2 = 0.297$; & 4.2F, right).

A week-long ester-odorant exposure does not alter the peak response amplitudes or overall spatial representations of two unexposed aldehydes.

Figure 4.3A-B shows resting fluorescence images of the dorsal olfactory bulb through the cranial window, as well as example pseudocolored difference maps showing

the pattern of HEPT- and HEX-evoked OSN synaptic input to olfactory bulb glomeruli before and after 7 days of HCC (Figure 4.3A) and BA (Figure 4.3B) exposure. As expected from the PRE-exposure (baseline) behavioral data (Figure 4.2E, left and Figure 4.2F, left), the initial neural representations of HEPT and HEX included highly-overlapping populations of OSNs – at baseline, 53% of glomeruli (pooled across all subjects) received OSN input evoked by both HEPT and HEX.

The effects of HCC and BA exposure on peak HEPT- and HEX-evoked response amplitudes (Figure 4.3C-D) were evaluated, as described above. On average, we observed no change in the HEPT- or HEX-evoked peak ΔF for either the HCC group (Figure 4.3C & 4.3E; $F_{1,3} = 0.054$, $p = 0.831$, $\eta_p^2 = 0.018$) or the BA-exposed group (Figure 4.3D & 4.3E; $F_{1,3} = 0.092$, $p = 0.782$, $\eta_p^2 = 0.030$), nor did we observe a difference when we pooled across individual ΔF values within each imaging session for each group (Figure 4.3F-G).

We next found that the average number of glomeruli receiving measurable synaptic input during HEPT and HEX presentations remained unchanged after 1 week of either HCC ($F_{1,3} = 2.227$, $p = 0.232$, $\eta_p^2 = 0.426$) or BA ($F_{1,3} = 0.226$, $p = 0.667$, $\eta_p^2 = 0.070$) exposure (Figure 4.4A). Additionally, the observed frequency of aldehyde-responsive glomeruli (that responded to HEPT alone, HEX alone, or to both HEPT and HEX) remained stable over time in the HCC group ($N_{\text{PRE}} = 99$, $N_{\text{POST}} = 88$; $\chi^2 = 0.647$, $p = 0.421$) and also in the BA-exposed group ($N_{\text{PRE}} = 125$, $N_{\text{POST}} = 115$; $\chi^2 = 0.417$, $p = 0.519$). We then assessed potential changes in the selectivity of HEPT-, HEX-, and dual-odorant-responsive glomeruli, and found that the relative frequency of glomeruli within each of the 3 selectivity categories for each group did not change across imaging sessions (Figure 4.4B; non-significant 3-way, higher order effect, $\chi^2_{(df=2)} = 1.666$, $p = 0.435$). Instead,

aldehyde-responsive glomerular populations were best accounted for by a model with a 1-way effect ($\chi^2_{(df=11)} = 232.45, p \leq 0.001$), where the selectivity categorization itself was the strongest predictor of frequency distributions (partial, 1-way association of selectivity, $\chi^2_{(df=2)} = 212.692, p \leq 0.001$). That is, the best predictor of a glomerulus' odorant-selectivity after exposure was its selectivity before exposure.

Because BA exposure had no effect on the average number of glomeruli contributing to peak HEPT- and HEX-evoked glomerular representations (Figure 4.4A), or on the selectivity of individual aldehyde-responsive glomeruli (Figure 4.4B), the overlapping spatial features of peak HEPT- and HEX-evoked glomerular response maps probably also remained quite similar after BA (or HCC) exposure. Investigation of heat maps showing the patterns of normalized HEPT- and HEX-evoked activity across all glomerular ROIs from each subject confirm that the spatial similarity between the 2 aldehydes was not altered by 7 days of home cage (Figure 4.4C) or ester-odorant (Figure 4.4D) exposure. Additionally, the correlation between peak HEPT- and HEX-evoked ΔF s across all glomerular ROIs for each subject was not reduced by 7 days of home cage (Figure 4.4E) or BA (Figure 4.4F) exposure, providing further evidence that the spatial similarity between the 2 aldehydes was stable over time in both groups.

Exposure to a single ester odorant can modify temporal properties of OSN responses to unexposed, aldehyde homologues and consequently enhance contrast between shared representational features.

Although 7 days of ester-odorant exposure did not alter the number of glomeruli receiving aldehyde-evoked OSN input (Figure 4.4), or the peak response magnitude of those inputs (Figure 4.3), it did induce a form of perceptual learning which lead to

behavioral discrimination of aldehyde homologues that were indiscriminable at baseline (Figure 4.2). Odor information is not solely represented by the static pattern of activity that is mapped across the glomerular layer of the olfactory bulb, but is also represented by the temporal structure of that activity (Wachowiak and Shipley, 2006). Thus, while BA exposure did not change the static patterns of HEPT- and HEX-evoked activity, it could have altered the temporal dynamics of those activity patterns in a way that would enhance contrast between shared features, and that would consequently parallel the perceptual effects shown in Figure 4.2.

To test this, fluorescence records (traces) from all glomerular ROIs that were statistically confirmed as HEPT- or HEX-evoked responses were normalized relative to the minimum and maximum fluorescence values throughout the full trial duration and across all ROIs within each odorant-evoked activity pattern during each preparation. Because the shape of the spH waveform indicates cumulative neurotransmitter release, this analysis permitted a qualitative evaluation of the temporal structure of the HEPT- and HEX-evoked input to the brain, independent of response magnitudes and static maps. The temporal dynamics of HEPT- and HEX-evoked activity were highly similar before the week-long exposure period in HCC (Figure 4.5A, left) and BA-exposed (Figure 4.5B, left) subjects. After one week of HCC exposure, the time course of HEPT- and HEX-evoked activity remained relatively similar (Figure 4.5A, right), whereas the temporal response profiles of HEPT- and HEX-evoked activity became more distinct after BA exposure (Figure 4.5B, right). While Figure 4.5A-B shows data from 2 representative mice, the same results were obtained when we plotted mean \pm SEM traces pooled across glomerular ROIs from all subjects in the HCC ($N_{\text{HEPT}} = 100$; $N_{\text{HEX}} = 70$) and the BA-exposed ($N_{\text{HEPT}} = 123$; $N_{\text{HEX}} =$

98) groups before and after exposure. This result suggests that after BA exposure, but not HCC exposure, HEPT- and HEX-evoked neural activity become more discriminable on the basis of their temporal structures (Figure 4.5A-B).

Discussion

Consistent with previous reports (Mandairon et al., 2006b) we found that a perceptually-indiscriminable aldehyde pair becomes discriminable to a mouse after one week of exposure to an ester (chemically-different) odorant. Visualizing aldehyde-evoked OSN synaptic output *in vivo* revealed no changes in the spatial patterns of activity across olfactory bulb glomeruli after the week of odorant exposure and no change in total neurotransmitter release in each glomerulus during the six second odor presentation. However, we did observe that the ester exposure induced modest changes in the temporal dynamics of OSN responses to the unexposed pair of homologous aldehydes. These results are concordant with a large body of research showing that sensory enrichment can enhance neural and perceptual contrast between olfactory stimuli in a relatively non-specific manner, and additionally show that experience-dependent modulation of olfactory temporal coding can occur in primary sensory representations.

Consistent with earlier reports (Kass et al., 2013d), we found that the number of glomeruli receiving aldehyde-evoked input from OSNs, and the peak magnitudes of those inputs, was not altered by seven days of exposure to an ester. In the present experiments, we extended those findings to show that these odor-evoked spatial response maps remained stable, even in an exposure paradigm that successfully induced a perceptual difference between the odors. However, we did observe a modest change in the temporal dynamics

of HEPT- and HEX-evoked OSN neurotransmitter release such that the timing of the odorant-evoked signal became more different between the odorants. This timing change would likely be perceptible to a mouse (Smear et al., 2013), and thus could potentially facilitate odor discrimination by downstream circuitry.

How could exposure to an ester odorant, which principally activates one subset of OSNs, alter the timing of the response to aldehydes in a different subset of OSNs? Odorant exposure has been reported to alter the transduction kinetics of MOR23-expressing OSNs, but not M71-expressing OSNs (Cadiou et al., 2014). It is therefore possible that ester exposure directly induced temporal changes in the odor response of some OSN populations, but not others, such that subsequent aldehyde presentation evoked more diverse timing. Alternatively, it is possible that the timing was being regulated by periglomerular feedback at the OSN synaptic terminal, which receives strong presynaptic inhibition arising from GABAergic and dopaminergic PG circuitry (McGann et al., 2005; Murphy et al., 2005; McGann, 2013). The multiglomerular nature of the latter circuitry makes it an appealing vehicle for this non-odor selective effect, and this circuitry has been shown to exhibit neurochemical plasticity after odor exposure (Woo and Leon, 1995; Bovetti et al., 2009; Bonzano et al., 2014).

Given the considerable evidence that static maps of peak or total glomerular activity predict the perceptual quality of an odor (Linster et al., 2001; Cleland et al., 2007), and that the difference between these maps predicts the discriminability of odors (Youngentob et al., 2006), it was perhaps unexpected that the OSN peak response maps remained unchanged while the mice began to discriminate the two aldehydes. In a way, the present finding that odor perception can change while the static OSN response map remains

constant is the complement of a previous finding that odor perception can remain at least relatively constant while the OSN response map changes dramatically (Homma et al., 2009). While the observed differences in OSN timing may certainly play a role in making the aldehyde patterns easier for the bulb to decorrelate (Linster and Cleland, 2010), it is also interesting if they do not, because it suggests that later circuitry in the olfactory system can produce perceptions that at least somewhat disagree with the glomerular map. This could include lateral inhibition arising from reciprocal synaptic interactions between mitral/tufted cells and olfactory bulb interneurons (Yokoi et al., 1995; Isaacson and Strowbridge, 1998), or feedback circuitry between the bulb and other structures. Olfactory sensory experience can refine lateral inhibition and thus sharpen odor-driven activity such that contrast is enhanced between stimulus representations, at least on some time scales (Fletcher and Wilson, 2003).

Activity in forebrain and brainstem transmitter systems that can modulate the inhibitory bulbar circuitry mediating lateral inhibition may also contribute to the exposure-induced perceptual and neural plasticity that we observed here. Acetylcholine, for example, has been implicated in normal odor discrimination abilities as well as in perceptual learning (Wilson et al., 2004), and pharmacologically manipulating cholinergic activity in the olfactory bulb can mimic the perceptual effects associated with odorant exposure (Mandairon et al., 2006c). Furthermore, odor-exposure-induced spontaneous discrimination between homologous esters is eliminated when a cholinergic antagonist is peripherally administered during the initial exposure period (Fletcher and Wilson, 2002). An alternative mechanism for the enhanced perceptual and neural contrast that we observed between homologous aldehydes after exposure could be related to noradrenergic-mediated

tuning of inhibitory circuitry in the olfactory bulb (Jiang et al., 1996; Shea et al., 2008; Linster et al., 2011; Eckmeier and Shea, 2014). Similar to the exposure-induced perceptual effects reported here, noradrenergic modulation of the olfactory bulb circuitry enhances the perceptual discriminability of highly similar odorants (Escanilla et al., 2010; Linster et al., 2011), and recent work has also shown that noradrenergic input to the olfactory bulb during the time of odorant exposure is necessary for the subsequent exposure-induced perceptual learning to occur (Moreno et al., 2012; Viner et al., 2015).

In sum, the results reported here exemplify the ability of the adult olfactory system to adapt coding strategies based on passive experience with stimuli in the surrounding environment. The underlying mechanisms for this neurophysiological plasticity may include stimulus-driven changes in the olfactory bulb circuitry mediating multiglomerular communication and lateral inhibition, as well as modulation of that circuitry by diffuse transmitter systems and top-down input from higher olfactory sensory regions.

Acknowledgements

I thank Stephanie Guang for assisting with the cross-habituation/dishabituation behavioral experiment, and Andrew Moberly for surgically implanting cranial windows prior to imaging procedures.

Chapter 4 Figures

Figure 4.1

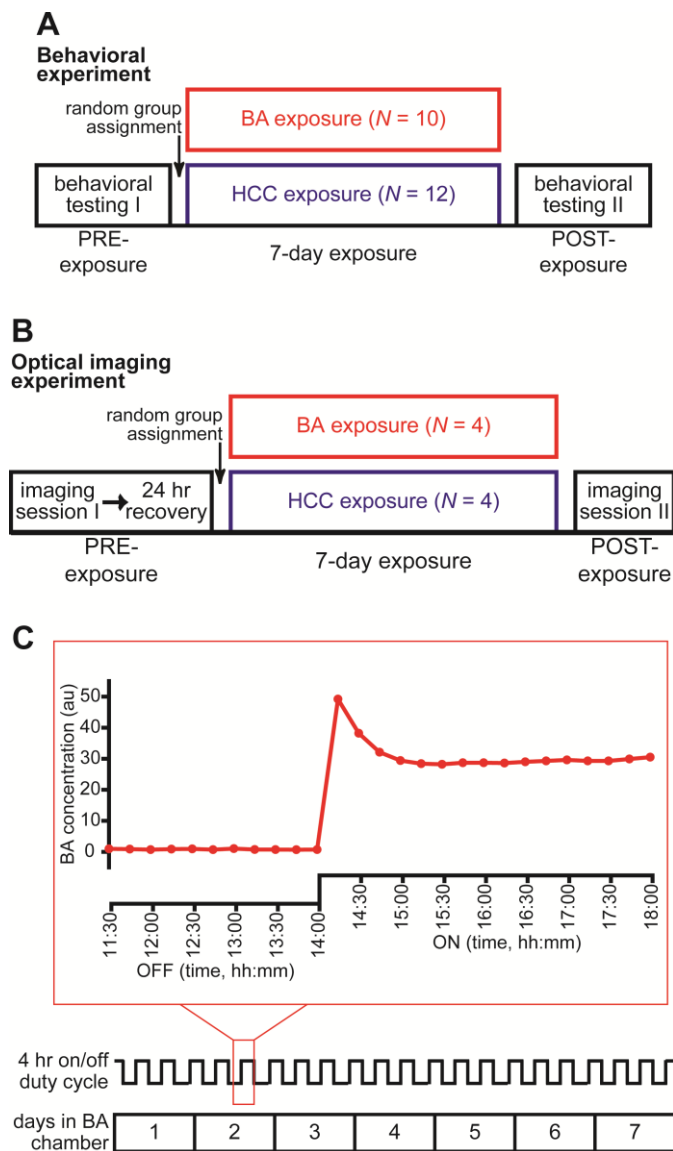


Figure 4.1. Summary of experimental procedures. (A-B) Timeline of the behavioral (A) and optical imaging (B) experiments showing HCC and BA group assignments. (C) Timeline of the 7-day exposure period in a BA exposure chamber (bottom) with a trace (middle) indicating the time course of the 4-hour duty cycle. The outlined portion of the duty cycle is expanded immediately above the trace (top) to show photoionization measurements that were continuously sampled once every 15 minutes during the last 2.5

hours of an OFF cycle and then during the entire 4-hour ON cycle. Animals that were assigned to the HCC group followed the same 7-day timeline, but were housed in standard cages.

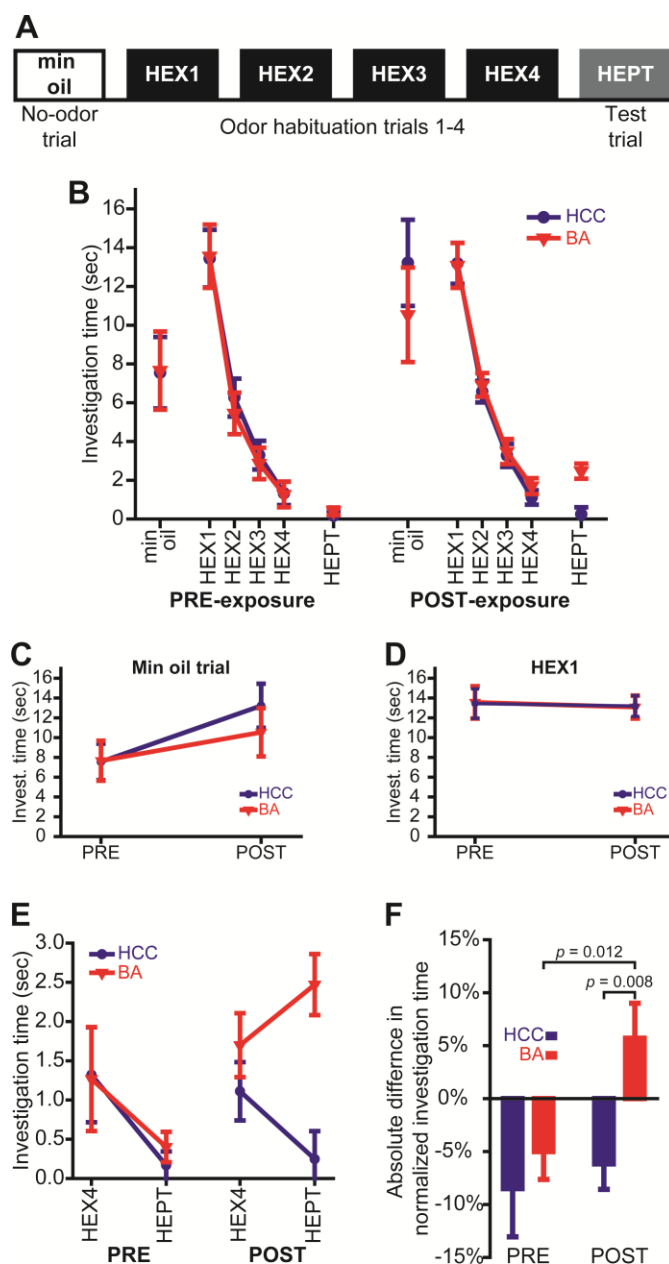
Figure 4.2

Figure 4.2. Chronic odorant exposure enhances olfactory discrimination abilities, but does not alter general motor activity or the propensity to investigate an odor object. (A) Procedure summary for the habituation/dishabituation testing protocol. (B) Summary of all data from PRE- and POST-exposure testing sessions. (C-D) Investigation time during the mineral oil (no odor) trial (C) and the first habituation trial (HEX1) (D) before (PRE) and after (POST) the 7-day exposure period. (E) Investigation time during the last

habituation trial (HEX4) and the test trial (HEPT) before and after HCC or BA exposure. **(F)** Difference scores (normed HEPT minus normed HEX4) for both groups during both behavioral test sessions. The data in **B-F** are shown as group means \pm SEMs, and p values are by between-groups or paired t tests.

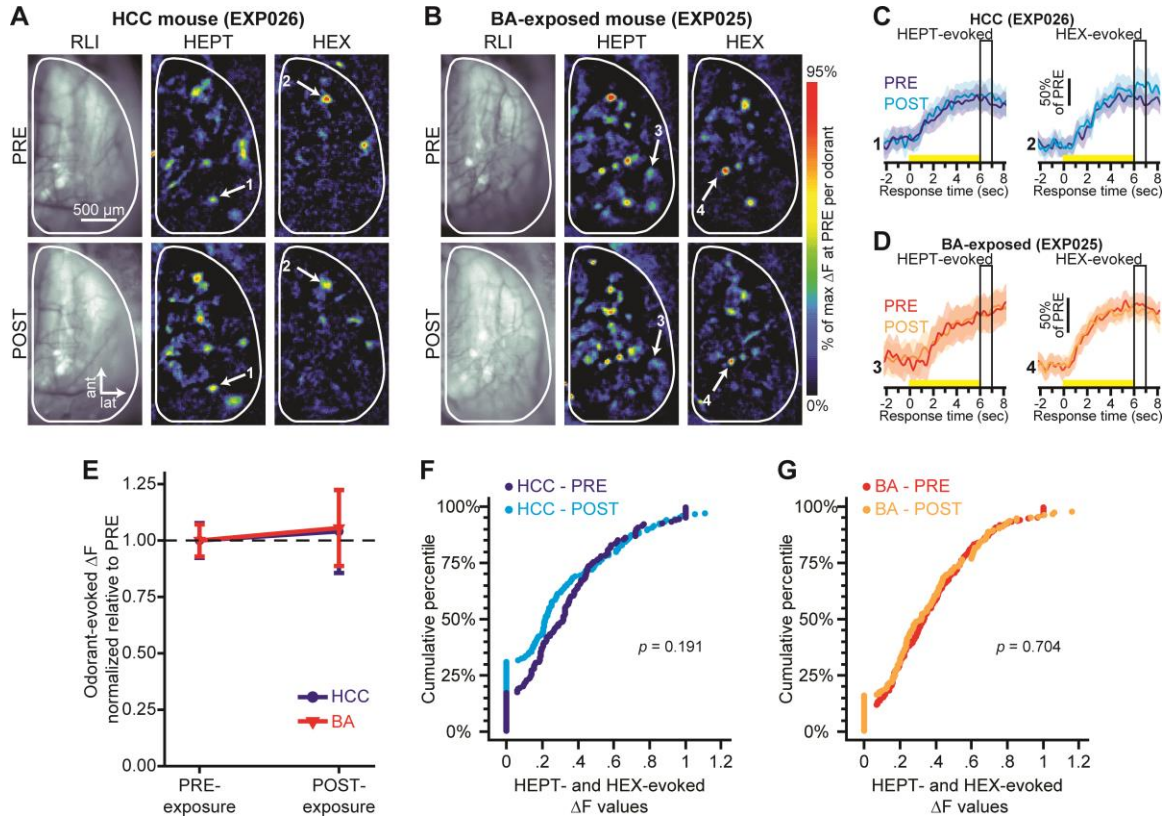
Figure 4.3

Figure 4.3. Peak HEPT- and HEX-evoked response amplitudes are stable over time in both HCC and BA-exposed groups. (A-B) Example resting light intensity (RLI) images (left) and pseudocolored HEPT- and HEX-evoked difference maps (middle and right) from a HCC mouse (A) and from a BA-exposed mouse (B) before (top, PRE) and after (bottom, POST) the 7-day exposure period. (C-D) Sets of traces from a HCC mouse (C) and a BA-exposed mouse (D) corresponding to the numbered callouts in A-B. Each set of traces was evoked by either HEPT (left) or HEX (right) both before and after the 7-day exposure period. Solid traces and surrounding shading show the mean \pm SEM HEPT- or HEX-evoked spH signal across 5-6 trials. Yellow stimulus bars indicate the time of odorant presentations. Boxed regions indicate the response time corresponding to the peak odorant-evoked response maps shown in A-B and the analyses that are summarized in E-G. (E) Mean \pm SEM normalized odorant-evoked change in fluorescence (ΔF) pooled across odorants in HCC and BA-exposed mice, and plotted as a function of the time of imaging. (F-G) Cumulative probability plots showing the distributions of normalized

odorant-evoked ΔF values before and after 7 days of housing in a home cage (**F**) or an exposure chamber (**G**). For each group, data are pooled across all subjects and odorants. P values are by Wilcoxon signed ranks test: HCC, $N_{\Delta Fs} = 156$; BA, $N_{\Delta Fs} = 198$.

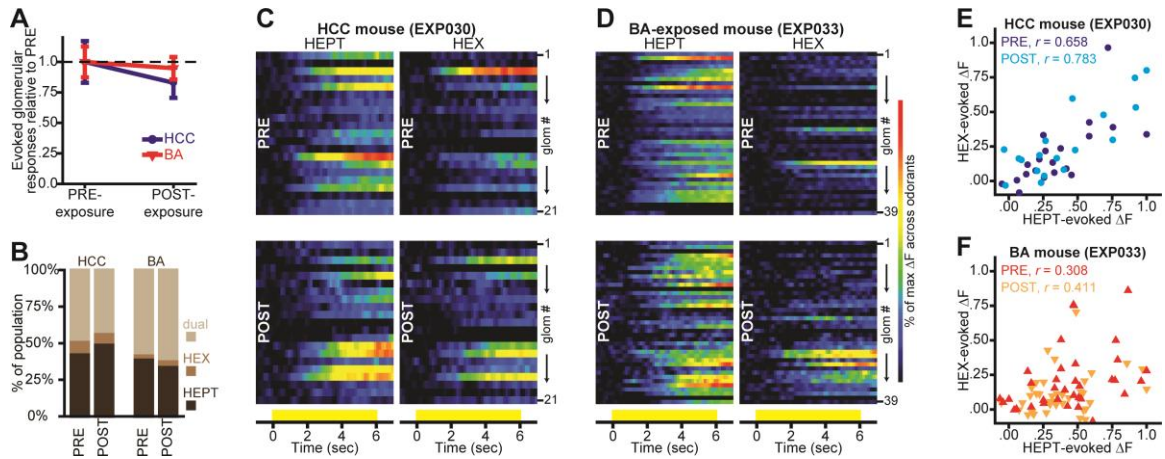
Figure 4.4

Figure 4.4. Aldehyde-evoked spatial maps are not altered by one week of HCC or ester-odorant exposure. (A) Mean \pm SEM number of odorant-evoked glomerular responses pooled across odorants in HCC and BA-exposed mice, and plotted as a function of the time of imaging. (B) Percentage of HCC and BA-exposed glomerular populations that were categorized as receiving input from OSNs stimulated by HEPT-alone, HEX-alone, or by both HEPT and HEX before (PRE) and after (POST) the week-long exposure period. (C-D) Pseudocolored heat maps from example HCC (C) and BA-exposed (D) mice, showing HEPT- (left) and HEX- (right) evoked activity across all glomerular ROIs PRE- (top) and POST- (bottom) exposure. Activity maps are scaled relative to the max across both odorant within each imaging session. Each row in a heat map represents the activity of a glomerular ROI (glom # $1 \rightarrow N$), and all ROIs are matched across all heat maps for each subject. Yellow bars indicate the time of odorant presentations. (E-F) Scatterplots from HCC (E) and BA-exposed (F) mice showing peak HEX-evoked ΔF values plotted as a function of peak HEPT-evoked ΔF values for all glomerular ROIs shown in C-D.

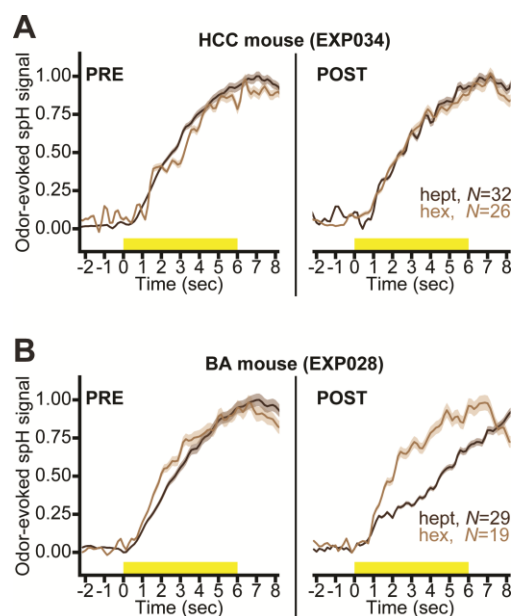
Figure 4.5

Figure 4.5. Ester-odorant exposure alters the temporal dynamics of activity in overlapping aldehyde-evoked glomerular response maps. (A-B) Normalized HEPT- and HEX-evoked spH signals before (PRE, left) and after (POST, right) HCC (**A**) or BA (**B**) exposure. Solid lines surrounded by shading show the mean \pm SEM odorant-evoked spH signals pooled across all glomerular ROIs (N s are indicated in each plot).

CHAPTER 5

Fear learning enhances neural responses to threat-predictive sensory stimuli

The results from this chapter are reported in Kass MD*, Rosenthal MC*, Pottackal J, McGann JP (2013b) Fear learning enhances neural responses to threat-predictive sensory stimuli. *Science* 342:1389-92. **co-first authors.*

Abstract

The central nervous system rapidly learns that particular stimuli predict imminent danger. This learning is thought to involve associations between neutral and harmful stimuli in cortical and limbic brain regions, though associative neuroplasticity in sensory structures is increasingly appreciated. We observed the synaptic output of olfactory sensory neurons (OSNs) in individual mice before and after they learned that a particular odor indicated an impending foot shock. OSNs are the first cells in the olfactory system, physically contacting the odor molecules in the nose and projecting their axons to the brain's olfactory bulb. OSN output evoked by the shock-predictive odor was selectively facilitated after fear conditioning. These results indicate that affective information about stimuli can be encoded in their very earliest representations in the nervous system.

Introduction

Associative learning can alter cortical and even pre-cortical processing in mammalian sensory systems (Kay and Laurent, 1999; Chen et al., 2011; Doucette et al., 2011; Gdalyahu et al., 2012). However, the primary sensory input is generally thought to be determined by the physical stimulus itself, independent of any prior information the subject may have learned about that stimulus. The development of stably expressed optical activity indicators in mice now permits longitudinal experiments testing whether sensory inputs to the brain remain constant as an individual mouse learns about specific sensory stimuli.

Associative fear conditioning, in which an animal learns that a neutral sensory stimulus predicts the occurrence of an aversive stimulus, can alter the processing of threat-predictive sensory stimuli (Barrett and Bar, 2009; Headley and Weinberger, 2013; Krusemark and Li, 2013). In the olfactory system, fear learning has been shown to enhance difficult olfactory discriminations (Li et al., 2008) and alter odorant-evoked neural activity in the piriform cortex and olfactory bulb (Li et al., 2008; Fletcher, 2012).

Methods

Subjects.

A total of 46 mice were used in the experiments reported here. Specifically, 14 heterozygous ($n = 7$) and homozygous ($n = 7$) OMP-spH mice were used for optical imaging experiments. Wild-type C57BL/6 mice (Charles River Laboratories) were used in experiments for behavioral testing ($N = 21$) and for respiration measurements ($N = 11$). All animals were adult males.

Discriminative olfactory fear conditioning.***Apparatus.***

Behavioral training and testing took place in conditioning chambers (model H10-11M-TC) located inside ventilated and sound-attenuated isolation cubicles (model H10-24A) from Coulbourn Instruments (Habitest System). During context pre-exposure and training days, the chamber floors were modular shock floors (model H10-11M-TC-SF) consisting of 16 metal bars that were controlled by a precision animal shocker (model H13-15). During behavioral testing, a separate chamber that was made distinct from the conditioning chambers by adding blue stripes to the walls and replacing the modular shock floor with a white, plastic floor was used to create a novel spatial context. The behavioral testing chamber was also equipped with a camera that was mounted inside of the isolation cubicle, providing an aerial view of the operant chamber for behavioral analysis. All chambers were operated through programs written in Graphic State 3.03 software. A house light was turned on for the duration of each (training and testing) session. All chambers were washed before and after each session using a tergazyme (10g/L) solution followed by an ethanol (70%) solution.

Each conditioning chamber was equipped with its own custom-built olfactometer and was modified to contain a port for odor delivery (2.5 cm above the floor) and a vacuum exhaust for odor removal. The (ester) odorants methyl valerate (MV) and *n*-butyl acetate (BA) were diluted 1:200 in mineral oil and were presented at a flow rate of 1 sL/min. Steady-state concentrations of odorant stimuli were achieved across training and testing days and between subjects by calibrating the odorants daily prior to experimentation via a photoionization detector (ppbRAE plus). Training and testing sessions did not begin until

the olfactometer calibrations yielded odorant concentrations (reported in arbitrary units, a.u.) that peaked at 8 a.u. (see Figure 5.1B, top) when measured from the center of the conditioning chamber at approximately the animal's nose height (~2.5 cm). To ensure that the odorant stimuli used during behavioral training and optical imaging sessions were matched, the same stimulus calibration procedure was used prior to imaging experiments.

Procedure.

The fear conditioning paradigm is illustrated in Figure 5.1A. All animals received 3 daily context pre-exposures that each consisted of a 10 min session in the conditioning chamber (without any odorant or shock stimuli being presented). Context pre-exposure was followed by a baseline imaging session and subsequent recovery day for mice used in the imaging experiment, while mice used in the behavioral and respiration experiments had 2 days of rest in the home cage (to match the study time line across experiments). All subjects were randomly assigned to 1 of 3 groups that then underwent 3 daily sessions of fear or control training. For subjects in the Paired group, each daily training session (see Figure 5.1B, bottom) began with a 180-sec acclimation period that was followed by 10 randomly-presented trials that were given at variable (140-200 sec) ITIs. Individual trials consisted of ~15-sec odorant presentations that either co-terminated with a 0.4-mA, 0.5-sec footshock (for the CS⁺ odorant, $n = 5$ trials; for sample trial see Figure 5.1B, top) or were presented without shock (for the CS⁻ odorant, $n = 5$ trials). Two esters (MV and BA) were counterbalanced as the CS⁺ and CS⁻ across subjects in the paired group. Daily training for subjects in the Odor Alone control group consisted of the same fear conditioning paradigm, but *without* the presentation of any shocks. Specifically, these subjects received a 180-sec acclimation period followed by 5 MV trials and 5 BA trials (~15 sec/trial) that

were presented in random order at the same variable ITI per daily session. Shock Alone control training consisted of the same fear conditioning paradigm used for the paired group, but *without* the presentation of any odorants. The duration of a shock alone control training session was equivalent to that in the other groups and consisted of a shock exposure that was equivalent to that in the paired group (i.e., 5 shocks/day, but with no odorants).

Twenty-four hours after the last fear or control training session, subjects in the optical imaging experiment underwent a second imaging session, subjects in the behavioral experiment underwent behavioral testing, and subjects in the respiration experiment underwent respiratory recordings. In the behavioral study, mice were tested for odorant-evoked conditioned freezing in a novel context. This test session consisted of 1) a CS⁺ trial, 2) a CS⁻ trial, and 3) a clean air control trial. The 3 trials were 60 sec in duration and randomly presented at variable ITIs ranging from 4 to 6 min. Note that no shocks were presented during the test session. Additionally, while there were always 3 trials presented during the test session, the 3 trials were only comprised of 2 odor types for subjects in the shock and odor alone control groups: 1) unpaired odorants (MV and BA) and 2) clean air. Behavioral test sessions were video-recorded and analyzed offline for conditional freezing. Freezing behavior was operationalized as the absence of all visible movement save for respiration and was manually scored during each 60-sec trial via Etholog 2.2 (Ottoni, 2000). The raw freezing data (in sec) from each subject was then converted into percent time freezing during each 60-sec trial and analyzed across groups and trial types.

In vivo optical imaging procedures and analyses.

Procedures for the implantation of chronic cranial windows and subsequent acquisition of odorant-evoked spH signals were performed as described under General

Methods. Subjects were anesthetized, secured under the imaging apparatus, and presented with a panel of up to 5 odorants including the CS⁺ and the CS⁻ (which were counterbalanced MV and BA), an unexposed ester (isoamyl acetate, IAA), and 2 unexposed aldehydes (heptanal, HEPT; hexanal, HEX). To determine if the effects of fear learning on early olfactory processing are concentration-dependent, we presented both of the training esters (i.e., MV and BA) at 3 concentrations, including 4 a.u., 8 a.u. (the training concentration), and 16 a.u. To investigate the odorant specificity of learning-induced plasticity in primary sensory representations of olfactory stimuli, we presented the other 3 unexposed/untrained odorants (i.e., IAA, HEPT, and HEX) at 8 a.u. to be comparable to the relative training concentration of the conditioning esters.

Glomerular ROIs were hand-selected in the blank-subtracted average response maps for each concentration of each odorant stimulus. To quantify the peak odorant-evoked change in fluorescence (ΔF), spH signals for each trace corresponding to a glomerular ROI were determined by subtracting 1 sec of baseline frames (acquired during the pre-odorant baseline) from 1 sec of frames centered around the peak trace inflection after odorant onset. Because spH provides an integrative signal of exocytosis over time, the peak response magnitudes typically occurred after the end of the 6-sec odorant presentation (frames 78-84 were used for this subtraction). To evaluate potential changes in the evolution of glomerular response maps evoked by the 2 conditioning esters, we then performed 3 more subtractions and generated a time course of sub-maximal (i.e., pre-peak) response maps that were evoked throughout an odorant presentation (see Figure 5.8). Specifically, we subtracted the average of 7 baseline frames from the average of frames 1) 36-42 (1-2 sec during odorant), 2) 50-56 (3-4 sec during odorant), and 3) 64-70 (5-6 sec

during odorant). SpH signals in the first second of the odorant presentation were not compared because of the low signal-to-noise ratio and to limit the influence of trial-to-trial variability in the respiratory phase at odorant onset. Non-parametric statistical tests, including Kolmogorov-Smirnov (K-S), Mann-Whitney (M-W), rank sign, Friedman, and χ^2 tests, were performed to evaluate changes in populations of glomerular responses. Parametric tests, including ANOVAs and t tests, were used to evaluate changes in central tendencies of groups based on means from individual subjects.

Odorant-evoked ΔF values were always normalized so that we could pool data across glomeruli and mice. To determine if the effects of fear learning were stimulus-specific, we normalized the peak evoked ΔF values relative to the maximum evoked ΔF value that was measured during pre-training imaging. This normalization was performed separately within each category of stimuli and was calculated across both pre- and post-imaging sessions per mouse. No differences in IAA-, HEPT-, and HEX-evoked spH signals were observed between imaging sessions in any group, and thus, as intended, the responses evoked by these 3 unexposed odorants were pooled together for all subsequent analyses. The distributions of normalized peak ΔF values are shown in Figure 5.2E-J.

In a separate set of analyses evaluating potential changes in the temporal evolution of CS⁺- and CS⁻-evoked response maps during the odorant presentation, we normalized all of the pre- and post-training ΔF values per mouse relative to the maximum evoked ΔF value across all response times measured within each conditioning odorant during pre-training imaging. The distributions of these normalized ΔF values are shown in Figure 5.9 and the means pooled across glomeruli are displayed in Figure 5.6C. A second normalization was performed separately on each time bin to determine if the CS⁺-specific

enhancement of odorant-evoked nerve output varied across time during the odorant presentation. For example, each measurable ΔF value that was evoked between 1 and 2 sec of an odorant presentation during both pre- and post-training imaging sessions was divided by the maximum evoked ΔF within that bin during the pre-training imaging session, etc. These data are shown in Figure 5.6D.

To generate odorant-specific concentration response functions, we normalized the peak ΔF values that were evoked by each concentration of the CS⁺ and CS⁻ (simply MV and BA for the control groups) relative to the maximum evoked ΔF across concentrations (and within each odorant) during the pre-training imaging session. The mean concentration response functions pooled across glomeruli are shown in Figure 5.12 and in Figure 5.14. We also repeated this normalization for activity measured within the first time bin (pre-peak responses, Figure 5.13) and generated concentration response functions for the earliest response time that we quantified. A second normalization was performed on these data to directly compare relative changes in OSN output per concentration. As shown in Figure 5.12F, peak evoked ΔF values that were evoked by each concentration of each odorant were normalized relative to the max evoked response per concentration during pre-training imaging.

The Euclidean distances (EDs) between CS⁺-, CS⁻-, and IAA-evoked glomerular response maps were calculated on a frame-by-frame basis (1 frame = ~0.143 sec) to permit a network-level analysis for each individual mouse in the paired group. Specifically, differences among odorant-evoked glomerular response maps were quantified as EDs in N -dimensional vector space, where N was equivalent to the number of glomerular regions of interest identified in each imaging session in each mouse. Note that glomerular regions

of interest included glomeruli that received odorant-evoked OSN input (per our statistical thresholding criterion) and control regions. Control regions were included in this analysis to more accurately capture the similarity-dissimilarity between overall odor representations. That is, areas of the bulb that are not receiving odorant-evoked OSN input affect the overall spatial features of a given odor map, and thus its discriminability from other odor representations. For both pre- and post-training imaging sessions, there were 6 individual ED comparisons that were made for all 3 combinations of odor maps: 1) CS^+ vs. CS^- , 2) CS^+ vs. IAA, and 3) CS^- vs. IAA. The 6 individual ED comparisons corresponded to 6 CS^+ trials, 6 CS^- trials, and 6 IAA trials that were paired up based on chronology of trial number (e.g., ED between CS^+_{t1} and CS^-_{t1} , ED between CS^+_{t2} and CS^-_{t2} , etc.). The mean \pm SEM ED between each pair of odor maps was calculated over the duration of the stimulus presentations for each mouse by averaging frames within the six trial-by-trial comparisons. An example of this analysis in one mouse is shown in Figure 5.6G-H and Figure 5.11A-C. The network-level analysis pooled across all mice in the paired group is shown in Figure 5.11D-G.

To perform odorant response selectivity analyses for the paired group, we first binarized the data per odorant. Specifically, if an ROI was statistically included as a glomerulus receiving odorant-evoked OSN input during any of the 4 time bins that we measured, then it was coded with a 1 (if not, it was coded with a 0). This binarization was first performed separately for CS^+ - and CS^- -evoked activity within each individual glomerulus. The binarized response profiles per glomerulus were then combined by summing across odorants, yielding 3 possible categories of response selectivity profiles: 1) CS^+ -selective glomeruli (1,0); 2) CS^- -selective glomeruli (0,1); and 3) non-selective (dual-

responsive) glomeruli (1,1). We used this glomerular categorization to evaluate changes in response magnitudes based on odorant selectivity.

Potential structural changes (Jones et al., 2008) were first assessed through quantifying the frequency of glomeruli considered to be receiving OSN input during odorant presentations. In addition to changes in the absolute number of glomeruli per (PRE vs. POST) population, we considered alterations in the distributions of glomeruli within each selectivity category (Figure 5.6F). Next, we quantified the odorant-evoked response size corresponding to each glomerular ROI by totaling the number of pixels per region and converting to μm^2 to determine the glomerular response area. Under the imaging conditions detailed above, 1 pixel was equivalent to $318.87751 \mu\text{m}^2$. The average glomerular surface response area, pooled across all (pre- and post-training) glomerular regions of interest, was $7264.56 \pm 152.04 \mu\text{m}^2$. These data are separated by imaging session and selectivity category and shown relative to baseline in Figure 5.6E.

Respiration recordings and analysis.

The piezosensor method was validated in a control experiment performed on a naïve, deeply-anesthetized mouse (Figure 5.5A-C). Respiration was monitored simultaneously by a thermocouple (Kass et al., 2013c) positioned extranasally and a force-transducing piezosensor strip positioned just below the diaphragm. The latencies of inhalation (and exhalation, not shown) onset-related events during a single respiration cycle were recorded by each method and compared across the full duration of the recordings. To further validate the piezosensor, we then demonstrated a quantitative relationship between the thermocouple- and piezosensor-generated waveforms. Average waveforms were obtained by aligning each cycle to the peak value recorded by the

piezosensor. For the n th point of the average waveform, the value of the antiderivative at time t_n was obtained by summing the value of the antiderivative at time t_{n-1} with the product of the average waveform at t_{n-1} and the sampling rate. The initial value of the first antiderivative at time t_0 was chosen such that the area bounded by the first antiderivative and the t -axis was zero. The second antiderivative was multiplied by a constant to match the amplitude of the thermocouple waveform and its initial value was chosen such that its maximum and minimum values were equal to those of the thermocouple waveform. To convert to phase (in radians), each time point was then multiplied by $2\pi/T_w$, where T_w is the period of the average waveform.

In a separate experiment, mice were trained on a discriminative fear conditioning paradigm that followed the same time line and used the same counterbalanced conditioning odorants as that used for behavioral and optical imaging studies, as detailed above (Figure 5.1A). Compared to that shown in Figure 5.1B, modifications to the olfactometers that were connected to the conditioning chambers prior to beginning this experiment caused modest differences in the timing of odor presentations during fear training. Approximately 24 hours after the last training day, mice were anesthetized with pentobarbital (as in the imaging experiments) and underwent surgical head-mounting procedures that were comparable to those used in the imaging procedures. While mice were mounted and deeply anesthetized, respiration was then recorded during presentations of the CS^+ and CS^- odor stimuli via a piezosensor (Figure 5.5D-G).

For post-fear conditioning respiration recordings, the CS^+ and CS^- were typically presented in blocks of 10 trials at 60-sec ITIs. Each mouse received between 8 and 60 trials of each odorant stimulus. All trials (per odorant) were then averaged together to

generate overall respiration rates during CS⁺ and CS⁻ presentations for each mouse. The piezosensor was configured such that inhalation onsets were marked by ascending zero-crossings of the output voltage trace, which was digitized (2000 Hz) and low-pass filtered (15 Hz) off-line. Individual odorant presentations were triggered by the first inhalation onset following a 60 sec ITI. In Figure 5.5F-G, the instantaneous respiration rate at a given piezosensor peak was calculated as the reciprocal of the preceding inter-peak interval. All data acquisition and analysis were performed using Spike2 software.

Results and Discussion

We used a trial-based, discriminative olfactory fear conditioning paradigm consisting of Paired, Shock Alone Control, and Odor Alone Control groups that underwent either repeated *in vivo* optical imaging procedures or behavioral testing (Figure 5.1A). During each of 3 consecutive days of training, mice assigned to the paired group received 5 ~15-sec presentations of each of 2 odorants, one of which (the CS⁺) always co-terminated with a footshock (Figure 5.1B) and one of which (the CS⁻) did not. Shock-alone and odor-alone groups underwent identical paradigms but without the odor or shock presentations, respectively. When tested in a novel context, mice in the paired group exhibited preferential freezing to the CS⁺ compared to the CS⁻, with comparatively little freezing observed in the shock- or odor-alone control groups, or to a clean air control stimulus (Figure 5.1C).

For optical imaging, odorant-evoked spH signals, indicating neurotransmitter release from OSN terminals into olfactory bulb glomeruli, were visualized *in vivo* in adult OMP-spH mice using wide-field fluorescence imaging through an implanted cranial

window (Czarnecki et al., 2011; Kass et al., 2013d) before and after behavioral training (Figure 5.1A). Olfactory fear conditioning induced a robust increase in the magnitude of spH responses evoked by the CS⁺ odorant compared to pre-conditioning baseline, while no changes were observed in the spH responses evoked by the CS⁻ or 3 non-presented control odorants (Figure 5.2A, 5.2D-G and 5.2K). Odorant-evoked spH signals did not differ across imaging sessions in the shock- and odor-alone control groups (Figure 5.2B-D and 5.2H-K). Identical results were obtained regardless of whether glomerular responses were pooled across mice (Figure 5.2) or averaged within each individual mouse (Figure 5.3). While fear learning augmented CS⁺-evoked spH signals, there was no change in the spatial arrangement of CS⁺-evoked glomerular response maps (Figure 5.4). In a parallel control experiment, no changes in respiration were observed during CS⁺ and CS⁻ presentations in identically-anesthetized, fear conditioned mice (Figure 5.5).

Each OSN in the mouse olfactory epithelium expresses one out of hundreds of odor receptor types (Buck and Axel, 1991). As OSN axons project ipsilaterally to the olfactory bulb, they segregate by receptor type so that each glomerulus receives projections exclusively from OSNs expressing a specific odor receptor (Mombaerts et al., 1996). Odorants bind to a subset of olfactory receptor types in the epithelium and thus drive OSN synaptic output into a corresponding subset of olfactory bulb glomeruli. Consequently, the global configuration of odorant-evoked OSN input to glomeruli across the bulb represents the chemical identity of that odorant (Malnic et al., 1999; Youngentob et al., 2006). Because the CS⁺ and CS⁻ were both esters, they drove OSN input to distinct but overlapping populations of glomeruli, reflecting their excitation of partially overlapping populations of OSNs. Some glomeruli selectively received OSN output evoked by the CS⁺, while others

were selective for the CS^- , and some responded to both odorants (dual-responsive). Separating the odorant-evoked OSN synaptic output based on the odorant-selectivity of each glomerulus revealed that the OSN input to CS^+ -selective glomeruli was greatly enhanced, whereas OSN input to glomeruli selective for the CS^- was unchanged (Figure 5.6A-B). In dual-responsive glomeruli, there was a selective enhancement when the OSN glomerular inputs were evoked by the CS^+ , but *not* when they were evoked by the CS^- (Figure 5.6A-B). This differential enhancement was not attributable to scattered light from the responses of CS^+ -selective glomeruli (Figure 5.7).

The selective enhancement of CS^+ -evoked OSN synaptic output in glomeruli whose OSNs are driven by both the CS^+ and the CS^- was unexpected. This discrimination presumably requires that information about the activity of other OSN populations reaches the dual-responsive OSNs to modulate their output. Because this could require feedback from other brain regions, we separated the spH signals into 4, 1-sec time bins (Figure 5.8) and tested whether the degree of enhancement varies across the duration of the odorant presentation. We observed the CS^+ -specific enhancement of OSN output not only at the peak of the spH response, but also in constant proportion throughout the entire odorant presentation (Figure 5.6C-D and Figs. 5.8-5.9). No changes were observed for CS^- -evoked synaptic input to CS^- -selective or dual-responsive glomeruli (Figure 5.6C-D and Figure 5.9), nor were they observed for time-binned shock- or odor-alone control data (Figure 5.10).

Fear conditioning with acetophenone increases the number of OSNs expressing its cognate M71 odorant receptor, and consequently increases the cross-sectional area of their target glomeruli when observed 3 weeks later (Jones et al., 2008). However, after fear

conditioning we did not observe a change in the cross-sectional area of OSN output signals from CS⁺-selective, CS⁻-selective, or dual-responsive glomeruli (Figure 5.6E), or in the distributions of glomeruli among these selectivity categories (Figure 5.6F). Moreover, the present results cannot be explained by changes in OSN number because an increase in the number of cells in OSN populations excited by both the CS⁺ and the CS⁻ would not selectively facilitate the response of that population to the CS⁺ (Figure 5.6B). In addition, only 3 days elapsed between fear conditioning and imaging (Figure 5.1A), which is less than the 7 days required for newborn OSNs to mature and express OMP ((Miragall and Monti Graziadei, 1982); whose promoter drives spH expression in these mice). It is also insufficient time for enhanced survival of mature CS⁺-responsive OSNs (which typically survive for months; (Carr and Farbman, 1993)) to disproportionately increase their numbers. The locus of plasticity may thus lie in the glomerular circuit that presynaptically modulates OSN output (McGann, 2013), instead of in changes in the population of OSNs.

Fear learning enhanced CS⁺-evoked OSN output on average across glomeruli (Figure 5.2 and Figure 5.6A-D), but in fact each mouse receives OSN input to many glomeruli at once. For each mouse, we thus quantified the differences in the overall patterns of OSN input evoked by the CS⁺, CS⁻, and an unexposed ester both before and after fear learning. The differences (quantified as Euclidean distances in vector space) between the primary sensory representations for the CS⁺ and CS⁻ and between the CS⁺ and an unexposed odorant were increased by fear learning (Figure 5.6G and Figure 5.11). When calculated as a function of time, the fear conditioning-induced difference in representations (presumably predictive of odor discriminability; (Youngentob et al., 2006))

was most pronounced during the first second of the stimulus presentations (Figure 5.6H and Figure 5.11).

Olfactory stimuli typically do not include sharp onsets and offsets. Instead, their concentration varies over time and with distance from the source. OSN firing frequency increases with higher odorant concentrations (Reisert and Matthews, 2001), resulting in more neurotransmitter release from axon terminals into olfactory bulb glomeruli (Bozza et al., 2004). It is possible that the CS⁺-selective enhancement of OSN output after fear conditioning is concentration-dependent, such that only OSN responses above some threshold evoke the enhancement. Alternatively, the augmented response to the CS⁺ could be concentration-independent, thus enhancing sensitivity to the threat-predictive odorant. We tested these possibilities by presenting the CS⁺ and CS⁻ odorants at 3 different concentrations, including the training concentration (Figure 5.1B), half, and double that concentration, during both imaging sessions.

During baseline imaging, the size of the peak spH signals increased as a function of concentration (Figure 5.12A-C). Following fear conditioning, CS⁺-evoked OSN output was enhanced at all 3 concentrations (Figure 5.12A and 5.12C-D), while CS⁻-evoked OSN output was unchanged (Figure 5.12B-C and 5.12E). The magnitude of spH signals stimulated by the training CS⁺ concentration (Figure 5.12D and 5.12F) was ~68% larger than before conditioning, comparable to the increase at the lower (~73% larger) and higher (~78% larger) concentrations. Similar results were obtained when concentration-response functions were measured earlier in the odorant presentation (Figure 5.13). No differences were observed in the concentration-response functions that were evoked by the CS⁻ (99.6% of baseline; Figure 5.12E-F) or in shock- or odor-alone control groups (Figure 5.14).

Notably, after conditioning, the OSN output that was evoked by the lowest concentration of the CS⁺ odorant (4 a.u.) was equivalent to the OSN output evoked by the highest concentration of that odorant (16 a.u.) before conditioning. This suggests that the effect of fear conditioning on OSN output was comparable to the effect of quadrupling the odorant concentration (Figure 5.12D and Figure 5.13).

These data demonstrate that fear learning can change the neural representation of threat-predictive odors at the synaptic output of the OSNs, which provide the primary olfactory input to the brain. This plasticity may serve to enhance the system's sensitivity to odors associated with an aversive event, perhaps by initiating a large "alarm signal" specific to the CS⁺. Such an enhancement could potentially underlie sensory symptoms of anxiety and affective disorders (Beck and Clark, 1997), including attentional bias or even PTSD-like hallucinations (Barrett and Bar, 2009; Felmingham et al., 2012).

Acknowledgements

I thank Michelle Rosenthal (who was a co-first author on the published manuscript) and Joseph Pottackal for their contributions to this project. Michelle contributed substantially to the project through the collection of behavioral and optical imaging data, and Joseph contributed to the collection of respiration data.

Chapter 5 Figures

Figure 5.1

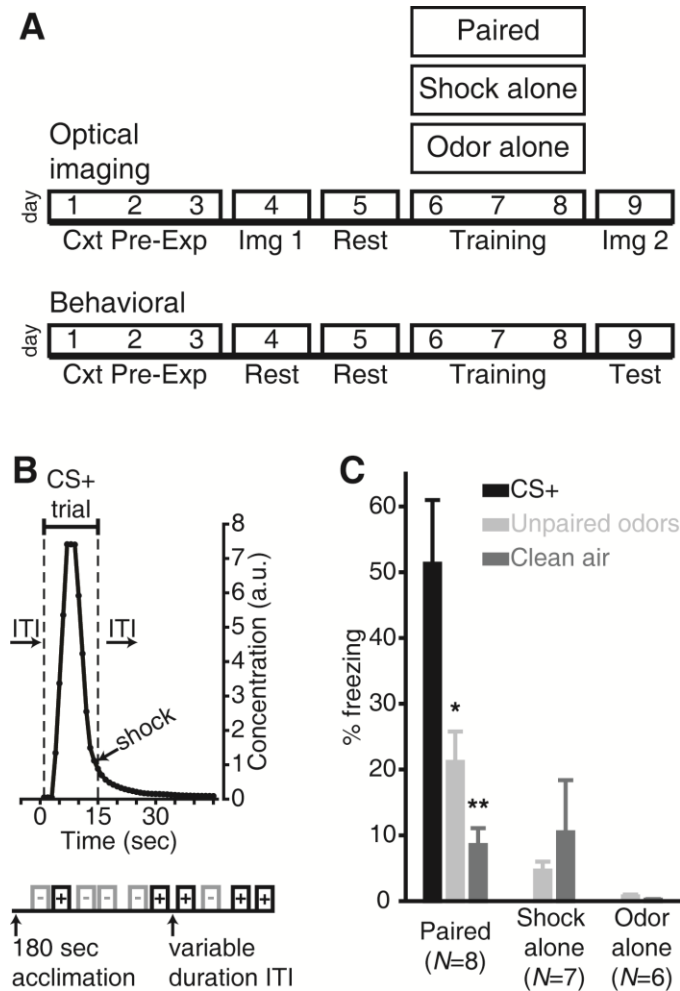


Figure 5.1. Olfactory fear learning and conditioned freezing. (A) Timeline of experiments. Cxt Pre-Exp, context pre-exposure; Img, imaging. (B) Protocol summary for 1 day of Paired training, with expanded CS⁺ trial showing the delivery of odorant (arbitrary units, a.u.) and shock stimuli. (C) Mean \pm SEM percent time freezing during the behavioral test session. * $P < 0.05$, ** $P < 0.01$ by Bonferroni-corrected *post-hoc* comparisons; N , mice/group.

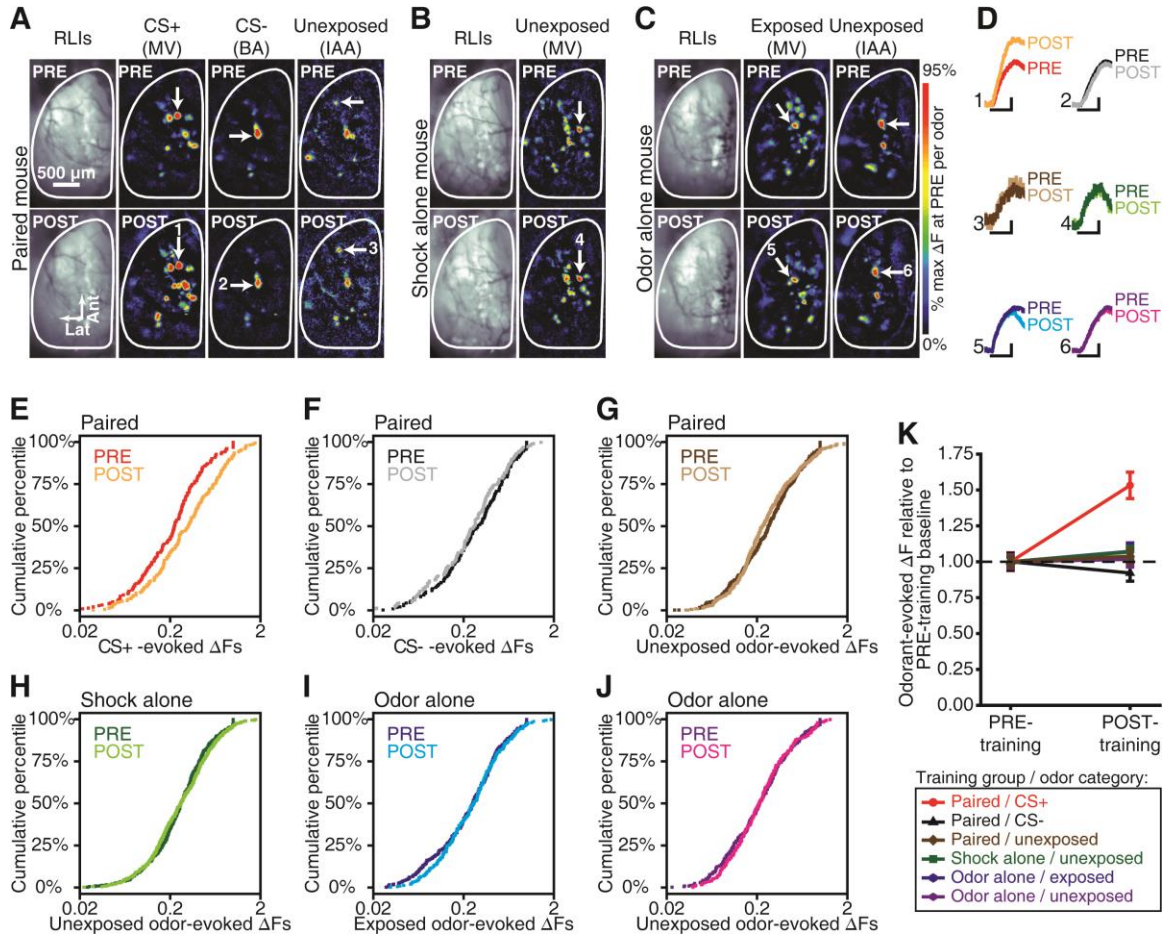
Figure 5.2

Figure 5.2. Fear learning-induced plasticity in odorant-evoked nerve output. (A-C) PRE vs. POST resting light images (RLIs) and pseudocolored difference maps from representative fear conditioned (A), shock alone (B), and odor alone (C) mice. MV, methyl valerate; BA, butyl acetate; IAA, isoamyl acetate. (D) Odorant-evoked change in fluorescence (ΔF) corresponding to callouts in A-C. Scale bars, 6-sec stimulus, 25% max of PRE. (E-J) Cumulative probability plots showing the distributions of PRE vs. POST ΔF values that were evoked by the CS⁺ (E; $P \leq 0.001$), CS⁻ (F; $P > 0.05$), and all other unexposed odorants (G; $P > 0.05$) in the paired group, all unexposed odorants in the shock alone group (H; $P > 0.05$), and all exposed (I; $P > 0.05$) and unexposed (J; $P > 0.05$) odorants in the odor alone group. P values are by K-S tests. (K) Mean \pm SEM ΔF pooled across glomeruli (dashed line, baseline). Number (N) of glomeruli contributing to data in

E-K: paired, $N_{\text{PRE}} = 267$, $N_{\text{POST}} = 285$; shock alone, $N_{\text{PRE}} = 163$, $N_{\text{POST}} = 173$; odor alone, $N_{\text{PRE}} = 209$, $N_{\text{POST}} = 180$.

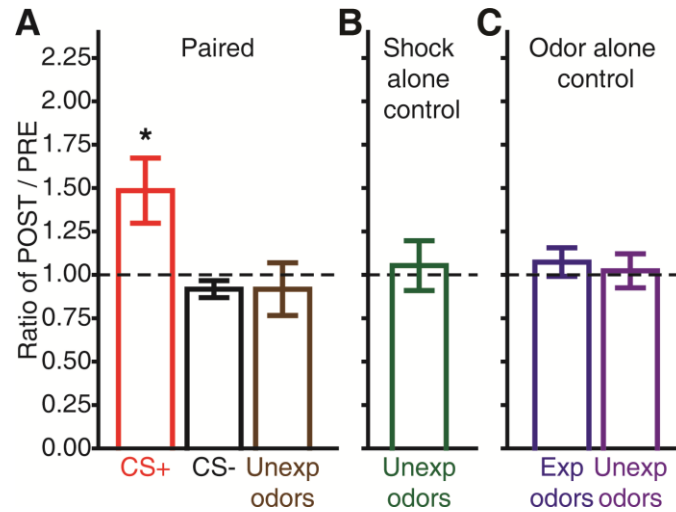
Figure 5.3

Figure 5.3. All subjects in the paired group exhibited associative, stimulus-specific neuroplasticity, whereas no plasticity was observed in shock or odor alone control groups. (A-C) For each mouse, glomerular responses evoked during both imaging sessions were first normalized relative to the max evoked response within each odorant category during pre-training imaging, as in Figure 5.2. To quantify the overall odorant-evoked change in fluorescence (ΔF) observed in response to each odorant per mouse, individual ΔF values (corresponding to the glomeruli receiving OSN input) that were measured in response to a given odorant were then averaged together for each imaging session in each mouse. Relative changes in odorant-evoked OSN activity per mouse were assessed by dividing the post-training average ΔF value by the pre-training average ΔF value. These ratios are summarized in A-C as the mean \pm SEM group ratio of average response magnitude evoked during post-training imaging / pre-training imaging (POST / PRE) for each odor category. * $P < 0.05$ by one-sample t test. Number of mice (N) contributing to group means: paired, $N = 6$; shock alone control, $N = 4$; odor alone control, $N = 4$. Unexp, unexposed; Exp, exposed.

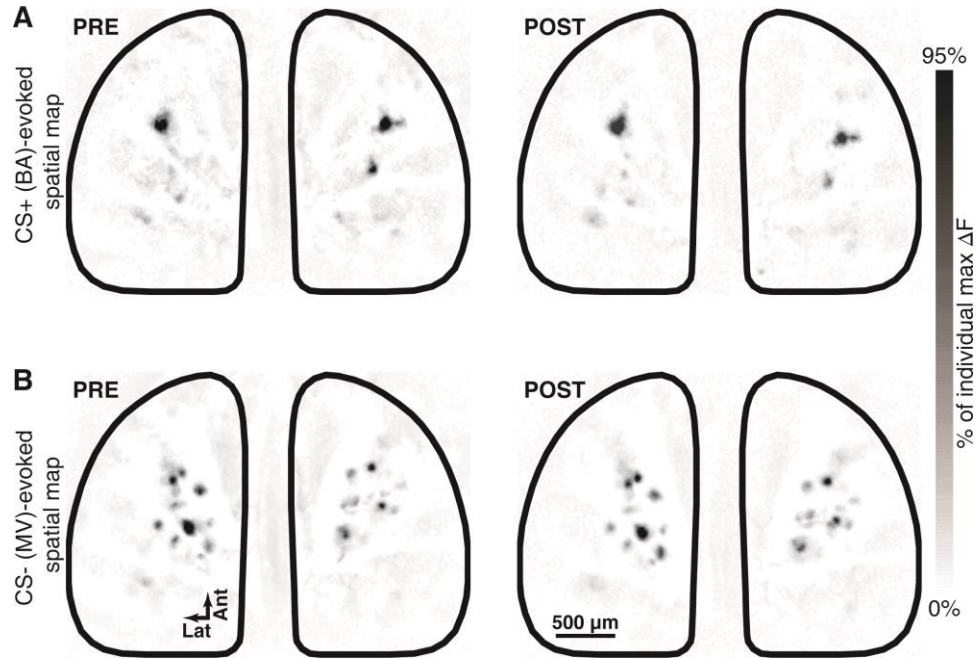
Figure 5.4

Figure 5.4. The spatial arrangement of odorant-evoked glomerular response maps is unaltered by fear conditioning. (A-B) Glomerular response maps evoked by the CS⁺ (A) and the CS⁻ (B) both before (left) and after (right) this representative subject underwent discriminative olfactory fear conditioning. BA, butyl acetate; MV, methyl valerate. All 4 maps are scaled relative to their individual maxima and shown in greyscale to illustrate the overall patterns of odorant-evoked activity, regardless of learning-induced changes in response magnitudes. While fear conditioning caused a ~35% increase in CS⁺-evoked spH signals in this subject, there was no change in the spatial distribution of glomeruli receiving CS⁺-evoked OSN input (A; $r = 0.811$, $P < 0.001$ by Pearson product-moment correlation coefficient). The areas receiving CS⁻-evoked OSN input in this subject (B) also remained very similar after fear conditioning ($r = 0.852$, $P < 0.001$). Note that to assess learning-induced alterations in OSN physiology, we normalized odorant-evoked glomerular response maps relative to the maximum change in fluorescence (ΔF) that was evoked during the baseline (pre-training) imaging session (as shown in Figure 5.2). The range of CS⁺-evoked ΔF values during the post-training imaging session exceeds that of the pre-training imaging session (recall, CS⁺-evoked spH signals became larger after fear conditioning). Thus, a consequence of imposing a single range of ΔF values (0-95% max

ΔF of PRE) on both PRE and POST CS⁺-evoked odor maps is a ceiling effect on the display of the pseudocolor scale for the POST map. This ceiling effect in the pseudocoloring causes the appearance of an increase in the number of CS⁺-evoked glomerular responses. However, there was *no* change in the number of glomeruli receiving measurable synaptic input during presentations of the CS⁺ after fear conditioning ($N_{\text{PRE}} = 195$, $N_{\text{POST}} = 218$; $P > 0.05$, by χ^2 test). If we scale each map relative to its own maximum (thus ignoring the relative enhancement of CS⁺-evoked response magnitudes, as shown here in Figure 5.4) we eliminate the ceiling effect and can more easily compare the overall spatial patterns of odorant-evoked activity.

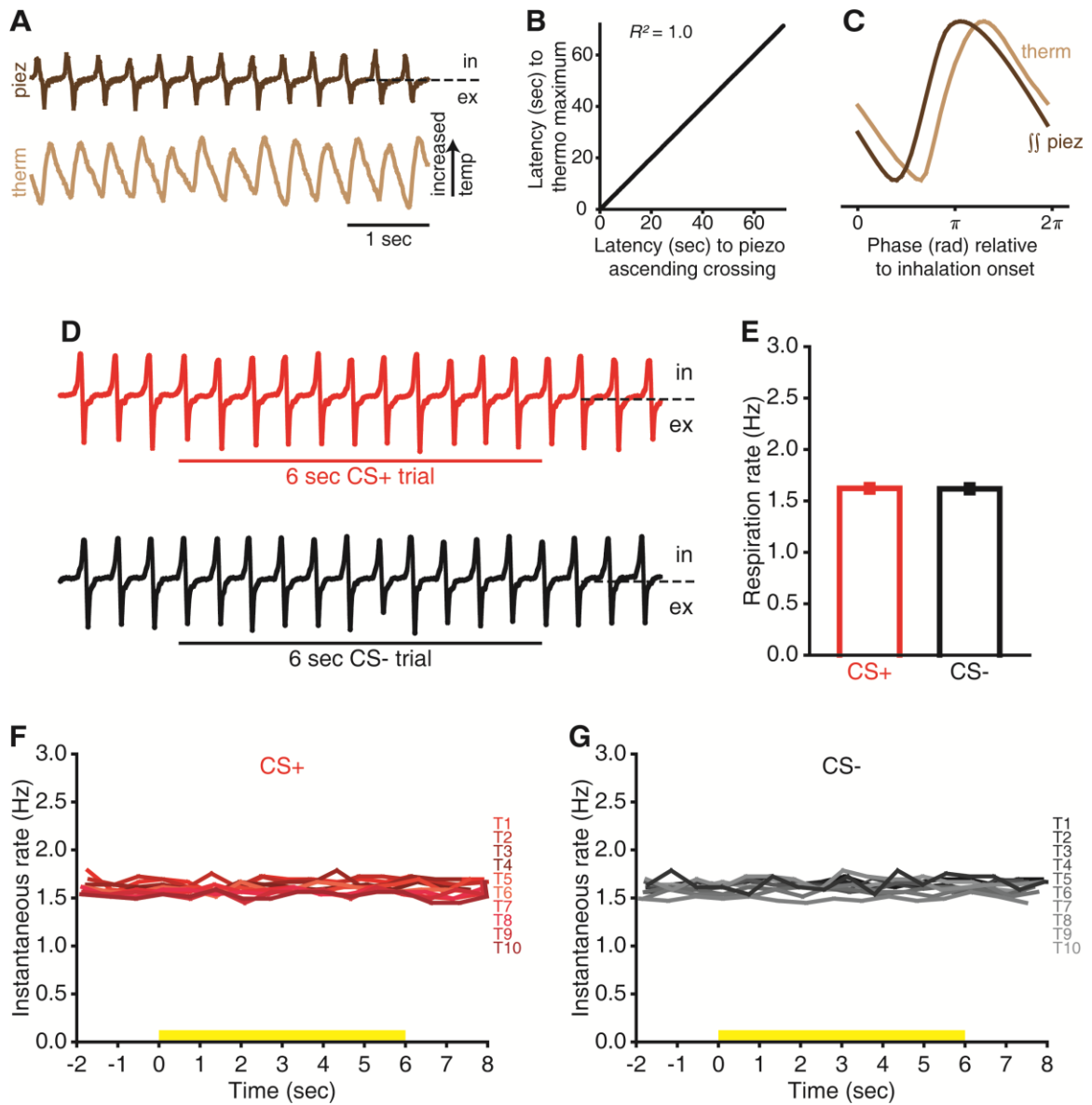
Figure 5.5

Figure 5.5. Respiration does not differ during CS⁺ and CS⁻ presentations in anesthetized mice that underwent discriminative fear conditioning. (A) Sample respiration traces acquired simultaneously from a naïve mouse by a piezosensor strip (brown, top) and an extranasal thermocouple (gold, bottom). The dashed line on the piezosensor trace indicates positive and negative regions of the trace, which show inhalation (in) and exhalation (ex) phases, respectively. Regions of positive slope in the thermocouple trace represent increasing temperature of extranasal air. (B) Latencies of inhalation onset-related events recorded simultaneously by thermocouple and piezosensor.

Each point gives the latencies of the inhalation onset-related event recorded by each method during a single cycle. An analysis conducted on the exhalation onset-related events (not shown here) yielded identical results. **(C)** Demonstration of a quantitative relationship between thermocouple- and piezosensor-generated waveforms. The average thermocouple waveform (gold) is related as a phase-shifted (lagging) scalar multiple of the second antiderivative of the average piezosensor waveform (brown). **(D)** Sample respiration traces recorded during presentations of the CS⁺ (red, top) and CS⁻ (black, bottom) that were measured in an anesthetized preparation after this representative mouse had undergone fear conditioning. **(E)** Mean \pm SEM respiration rate during CS⁺ and CS⁻ trials from 11 subjects that underwent discriminative fear conditioning. $P > 0.05$ by paired t test. **(F)** Instantaneous respiration rates during 10 individual trials (T1-T10) of the CS⁺ (**F**, red) and the CS⁻ (**G**, black) from a representative mouse. The yellow bars indicate the timing of stimulus presentation. Post-fear conditioning respiration (shown in **D-G**) was monitored via a force-transducing piezosensor strip positioned just below the diaphragm.

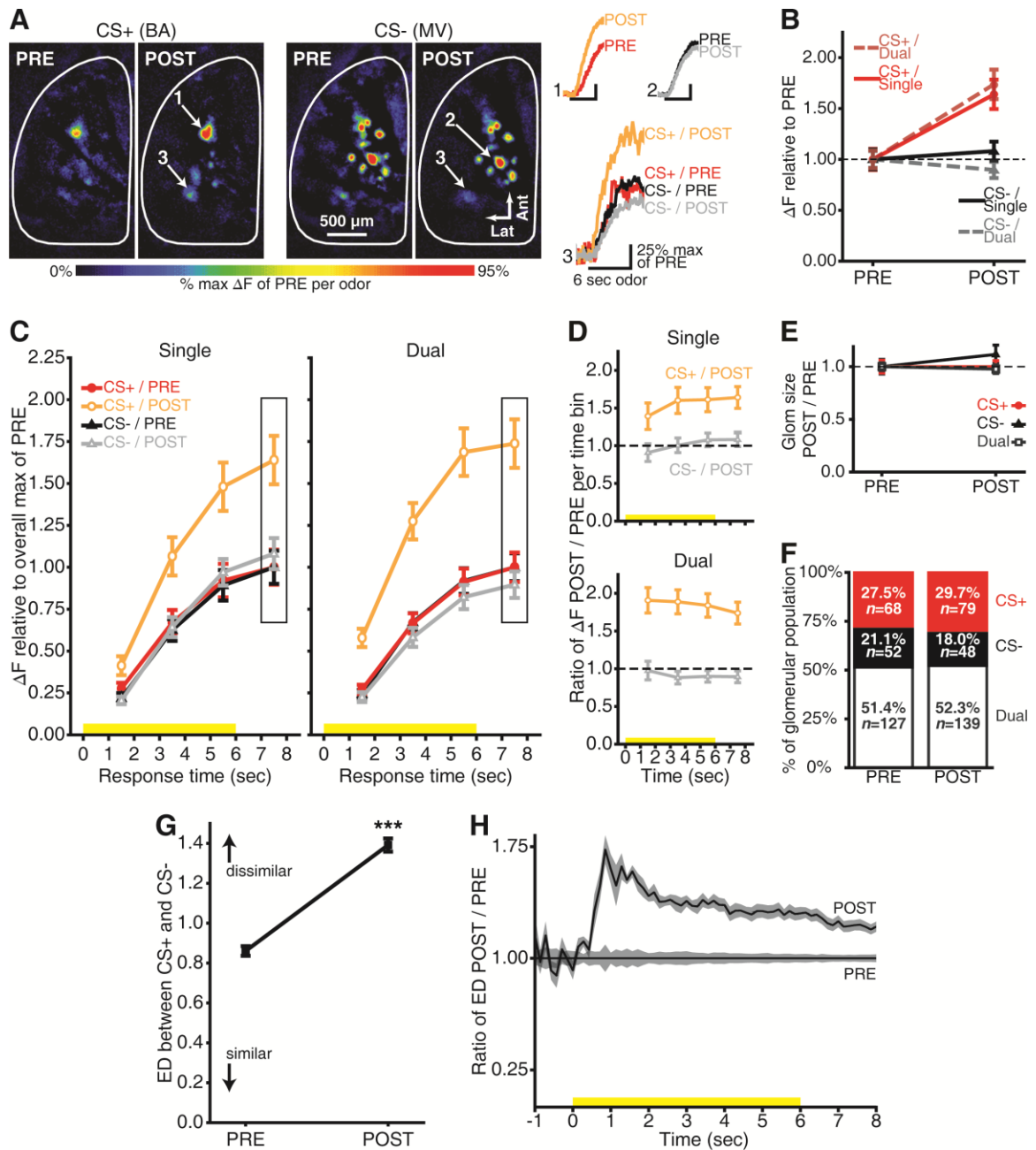
Figure 5.6

Figure 5.6. Stimulus-specific enhancement of nerve output. (A) PRE vs. POST CS⁺- and CS⁻-evoked maps from a representative mouse. Numbered callouts show example traces from single- and dual -responsive glomeruli. Butyl acetate, BA; methyl valerate, MV. (B) Peak odorant-evoked change in fluorescence (ΔF) separated by selectivity (dashed line, baseline). (C) Time-binned odorant-evoked ΔF for single- and dual-

responsive glomeruli. Boxed regions indicate the bin corresponding to peak responses in **A-B**. Yellow stimulus bars show odorant presentations. **(D)** Ratio of CS⁺ and CS⁻-evoked ΔF s during POST / PRE per bin per selectivity category (dashed line, baseline). **(E)** Glomerulus response size shown relative to PRE (dashed line). **(F)** Percent of PRE- and POST-training glomerular populations per selectivity category. $P > 0.05$, by χ^2 ; N s, number of glomeruli contributing to means \pm SEM in **B-E**. **(G-H)** Example network-level analysis from one mouse. **(G)** PRE vs. POST mean \pm SEM Euclidean distance (ED) between CS⁺- and CS⁻-evoked maps pooled across trial pairs and response times (0-8 sec). *** $P < 0.001$ by factorial ANOVA. **(H)** Proportional increase in dissimilarity between odor representations as a function of time. Solid lines \pm shading, mean \pm SEM.

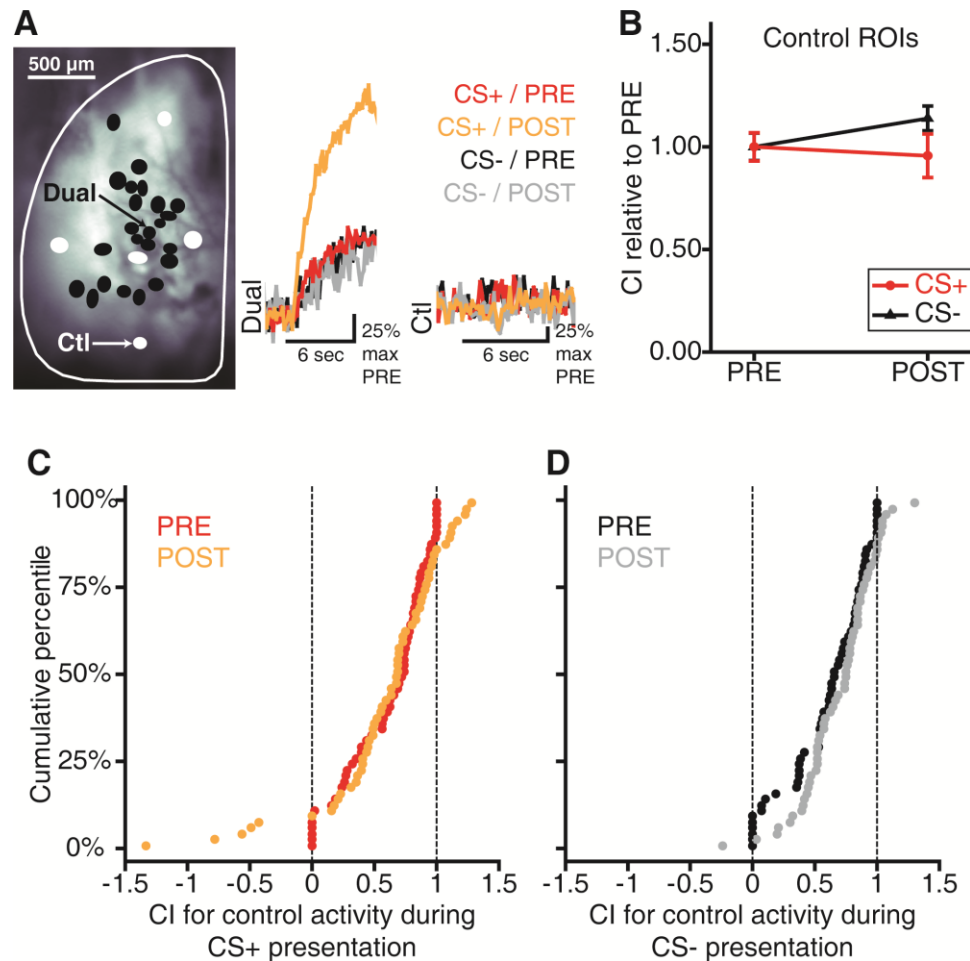
Figure 5.7

Figure 5.7. The stimulus-specific enhancement of CS⁺-evoked nerve output is *not* caused by odor-dependent light scatter. (A) Sample resting light image (RLI) from a subject in the paired group. Black circles, glomerular regions of interest (ROIs); white circles, control (Ctl) ROIs. To assess potential light scatter across the entire olfactory bulb, 5 Ctl ROIs spanning the *X* and *Y* axes of activity were selected per olfactory bulb per mouse. To determine if there were CS⁺- and CS⁻-evoked changes in fluorescence in these Ctl regions, we then analyzed the Ctl data in the same manner as the experimental data. Example traces corresponding to the callouts shown on the RLI are displayed at right. There is an example glomerulus (Dual, left) that received input from OSNs stimulated by both the CS⁺ and the CS⁻ during pre- and post-training imaging sessions. Although responses to both odors were observed in this glomerulus during both imaging sessions, only the CS⁺-evoked response was enhanced after fear conditioning. An example Ctl ROI

(Ctl, right) shows no change in fluorescence during presentations of the CS⁺ and CS⁻ and no stimulus-specific enhancement in control activity after fear conditioning. **(B-D)** To assess alterations in Ctl activity between pre- and post-training imaging sessions, change indexes (CIs) were calculated separately for each control ROI during CS⁺ and CS⁻ presentations. CIs were quantified per mouse and within odorants by (Ctl ROI – min Ctl ROI value of PRE)/(max Ctl ROI of PRE – min Ctl ROI of PRE), and thus always ranged between 0 and 1 for Ctl activity measured during pre-training imaging. **(B)** Mean \pm SEM CIs are averaged for the CS⁺ and CS⁻ by pooling across all Ctl ROIs from all subjects and are shown as a function of imaging session. $P > 0.05$ for odorant \times imaging session interaction by 2-way, repeated measures ANOVA; $N = 60$ Ctl ROIs. **(C-D)** Cumulative probability plots showing the distribution of CIs corresponding to each individual control ROI for the CS⁺ (**C**; $P > 0.05$ by K-S test) and CS⁻ (**D**; $P > 0.05$ by K-S test). Dashed lines indicate the min and max values during pre-training imaging.

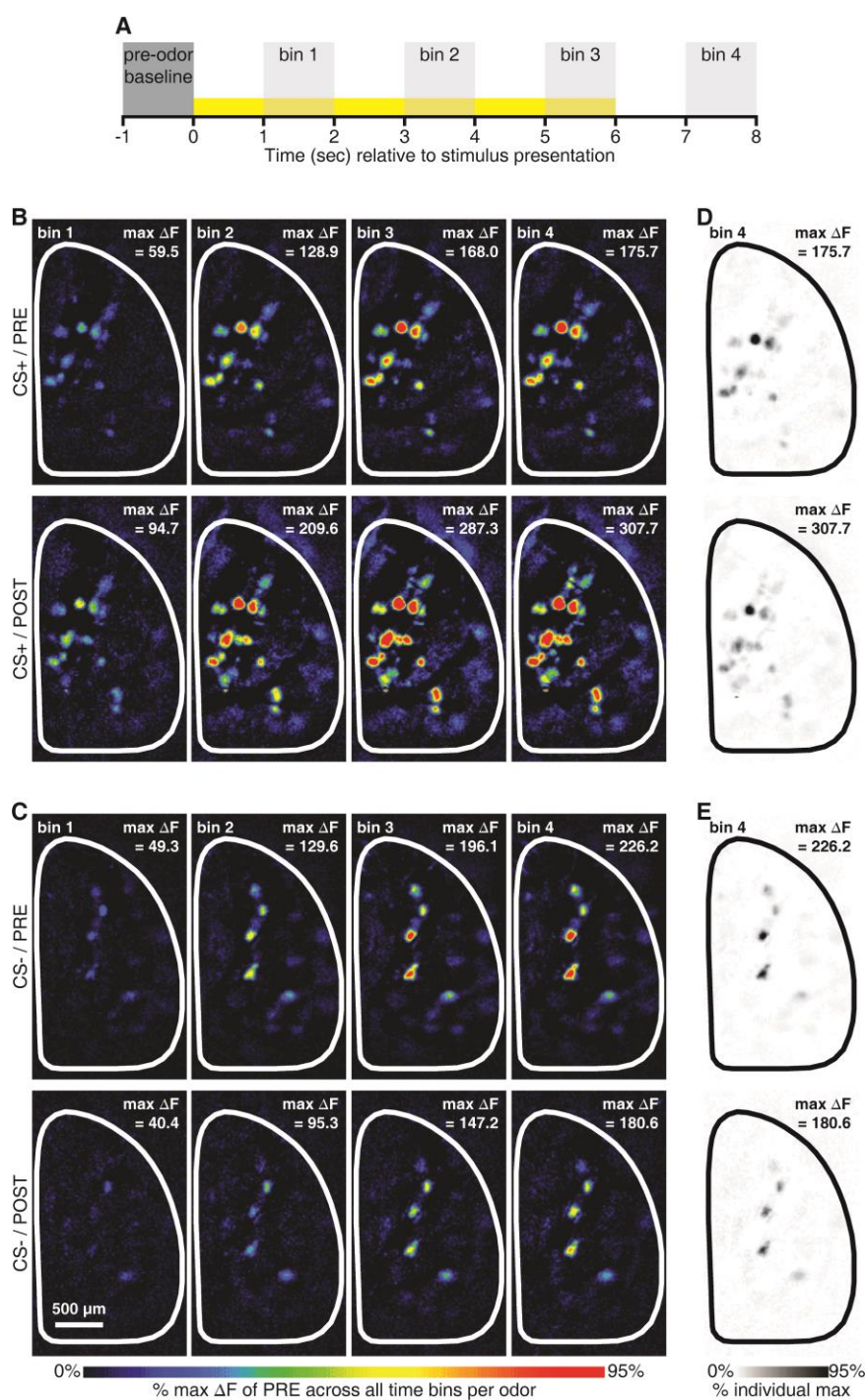
Figure 5.8

Figure 5.8. Temporal evolution of CS⁺- and CS⁻-evoked odor maps. (A) Timeline illustrating the 4, 1-sec time bins relative to stimulus presentation (yellow stimulus bar). One sec of baseline frames was subtracted separately from each time bin to generate

difference maps and to quantify the corresponding response magnitudes in glomeruli receiving odorant-evoked OSN input. CS⁺- (**B**) and CS⁻- (**C**) evoked pseudocolored difference maps measured during each time bin both before and after this subject underwent discriminative olfactory fear conditioning. CS⁺- (**D**) and CS⁻- (**E**) evoked maps from bin 4 are shown again in greyscale and are scaled to their individual maxima, permitting a more accurate evaluation of the similarity in the spatial arrangement of each pre- versus post-training pair of odor maps (as in Figure 5.4). During this mouse's discriminative fear conditioning training, methyl valerate and butyl acetate were used as the CS⁺ and CS⁻, respectively.

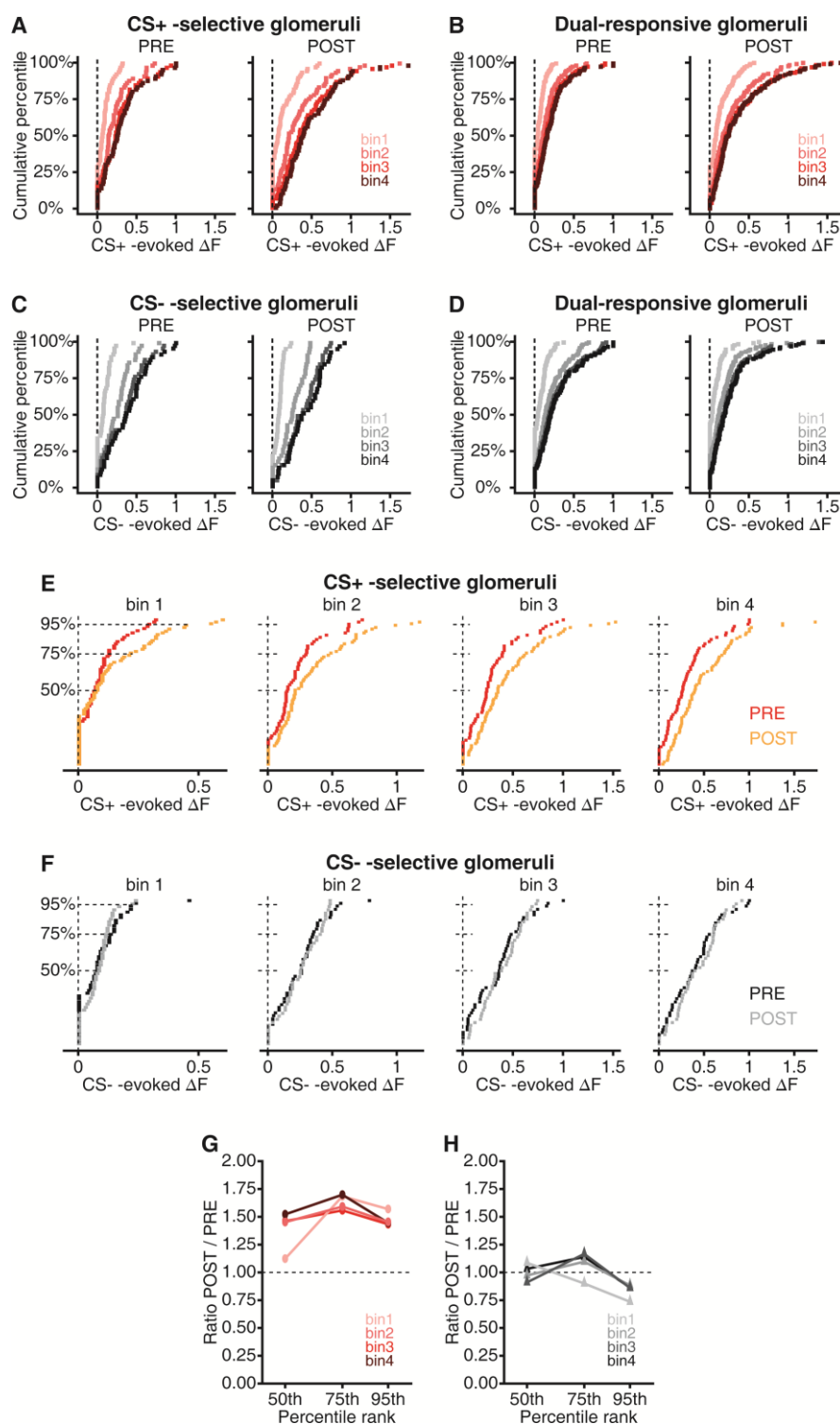
Figure 5.9

Figure 5.9. Analyzing the time course of odorant-evoked spH signals. (A-D) Cumulative probability plots showing the distributions of odorant-evoked change in

fluorescence (ΔF) values that were measured in 4, 1-sec time bins after odor onset: 1) bin 1, 1-2 sec after odor onset; 2) bin 2, 3-4 sec after odor onset; 3) bin 3, 5-6 sec after odor onset; 4) bin 4, 7-8 sec after odor onset (corresponds with time of peak responses). CS^+ - and CS^- -evoked ΔF s from both imaging sessions were normalized relative to the max evoked ΔF of PRE across all 4 time bins per odorant. Panels **A-D** are separated by the 3 categories of glomerular response selectivity profiles. These categories were characterized by glomeruli that were selective for the CS^+ (**A**), selective for the CS^- (**C**), or dual-responsive, which was the population of glomeruli receiving input from OSNs stimulated by both the CS^+ (**B**) and the CS^- (**D**). Individual plots within each panel are separated by imaging session (PRE- and POST-training imaging). During pre-training imaging, the magnitude of CS^+ - and CS^- -evoked spH signals increased throughout the duration of the odorant presentations, as indicated by the rightward shifting ΔF distributions corresponding to time bins 1-4. During post-training imaging, the temporal evolution of CS^- -evoked spH signals throughout the stimulus presentation was identical to that observed during the baseline session. However, CS^+ -evoked spH signals that were measured in each time bin throughout the stimulus presentation were enhanced after fear conditioning. (**E-F**) Example PRE versus POST pairwise comparisons showing distributions of CS^+ - and CS^- -evoked ΔF values within each time bin from glomeruli that were selective for the CS^+ (**E**) or the CS^- (**F**). The x -axes are truncated and expanded in plots showing PRE versus POST ΔF distributions from bins 1-3. (**G-H**) Examples showing that the learning-induced enhancement of CS^+ -evoked activity was a constant proportion of the response magnitude throughout the odorant presentation. ΔF values that were ranked at the 50th, 75th, and 95th percentiles were determined for each time bin of each session, as indicated by the horizontal dashed lines in **E-F**. A ratio of ΔF during POST relative to ΔF during PRE was then calculated for each time bin and plotted as a function of percentile ranking for the examples of CS^+ - (**G**) and CS^- - (**H**) selective glomeruli. The response distributions shown in **A-D** correspond to the summary plots (means \pm SEM) shown in Figure 5.6B-C.

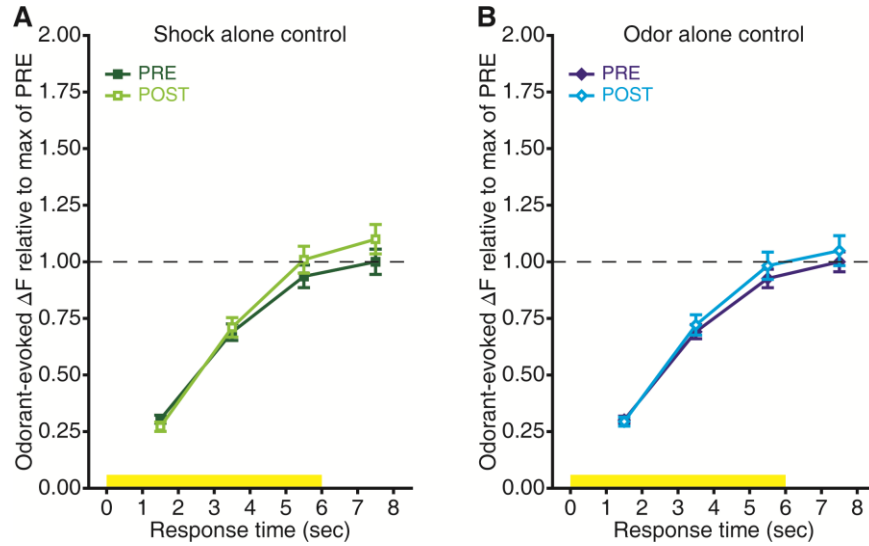
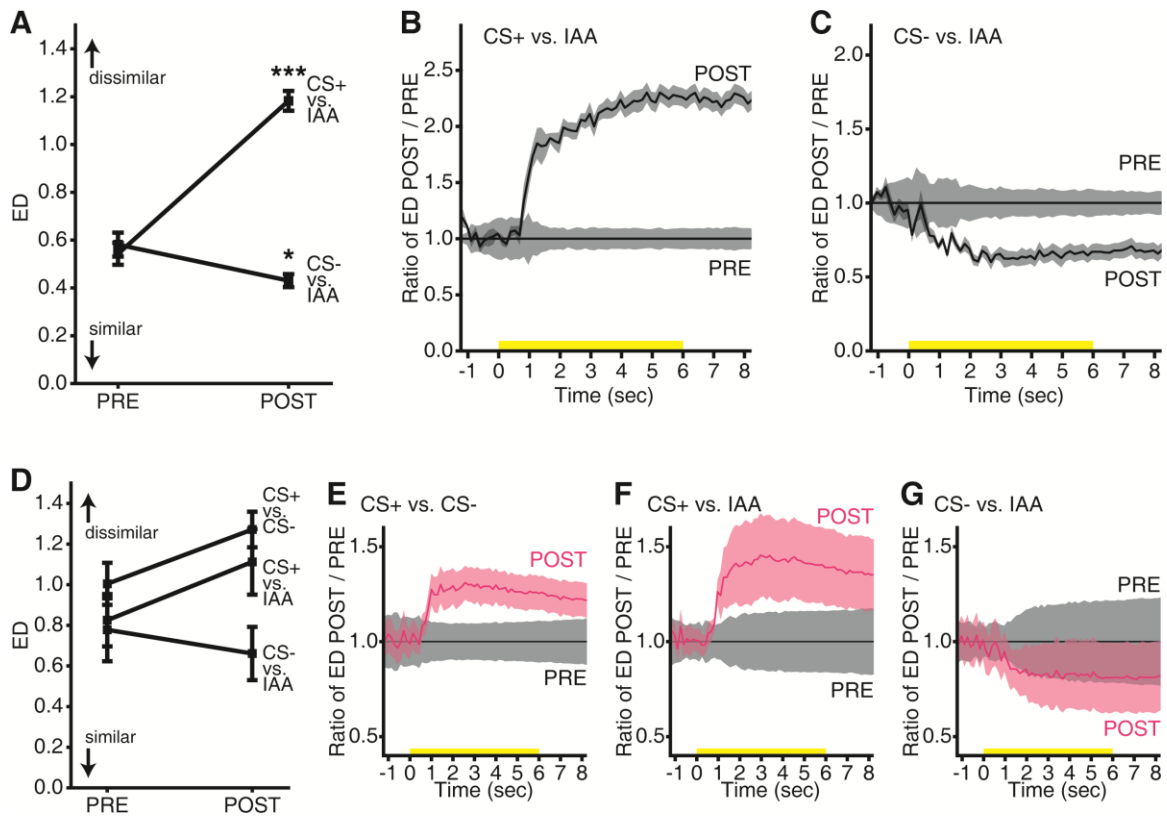
Figure 5.10

Figure 5.10. The time course of responses evoked by the two conditioning odorants is not affected by shock alone or odor alone control exposures. (A-B) Mean \pm SEM change in fluorescence (ΔF) that was evoked by the 2 counterbalanced conditioning odorants shown as a function of response time relative to stimulus presentation (yellow bars). Individual ΔF s from PRE- and POST- shock alone control training (**A**) and from odor alone control training (**B**) are normalized relative to the max of baseline (dashed lines) across all response times and pooled together within each time bin. There were no odor-shock pairings during either control training protocol and thus the 2 conditioning odorants were simply unexposed and exposed stimuli for the shock alone and odor alone control groups, respectively. Number (N) of glomeruli contributing to data shown in **A-B**: shock alone control, $N_{\text{PRE}} = 155$, $N_{\text{POST}} = 160$; odor alone control, $N_{\text{PRE}} = 195$, $N_{\text{POST}} = 171$.

Figure 5.11**Figure 5.11. Fear learning enhances the contrast between primary neural representations of a threat-predictive olfactory stimulus and other olfactory stimuli.**

To consider the discriminability between the overall sensory representations of the CS⁺, CS⁻, and IAA (an unexposed ester odorant) in each individual mouse both before and after fear conditioning, differences between odor maps were determined by Euclidean distances (EDs) in *N*-dimensional vector space, when *N* is equivalent to the number of glomerular regions of interest identified in each mouse (in each imaging session). **(A-C)** Additional results from the network-level analysis conducted on the same example mouse shown in Figure 5.6G-H. **(A)** After this mouse was fear conditioned, the neural representation of the CS⁺ was further in Euclidean space from the neural representation of IAA, whereas the CS⁻-evoked odor map became slightly more similar to the IAA-evoked odor map. EDs are summarized as means \pm SEM (averaged across 6 trial pairs and 0-8 sec relative to stimulus onset) and plotted as a function of imaging session. *** $P < 0.001$, * $P < 0.05$ by repeated measures ANOVA. **(B-C)** These data are normalized relative to baseline (PRE) and plotted

as a function of response time relative to stimulus presentations (yellow bar). Specifically, to analyze the relative change in ED between odor maps throughout the stimulus presentation, the mean \pm SEM ED (across 6 trial pairs) between CS⁺- and IAA-evoked maps (**B**) and between CS⁻- and IAA-evoked maps (**C**) during the post-training imaging session was divided by that of the pre-training imaging session for each frame that was acquired. The baseline (PRE) ED between odorant-evoked response maps across trials is shown as 1.0 and the relative change in ED (POST) is plotted as a ratio of baseline. The solid traces show the mean ED across trial pairs and the shaded regions show the SEM. (**D-G**) Network level analysis averaged across 6 mice that underwent discriminative olfactory fear conditioning (includes data from the example mouse shown in Figure 5.6G-H and Figure 5.11A-C). For each set of map comparisons, the average ED across 6 trial pairs (as in the solid traces in **B-C**) for each mouse was used to generate an overall group mean. (**D**) Group mean \pm SEM ED between odorant-evoked response maps before and after fear conditioning (pooled across time 0-8 sec). Group mean \pm SEM (solid lines \pm shaded regions) ED between (**E**) CS⁺ and CS⁻, (**F**) CS⁺ and IAA, and (**G**) CS⁻ and IAA sensory representations before and after fear conditioning plotted relative to baseline and as a function of time. Yellow stimulus bars indicate the time of odorant presentations.

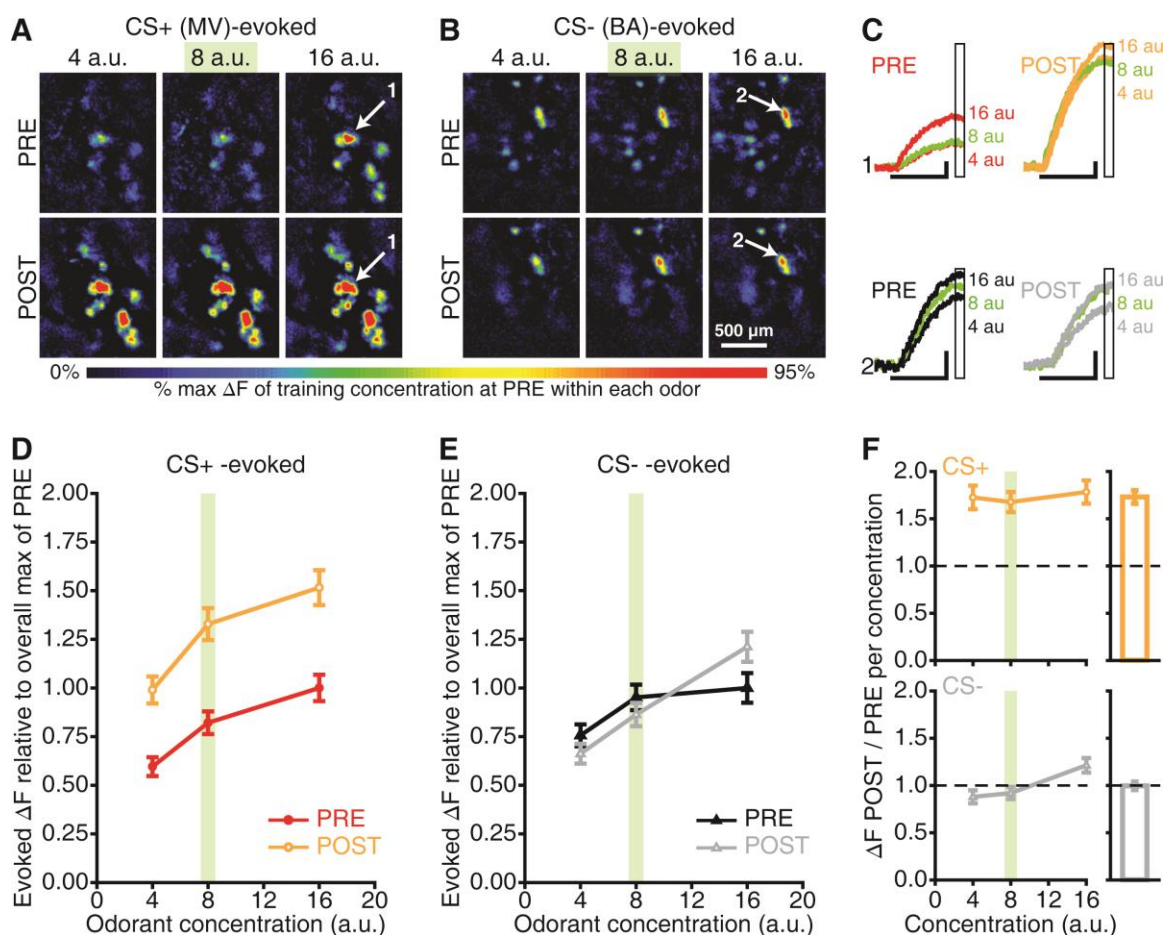
Figure 5.12

Figure 5.12. Enhanced sensitivity to the CS⁺. (A-B) Maps evoked by 3 concentrations (arbitrary units, a.u.) of the CS⁺ and CS⁻ before and after this mouse underwent fear conditioning. MV, methyl valerate; BA, butyl acetate. (C) Response amplitudes (ΔF s) for callouts (A-B). Scale bars, 6-sec stimulus, 25% max of PRE. Boxed regions indicate the bin used to generate peak maps (A-B) and concentration analyses (D-F). (D-E) PRE vs. POST CS⁺- and CS⁻-evoked concentration-response functions. (F) Ratio of CS⁺- and CS⁻-evoked ΔF s during POST / PRE per concentration (dashed lines, baseline). Outsets are scaled to the main y-axis and show overall ratios pooled across concentrations. Data are pooled across glomeruli (mean \pm SEM) in D-F. The training concentration is indicated in green in A-F.

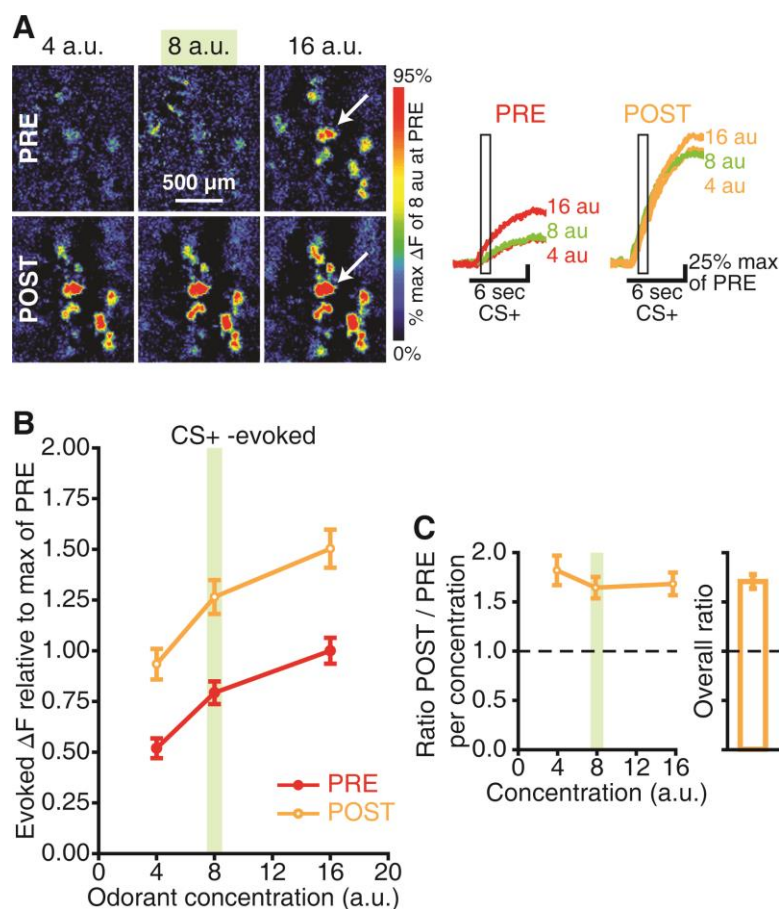
Figure 5.13

Figure 5.13. Sub-maximal CS⁺-evoked response amplitudes exhibit enhanced sensitivity after fear learning. This figure is analogous to Figure 5.12 (which summarizes “peak” evoked spH signals that were measured during bin 4), but uses measurements taken earlier (bin 1) in the odorant presentation before the peak of the spH response. **(A)** Pseudocolored difference maps evoked by a range of concentrations (represented in arbitrary units, a.u.) centered around the training concentration (8 a.u.) of the CS⁺ before (top) and after (bottom) this mouse underwent fear conditioning. During the 6-sec CS⁺ presentations, these early response maps evolved into the peak response maps shown in Figure 5.12A. Example traces correspond to the callouts shown in the maps directly above. Scale bars indicate 6-sec stimulus presentations and 25% max of PRE. The boxed regions indicate the frames from bin 1 that were used to generate the corresponding early odor maps and quantify sub-maximal CS⁺-evoked responses for concentration analyses shown in **B-C**. **(B)** Early (bin 1) concentration response functions evoked by the CS⁺ during pre-

and post-training imaging sessions. Odorant-evoked change in fluorescence (ΔF) values are normalized relative to the max evoked ΔF *across* concentrations during pre-training imaging and pooled across glomeruli (mean \pm SEM). (C) Left, early odorant-evoked ΔF s were normalized to the max evoked ΔF of PRE *within* each concentration of the CS⁺ and are plotted as mean \pm SEM ratios to show the relative change from baseline (dashed lines) across concentrations. Right, overall ratio (pooled across all 3 concentrations) of early odorant-evoked ΔF during post-training imaging relative to pre-training imaging. Left and right plots are scaled to the same y-axis. The target concentration used during training is indicated in A-C by the color green.

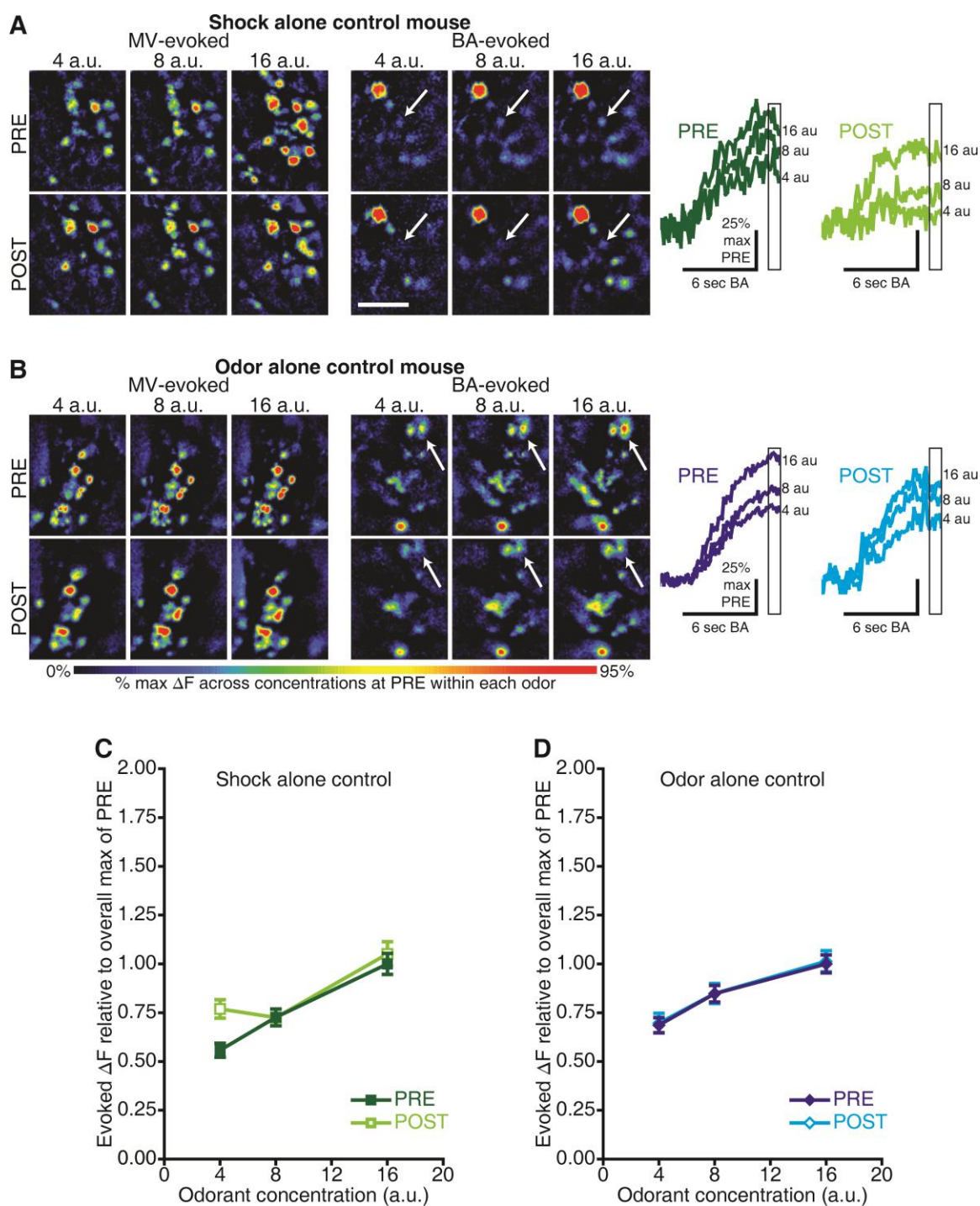
Figure 5.14

Figure 5.14. Exposures to shock or odorant stimuli alone do not alter the sensitivity of OSNs stimulated by the 2 conditioning esters. For subjects that underwent shock or odor alone control training, methyl valerate (MV) and butyl acetate (BA) (the 2

counterbalanced conditioning odorants for the paired group) were simply *unexposed* or *exposed* stimuli, respectively. The concentration (in arbitrary units, a.u.) used for ester (alone) exposures was 8 a.u., paralleling that in the paired group. **(A-B)** Pseudocolored difference maps across a range of concentrations of MV and BA that were evoked both before and after these 2 mice underwent either shock alone exposure **(A)** or odor alone exposure **(B)**. Scale bar, 500 μm . Example response amplitudes (ΔFs) corresponding to callouts in **A-B** are shown right. Boxed regions show the frames from bin 4, which were used to generate the corresponding odor maps and quantify the peak evoked glomerular responses for concentration analyses shown in **C-D**. **(C-D)** Concentration response functions evoked by the 2 conditioning esters before and after shock alone control exposure **(C)** or odor alone control exposure **(D)**. ΔFs are normalized relative to the max evoked ΔF *across* concentrations during pre-training imaging per odor, pooled across glomeruli (**C**, $N_{\text{PRE}} = 163$, $N_{\text{POST}} = 167$; **D**, $N_{\text{PRE}} = 197$, $N_{\text{POST}} = 169$), and shown as the mean \pm SEM.

CHAPTER 6

Persistent, generalized hypersensitivity of olfactory bulb interneurons after olfactory fear generalization

The results from this chapter are reported in Kass MD, McGann JP (Submitted) Persistent, generalized hypersensitivity of olfactory bulb interneurons after olfactory fear generalization.

Abstract

Generalization of fear from previously threatening stimuli to novel but related stimuli can be beneficial, but if fear overgeneralizes to inappropriate situations it can produce maladaptive behaviors and contribute to pathological anxiety. Appropriate fear learning can selectively facilitate early sensory processing of threat-predictive stimuli, but it is unknown if fear generalization has similarly generalized neurosensory consequences. We performed *in vivo* optical neurophysiology to visualize odor-evoked neural activity in populations of periglomerular interneurons in the olfactory bulb one day before, one day after, and one month after each mouse underwent an olfactory fear conditioning paradigm designed to produce generalized fear of odors. Behavioral and neurophysiological changes were assessed in response to a panel of odors that varied in similarity to the threat-predictive odor at each time point. After conditioning, all odors evoked similar levels of freezing behavior, regardless of similarity to the threat-predictive odor. Freezing significantly correlated with large changes in odor-evoked periglomerular cell activity, including a robust, generalized facilitation of the response to all odors, broadened odor tuning, and increased neural responses to lower odor concentrations. These generalized effects occurred within 24 hours of a single conditioning session, persisted for at least one month, and were detectable even in the first moments of the brain's response to odors. The finding that generalized fear includes altered early sensory processing of not only the threat-predictive stimulus but also novel though categorically-similar stimuli may have important implications for the etiology and treatment of anxiety disorders with sensory sequelae.

Introduction

Generalization of learned fear is an adaptive mechanism that promotes flexible responding to novel but potentially dangerous situations. Learned fear is studied through classical conditioning paradigms that pair a neutral sensory stimulus such as an odor (the conditioned stimulus, CS) with an aversive stimulus such as a shock (the unconditioned stimulus, US) that elicits an unconditioned defensive response. After conditioning, the defensive response will be elicited by the CS but will also generalize to non-threatening stimuli related to the CS (Lissek et al., 2008; Dunsmoor et al., 2009; Dunsmoor et al., 2011a; Resnik et al., 2011; Resnik and Paz, 2015; Rajbhandari et al., 2016). Generalization of conditioned fear typically falls off gradually as stimuli become more dissimilar to the CS along continuous, physical axes, such as tone frequency (Resnik et al., 2011; Aizenberg and Geffen, 2013; Resnik and Paz, 2015) or geometric size (Lissek et al., 2008; Lissek et al., 2010; Lissek et al., 2014), though generalization also can occur within conceptual categories (Dunsmoor et al., 2011a; Dunsmoor and Murphy, 2015). Fear overgeneralization occurs when cues that do not actually predict dangerous outcomes evoke maladaptive fearful or defensive responses (van Meurs et al., 2014). Patients with anxiety disorders exhibit broadened fear generalization compared to healthy controls (Lissek et al., 2010; Lissek et al., 2014), suggesting that overgeneralization of learned fear may contribute to the etiology or maintenance of pathological fear (Dunsmoor and Paz, 2015; Resnik and Paz, 2015).

Most research addressing the neurobiology of conditioned fear has focused on structures such as the amygdala, hippocampus, and prefrontal cortex (LeDoux, 2000; Maren and Quirk, 2004; Phelps and LeDoux, 2005; Jovanovic and Ressler, 2010;

Dunsmoor and Paz, 2015). However, fear learning also induces dramatic changes in sensory regions (Bakin and Weinberger, 1990; Quirk et al., 1997; Weinberger, 2007; Li et al., 2008; Chen et al., 2011; Fletcher, 2012; Gdalyahu et al., 2012; McGann, 2015), including CS-specific hypersensitivity in primary sensory neurons (Jones et al., 2008; Kass et al., 2013b; Dias and Ressler, 2014). This plasticity can have explicitly sensory consequences, such as lowered detection thresholds (Ahs et al., 2013; Parma et al., 2015) or altered perceptual discrimination abilities (Fletcher and Wilson, 2002; Li et al., 2008; Chen et al., 2011; Resnik et al., 2011; Aizenberg and Geffen, 2013; Resnik and Paz, 2015), but it may also be important for non-sensory functions like recruiting attention or triggering defensive behavior (McGann, 2015). Fear generalization has been presumed to reflect changes in higher-order structures responding to sensory inputs (Ciocchi et al., 2010; Dunsmoor et al., 2011b; Dunsmoor and Paz, 2015; Ghosh and Chattarji, 2015; Resnik and Paz, 2015), but sensory regions might be responsible for labeling CS-resembling stimuli as potentially threatening (Chen et al., 2011; Krusemark and Li, 2012; Miasnikov and Weinberger, 2012; Aizenberg and Geffen, 2013). Psychopathologies like post-traumatic stress disorder (PTSD) include alterations in attentional and neurosensory processing (Bryant et al., 2005; Mueller-Pfeiffer et al., 2013; Olatunji et al., 2013; Todd et al., 2015; Clancy et al., 2017) that might reflect dysfunctional plasticity in early sensory brain regions.

In the olfactory system, odors are initially processed in the olfactory bulb, where “bottom-up” sensory input from olfactory sensory neurons (OSNs) in the nose converges with “top-down” projections from structures involved in fear learning (de Olmos et al., 1978; Zaborszky et al., 1986; Carmichael et al., 1994; Shipley and Ennis, 1996). After

olfactory fear conditioning, odor-evoked neural activity is enhanced in the olfactory bulb (Sevelinges et al., 2007; Fletcher, 2012), even as early as the synaptic terminals of OSNs (Kass et al., 2013b). To investigate whether fear generalization would alter bulbar processing, we focused on the physiology of inhibitory periglomerular (PG) interneurons, which shape the input and output of the olfactory bulb (McGann et al., 2005; Murphy et al., 2005; Shao et al., 2009; Shao et al., 2012; McGann, 2013). PG interneurons integrate peripheral input from receptor-specific populations of OSNs with lateral information about other OSN populations (Aungst et al., 2003; Liu et al., 2013) and also with top-down information from cortical and neuromodulatory structures (Shipley and Ennis, 1996; Boyd et al., 2012; Ma and Luo, 2012; Markopoulos et al., 2012; Eckmeier and Shea, 2014; Liu et al., 2015). Notably, PG cell activity is influenced by interactions between the amygdala and locus coeruleus (LC) (Fast and McGann, 2017b), which are both involved in emotional processes (Aston-Jones et al., 1996; LeDoux, 2000). Such modulation might enable PG cells to facilitate the detection of potentially threatening sensory cues.

Methods

Subjects.

Mice in the imaging experiment ($N = 18$; listed in Supplementary Table S6.1) expressed either GCaMP3 (Zariwala et al., 2012) or GCaMP6f (Chen et al., 2013) in GAD65-expressing (Taniguchi et al., 2011) PG interneurons in the olfactory bulb^{35,85}. Purely behavioral experiments ($N = 48$) included either wild-type C57BL/6J mice or GCaMP^{-/-} littermates. All subjects were adult (5.5 ± 0.12 months) males, and all

experiments were performed in accordance with protocols approved by the Rutgers University Institutional Animal Care and Use Committee.

Olfactory fear conditioning.

Behavioral procedures took place in one of two distinct contexts (Figure 6.1A, CTX A versus CTX B), as previously described (Kass et al., 2013b). Subjects were randomly assigned to 1 of 3 groups, and subsequently underwent an approximately month-long paradigm (Figure 6.1A) that consisted of 2 15-min context pre-exposure sessions (to minimize shock-context associations), 1 day of training, and repeated post-training behavioral tests in a novel context. To promote fear generalization (Fanselow, 1980; Laxmi et al., 2003; Baldi et al., 2004; Shaban et al., 2006; Chen et al., 2011; Aizenberg and Geffen, 2013; Ghosh and Chattarji, 2015; Poulos et al., 2016), paired training included 10 trials (Figure 6.1B, top) of an ~15-sec ester-odor (methyl valerate, MV) that approximately co-terminated with a strong 1.2-mA, 0.5-sec footshock (Figure 6.1C). Shock-alone and odor-alone control training consisted of the same paradigm, but *without* the presentation of any odors (Figure 6.1B, middle) or any shocks (Figure 6.1B, bottom), respectively. Training sessions began with a 180-sec acclimation period and employed long, variable inter-trial intervals (ITIs; 228-348 sec).

During both the 3-day test and the 1-month retest (Figure 6.1A), subjects were pseudo-randomly presented with 3 trials of each of 4 odorants (12 trials total) at variable duration ITIs (example protocols in Figure 6.1D and Supplementary Figures S6.1 and S6.2). These stimuli included the CS and 3 other unexposed odors that varied in chemical similarity to the CS, including a similar ester (ethyl valerate, EV, smells very similar to

MV), a less-similar ester (*n*-butyl acetate, BA, which is readily discriminable from MV), and a ketone (2-hexanone, 2H, smells very different from MV). Test sessions were recorded, tracked (Figure 6.1D and Supplementary Figures S6.1 and S6.2), and analyzed with FreezeFrame 4 software. Odorant-evoked freezing was scored during 3 consecutive 20-sec bins for each trial (pre-odor, odor, and post-odor). Data were analyzed with mixed-model ANOVAs and planned *post-hoc* ANOVAs that included group, odor, trial number, and trial phase as factors. Tests with multiple comparisons were Bonferroni-corrected.

We ran a series of purely behavioral experiments in parallel with the above imaging experiment to determine: 1) if the imaging procedures affected the generalization of conditioned fear (Supplementary Figure S6.3); 2) if fear generalization is exhibited within 24 hours of training (Supplementary Figure S6.4); and 3) to confirm that fear generalization persists up to 1 month after learning (Supplementary Figure S6.5).

In vivo optical recordings and analyses.

Optical neurophysiology procedures and analyses are detailed in the General Methods section. Briefly, cranial windows (Figure 6.1G-I) were surgically implanted (Czarnecki et al., 2012; Kass et al., 2013d; Kass et al., 2013b; Kass et al., 2016) and *in vivo* imaging procedures were performed (Czarnecki et al., 2011; Czarnecki et al., 2012; Kass et al., 2013a; Kass et al., 2013d; Kass et al., 2013c; Kass et al., 2013b; Kass et al., 2016; Kass et al., 2017) to visualize odorant-evoked GCaMP signals from populations of GAD65-expressing PG cells (Fast and McGann, 2017b) 1 day before, 1 day after, and 1 month after fear conditioning (Figure 6.1A). Vapor dilution olfactometry was used to present up to 3 concentrations of up to 5 odors during each imaging session. The odor-panel included 3 esters (MV, which was used as the CS, EV, and BA), 1 ketone (2H), and

1 aldehyde (*trans*-2-methyl-2-butenal, 2M2B), yielding 3 odor categories for paired and odor-alone subjects (training ester, unexposed esters, and unexposed “other”) and 1 odor category for shock-alone subjects (unexposed odors). Blocks of 3-6 trials (20-sec/trial, 60-sec ITI) were presented to anesthetized subjects. Respiration was monitored (Kass et al., 2013b; Kass et al., 2017), and odor presentations (6-sec/presentation) were timed to begin during the exhalation phase of the respiration cycle to ensure reliable odor concentrations during the first inhalation of odor.

Optical data were spatially low-pass filtered with a 3×3 pixel median filter, and spatially high-pass filtered with a 2-dimensional Gaussian filter. To prevent aliasing artifacts, low-pass temporal filtering was applied at 6.25 Hz. To capture potential differences in the dynamics of PG cell activity, odor-evoked response amplitudes ($\Delta F/F$) were quantified as the change in fluorescence during the first inhalation of odor and as the integrated change from baseline fluorescence during the 6-sec odor presentation. Glomerular regions of interest (ROIs) were matched across imaging sessions for each subject. The raw data set included 787 glomerular ROIs from 8 paired subjects, 443 ROIs from 5 shock-alone subjects, and 464 ROIs from 5 odor-alone subjects. Candidate ROIs were included as responses if the mean odor-evoked GCaMP signal across 3-6 trials was greater than 3 standard errors above 0.

$\Delta F/F$ s were normalized relative to the maximum $\Delta F/F$ within each odor and across all imaging sessions per subject (Figures 6.1 and 6.2), and the corresponding number of odor-evoked glomerular responses was quantified (Figure 6.3). Odor-response selectivity (Figure 6.4) was quantified as the number of odors (from 0-5) that evoked a response in each glomerulus. Note that within a given subject the same array of glomerular ROIs was

identified across imaging sessions, so it was possible for the selectivity of an individual glomerulus to be 0 during baseline imaging if that glomerulus did not respond to any odors in the panel at baseline, but later responded to at least 1 odor during at least 1 of the 2 post-training imaging preparations. As a measure of similarity between odor pairs (Figure 6.4) we calculated uncentered correlation coefficients (Soucy et al., 2009) across the 5 odors, yielding 10 odor pairs per subject, per imaging session (e.g., CS-EV, CS-BA, CS-2H, etc). Two PG cell activity maps with the same odor tuning will have a similarity of 1, whereas odor-evoked maps with completely non-overlapping PG cell activity have a similarity of 0. Correlational analyses (Figure 6.5) related the magnitude of baseline $\Delta F/F_s$ with change indexes that represented that effect of fear conditioning in each glomerulus. Change indexes were computed as $(\text{Post}_{\Delta F/F} - \text{Pre}_{\Delta F/F}) / (\text{Post}_{\Delta F/F} + \text{Pre}_{\Delta F/F})$, and thus ranged from -1.0 to +1.0, with +1.0 representing a 100% increase in activity (i.e., a glomerulus that started to respond to the CS after fear conditioning) and -1.0 representing a 100% decrease in activity (i.e., a glomerulus that stopped responding to the CS after fear conditioning). Additionally, change indexes from 1 day post-training imaging sessions were pooled across glomeruli from all subjects in a group, ranked from lowest to highest by their normalized CS-evoked $\Delta F/F_s$ from the pre-training imaging session, and then separated into quartiles of the pre-training CS-evoked $\Delta F/F$ distribution. During imaging, the CS and the other unexposed esters were presented across a 4-fold range of concentrations that included the training concentration (Figure 6.1C, 9 au) and half and double that concentration. These data were normalized across concentrations and imaging sessions per odor to assess potential changes in sensitivity (Figure 6.6).

Statistical analyses included omnibus factorials to assess planned interactions across groups, imaging sessions, odors, and concentrations. These were followed with planned *post-hoc* ANOVAs and *t*-tests. Differences across glomerular distributions were assessed with Wilcoxon signed-ranks tests, Friedman's ANOVAs, and Kruskal-Wallis tests. *P* values were adjusted for multiple comparisons.

Results

Long-lasting generalization of conditioned fear to odors.

To induce generalized fear of odors, we employed a conditioning paradigm (Figure 6.1A-C) in which 1 day of non-discriminative training (Chen et al., 2011; Aizenberg and Geffen, 2013; Resnik and Paz, 2015) included 10 paired presentations of a single odor with a strong footshock (Fanselow, 1980; Laxmi et al., 2003; Baldi et al., 2004; Shaban et al., 2006; Ghosh and Chattarji, 2015; Poulos et al., 2016). This model parallels naturally occurring traumatic events, which are very salient and do not alternate between threatening and safe stimuli (Resnik and Paz, 2015).

During testing 3 days post-conditioning (Figure 6.1A, 3-day test), there was a significant difference in odor-evoked freezing between groups (Figure 6.1E, left, $F_{(2,25)} = 232.461$, $p < 0.001$). Regardless of which odor was being presented (group \times odor, $F_{(6,75)} = 0.604$, $p = 0.727$), paired mice exhibited significantly ($P_s < 0.001$) more odor-evoked freezing than shock-alone and odor-alone controls (which did not differ from each other, $p = 0.189$). Remarkably, paired subjects froze equally to all 4 odors (Figure 6.1E, left, non-significant odor effect, $F_{(3,36)} = 0.666$, $p = 0.578$), demonstrating broad fear generalization. Importantly, they did not freeze continuously (Figure 6.1D and Supplementary Figures

S6.1 and S6.2), exhibiting comparable freezing to shock-alone controls prior to odor onset, and then freezing much more during the odor and immediate post-odor periods (Figure 6.1F, left). These mice were tested 3 days post-training to permit interleaved imaging sessions (Figure 6.1A), but parallel experiments demonstrated that the intervening imaging procedures did not influence fear generalization (Supplementary Figure S6.3), and that fear generalization is observed by 24 hours post-conditioning (Supplementary Figure S6.4).

To determine if the observed fear generalization parallels the long-lasting phenotype that occurs in anxiety (Jovanovic and Ressler, 2010), we performed a second behavioral test 1 month post-training (Figure 6.1A, 1-month retest). Paired mice continued to exhibit generalized freezing behavior to all 4 odors (Figure 6.1E, right), while shock-alone and odor-alone controls continued to show minimal odor-evoked freezing (between-groups, $F_{(2,25)} = 43.225$, $p < 0.001$; group \times odor, $F_{(6,75)} = 1.234$, $p = 0.299$). However, paired mice exhibited a reduction in odor-evoked freezing during the 1-month retest compared to the 3-day test (Figure 6.1E-F, $F_{(1,12)} = 19.719$, $p = 0.001$). This reduction likely reflects partial extinction learning during the 3-day test, because a parallel experiment found no difference in freezing between mice tested for the first time 3 days post-training and those tested for the first time 1 month post-training (Supplementary Figure S6.5). Shock-alone ($F_{(1,7)} = 0.063$, $p = 0.809$) and odor-alone ($F_{(1,6)} = 0.259$, $p = 0.629$) controls exhibited no change in odor-evoked freezing between tests (Figure 6.1E,F).

Long-lasting enhancement of CS-evoked PG interneuron activity after conditioning.

We used reporter mice (Taniguchi et al., 2011; Zariwala et al., 2012; Chen et al., 2013) (Supplementary Table S6.1) to visualize CS-evoked GCaMP signals in populations of PG interneurons (Wachowiak et al., 2013; Fast and McGann, 2017b) 1 day before, 1 day

after, and 1 month after fear conditioning (Figure 6.1A). Because of the orderly mapping of odor receptors in the nose onto the olfactory bulb glomeruli, odors evoke focal increases in fluorescence in PG cells innervating odor-specific subsets of glomeruli (Figure 6.1G-I). PG cell activity evoked by the first inhalation of the CS was strongly facilitated by fear conditioning (Figure 6.1G,J; Supplementary Figure S6.6A-H,N and Supplementary Table S6.2). Overall, paired mice exhibited a robust enhancement of CS-evoked GCaMP signals 1 day after conditioning that persisted (to a lesser extent) 1 month later (Figure 6.1M, left, $F_{2,14} = 11.219$, $p = 0.001$; and Figure 6.1N, $\chi^2_{(df=2)} = 105.771$, $p < 0.001$). This sensory facilitation may not require feedback from other brain regions because it was even visible during the rising phase of the first inhalation (e.g., Figure 6.1J). Identical results were obtained when GCaMP signals were integrated across the entire 6-sec CS presentation (Figure 6.1M, right and Supplementary Figure S6.7A,D,G), with all individual subjects exhibiting significant enhancements (Supplementary Figure S6.8 and Supplementary Table S6.3).

The odor-alone control group showed no change across imaging sessions in MV-evoked activity on the first inhalation (Figure 6.1I,L,M, $F_{(2,8)} = 2.356$, $p = 0.157$) or integrated across the odor presentation (Figure 6.1M, right, $F_{(2,8)} = 0.120$, $p = 0.888$; Supplementary Figure S6.7C,F,G). Unexpectedly, PG cell physiology was altered in shock-alone controls that received multiple footshocks but no odors during training (Figure 6.1H,K,M,O). After training, most shock-alone subjects (Supplementary Figure S6.6I-M,N and Supplementary Table S6.2) exhibited a small, but persistent reduction of MV-evoked GCaMP signals during the first inhalation (Figure 6.1M, left, $F_{(2,8)} = 5.283$, $p = 0.034$; and Figure 6.1O, $\chi^2_{(df=2)} = 84.351$, $p < 0.001$) and also integrated across multiple

inhalations (Figure 6.1M, right and Supplementary Figure S6.7B,E,G). The opposing effects that occurred in the paired and shock-alone groups, but not in the odor-alone group, could not be attributed to differences in respiration between groups (Figure 6.1P, $F_{(2,15)} = 1.129$, $p = 0.349$) or across imaging sessions (Figure 6.1P, group \times session, $F_{(4,30)} = 1.560$, $p = 0.211$).

Neural generalization to non-threatening odors and correlation with freezing behavior.

We also visualized neural responses to unexposed odors before and after conditioning (e.g., Figure 6.2A-C). After conditioning with MV as the CS, all paired subjects (Supplementary Figure S6.9 and Supplementary Table S6.4) exhibited an enhancement of the PG cell activity that was evoked by all of the unexposed odors (Figure 6.2A,D,G, $F_{(2,14)} = 8.989$, $p = 0.003$). This enhancement was comparable across odors (Figure 6.2A, unexposed-odor \times prep, $F_{(2,14)} = 0.320$, $p = 0.731$; Supplementary Figure S6.10), and equivalent in magnitude to the change in CS-evoked activity (Figures 6.1J,M vs. 6.2D,G, odor-category \times prep, $F_{(4,28)} = 0.156$, $p = 0.958$), paralleling the observed behavioral generalization (Figure 6.1E). This generalized sensory facilitation after fear conditioning cannot be attributed to respiratory effects (Supplementary Figure S6.10). No changes were observed in the odor-alone control group (Figure 6.2C,F,G), while the shock-alone control group exhibited a modest reduction in their responses to these odors (Figure 6.2B,E,G).

The tested odors activate distinct but overlapping sets of glomeruli because they have some chemical similarities. Consequently, there was some overlap between the population of glomeruli that responded to the CS and the populations that responded to the unexposed odors. If fear conditioning had only enhanced activity in glomeruli driven by

the CS, then the degree of generalization would depend on the degree of overlap between each odor and the CS, as occurs in generalization gradients (Lissek et al., 2008; Resnik et al., 2011; Aizenberg and Geffen, 2013). However, that is not what we observed – instead, all odors were equally facilitated and equally fearful. This suggested that olfactory fear conditioning had actually induced plasticity in glomeruli that did not respond to the CS at all. To test this, we isolated a subset of glomeruli that were activated by unexposed odors but did not respond to the CS at baseline (e.g., Figure 6.2H), and compared their response to their preferred odors before and after conditioning. Surprisingly, responses in these glomeruli were facilitated (Figure 6.2I, $\chi^2_{(df=2)} = 120.096$) 1 day ($p < 0.001$) and 1 month ($p < 0.001$) after fear conditioning, though the facilitation was not as robust 1 month later (1d post vs. 1m post, $p < 0.001$). This facilitation did not differ among unexposed odors (Supplementary Figure S6.11).

There was some variability across animals in both physiological (Supplementary Figures S6.6 and S6.8, and S6.9) and behavioral (Supplementary Figure S6.1) responses to odors after conditioning. Remarkably, there was a significant positive correlation such that the subjects exhibiting the largest proportional enhancements of odor-evoked PG cell activity across all odors 1 day after training also tended to spend the most time freezing to odors during the 3-day test (Figure 6.2J, $r = 0.728$, $p = 0.040$).

Broader odor tuning and increased similarity of odor representations after fear generalization.

Paired conditioning modestly increased the number of glomeruli exhibiting a measureable response to each odor in the panel across imaging sessions (Figure 6.3A,D, $F_{(1,2,8,1)} = 9.796$, $p = 0.002$), whereas no difference was observed after shock-alone (Figure

6.3B,E, $F_{(2,8)} = 1.053$, $p = 0.393$) or odor-alone (Figure 6.3C,F, $F_{(2,8)} = 1.557$, $p = 0.269$) training. This change reflected a decrease in the odor-selectivity of individual glomeruli after paired training, but not after shock-alone or odor-alone training (Figure 6.4A-J, group \times session, $F_{(4,30)} = 8.110$, $p < 0.001$). On average, glomeruli responded to slightly more odors (from 0-5) after paired conditioning (e.g., Figure 6.4G; $F_{(2,14)} = 16.781$, $p < 0.001$; pre, 1.64 ± 0.04 ; 1d-post, 2.02 ± 0.04 ; 1m-post, 1.87 ± 0.04). This tuning shift included glomeruli that did not respond to any odors at baseline but began responding to 1 or more odors after conditioning (Supplementary Figure S6.11A,C,G).

The relative decrease in odor selectivity could potentially contribute to the generalized behavioral fear by increasing the similarity between neural representations of different odors. To quantify this, we calculated similarity indexes (from 0-1) between pairs of PG cell activity maps (CS-EV, CS-BA, etc.) before and after conditioning. Pre-training neural representations reflected the chemical and perceptual similarity between odors (Figure 6.4K, pre). After conditioning, the representations of unexposed odors tended to become more similar to that of the CS (Figure 6.4K,L) and to each other (Supplementary Figure S6.12). The largest proportional changes occurred in pairs that were relatively dissimilar at baseline (e.g., CS-2M2B; Figure 6.4K,L). However, even after this change, most similarity indexes were still well below 1 (Figure 6.4K), suggesting that neural representations of non-threatening odors remained discriminable from the CS.

Fear conditioning preferentially boosts CS-evoked activity in weakly-responsive glomeruli.

On average, CS-evoked activity was robustly increased in paired subjects, and slightly reduced in shock-alone subjects (Figure 6.1M). However, there is broad variance

in response to the CS across glomeruli at baseline (Figure 6.5A-F). To test whether fear conditioning had equivalent effects on glomeruli that were weakly- and strongly-responsive at baseline, we compared baseline responsiveness to the effect of fear conditioning in individual glomeruli. Glomeruli that were most weakly activated by the CS at baseline tended to exhibit the largest enhancement of CS-evoked PG cell activity 1 day (Figure 6.5G, $r = -0.627$, $p < 0.001$) and 1 month (Supplementary Figure S6.13 and Supplementary Table S6.5) after paired training. By contrast, the day after shock-alone exposure, MV-evoked responses tended to be reduced in glomeruli that exhibited the largest amplitudes at baseline (Figure 6.5H, $r = -0.157$, $p = 0.009$; and Supplementary Figure S6.13 and Supplementary Table S6.5).

To more clearly illustrate these relationships, glomeruli were ranked from lowest-to-highest based on pre-training MV-evoked $\Delta F/F_s$ within each group, and then separated into quartiles of the pre-training distributions (Figure 6.5I). After conditioning, the glomeruli in the bottom 75% of the paired distribution (Figure 6.5I, left) were enhanced relative to baseline ($P_s < 0.001$ by 1-sample t tests), whereas glomeruli within the top 25% of the pre-training response distribution were unchanged ($p = 0.920$; see Supplementary Table S6.6). By contrast, glomeruli in the bottom half of the shock-alone distribution exhibited no change in response amplitude 1 day post-training (Figure 6.5I, right, $P_s > 0.05$), while those in the top half of the distribution were reduced relative to baseline (Figure 6.5I, right, $P_s < 0.001$).

Olfactory fear conditioning increases odor sensitivity in PG interneurons.

Higher odor concentrations evoke stronger activity in the olfactory bulb (Stewart et al., 1979; Meister and Bonhoeffer, 2001), so the preferential boosting of weak activity

could increase the sensitivity of the system to lower concentrations. To test this, we compared PG cell activity across a 4-fold range of odor concentrations. Before conditioning, the lowest concentration evoked the weakest responses and the highest concentration evoked the strongest responses (Figure 6.6A-I, pre), as expected. After fear generalization, paired subjects (Supplementary Figure S6.14A-H) exhibited enhanced responses across all tested concentrations of the CS (Figure 6.6A,D,G, $F_{(2,14)} = 12.525$, $p = 0.001$) and the unexposed odors (Supplementary Figure S6.15). The proportional effect of fear conditioning was inversely related to the effect of concentration at baseline (Figure 6.6J) because lower concentrations evoked weaker baseline responses that were preferentially boosted, as in Figure 6.5. Note that after conditioning the response to the lowest concentration of the CS was even larger than the activity evoked by the highest CS concentration at baseline (Figure 6.6G), demonstrating that the effect of fear conditioning on PG cell activity was even greater than the effect of quadrupling the odor concentration.

Odor-alone training had no effect on sensitivity to the exposed odor (Figure 6.6C,F,I, $F_{(2,8)} = 1.855$, $p = 0.218$) or to unexposed odors (Supplementary Figure S6.15). However, shock-alone training induced a modest but persistent decrease in PG cell activity across a range of concentrations of MV (Figure 6.6B,E,H, marginally-significant effect across sessions, $F_{(2,8)} = 4.423$, $p = 0.051$), suggesting that footshock exposure by itself may cause slight decreases in sensitivity to odors (Supplementary Figures S6.14 and S6.15).

Discussion

Here, we used fear conditioning to explore the neurosensory effects of generalized fear across odors. Conditioning resulted in equivalent fear of multiple odors, regardless of

similarity to the CS. This fear was correlated with large changes in early sensory processing, including hyper-responsiveness of PG cells, broadened odor tuning, and increased neural sensitivity to lower odor concentrations. These generalized effects occurred within 24 hours of conditioning, persisted for at least a month (with some evidence of reversal with extinction), and were detectable even in the first moments of the brain's response to odors. The finding that fear generalization alters early neural processing of harmless sensory cues may have important implications for the etiology and treatment of anxiety disorders.

Anxiety disorders, especially PTSD, include sensory symptoms like hypervigilance and attentional bias (McNally et al., 1990; Bar-Haim et al., 2007; Eldar et al., 2010; Notebaert et al., 2011; Krusemark and Li, 2012; Dowd et al., 2016). Recent evidence suggests these symptoms may be caused by hyper-reactivity in sensory processing circuitry (Bryant et al., 2005; Stewart and White, 2008; Clark et al., 2009; Krusemark and Li, 2012; Mueller-Pfeiffer et al., 2013), such as in visual cortex while viewing trauma-associated cues (Todd et al., 2015), or even at rest as part of a hypervigilant sensory state (Clancy et al., 2017). Such alterations in sensory function often have some content specificity because they generalize across trauma-related stimuli, but not across neutral stimuli (Cortese et al., 2015; Todd et al., 2015; Zinchenko et al., 2017). Thus, in humans, fear generalization may be based on shared stimulus categories and not just shared features (Dunsmoor et al., 2011a; Dunsmoor and Murphy, 2015). Our study supports this category-based model and demonstrates that when fear has generalized to “odors” rather than “methyl valerate-like odors,” the brain's earliest olfactory sensory regions show strongly facilitated responses that do not require overlapping features between the CS and other stimuli.

We observed that broad fear generalization was accompanied by modest changes in the odor tuning of olfactory bulb glomeruli, causing non-threatening odor representations to become more similar to each other and to the representation of the shock-predictive odor. This contrasts with discriminative conditioning, which increases the difference between the representations of threat-predictive and explicitly safe odors (Li et al., 2008; Kass et al., 2013b). Such plasticity could potentially underlie the perceptual effects of fear conditioning, including either increases or decreases in odor discrimination acuity (Fletcher and Wilson, 2002; Li et al., 2008; Chen et al., 2011; Ahs et al., 2013) depending on the training parameters (Fanselow, 1980; Laxmi et al., 2003; Baldi et al., 2004; Shaban et al., 2006; Chen et al., 2011; Chapuis and Wilson, 2012; Aizenberg and Geffen, 2013; Ghosh and Chattarji, 2015; Poulos et al., 2016). However, even with the increase in similarity between odor representations that occurred after fear generalization, the neural representations of different odors were still quite dissimilar (Figure 6.4K). This suggests that mice are not behaviorally generalizing because they are mistaking other odors for the CS, but they are now representing all odors as potential threats. Notably, PG interneuron activity exhibited enhanced sensitivity to the shock-predictive odor as well as to non-threatening odors, suggesting that the behavioral generalization may have been mediated by a global facilitation of threat detection (Resnik et al., 2011) across a dangerous category of sensory stimuli. Thus, the increased odor-evoked neural activity likely serves non-perceptual functions, such as providing a “warning signal” to recruit attention or prioritize the odor for evoking defensive behavior.

The mechanism of the observed plasticity presumably involves the amygdala, which is a key structure in fear learning (LeDoux, 2000; Maren and Quirk, 2004; Phelps

and LeDoux, 2005) that has been implicated in anxiety disorders such as PTSD (Liberzon et al., 1999; Rauch et al., 2000; Bryant et al., 2005; Protopopescu et al., 2005; Jovanovic and Ressler, 2010; Stevens et al., 2017), and also LC noradrenaline, which is involved in odor perception, olfactory learning, and odor memory formation (Sullivan et al., 1992; Sullivan et al., 2000; Mandairon et al., 2008b; Linster et al., 2011; Moreno et al., 2012; Eckmeier and Shea, 2014). Recent studies using auditory fear conditioning have found that the specificity of cue-evoked freezing was paralleled by the specificity of cue-evoked amygdala activity (Ghosh and Chattarji, 2015), and that the effect of fear generalization on tuning curves in the amygdala was dependent upon the neuron's preferred stimulus, with the broadest shifts in tuning occurring when the preferred stimulus was relatively far from the CS (Resnik and Paz, 2015). Comparable effects of fear generalization are reported here, with glomeruli that exhibited the weakest responses before conditioning being robustly facilitated and the largest baseline responses showing minimal change. We recently demonstrated that PG interneuron activity is influenced by the output of the amygdala and that this effect is mediated by interactions with LC (Fast and McGann, 2017b). Notably, the amygdala-dependent noradrenergic tuning of PG circuitry preferentially affected weakly- over strongly-activated glomeruli, paralleling the effect of fear generalization.

Unexpectedly, odor-evoked PG interneuron activity was reduced in the shock-alone group, even though these subjects did not experience discrete odor cues during conditioning. However, LC densely innervates the olfactory bulb (Shipley and Ennis, 1996; Linster et al., 2011) and salient events can stimulate LC noradrenaline release (Aston-Jones et al., 1996). Further, LC stimulation that is delivered in the absence of any

odors induces a subsequent suppression of odor-evoked responses in the olfactory bulb (Eckmeier and Shea, 2014), consistent with the decrease in sensitivity that was observed here. It is possible that the highly aversive (and salient) footshocks stimulated noradrenaline release in the olfactory bulb, resulting in plasticity in PG interneurons.

In sum, these data show that broad fear generalization is associated with enhanced processing of stimuli in the same category, and that this sensory plasticity is relatively long-lasting, paralleling the pathological fear that can persist for years after a traumatic event in humans. Activity in this circuitry might normally facilitate the detection of threatening sensory cues, but perturbations in this activity might promote vigilance towards harmless cues that resemble danger cues, and thus contribute to anxiety.

Chapter 6 Figures

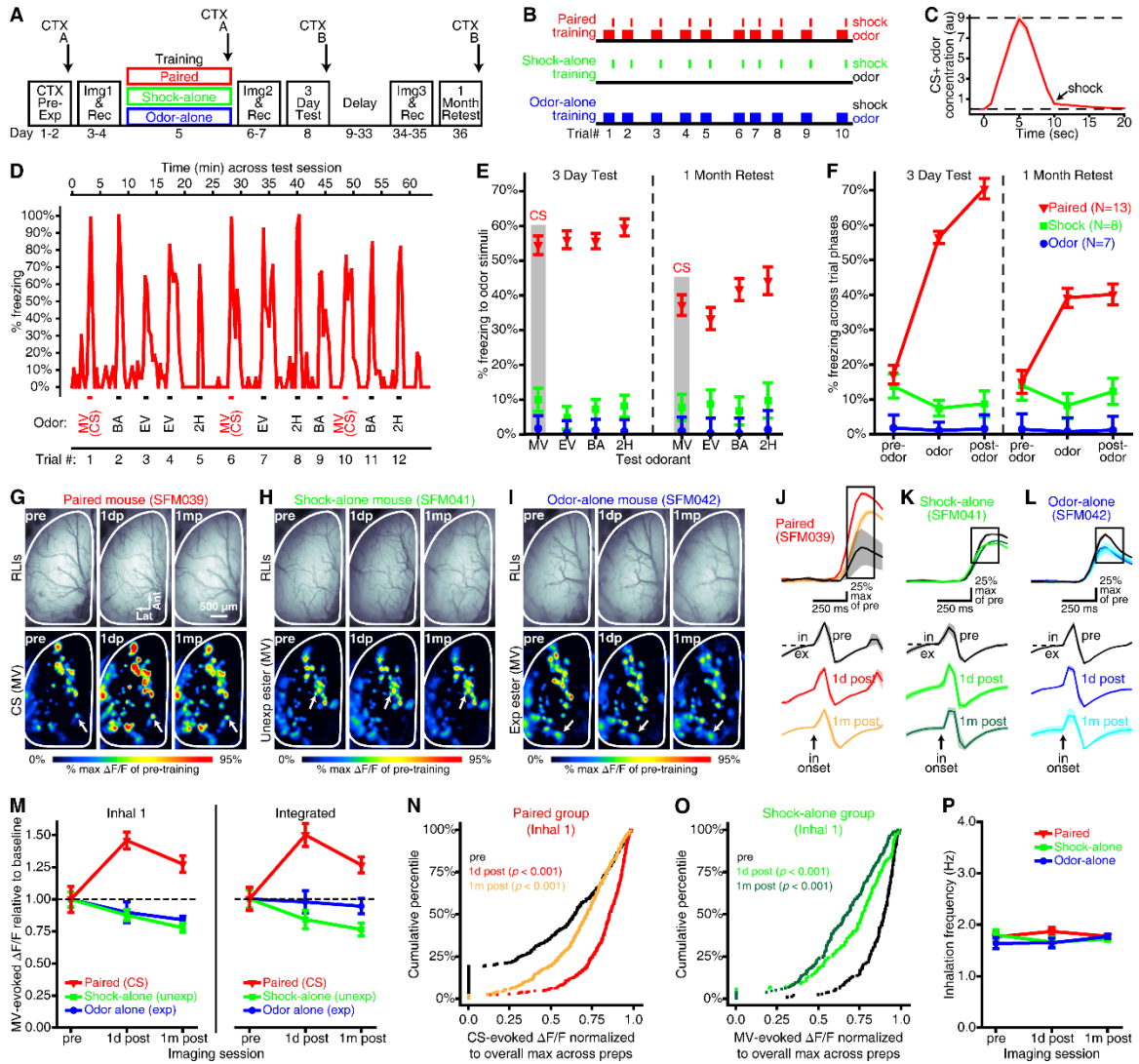
Figure 6.1

Figure 6.1. Olfactory fear conditioning results in a long-lasting, generalized fear response and an enhancement of CS-evoked PG interneuron activity. (A) Experimental timeline. CTX Pre-Exp, context pre-exposure; Img, imaging; Rec, recovery. (B) Sample paired (top), shock-alone (middle), and odor-alone (bottom) training protocols. (C) Mean±SEM CS concentration (in arbitrary units, au) across 10 paired trials. Dashed lines: 9 au, target concentration; 0 au, odor-free. (D) Representative freezing histogram that is plotted against the protocol from that paired subject's 3-day test session. Tick marks

(bottom) are labeled to show odor presentations (MV/CS, EV, BA, and 2H) during all 12 trials. **(E)** Paired subjects exhibited odor-evoked freezing that generalized across odors, whereas comparatively little odor-evoked freezing was observed in either control group. These data are collapsed across odors in **F** and shown as the “odor” trial phase. **(F)** Freezing data are pooled across all 12 trials and separated by trial phase to show relative increases and decreases in freezing that were evoked by odor presentations in the paired and shock-alone groups, respectively. **E-F** show group means \pm SEMs from the 3-day (left) and 1-month (right) tests. **(G-I)** Representative resting light images (RLIs) and pseudocolored difference maps from 1 day before (pre), 1 day after (1dp), and 1 month after (1mp) paired **(G)**, shock-alone **(H)**, or odor-alone **(I)** training. **(J-L)** Mean \pm SEM fluorescence (top; $\Delta F/F$) and piezosensor (bottom: in, inhalation; ex, exhalation) records correspond with the glomerular callouts in **G-I**. All records are aligned relative to the first inhalation after odor onset. Boxed regions indicate the frames that were used for inhalation 1-evoked activity maps **(G-I)** and analyses **(M, left and N-O)**. Traces and activity maps **(G-L)** are averaged across 3-6 trials of MV, which was the CS for paired subjects, an unexposed ester for shock-alone subjects, and the exposed ester for odor-alone subjects. **(M)** Mean \pm SEM CS-evoked activity during the first inhalation (left) and integrated across the entire odor presentation (right) plotted relative to baseline (dashed line) across imaging sessions. **(N-O)** Cumulative frequency histograms pooling glomeruli across subjects. CS-evoked PG cell activity was enhanced after paired training **(N)** but reduced after shock-alone training **(O)**. *P* values are compared with pre-training baseline. **(P)** Mean \pm SEM inhalation frequency did not differ between groups or across imaging sessions.

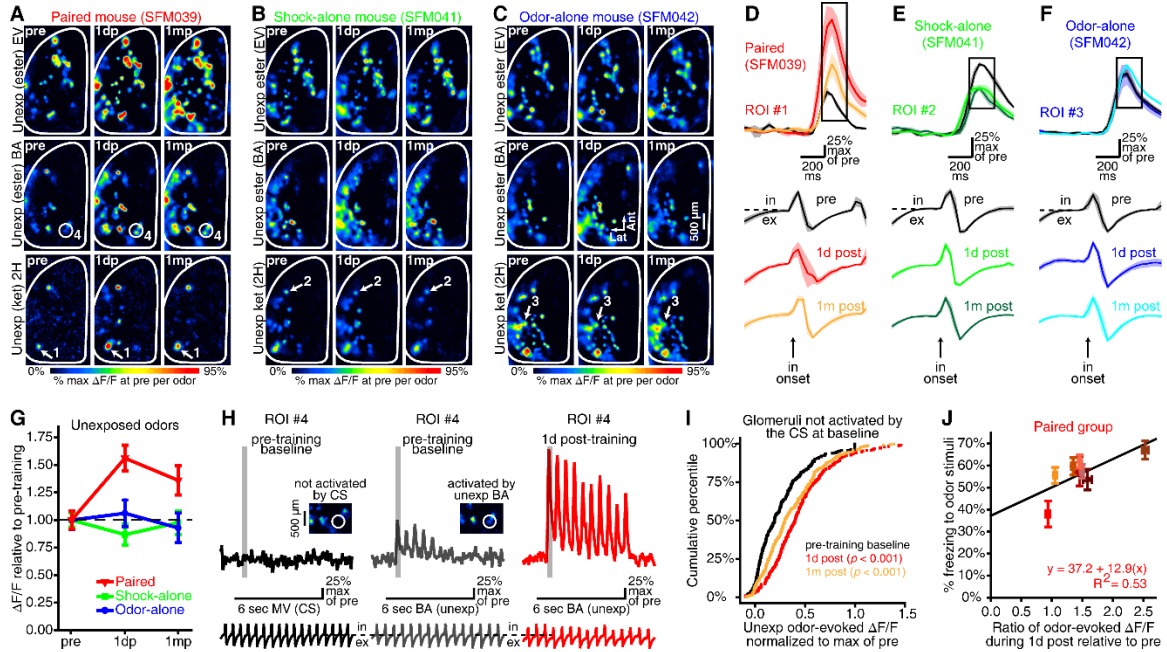
Figure 6.2

Figure 6.2. Generalized enhancement of odor-evoked PG interneuron activity after olfactory fear conditioning. (A-C) Activity maps from paired (A), shock-alone (B), and odor-alone (C) subjects that were evoked by 3 unexposed (unexp) odors (top, EV; middle, BA; bottom, 2H). (D-F) Traces show the mean \pm SEM odor-evoked change in fluorescence ($\Delta F/F$, top) and respiration (bottom; in, inhalation; ex, exhalation) records 1 day before (pre), 1 day after (1d post), and 1 month after (1m post) training. Traces correspond to the numbered glomeruli in A-C and are aligned relative to the first inhalation after odor onset. Boxed regions note the frames that were used for inhalation 1-evoked maps (A-C) and analyses (G-I). The examples in A-F are averaged across 3-6 trials. (G) Mean \pm SEM odor-evoked $\Delta F/F$ pooled across all unexposed odors for each group and plotted across imaging preparations (dashed line, pre-training baseline). (H-I) Glomeruli that were not activated by the CS at baseline were still facilitated after fear conditioning. (H) ROI #4 (which corresponds to the callout in A) did not respond to the CS at baseline (left), but nonetheless exhibited an enhanced response to BA after fear conditioning (middle and right). Each set of 3 traces shows ROI #4's fluorescence (top) and respiration (bottom) records relative to the 6-sec odor presentation (middle) from that trial. Inhalation 1 (G,I) and integrated (J) measurements correspond with the shaded regions and the 6-sec odor presentations,

respectively. **(I)** Cumulative frequency histogram illustrating the odor-evoked $\Delta F/F_s$ in glomeruli that did not respond to the CS at baseline, but still exhibited enhanced responses to unexposed odors after fear conditioning. Data are pooled across 4 unexposed odors and 313 glomeruli that did not respond to the CS at baseline. **(J)** Odor-evoked freezing behavior (y-axis) was positively correlated with the relative enhancement of odor-evoked PG cell activity after fear conditioning (x-axis). For each paired subject, freezing was averaged across all 12 trials during the 3-day test and odor-evoked GCaMP signals were averaged across all glomeruli and odors.

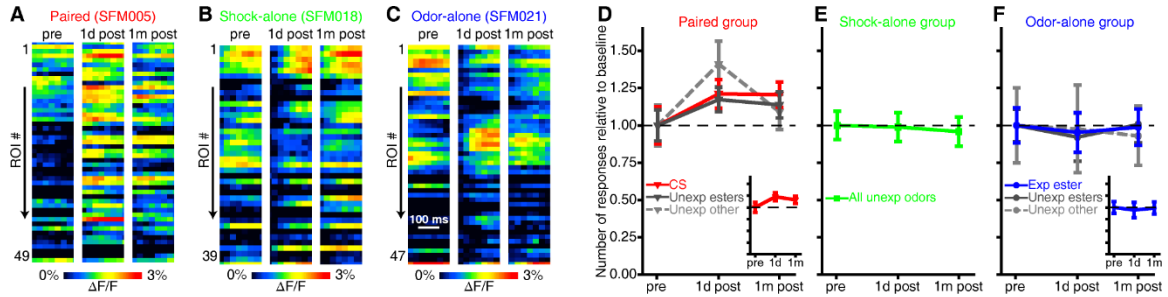
Figure 6.3

Figure 6.3. Olfactory fear conditioning increases the number of glomeruli exhibiting odor-evoked responses. (A-C) Pseudocolored heat maps from imaging sessions that were performed 1 day before (pre, left), 1 day after (1d post, middle), and 1 month after (1m post, right) paired (A), shock-alone (B), or odor-alone (C) training in these representative subjects. Each heat map depicts the MV-evoked change in fluorescence ($\Delta F/F$) across a population of glomeruli (ROI #1 \rightarrow N) during a 200 ms window corresponding to the first inhalation of MV (which was, respectively, the CS and exposed ester for paired and odor-alone subjects). Examples in A-C are from single trials. (D-E) The mean \pm SEM number of odor-evoked glomerular responses is shown as a ratio of pre-training baseline (dashed lines centered on 1.0) and plotted as a function of imaging session for paired (D), shock-alone (E), and odor-alone (F) groups. The data are pooled across relevant odor categories for each group. The insets (D,F) show the mean \pm SEM number of responses pooled across all 3 odor categories and are scaled to the same y-axes of the main panels.

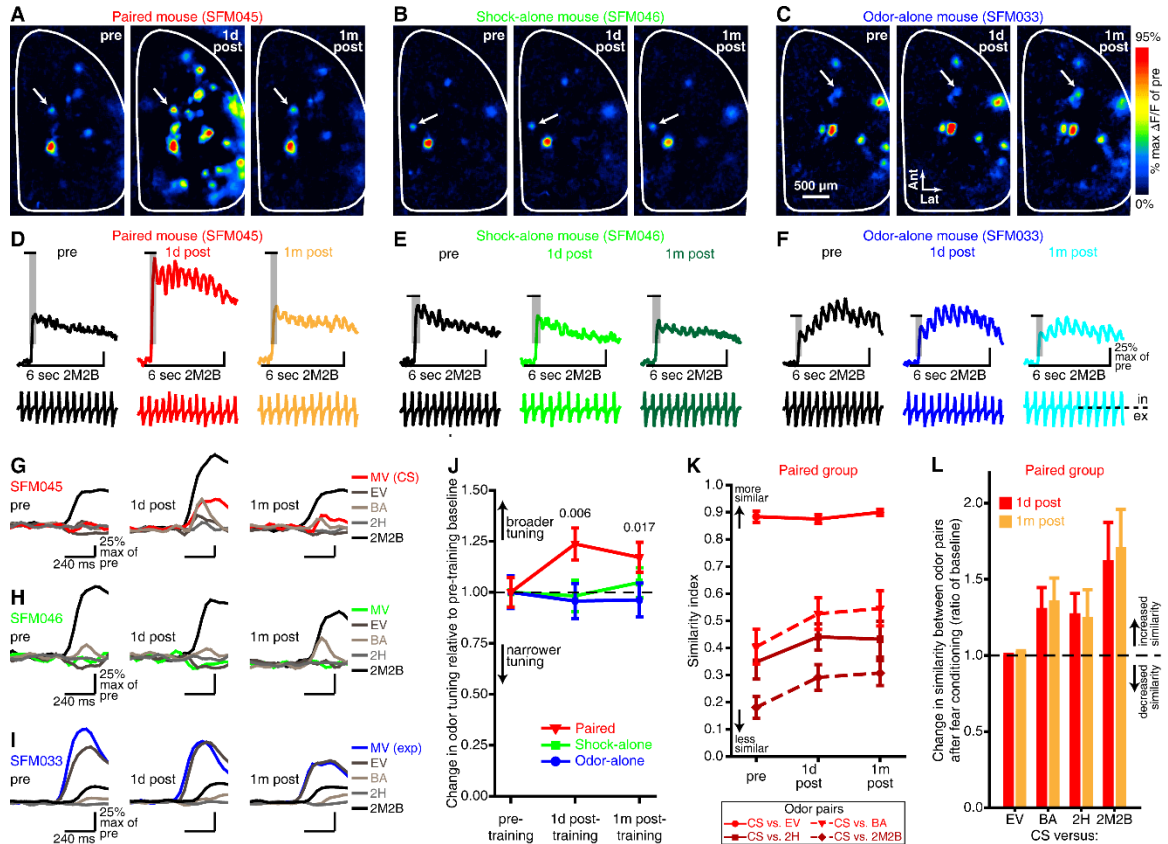
Figure 6.4

Figure 6.4. PG interneurons exhibit a decrease in odor response selectivity after olfactory fear conditioning with a single CS. (A-F) Difference maps (A-C) and corresponding fluorescence (top) and respiration (bottom) records (D-F) that were measured from single trials of 2M2B that were presented 1 day before (left, pre), 1 day after (middle, 1d post), and 1 month after (right, 1m post) each representative subject underwent either paired (A,D), shock-alone (B,E), or odor-alone (C,F) training. 2M2B was an unexposed odor for all 3 groups. The shaded regions on the response amplitudes in D-F indicate the frames corresponding with inhalation 1-evoked maps (A-C) and analyses (J-L). Tick marks shown immediately above the shaded regions note the frames that are expanded in G-I. (G-I) Example odor response selectivity patterns across imaging sessions from the glomeruli in A-F. GCaMP signals that were evoked by the first inhalation of each of the other 4 odors in the panel were superimposed on the 2M2B-evoked amplitude from each imaging session for each glomerulus. (J) Odor-evoked activity in PG interneurons from paired mice exhibited a decrease in selectivity (broader tuning) relative

to pre-training baseline (dashed line), while no change in selectivity was observed across imaging sessions in the shock-alone or odor-alone groups. *P* values are compared to pre-training baseline for paired mice. **(K-L)** After olfactory fear conditioning, PG cell activity maps that were evoked by unexposed odors tended to become slightly more similar to the CS-evoked PG cell activity map, with the largest change in odor map similarity occurring between maps that were the least similar at baseline. **(K)** Mean \pm SEM similarity index between the CS and the other 4 unexposed odors across imaging sessions, where a value of 1 notes complete similarity between an odor pair and 0 notes complete dissimilarity between an odor pair. **(L)** Relative changes in similarity between the CS versus each of the other 4 unexposed odors 1 day and 1 month after training.

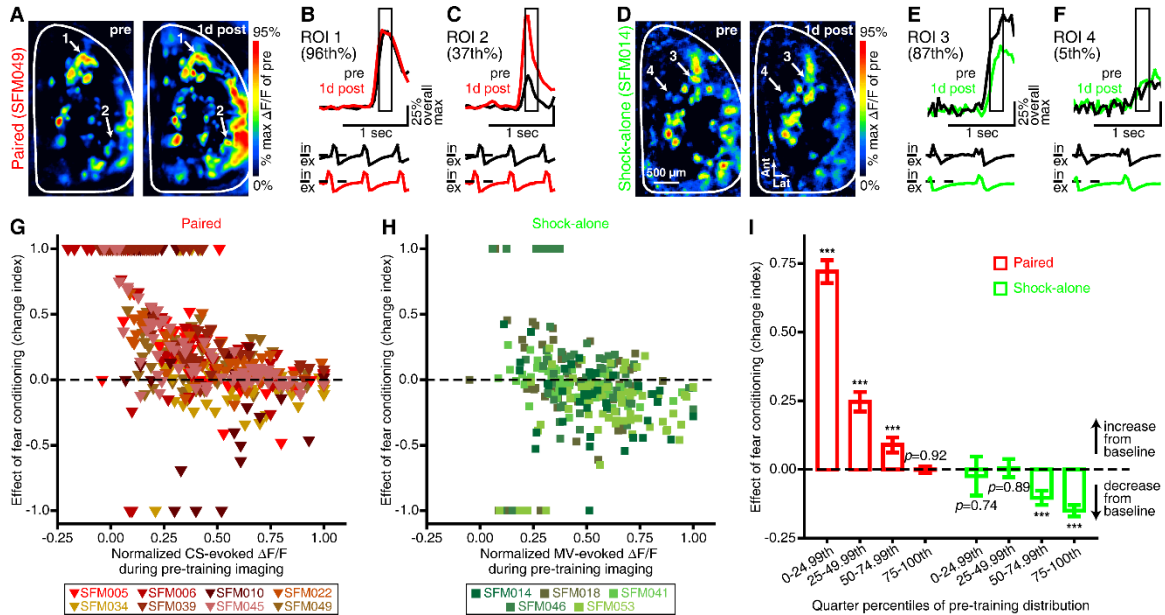
Figure 6.5

Figure 6.5. Fear conditioning-induced alterations in PG interneuron activity are dependent upon baseline response amplitudes. (A,D) Pseudocolored difference maps that were evoked by the CS 1 day before (pre, left) and 1 day after (1d post, right) either paired (A) or shock-alone (D) conditioning. Examples in A-F are from individual trials. These representative paired (A-C) and shock-alone (D-F) subjects respectively had 66 and 42 CS-responsive glomeruli (across both olfactory bulbs) that were rank-ordered from lowest to highest based on pre-training response amplitudes ($\Delta F/F$ s). The sample traces show CS-evoked $\Delta F/F$ s (top) in high-ranking (B, 96th percentile; E, 87th percentile) and low-ranking (C, 37th percentile; F, 5th percentile) glomeruli from 1 day before and 1 day after paired (B,C) or shock-alone (E,F) conditioning. $\Delta F/F$ s are scaled relative to the overall max of pre-training across both ROIs per subject and are aligned relative to the first second of the CS (stimulus bar, middle) and the corresponding respiration records (bottom; in, inhalation; ex, exhalation). Boxed regions indicate inhalation 1-evoked difference maps (A,D) and analyses (G-I). (G,H) Scatterplots showing the changes in CS-evoked PG cell activity 1 day after paired (G, $N = 449$) or shock-alone (H, $N = 277$) conditioning (y-axes) relative to normalized pre-training response amplitudes (x-axes). Data points above and below the dashed lines respectively indicate increases and decreases from pre-training baseline. Each data point represents a single glomerulus, and all glomeruli from a given

subject are color-coded per the keys. **(I)** Mean \pm SEM effect of paired (left, red) or shock-alone (right, green) conditioning 1 day after training for glomeruli that are grouped into quarter percentiles of the pre-training response distribution. Note that ***indicates $p < 0.001$, and all P values are against pre-training baseline by one-sample t tests. Fear conditioning **(A,B,C,G,I)** enhanced PG cell activity more in glomeruli that exhibited the weakest CS-evoked responses during pre-training imaging, whereas shock-alone training **(D,E,F,H,I)** reduced PG cell activity in glomeruli that exhibited the largest baseline responses to the CS (which was just an unexposed odor for this group).

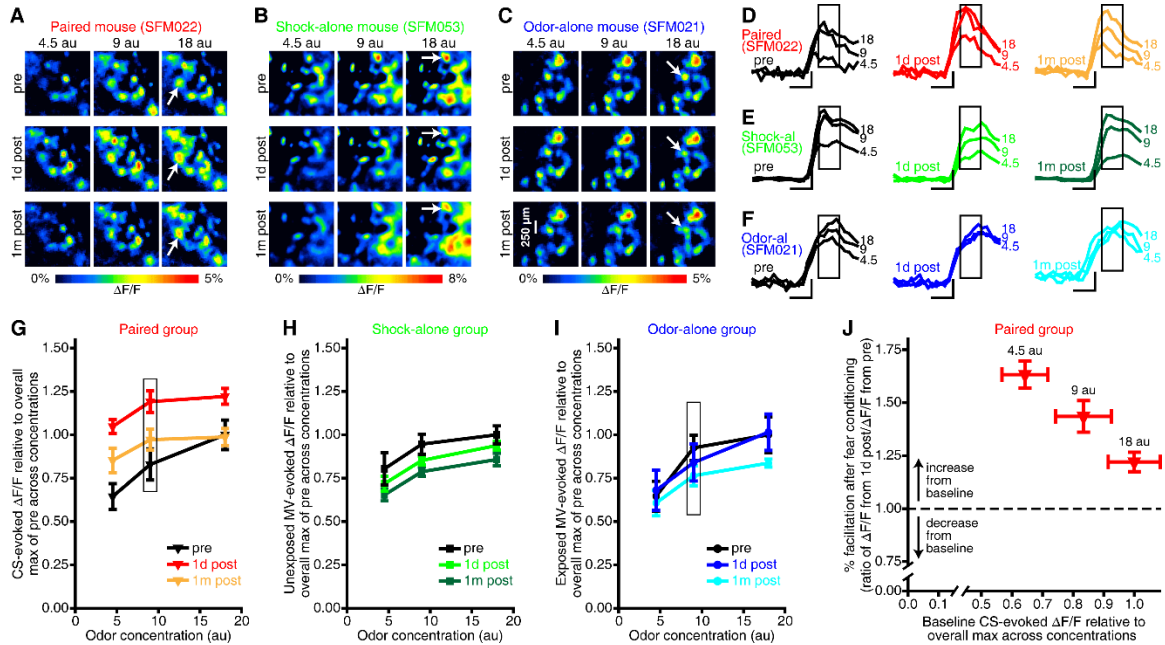
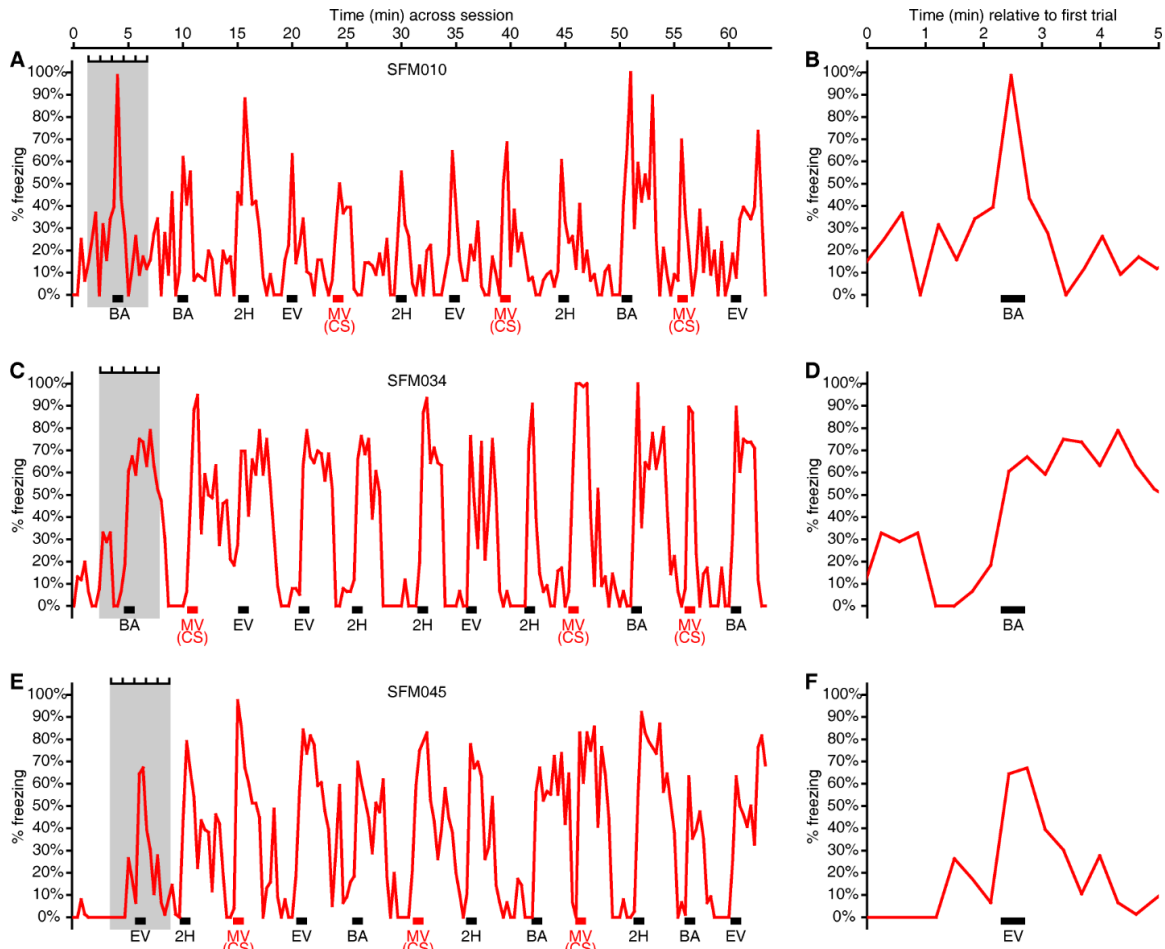
Figure 6.6

Figure 6.6. Enhanced sensitivity of PG interneurons after fear conditioning. (A-F) PG activity maps (A-C) and fluorescence records (D-F) from 1 day before, 1 day after, and 1 month after each representative subject underwent either paired (A,D), shock-alone (B,E), or odor-alone (C,F) training. Examples in A-F are from the first inhalation of odor during individual trials of each of 3 concentrations of MV, which was the CS for paired subjects, an unexposed ester for shock-alone subjects, and the exposed ester for odor-alone subjects. Traces for each ROI (D-F) are scaled relative to the overall max $\Delta F/F$ across concentrations from pre-training (scale bar: vertical, 25% overall max of pre; horizontal, 200 ms). Boxed regions note the frames corresponding with inhalation 1-evoked activity maps (A-C) and analyses (G-J). (G-I) The mean \pm SEM MV-evoked $\Delta F/F$ is plotted as a function of odor concentration (shown in arbitrary units, au) for each imaging session from paired (G), shock-alone (H), and odor-alone (I) groups. Boxed data points indicate the training concentration for paired and odor-alone groups. (J) Scatterplot showing the facilitation of CS-evoked PG cell activity 1 day after training (y-axis) relative to normalized baseline response amplitudes (x-axis) for each concentration of the CS. These data are pooled across 8 paired subjects and displayed as mean \pm SEM $\Delta F/F$ ratios (y-axis) and mean \pm SEM baseline $\Delta F/F$ s (x-axis).

Chapter 6 Supplementary Information

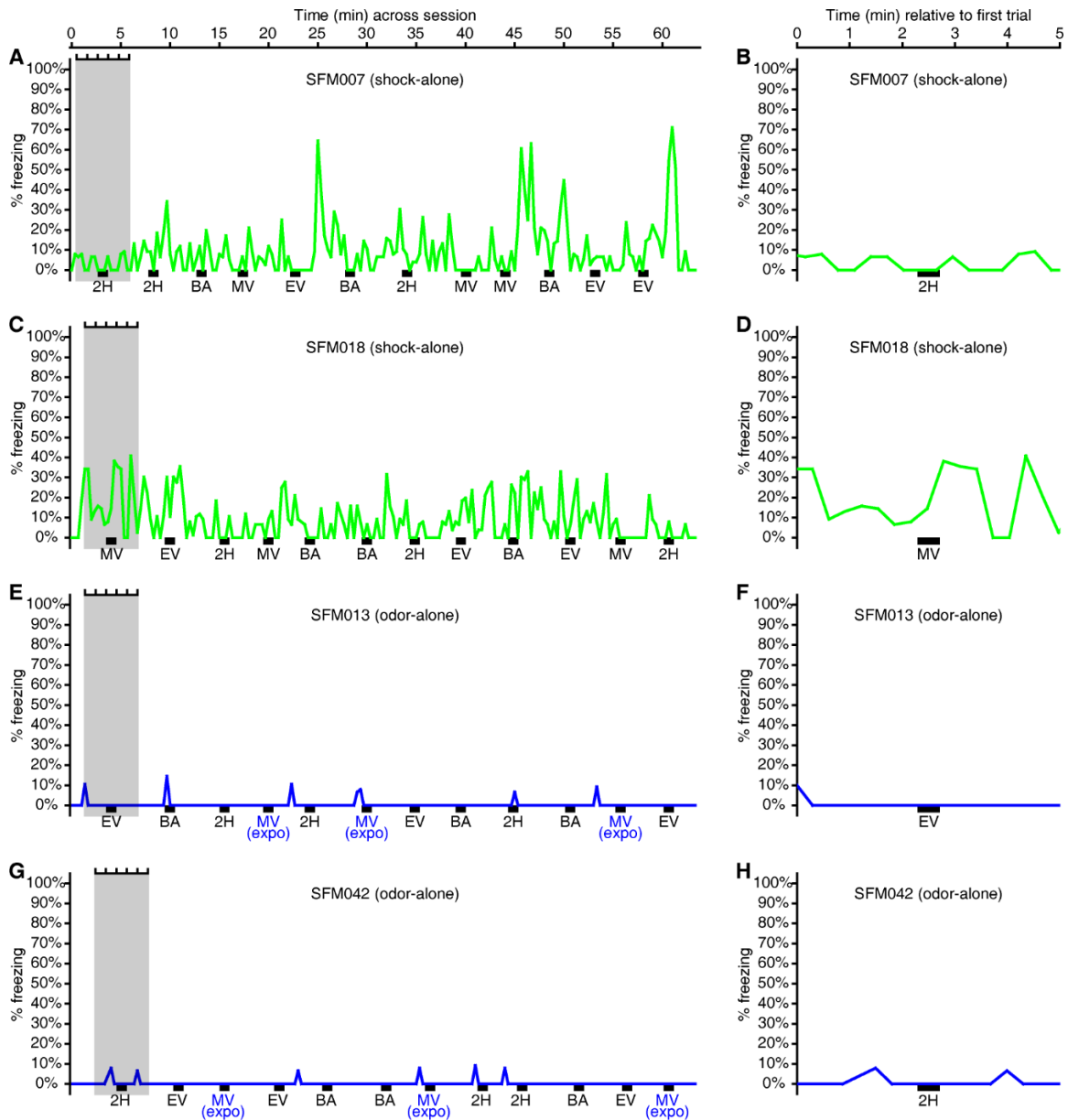
Supplementary Figure S6.1



Supplementary Figure S6.1. Stimulus-evoked freezing patterns in mice that underwent olfactory fear conditioning. The example freezing histograms from SFM010 (A-B), SFM034 (C-D), and SFM045 (E-F) demonstrate that classical olfactory fear conditioning results in broad fear generalization across a range of novel (unexposed) odors that vary in similarity to the CS. (A,C,E) Freezing data from 3 representative paired subjects throughout the entire duration of the 3-day test (see Figure 6.1A). Each subject's behavior was scored as the percent time spent freezing across consecutive 20-sec bins and was then plotted against the session time (63.68 min shown at the top of the figure). Note

that the freezing histogram from the representative subject shown in Figure 6.1D was also calculated across 20-sec bins. During testing, each subject received 3 presentations of each of 4 different odors. The test stimuli included the CS which (which was an ester odor; methyl valerate, MV) and 3 other unexposed odors that varied in chemical similarity to the CS, including a highly similar ester (ethyl valerate, EV, smells very similar to MV), a less similar ester (*n*-butyl acetate, BA, is readily discriminable from MV), and a ketone (2-hexanone, 2H, smells very different from MV). As shown by the protocols that are plotted at the bottom of each histogram, individual trials were presented at variable duration inter-trial intervals (ITIs) and odors were presented in pseudo-random order, allowing no more than 2 consecutive trials of the same odor. **(B,D,F)** These panels correspond with the shaded areas in **A**, **C**, and **E**, which show 5-min bins (scale bars show 1-min intervals) that are centered on the first trial for each subject. Each 5-min bin is expanded to show examples of changes in freezing behavior relative to odor onset and offset for a single trial. As shown here, there was some individual variability between subjects, but overall the paired group tended to exhibit relatively equal levels of stimulus-evoked freezing from trial to trial regardless of which odor was being presented. Additionally, the very first trial typically elicited robust freezing behavior, even when a novel odor was being presented. These sample behavioral patterns are representative of the paired group. In general for paired mice, the presentation of any of the 4 test odors would elicit relatively high levels of freezing behavior. After odor offset (i.e., the end of the trial) freezing behavior tended to remain relatively high for a period of time (which varied from mouse to mouse, as shown here), and would then gradually decline throughout the ITI.

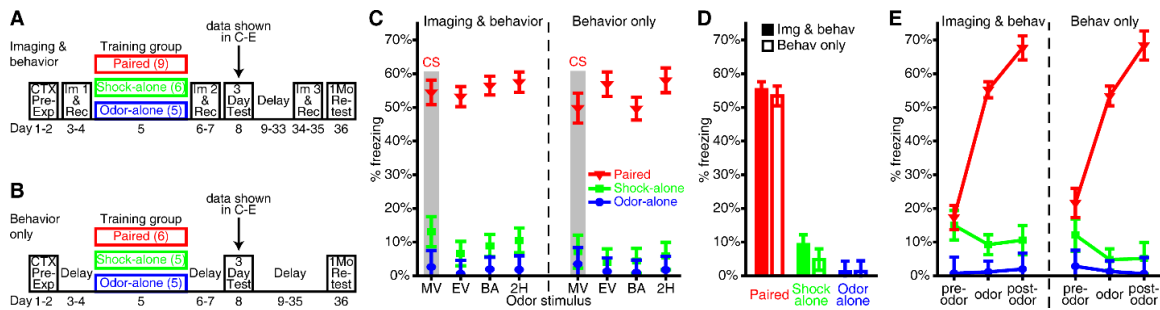
Supplementary Figure S6.2



Supplementary Figure S6.2. Freezing behavior in mice that underwent shock-alone or odor-alone control training. Example freezing data are shown for representative subjects from the shock-alone (**A-B**) and odor-alone (**E-F**) control groups. (**A,C,E,G**) Freezing histograms from 4 individual control subjects throughout the entire duration of the 3-day test (see Figure 6.1A). Each subject's behavior was scored as the percent time spent freezing across consecutive 20-sec bins and was then plotted against the session time

(63.68 min shown at the top of the figure). **(B,D,F,H)** These panels correspond with the 5-min bins (shaded regions) in **A, C, E, and G**. Mice that underwent odor-alone-control training **(E-H)** did not engage in any bouts of odor-evoked freezing, and overall these subjects exhibited near-zero freezing behavior throughout the duration of their test sessions. Mice that underwent shock-alone control training **(A-D)** exhibited low-to-moderate levels of freezing throughout the duration of their test sessions. Importantly, the amount of time that shock-alone controls spent freezing was typically lower than that in paired subjects, and the overall pattern of their freezing behavior was also notably different. Paired mice exhibited robust bouts of freezing that were initiated by an odor presentation and that subsided during the ITIs (Supplementary Figure S6.1), whereas shock-alone mice did not exhibit odor-evoked bouts of freezing. In fact, shock-alone subjects tended to exhibit the opposite behavioral pattern, with relatively higher levels of freezing during the ITIs and relatively lower levels of freezing during the odor presentations **(A-D)**. The relative suppression of freezing during odor presentations can presumably be attributed to an increase in investigatory behavior, which importantly suggests that shock-alone controls were not exhibiting a fear response to any of the odors. Nonetheless, the low levels of freezing that were observed across the entire test session during the ITIs suggests that shock-alone subjects generalized a learned fear response from the training context to the novel testing context, which is consistent with the context generalization that occurs after conditioning with relatively high US intensities (Fanselow, 1980; Laxmi et al., 2003; Baldi et al., 2004; Poulos et al., 2016).

Supplementary Figure S6.3



Supplementary Figure S6.3. Freezing behavior was not affected by the general anesthesia and optical imaging procedures. It was not clear if the presentation of odors (or the anesthesia that was used) during the imaging preparations would alter subsequent stimulus-evoked fear responses during the 3-day test. To address this concern, we ran a parallel “behavior only” experiment in which subjects underwent the same protocol as subjects that underwent the imaging procedures, except that the behavior only subjects had a 2-day delay in the home cage on imaging and recovery days. By comparing test sessions between the behavior only and optical imaging experiments, we were able to determine that 1 day of fear conditioning with a single CS results in stimulus-evoked freezing behavior that generalizes to novel stimuli, and that our optical imaging procedures (which include general anesthesia and surgical procedures) do not interfere with the expression of this generalized fear response.

(A-B) Protocol summaries comparing the paradigm that included imaging and behavioral experiments (A) with the paradigm that only included behavioral experiments (B). The arrows indicate the data that was analyzed and summarized in C-E. The *Ns* per group are shown in parentheses next to each group label. (C) The percent time freezing to MV (the CS), EV, BA, and 2H are averaged across 3 trials per odor within each group and shown separately for imaging and behavior subjects (left) and behavior only subjects (right). (D) The freezing data are then collapsed across all odors in each group to demonstrate that odor-evoked freezing did not differ overall across experiments. (E) Freezing data is pooled across all 12 trials (4 odors, 3×each) and plotted relative to trial phase (pre-odor, odor, and post-odor) for each group in each experiment to show relative

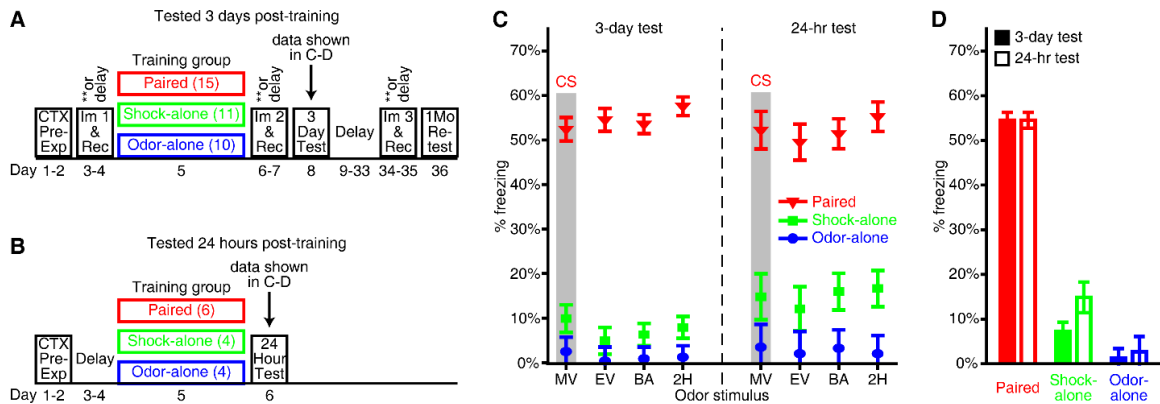
changes in freezing behavior before, during, and after odor presentations. The data presented in **C-E** are shown as the mean \pm SEM.

The data in **C-D** were quantified as the percent of time spent freezing during each 20 sec odor presentation. Importantly, the effect of fear conditioning on stimulus-evoked freezing was not affected by the optical imaging procedures (non-significant effect of experimental paradigm, $F_{(1, 30)} = 0.706$, $p = 0.407$, $\eta_p^2 = 0.023$; non-significant group \times paradigm interaction, $F_{(2, 30)} = 0.271$, $p = 0.765$, $\eta_p^2 = 0.018$). Stimulus-evoked freezing was equal across all 4 odors for the paired group (non-significant effect of odor, $F_{(3, 39)} = 1.048$, $p = 0.382$, $\eta_p^2 = 0.075$), and this was true for imaging and behavior subjects as well as behavior only subjects (non-significant, paradigm \times odor interaction, $F_{(3, 39)} = 0.959$, $p = 0.422$, $\eta_p^2 = 0.069$).

The data shown in **E** were divided into 3 trial phases (pre-odor, odor, and post-odor) that were quantified as the percent of time spent freezing during 3 consecutive 20-sec bins per trial. The pattern of freezing behaviors that was observed across trial phases differed between groups (significant trial phase \times group interaction, $F_{(2.7, 40.5)} = 42.704$, $p < 0.001$, $\eta_p^2 = 0.740$), but was not affected by the optical imaging procedures (non-significant trial phase \times paradigm interaction, $F_{(1.4, 40.5)} = 0.400$, $p = 0.672$, $\eta_p^2 = 0.013$; and non-significant trial phase \times group \times paradigm interaction, $F_{(2.7, 40.5)} = 0.085$, $p = 0.958$, $\eta_p^2 = 0.006$). Freezing behavior varied across trial phases in the paired group (significant effect of trial phase, $F_{(1.3, 17.5)} = 57.812$, $p < 0.001$, $\eta_p^2 = 0.816$), such that each odor presentation evoked a significant increase in freezing (pre-odor versus odor, $p < 0.001$) that remained elevated immediately after odor offset (post-odor versus both pre-odor and odor, $P_s < 0.001$). The stimulus-evoked enhancement of freezing relative to pre-odor baseline did not differ between animals that underwent imaging procedures and animals that did not (non-significant paradigm \times trial phase interaction, $F_{(1.3, 17.5)} = 0.220$, $p = 0.716$, $\eta_p^2 = 0.017$), and it was equal across all 4 odors (non-significant odor \times trial phase interaction, $F_{(3.2, 42.1)} = 1.153$, $p = 0.341$, $\eta_p^2 = 0.081$). By contrast, the change in freezing that was observed across trial phases in shock-alone controls (significant effect of trial phase, $F_{(2, 18)} = 9.082$, $p = 0.002$, $\eta_p^2 = 0.502$) was characterized by an odor-evoked suppression of freezing (pre-odor versus odor, $p = 0.009$) that remained slightly suppressed during the 20-sec interval after

odor offset (post-odor versus odor, $p = 1.00$, post-odor versus pre-odor, $p = 0.071$). This trial phase-dependent modulation of freezing behavior was not affected by the optical imaging procedures (non-significant paradigm \times trial phase interaction, $F_{(2, 18)} = 1.717$, $p = 0.208$, $\eta_p^2 = 0.160$). There was no change in behavior across trial phases in odor-alone controls, as this group exhibited near-zero levels of freezing before, during, and after each odor presentation (non-significant effect of trial phase, $F_{(2, 16)} = 0.389$, $p = 0.684$, $\eta_p^2 = 0.046$), regardless of which paradigm they were included in (imaging and behavior versus behavior only) and which odor was presented (non-significant paradigm \times odor \times trial phase interaction, $F_{(1.8, 14.3)} = 0.761$, $p = 0.604$, $\eta_p^2 = 0.087$). In sum, these results demonstrate that our optical imaging procedures did not have an effect on freezing behavior during odor presentations or during odor-free intervals.

Supplementary Figure S6.4

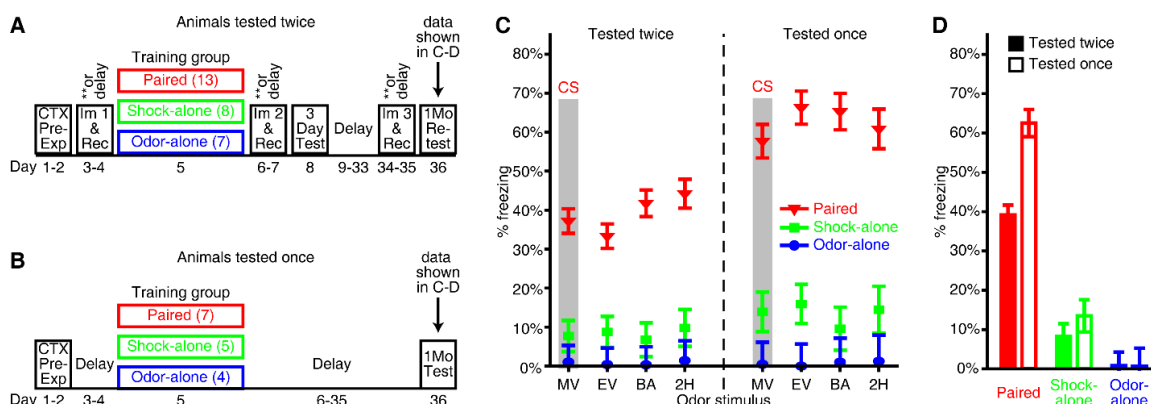


Supplementary Figure S6.4. Fear generalizes to non-threatening odors within 24 hours of olfactory fear conditioning. Subjects that were in the imaging and behavior experiment were tested for stimulus-evoked freezing 3 days after training because they could not be tested prior to imaging (to prevent potential extinction effects), and then a 1-day rest period was needed after imaging to ensure full recovery from the effects of anesthesia. Due to those limitations, we added a parallel experiment in which subjects were tested 24 hours after training.

(A-B) Protocol summaries comparing the paradigms in which the behavioral test was performed either 3 days **(A)** or 24 hours **(B)** after training. The arrows indicate the data that was analyzed and summarized in **C-D**. The *Ns* per group are shown in parentheses next to each group label. Because the imaging procedures did not have an effect on freezing behavior (Supplementary Figure S6.3) data from the 3-day test **(A)** was pooled across the “Imaging and behavior” and “Behavior only identical” paradigms (Supplementary Figure S6.3A-B). **(C)** The percent time freezing to MV (the CS), EV, BA, and 2H are averaged across 3 trials per odor within each group and shown separately for the 3-day (left) and 24-hour (right) test sessions. **(D)** Odor-evoked freezing is pooled across all odors and trials in each group and shown separately for subjects that were tested 3 days after training (solid bars) and subjects that were tested 24 hours after training (open bars). The data in **C-D** are presented as the mean \pm SEM. There was an overall effect of group ($F_{(2, 44)} = 234.436$, $p < 0.001$, $\eta_p^2 = 0.914$), such that the paired group exhibited significantly more odor-evoked freezing than the shock-alone and odor-alone control

groups ($P_s < 0.001$), regardless of the odor that was being presented (non-significant effect of odor, $F_{(3, 132)} = 1.120$, $p = 0.343$, $\eta_p^2 = 0.025$; non-significant group \times odor interaction, $F_{(6, 132)} = 0.521$, $p = 0.792$, $\eta_p^2 = 0.023$). Importantly, there was no difference in freezing behavior between animals that were tested 3 days after training and animals that were tested 24 hours after training (non-significant effect of test time, $F_{(1, 44)} = 1.019$, $p = 0.318$, $\eta_p^2 = 0.023$; non-significant group \times test time interaction, $F_{(2, 44)} = 1.873$, $p = 0.166$, $\eta_p^2 = 0.078$). These data demonstrate that odor-cued fear conditioning results in conditioned fear that generalizes to non-threatening odors within 1 day of training, which is the same behavioral phenotype expressed by subjects that were tested 3 days after training.

Supplementary Figure S6.5



Supplementary Figure S6.5. Olfactory fear conditioning results in broad fear generalization across odors that lasts up to at least 1 month after learning. Subjects underwent behavioral testing twice (Figure 6.1A) because we were primarily concerned with whether or not the effects of fear conditioning could persist up to 1 month after learning, rather than evaluating potential differences in the strength of the initial memory over time. However, no shocks are delivered during behavioral test sessions, so it is possible for subjects in the paired group to undergo some form of extinction learning during the 3-day test, and consequently the results obtained during the 1-month retest could be difficult to interpret. As an attempt to parse apart any behavioral extinction effects that might be induced by the 3-day test from any potential forgetting that might occur during the month-long delay prior to the 1-month retest, we included an additional cohort of behavior only animals that underwent the same fear conditioning protocol and timeline as the imaging and behavior experiment, except that these subjects were only tested once 1 month after the initial training. The results from this control experiment show that the generalized fear response that is expressed 1 month after training is equal to that expressed 3 days (or 24 hours) after learning, suggesting that broad generalization of conditioned fear can be relatively persistent.

(A-B) Protocol summaries comparing the paradigm in which subjects were being retested 1 month after training (A) with the paradigm in which subjects were being tested for the first time 1 month after training (B). The arrows indicate the data that was analyzed and summarized in C-D. The *Ns* per group are shown in parentheses next to each group

label. Because generalization of conditioned fear was not affected the optical imaging procedures (Supplementary Figure S6.3) we pooled data across the 1-month retests (**A**) from animals in the “Imaging and behavior” and “Behavior only” experiments (Supplementary Figure S6.3A-B). (**C**) The percent time freezing to MV (the CS), EV, BA, and 2H are averaged across 3 trials per odor within each group and shown separately for the subjects being retested (tested twice, left) and the subjects being tested for the first time (tested once, right). (**D**) Odor-evoked freezing is pooled across all odors and trials in each group and shown separately for subjects in each experiment (closed versus open bars). All data are shown as the mean \pm SEM.

During the 1-month retest (**C**, left), the paired group exhibited significantly more freezing to odors ($P_s < 0.001$) than the shock-alone and odor-alone control groups (which did not differ from each other, $p = 0.469$), suggesting that the generalized fear response is somewhat long-lasting. However, as shown in Figure 6.1E-F, the paired group also exhibited a reduction in odor-evoked freezing during the 1-month retest relative to their own freezing during the 3-day test. To address this, we directly compared freezing data from subjects being *retested* 1 month after training (**C**, left) with freezing data from subjects being tested for the first time 1 month after training (**C**, right). There was a significant interaction between training group and testing history ($F_{(2, 38)} = 6.563$, $p = 0.004$, $\eta_p^2 = 0.257$), such that the paired subjects that were being retested exhibited less odor-evoked freezing than the paired subjects that were being tested for the first time ($F_{(1, 18)} = 17.800$, $p = 0.001$, $\eta_p^2 = 0.497$). However, freezing from shock-alone ($F_{(1, 11)} = 1.360$, $p = 0.268$, $\eta_p^2 = 0.110$) and odor-alone ($F_{(1, 9)} = 0.074$, $p = 0.791$, $\eta_p^2 = 0.008$) control groups during the 1-month retest did not differ from the same-group counterparts that were tested for the first time 1 month after training. Additionally, there was no difference in odor-evoked freezing in the paired group ($F_{(1, 18)} = 2.303$, $p = 0.147$, $\eta_p^2 = 0.147$) when we compared data from the 3-day test (data shown in Supplementary Figure S6.3) with data from the test that was performed 1 month after training. These results indicate that 1 month after training paired subjects can express a generalized fear response that is equivalent in magnitude to the response that is expressed 1-3 days after training (Supplementary Figures S6.3 and S6.4). This suggests that it is unlikely for the modest reduction in freezing that occurred between the 3-day test and the 1-month retest (Figure 6.1E-F) to be attributable

to forgetting during the month-long delay in between tests. It further demonstrates that the maladaptive behavioral consequences (i.e., freezing to odors that have not been associated with shock) of our odor-cued fear conditioning paradigm are relatively long-lasting, which is consistent with the persistent nature of maladaptive behaviors that are associated with pathological fear in humans.

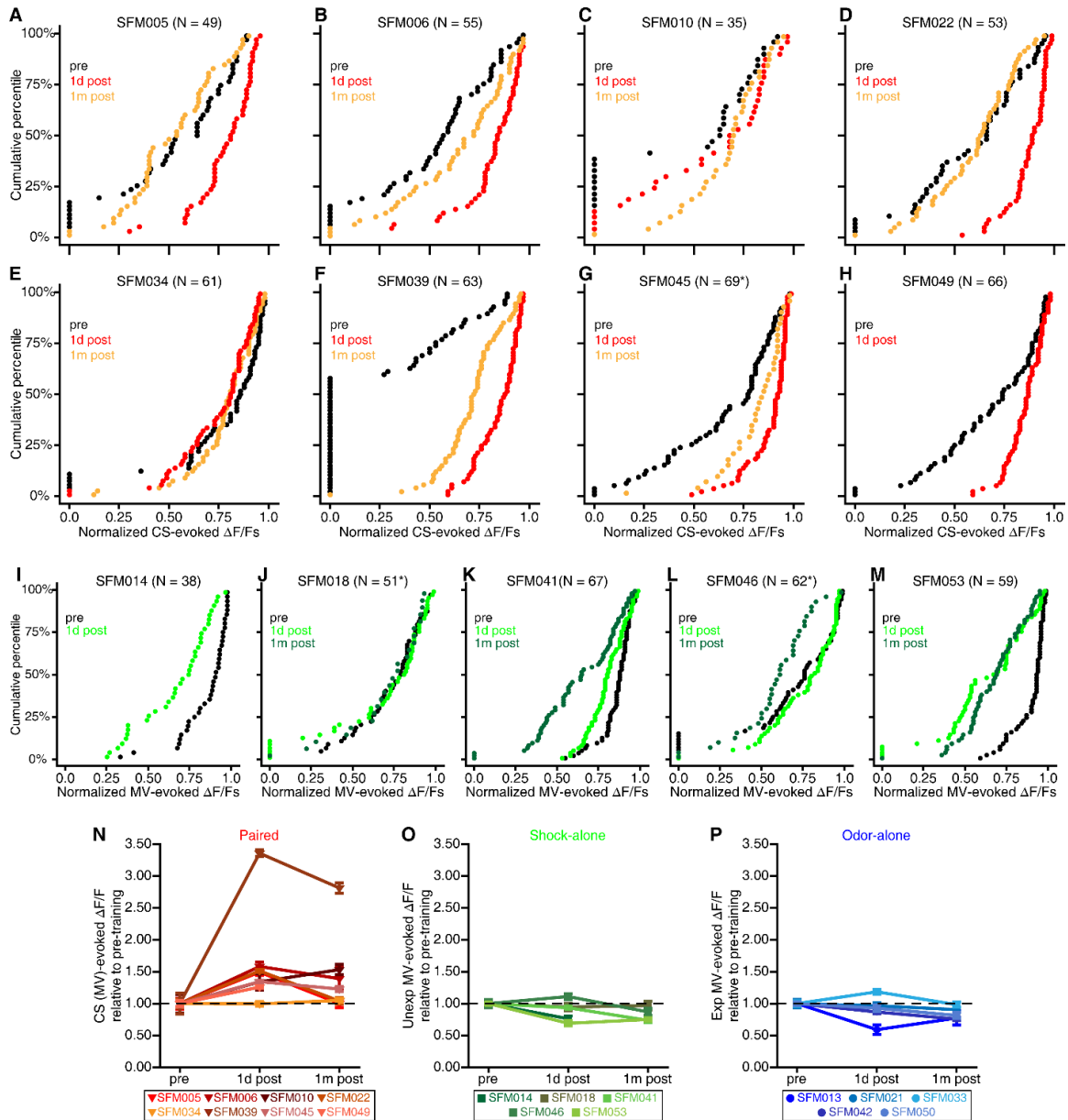
Supplementary Table S6.1

Animal ID	Gene	Group	Example in Figure #:	Example in Sup. Figure S#:	Data sets in Sup. Figure S#:	Analyses in Sup. Table S#:
SFM005	G2×G3	Paired	6.3A	S6.7A	S6.6A,N; S6.8A,I; S6.9A,I; S6.13A; & S6.14A	S6.2, S6.3, S6.4, & S6.5
SFM006	G2×G3	Paired			S6.6B,N; S6.8B,I; S6.9B,I; S6.13B; & S6.14B	S6.2, S6.3, S6.4, & S6.5
SFM010	G2×G3	Paired			S6.6C,N; S6.8C,I; S6.9C,I; S6.13C; & S6.14C	S6.2, S6.3, S6.4, & S6.5
SFM022	G2×G3	Paired	6.6A,D	S6.15A,D,G	S6.6D,N; S6.8D,I; S6.9D,I; S6.13D; & S6.14D	S6.2, S6.3, S6.4, & S6.5
SFM034	G2×G6	Paired		S6.1C-D	S6.6E,N; S6.8E,I; S6.9E,I; S6.13E; & S6.14E	S6.2, S6.3, S6.4, & S6.5
SFM039	G2×G6	Paired	6.1G,J & 6.2A,D,H	S6.1E-F	S6.6F,N; S6.8F,I; S6.9F,I; S6.13F; & S6.14F	S6.2, S6.3, S6.4, & S6.5
SFM045	G2×G6	Paired	6.4A,D,G		S6.6G,N; S6.8G,I; S6.9G,I; S6.13G; & S6.14G	S6.2, S6.3, S6.4, & S6.5
SFM049	G2×G6	Paired	6.5A-C		S6.6H,N; S6.8H,I; S6.9H,I; S6.13H; & S6.14H	S6.2, S6.3, S6.4, & S6.5
SFM014	G2×G3	Shock	6.5D-F	S6.2C-D	S6.6I,O; S6.13I; & S6.14I	S6.2 & S6.5
SFM018	G2×G3	Shock	6.3B		S6J,O; S13J; & S14J	S6.2 & S6.5
SFM041	G2×G6	Shock	6.1H,K & 6.2B,E	S6.7B	S6.6K,O; S6.13K; & S6.14K	S6.2 & S6.5
SFM046	G2×G6	Shock	6.4B,E,H	S6.15B,E,G	S6.6L,O; S6.13L; & S6.14L	S6.2 & S6.5
SFM053	G2×G6	Shock	6.6B,E		S6.6M,O; S6.13M; & S6.14M	S6.2 & S6.5
SFM013	G2×G3	Odor		S6.2E-F	S6.6P	
SFM021	G2×G3	Odor	6.3C & 6.6C,F	S6.15C,F,G	S6.6P	
SFM033	G2×G6	Odor	6.4C,F,I	S6.7C	S6.6P	
SFM042	G2×G6	Odor	6.1I,L & 6.2C,F	S6.2G-H	S6.6P	
SFM050	G2×G6	Odor			S6.6P	

Supplementary Table S6.1. Summary of representative examples and individual data sets. This table identifies which subjects were used as representative examples, and also notes where individual data sets and (corresponding analyses) can be found. Abbreviation key: Gene, genotype; WT, wild-type C57BL/6J mice (Jackson Laboratory, stock

#000664); G2×G3, GAD2-IRES-Cre driver line (Taniguchi et al., 2011) (Jackson Laboratory, stock #010802) crossed with the Ai38(RCL-GCaMP3) reporter line (Zariwala et al., 2012) (Jackson Laboratory, stock # 014538); G2×G6, GAD2-IRES-Cre driver line crossed with the Ai95D reporter line (Chen et al., 2013) (Jackson Laboratory, stock #024105); Shock, shock-alone; Odor, odor-alone; Behav, behavior only paradigm; Img-behav, optical imaging with behavior.

Supplementary Figure S6.6



Supplementary Figure S6.6. Individual variability in the effect of fear conditioning on CS-evoked PG interneuron activity during the first inhalation of odor. Data that were pooled across all subjects in the paired and shock-alone groups respectively exhibited an increase and decrease in CS-evoked PG cell activity after training (Figure 6.1M, left and Figures 6.1N-O). After identifying these overall group effects, we performed a mouse-by-mouse analysis to assess individual variability in the extent of the training-induced

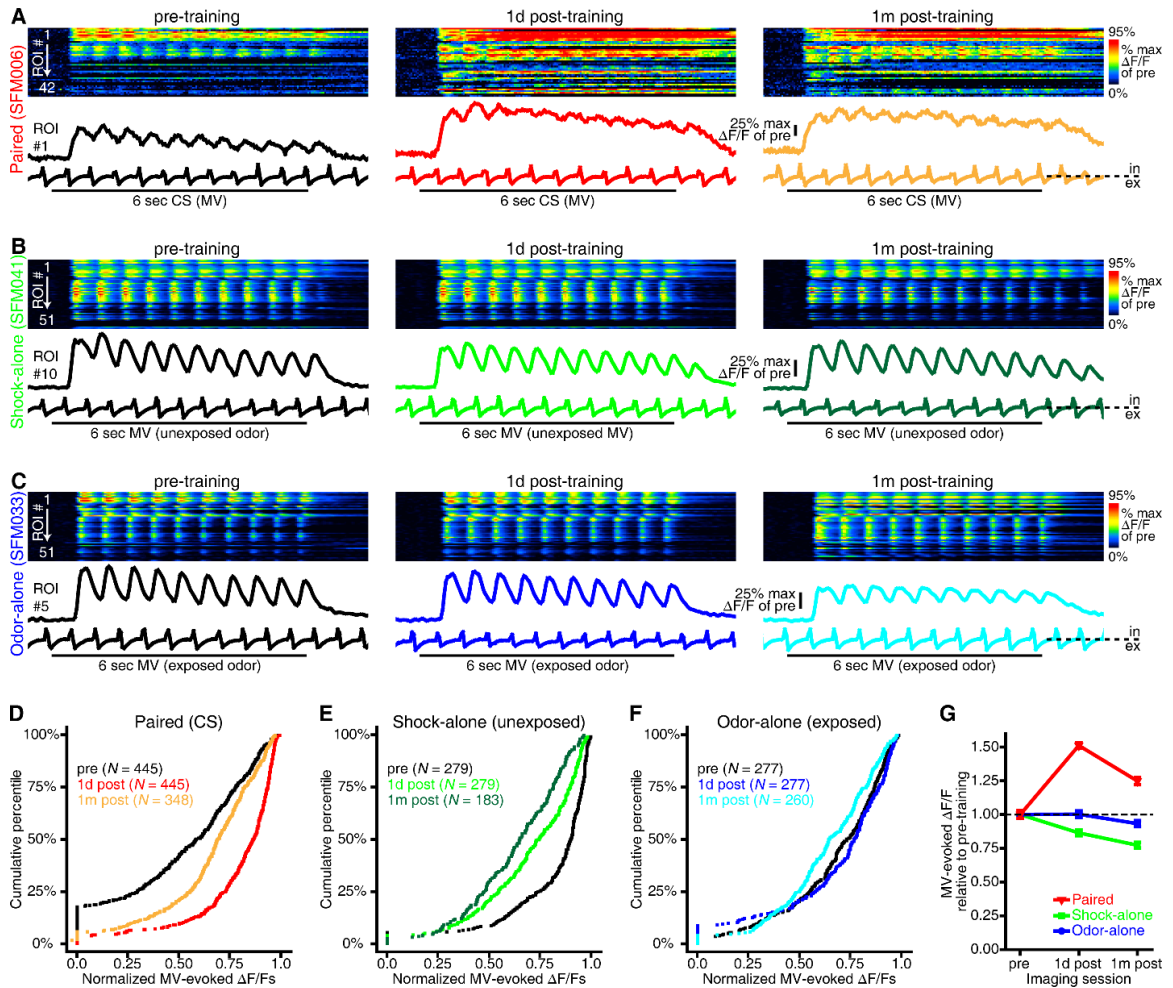
effects in those two groups. Note that the CS odor was simply an unexposed ester (MV) for the shock-alone group, because this group did not receive any odor presentations during training. **(A-M)** Cumulative probability plots from individual mice in the paired **(A-H)** and shock-alone **(I-M)** groups showing the distributions of GCaMP signals that were evoked by the first inhalation of the CS 1 day before (pre), 1 day after (1d post), and 1 month after (1m post) fear conditioning. Examples of inhalation 1-evoked responses to the CS can be seen in Figure 6.1J-L. *N*s indicate the population of glomeruli per mouse that responded to the CS during any of the imaging preparations. Asterisks in **G,J,L** indicate that 1m post was only able to include data from 1 olfactory bulb in each mouse. **(N-P)** Data are pooled across glomeruli for each subject and plotted as the mean \pm SEM ratio of pre-training baseline (dashed lines) for each imaging preparation to show relative changes in PG cell physiology after paired **(N)**, shock-alone **(O)**, or odor-alone **(P)** conditioning. Individual subjects are color-coded per the corresponding keys.

Supplementary Table S6.2

Animal ID	Group	Data shown in Figure:	<i>P</i> values from pairwise comparisons between imaging preparations		
			Pre vs. 1d Post	Pre vs. 1m Post	1d Post vs. 1m Post
SFM005	Paired	Fig. S6.6A	< 0.001	= 1.00	< 0.001
SFM006	Paired	Fig. S6.6B	< 0.001	= 0.085	= 0.011
SFM010	Paired	Fig. S6.6C	= 0.091	= 0.015	= 0.265
SFM022	Paired	Fig. S6.6D	< 0.001	= 1.00	< 0.001
SFM034	Paired	Fig. S6.6E	= 0.581	= 0.782	= 0.628
SFM039	Paired	Fig. S6.6F	< 0.001	< 0.001	= 0.001
SFM045	Paired	Fig. S6.6G	< 0.001	= 0.593	= 0.451
SFM049	Paired	Fig. S6.6H	= 0.002	NA	NA
SFM014	Shock-alone	Fig. S6.6I	= 0.001	NA	NA
SFM018	Shock-alone	Fig. S6.6J	= 0.546	= 0.886	= 0.287
SFM041	Shock-alone	Fig. S6.6K	= 0.047	< 0.001	< 0.001
SFM046	Shock-alone	Fig. S6.6L	= 0.229	< 0.001	= 0.219
SFM053	Shock-alone	Fig. S6.6M	< 0.001	< 0.001	= 1.00

Supplementary Table S6.2. Results from statistical analyses that were performed on the first inhalation of the CS in all individual paired and shock-alone subjects. This table lists the adjusted *P* values from all planned pairwise comparisons between imaging sessions for each mouse. These analyses accompany the cumulative frequency histograms in Supplementary Figure S6.6A-M.

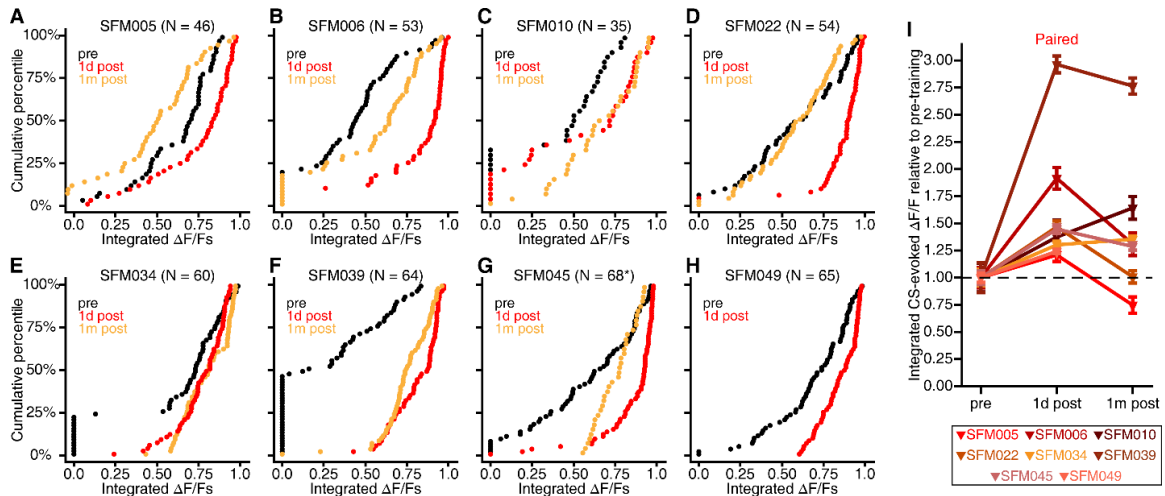
Supplementary Figure S6.7



Supplementary Figure S6.7. CS-evoked PG interneuron activity is enhanced throughout the duration of an odor presentation after paired fear conditioning, but reduced after shock-alone control training. (A-C) GCaMP signals across a population of GAD65-expressing PG interneurons during individual trials consisting of 6-sec presentations of MV. Each set of 3 pseudocolored heat maps corresponds to a population of glomerular ROIs from 1 olfactory bulb from a paired subject (A), a shock-alone subject (B), and an odor-alone subject (C). Each row in a heat map corresponds to a single glomerular ROI (ROI #1 → ROI #N), with each population of ROIs being matched across imaging sessions that were performed 1 day before (left), 1 day after (middle), and 1 month after (right) fear (or control) conditioning. The 3 traces placed immediately below each heat map show an example fluorescence record (top) from 1 of the ROIs in the

corresponding heat map, the respiration record that was recorded from the piezosensor (middle), and the time of the 6-sec MV presentation during that trial (bottom). All heat maps and traces are aligned to 0.5 sec prior to MV onset. **(D-F)** Cumulative frequency histograms showing the distributions of GCaMP signals that are integrated across the entire 6-sec MV presentation 1 day before, 1 day after, and 1 month after paired **(D)**, shock-alone **(E)**, or odor-alone **(F)**, training. Distributions for each group are pooled across MV-responsive glomeruli from all subjects. **(G)** The mean \pm SEM integrated MV-evoked $\Delta F/F$ is pooled across glomeruli from each group, plotted as a function of imaging preparation, and shown as a ratio of pre-training baseline (dashed line). Integrated PG cell activity was affected by paired and shock-alone training, but not by odor-alone training (interaction between group and imaging session, $F_{(4, 30)} = 5.568$, $p = 0.002$, $\eta_p^2 = 0.426$). Specifically, there was an effect of paired training across the population of CS-responsive glomeruli **(D)**, $\chi^2_{(df=2)} = 155.162$, $p < 0.001$), such that integrated PG cell activity was robustly enhanced 1 day after fear conditioning (pre vs. 1d post, $p < 0.001$), and it remained enhanced 1 month later (pre vs. 1m post, $p < 0.001$), albeit to a lesser extent than the initial increase (1d post vs. 1m post, $p < 0.001$). By contrast, the effect of shock-alone control exposure **(E)**, $\chi^2_{(df=2)} = 155.162$, $p < 0.001$) consisted of a persistent reduction in integrated MV-evoked PG cell activity (pre vs. 1d post, $p < 0.001$; pre vs 1m post, $p < 0.001$).

Supplementary Figure S6.8



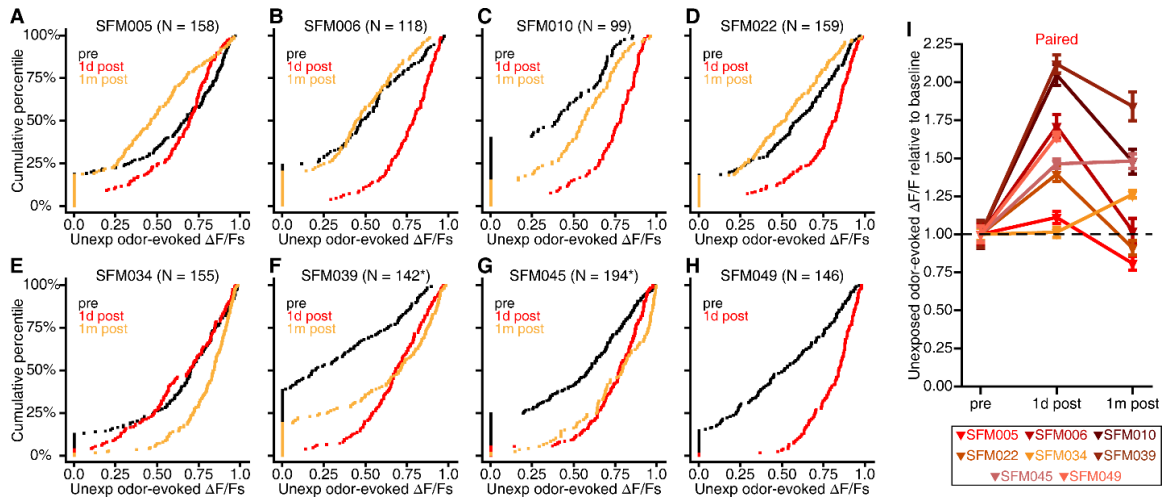
Supplementary Figure S6.8. Individual variability in the effects of olfactory fear conditioning on integrated CS-evoked PG interneuron activity. (A-H) Cumulative probability plots from individual mice in the paired group showing the distributions of integrated GCaMP signals that were evoked in PG interneurons by 6-sec presentations of the CS 1 day before (pre), 1 day after (1d post), and 1 month after (1m post) fear conditioning. Integrated GCaMP signals include multiple inhalations of odor across each 6-sec presentation, and examples of integrated activity can be seen in Supplementary Figure S6.7A-C. *Ns* indicate the population of glomeruli per mouse that responded to the CS during any of the imaging preparations. The asterisk in **G** indicates that 1m post was only able to include data from 1 olfactory bulb. (**I**) Data are pooled across glomeruli per subject and displayed as the mean \pm SEM ratio of pre-training baseline (dashed line) to show relative changes in integrated CS-evoked PG cell activity after fear conditioning.

Supplementary Table S6.3

Animal ID	Data shown in Figure:	<i>P</i> values from pairwise comparisons between imaging preparations		
		Pre vs. 1d Post	Pre vs. 1m Post	1d Post vs. 1m Post
SFM005	Figure S6.8A	= 0.027	= 0.011	< 0.001
SFM006	Figure S6.8B	< 0.001	= 0.026	< 0.001
SFM010	Figure S6.8C	= 0.031	= 0.026	= 1.0
SFM022	Figure S6.8D	< 0.001	= 1.00	< 0.001
SFM034	Figure S6.8E	< 0.001	< 0.001	= 1.00
SFM039	Figure S6.8F	< 0.001	< 0.001	= 0.231
SFM045	Figure S6.8G	< 0.001	= 0.987	= 0.683
SFM049	Figure S6.8H	< 0.001	NA	NA

Supplementary Table S6.3. Integrated CS-evoked PG interneuron activity was significantly enhanced 24 hours after olfactory fear conditioning in all 8 paired subjects. This table lists the adjusted *P* values from all planned pairwise comparisons between imaging sessions for each mouse. These analyses accompany the cumulative frequency histograms in Supplementary Figure S6.8A-H.

Supplementary Figure S6.9



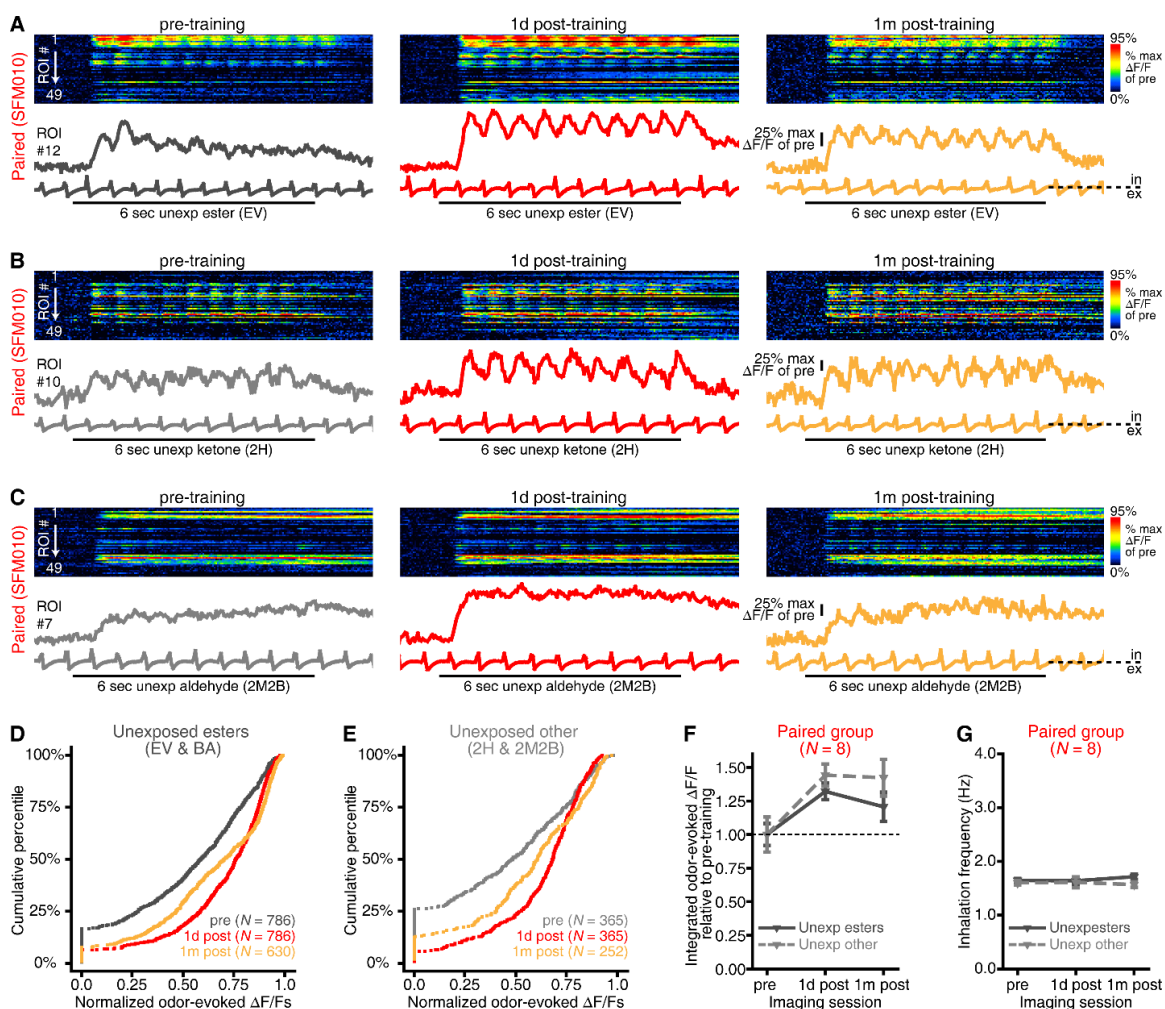
Supplementary Figure S6.9. Fear learning-induced plasticity in PG interneurons generalizes to non-threatening odors. (A-H) Cumulative probability plots from individual mice in the paired group showing the distributions of GCaMP signals that were evoked by the first inhalation of all unexposed odors 1 day before (pre), 1 day after (1d post), and 1 month after (1m post) odor-cued fear conditioning. These data are pooled across all 4 unexposed odors (EV, BA, 2H, and 2M2B) for each mouse because the effect of fear conditioning on PG cell activity was the same across all stimuli. An example of an inhalation 1-evoked response to an unexposed odor can be seen in Figure 6.2D. *Ns* indicate the number of response amplitudes (ΔF/Fs) that are pooled across glomeruli and odors per mouse. Asterisks in **F,G** indicate that the distributions shown for 1 month post-training do not contain the same number of ΔF/Fs as the other 2 distributions. (**I**) Data are pooled across glomeruli per subject and displayed as the mean±SEM ratio of pre-training baseline (dashed line) to show the relative effect of fear conditioning on inhalation 1-evoked PG cell activity that was stimulated by unexposed odors.

Supplementary Table S6.4

Animal ID	Group	Data shown in Figure:	<i>P</i> values from pairwise comparisons between imaging preparations		
			Pre vs. 1d Post	Pre vs. 1m Post	1d Post vs. 1m Post
SFM005	Paired	Fig. S6.9A	= 0.004	= 0.052	= 0.874
SFM006	Paired	Fig. S6.9B	< 0.001	= 0.299	< 0.001
SFM010	Paired	Fig. S6.9C	< 0.001	= 0.009	= 0.013
SFM022	Paired	Fig. S6.9D	< 0.001	= 0.001	< 0.001
SFM034	Paired	Fig. S6.9E	= 0.759	< 0.001	< 0.001
SFM039	Paired	Fig. S6.9F	< 0.001	<0.001	= 1.00
SFM045	Paired	Fig. S6.9G	< 0.001	= 0.716	= 0.006
SFM049	Paired	Fig. S6.9H	< 0.001	NA	NA

Supplementary Table S6.4. Olfactory fear conditioning results in a generalized enhancement of odor-evoked PG interneuron activity in most individual paired subjects. This table provides a summary of the results from the statistical analyses that accompany the cumulative probability plots in Supplementary Figure S6.9A-H. Adjusted *P* values from planned pairwise comparisons between imaging sessions are listed for each mouse. These analyses were performed on a mouse-by-mouse basis to look for individual variability in the extent to which fear conditioning resulted in a generalized enhancement of odor-evoked PG cell activity.

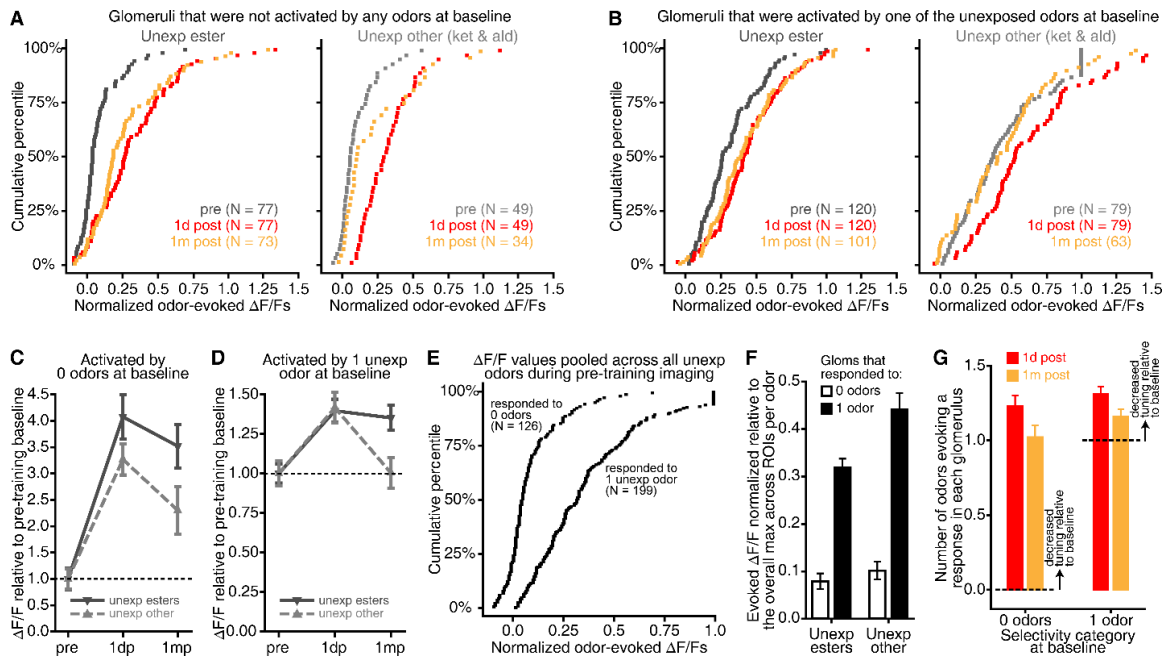
Supplementary Figure S6.10



Supplementary Figure S6.10. The generalized enhancement of PG interneuron activity occurs throughout the entire length of a trial. (A-C) GCaMP signals across a population of GAD65-expressing PG interneurons during individual trials consisting of 6-sec presentations of EV (A), 2H (B), and 2M2B (C). Each set of 3 pseudocolored heat maps shows the same population of glomerular ROIs from 1 olfactory bulb from a paired subject. Each row in a heat map corresponds to a single glomerular ROI (ROI #1 → ROI #49), with all ROIs being matched across imaging sessions that were performed 1 day before (left), 1 day after (middle), and 1 month after (right) fear conditioning. The 3 traces placed immediately below each heat map show an example fluorescence record (top) from 1 of the ROIs in the corresponding heat map, the respiration record that was recorded from

the piezosensor (middle), and the time of the 6-sec odor presentation during that trial (bottom). All heat maps and traces are aligned to 1 sec prior to odor onset. **(D-E)** Cumulative frequency histograms showing the distributions of integrated GCaMP signals that were evoked by unexposed esters **(D)** and by unexposed odors of other chemical classes **(E)** 1 day before, 1 day after, and 1 month after fear conditioning. Distributions are pooled across integrated $\Delta F/F$ s from all 8 paired subjects. **(F)** The mean \pm SEM integrated odor-evoked $\Delta F/F$ was calculated across individual subjects, plotted as a function of imaging preparation for both unexposed odor categories, and shown as a ratio of pre-training baseline (dashed line). On average **(F)**, integrated PG cell activity was enhanced after paired training ($F_{(2, 14)} = 6.355$, $p = 0.011$, $\eta_p^2 = 0.476$), and the effect of fear conditioning generalized equally across the CS and unexposed odors (non-significant interaction between imaging preparation and odor category, $F_{(2.4, 17.0)} = 1.203$, $p = 0.331$, $\eta_p^2 = 0.147$). The generalized effect of fear conditioning is also exemplified by the distributions of integrated GCaMP signals **(D,E)**; $\chi^2_{(df=2)} = 224.487$, $p < 0.001$), which were enhanced the day after fear conditioning (pre vs. 1d post, $p < 0.001$), and remained enhanced 1 month later (pre vs. 1m post, $p = 0.002$), albeit to a lesser extent (1d post vs. 1m post, $p < 0.001$). **(G)** Importantly, the respiration rates that were recorded during trials with unexposed odors did not differ across unexposed odor categories or imaging sessions in the paired group (non-significant effect of imaging session, $F_{(2, 14)} = 0.051$, $p = 0.950$, $\eta_p^2 = 0.007$; non-significant imaging session \times odor category interaction, $F_{(1.1, 7.8)} = 1.371$, $p = 0.286$, $\eta_p^2 = 0.164$), so the non-specific enhancement of odor-evoked PG cell activity is likely the result of learning-induced sensory plasticity and not changes in respiration.

Supplementary Figure S6.11

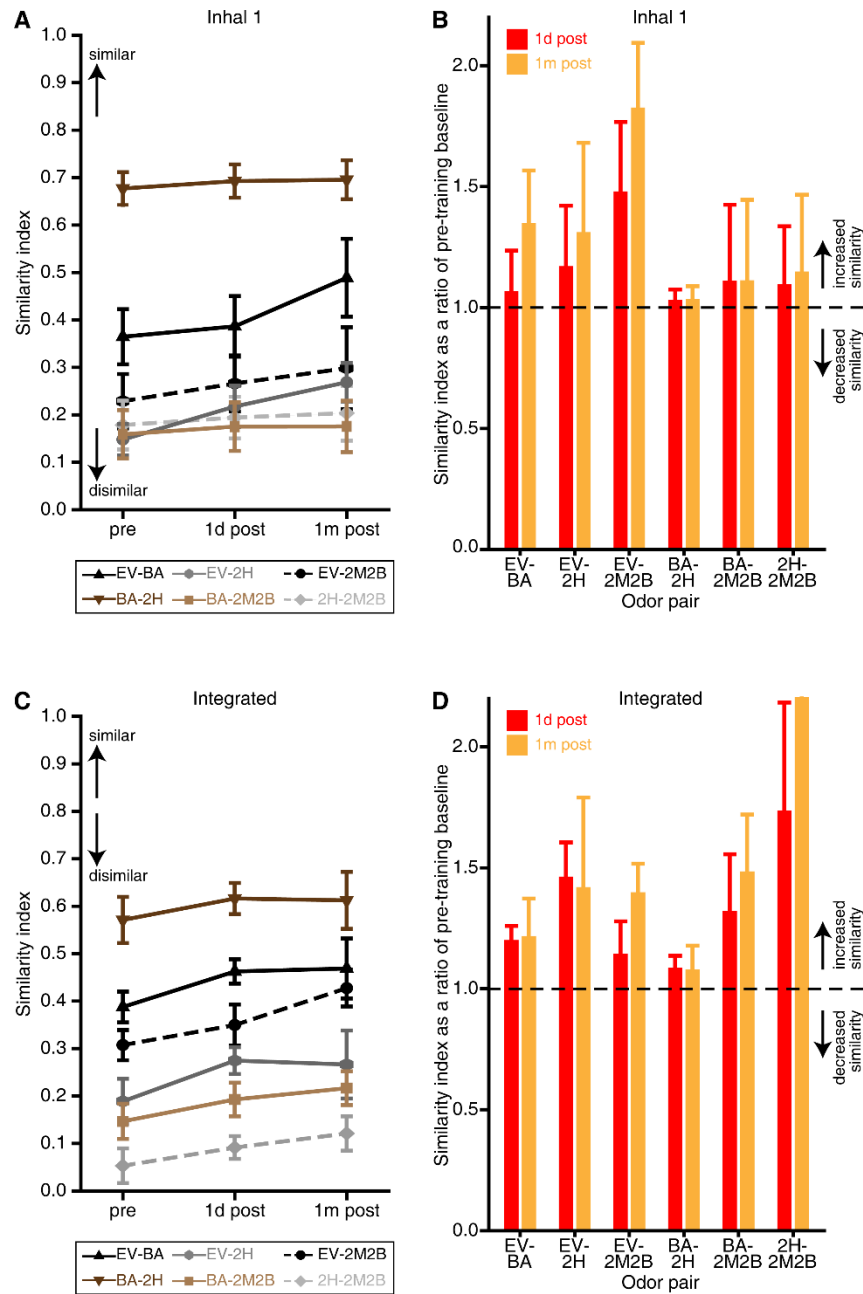


Supplementary Figure S6.11. The generalized enhancement of PG interneuron activity that occurred after fear conditioning was observed in glomeruli that did not respond to the CS at baseline. (A-B) Cumulative frequency histograms showing the distributions of response amplitudes ($\Delta F/Fs$) that were evoked by the first inhalation of an unexposed odor 1 day before (pre), 1 day after (1d post), and 1 month after (1m post) fear conditioning in glomeruli that did not respond to any odors at baseline (A) and glomeruli that only responded to 1 of the 4 unexposed (unexp) odors at baseline (B). Note that the glomeruli that did not respond to any odors at baseline (A) had below- or near-zero response amplitudes that did not exceed our statistical thresholding criterion. The activity that was evoked by unexposed esters (left; EV and BA) and by unexposed odors of “other” chemical classes (right; 2H and 2M2B) is displayed separately in each panel. (C-D) The distributions in A-B were averaged across glomeruli and are plotted here as a ratio of pre-training baseline (dashed line) to show relative changes across imaging sessions in PG cell activity that was evoked by unexposed odors. (E-F) Cumulative frequency histogram (E) and mean \pm SEM summary plot (F) comparing the normalized unexposed odor-evoked $\Delta F/Fs$ between glomeruli that did not respond to any odors and glomeruli that only responded to 1 unexposed odor during pre-training imaging. (G) The mean \pm SEM number

of odors evoking a measurable response in each glomerulus 1 day (red) and 1 month (orange) after fear conditioning is shown for populations of glomeruli that are separated by their baseline selectivity (left, responded to 0 odors; right, responded to 1 unexposed odor). The dashed lines indicate baseline odor response selectivity for each selectivity category. Values above and below the dashed lines respectively indicate decreases and increases in odor tuning relative to baseline.

The results that are summarized above in Supplementary Figure S6.11 show that there were glomeruli that were not activated by the CS at baseline, but were nonetheless facilitated after fear conditioning (**A-D**), confirming a generalized enhancement of odor-evoked PG interneuron activity. This generalized enhancement was equal across unexposed odor categories (i.e., unexposed esters vs. unexposed other) and was even observed in glomeruli that did not exhibit a measurable response to any of the odors in our panel at baseline, but that began to respond to at least 1 of the unexposed odors after fear conditioning (**A,C**). Notably, the facilitation was larger in glomeruli that did not respond to any odors at baseline (**C**) than in glomeruli that responded to 1 unexposed odor at baseline (**D**). The population that did not respond to any odors at baseline consisted of glomeruli that had below- or near-zero amplitudes that did not exceed our statistical thresholding criterion, and were therefore substantially smaller than the baseline amplitudes that were measured from glomeruli that responded to 1 unexposed odor (**E-F**). We found that fear conditioning differentially affected CS-evoked PG interneuron activity based on pre-training response amplitudes, such that glomeruli with the smallest CS-evoked amplitudes at baseline exhibited the largest facilitation after fear conditioning (Figure 6.5 and Supplementary Figure S6.13). We extended those findings here by demonstrating that the generalized enhancement of PG interneuron activity was more robust in the glomeruli that did not respond to any odors and thus had the weakest responses at baseline. The generalized facilitation of odor-evoked PG cell activity may be related to changes in odor tuning (see Figure 6.4 for more extensive selectivity analysis) because glomeruli that did not respond to the CS at baseline exhibited a decrease in odor tuning (i.e., responded to more odors) after fear conditioning, regardless of their baseline odor selectivity category (**G**).

Supplementary Figure S6.12

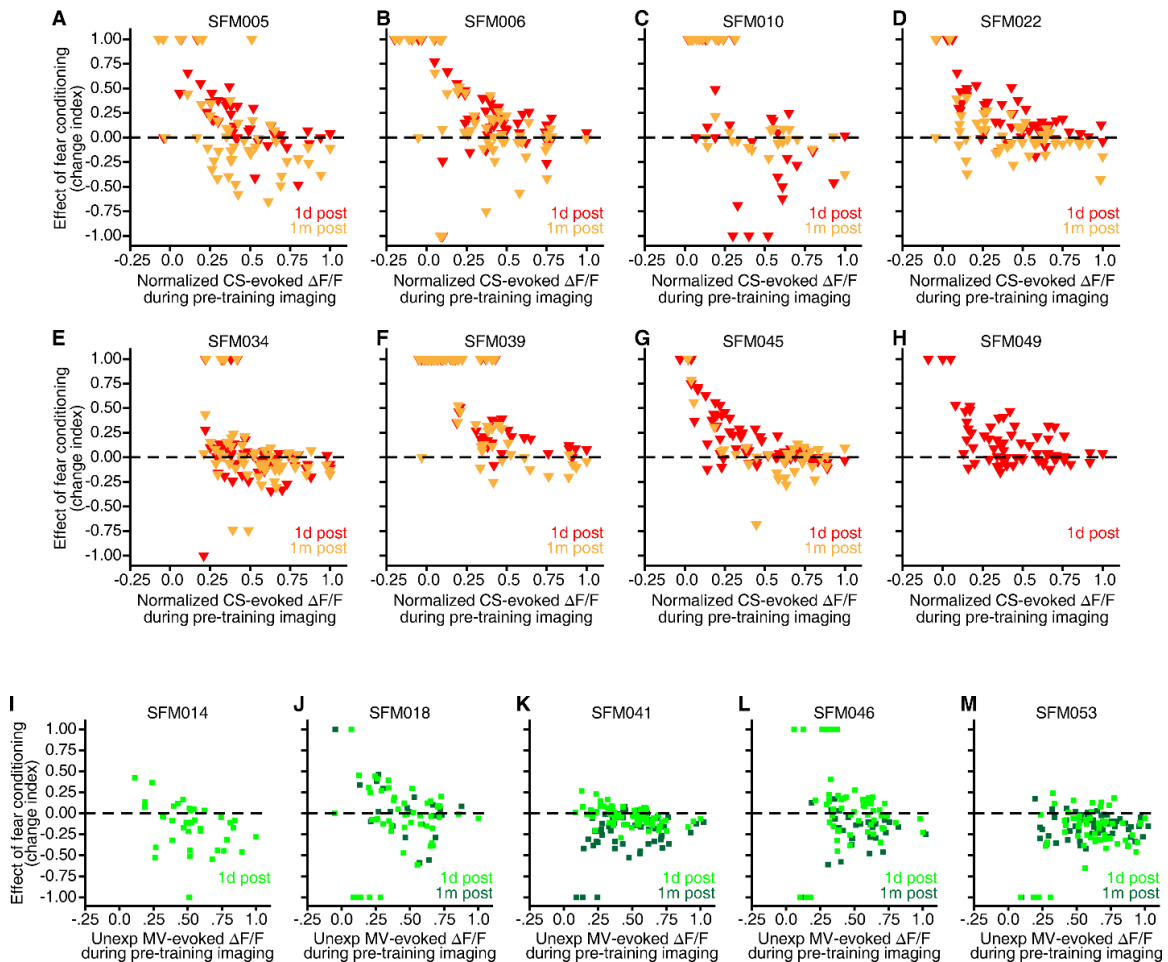


Supplementary Figure S6.12. Activity maps that are evoked by non-threatening odors tend to become more similar to each other after olfactory fear conditioning. Mice that underwent fear conditioning exhibited a generalized behavioral fear response to novel odors that was paralleled by a generalized enhancement of odor-evoked PG interneuron activity and by a decrease in glomerular odor response selectivity. It is possible that these

parallel changes in PG interneuron physiology increase the similarity (i.e., decrease the discriminability) between neural representations of the CS and unexposed odors (Figure 6.4K-L), and also between unexposed odors versus each other. To assess this possibility, we calculated similarity indexes for all possible pairwise comparisons of PG cell activity that was evoked by each of the 5 odors in our panel, yielding 10 odor pairs (see Figure 6.4K-L for CS versus unexposed odors).

(A,C) The mean \pm SEM similarity between pairs of unexposed odors was calculated across all 8 paired subjects and is plotted as a function of imaging preparation. The similarity index ranged from 0-1, with 0 indicating complete dissimilarity between odor-evoked PG cell activity and 1 indicating complete similarity. This analysis was performed on PG interneuron activity that was evoked by the first inhalation **(A)**, and also integrated across the trial **(C)**. **(B,D)** The 6 odor pairs differed in similarity at baseline – for example, at baseline EV- and BA-evoked PG activity maps were more similar to each other than EV- and 2H-evoked PG activity maps. Because of these baseline differences in odor map similarity we calculated ratios between the similarity indexes from 1 day and 1 month post-training relative to the similarity indexes from pre-training. This permitted a qualitative evaluation of changes in PG activity map discriminability relative to baseline (dashed line) for responses that occurred after the first inhalation **(B)** and responses that were integrated across the entire 6-sec odor **(D)**. After fear conditioning, most odor pairs tended to be more similar to each other than they were during baseline, regardless of if we were looking at PG activity that was evoked by the first inhalation of odor **(A-B)** or activity that was integrated across 6-sec odor presentations **(C-D)**. However, the increase in similarity was not equal for all odor pairs, and seemed to be inversely related to baseline similarity. For example, there was almost no change in the similarity between BA- and 2H-evoked activity maps after fear conditioning **(B,D)**, but out of all of the unexposed odor pairs, BA and 2H were the most similar at baseline **(A,C)**. Overall, these data suggest that PG activity maps that are evoked by novel odors may become more similar to each other after fear learning.

Supplementary Figure S6.13



Supplementary Figure S6.13. Paired mice exhibited the largest enhancement of PG cell activity in glomeruli that had the weakest responses to the CS at baseline, while most shock-alone mice tended to exhibit a reduction of activity in glomeruli that had larger response amplitudes at baseline. (A-M) Scatter plots from individual paired mice (A-H) and individual shock-alone mice (I-M) showing the effect of fear conditioning on CS-evoked PG cell activity 1 day and 1 month after fear conditioning (y-axes) relative to pre-training response amplitudes ($\Delta F/F$ s, x-axes). Glomeruli that did not respond to the CS at baseline, or glomeruli that were very weakly activated by the CS at baseline, had normalized CS-evoked $\Delta F/F$ s that were below or near 0 (along the x-axes). Data points that are above or below the dashed line are respectively increased or decreased from baseline.

Supplementary Table S6.5

Animal ID	Group	Data shown in Figure:	Correlation between CS-evoked $\Delta F/F$ during pre-training imaging and:					
			Change index 1d post-training			Change index 1m post-training		
			<i>N</i>	Pearson's <i>r</i>	<i>P</i> value	<i>N</i>	Pearson's <i>r</i>	<i>P</i> value
SFM005	Paired	Fig. S6.13A	49	-0.648	< 0.001	49	-0.557	< 0.001
SFM006	Paired	Fig. S6.13B	55	-0.523	< 0.001	55	-0.515	< 0.001
SFM010	Paired	Fig. S6.13C	34	-0.617	< 0.001	34	-0.745	< 0.001
SFM022	Paired	Fig. S6.13D	53	-0.732	< 0.001	51	-0.493	< 0.001
SFM034	Paired	Fig. S6.13E	60	-0.319	= 0.013	60	-0.383	= 0.003
SFM039	Paired	Fig. S6.13F	63	-0.800	< 0.001	63	-0.777	< 0.001
SFM045	Paired	Fig. S6.13G	69	-0.728	< 0.001	36	-0.549	= 0.001
SFM049	Paired	Fig. S6.13H	66	-0.543	< 0.001	-	-	-
SFM014	Shock-AI	Fig. S6.13I	38	-0.380	= 0.019	-	-	-
SFM018	Shock-AI	Fig. S6.13J	51	0.052	= 0.718	24	-0.304	= 0.149
SFM041	Shock-AI	Fig. S6.13K	67	-0.507	< 0.001	67	-0.293	= 0.016
SFM046	Shock-AI	Fig. S6.13L	62	-0.287	= 0.024	35	0.223	= 0.197
SFM053	Shock-AI	Fig S6.13M	59	-0.238	= 0.011	59	0.202	= 0.126

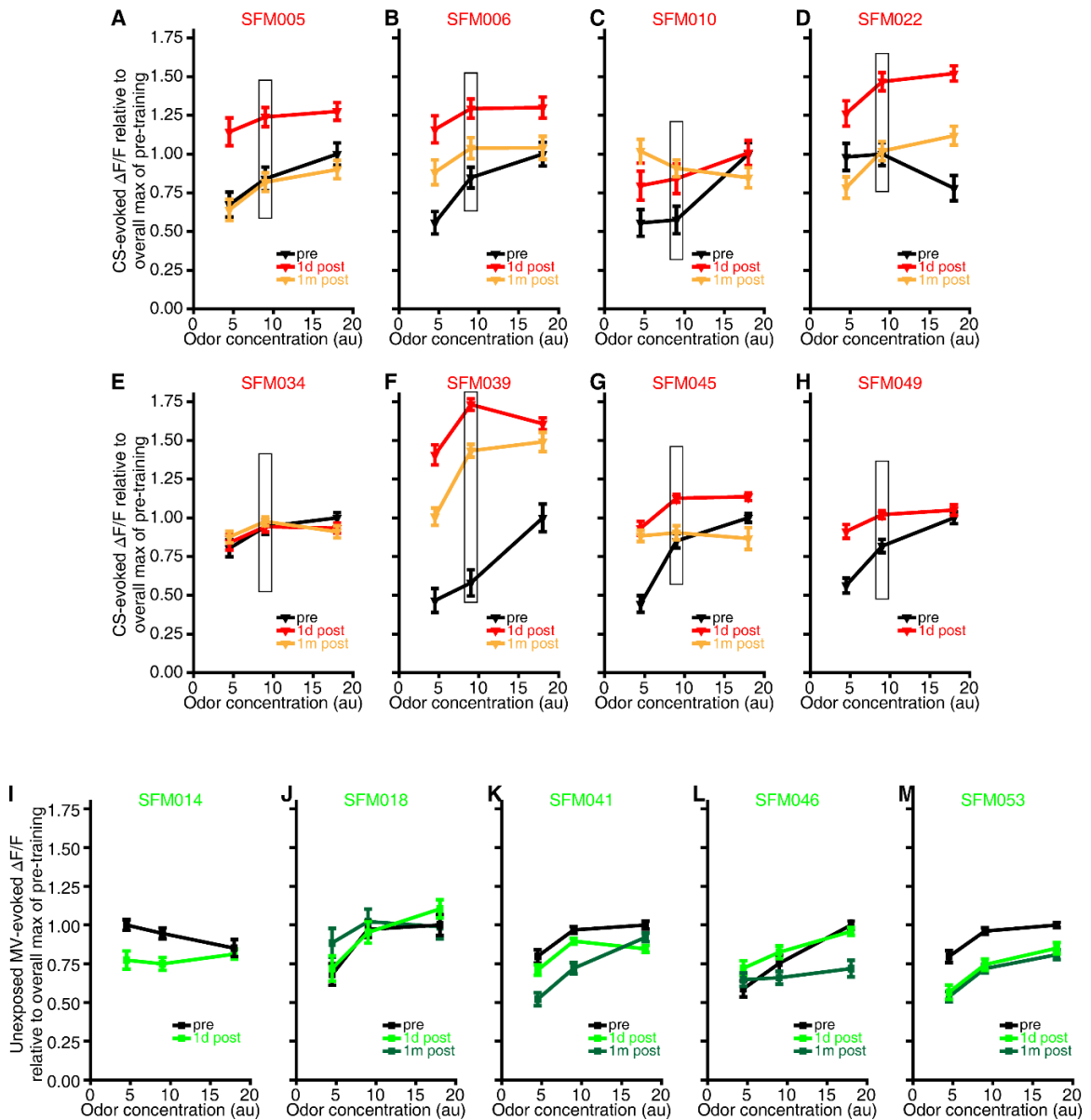
Supplementary Table S6.5. The change in CS-evoked PG interneuron activity after fear conditioning was negatively correlated with baseline response amplitudes. This table provides a summary of the results from the statistical analyses that accompany the individual scatter plots in Supplementary Figure S6.13A-M.

Supplementary Table S6.6

	Grouped change indexes from 1d post-training for Paired subjects				Grouped change indexes from 1d post-training for Shock-Alone subjects			
	0 th -	25 th -	50 th -	75 th -	0 th -	25 th -	50 th -	75 th -
	24.99 th	49.99 th	74.99 th	100 th	24.99 th	49.99 th	74.99 th	100 th
0 th -	-	< 0.001	< 0.001	< 0.001	-	= 1.00	= 0.016	< 0.001
24.99 th	-	-	= 0.004	< 0.001	-	-	= 0.557	= 0.003
25 th -	-	-	-	= 0.010	-	-	-	= 0.472
49.99 th	-	-	-		-	-	-	
50 th -	-	-	-		-	-	-	
74.99 th	-	-	-		-	-	-	

Supplementary Table S6.6. The effect of fear conditioning on CS-evoked PG interneuron activity was modulated by baseline response amplitudes. This table lists the results from the statistical analyses that accompany the summary plot in Figure 6.5I. Change indexes were pooled across all glomeruli, ranked from lowest-to-highest based on pre-training response amplitudes, and then separated into 4 groups that represented quartiles of the pre-training CS-evoked $\Delta F/F$ distribution (Figure 6.5I). There was a significant effect of group ranking on the change indexes from 1 day post-training for the paired group ($H_{(N=449, df=3)} = 188.534, p < 0.001$, by Kruskal-Wallis test) and also for the shock-alone group ($H_{(N=277, df=3)} = 20.809, p < 0.001$, by Kruskal-Wallis test). This table summarizes the adjusted significance levels from all planned *post-hoc* comparisons between change indexes that were grouped by quartiles of the normalized pre-training CS-evoked $\Delta F/F$ distributions.

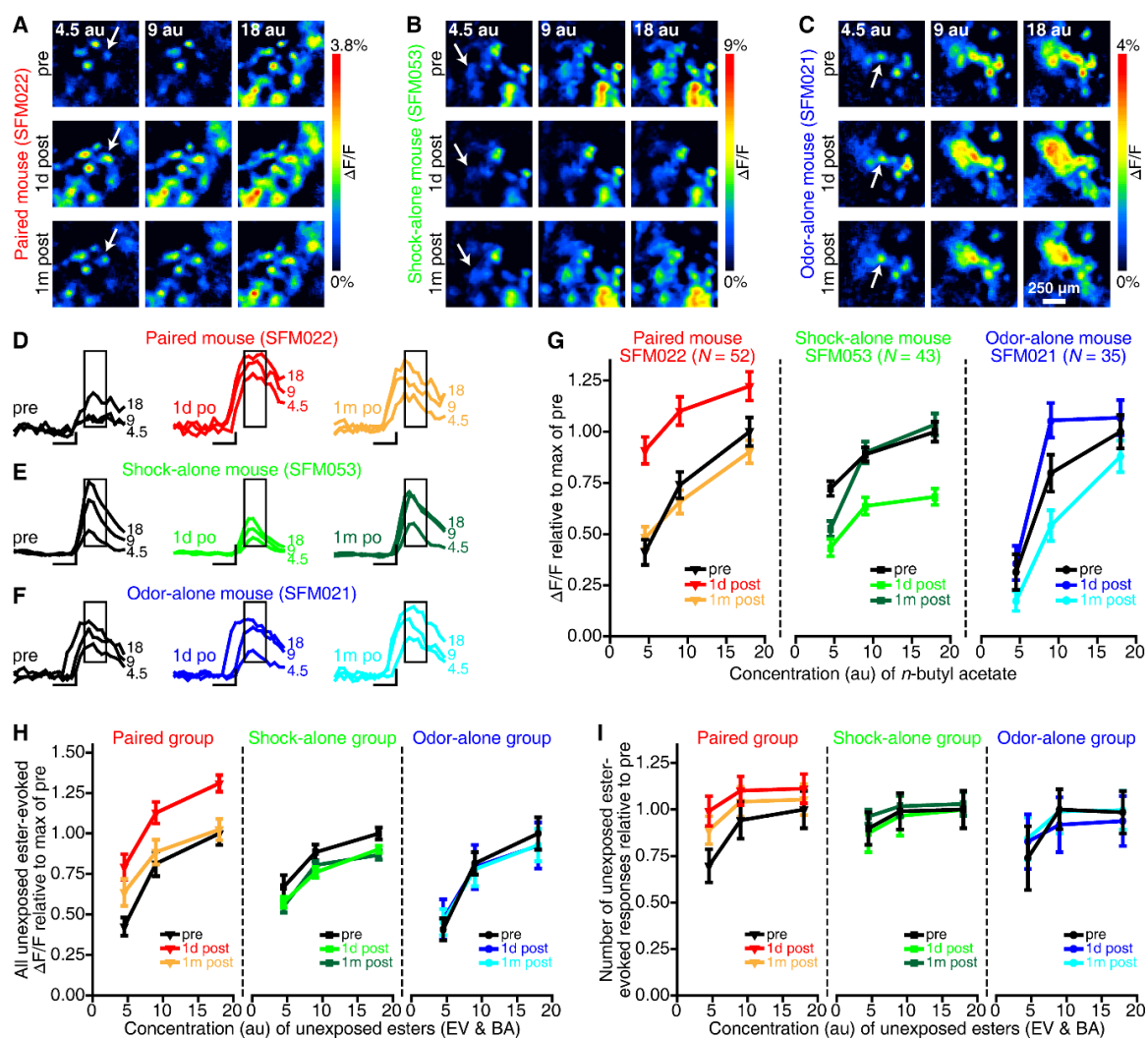
Supplementary Figure S6.14



Supplementary Figure S6.14. Altered sensitivity to the CS after conditioning in individual subjects. Because the group averages that were calculated for the paired and shock-alone subjects exhibited changes in sensitivity after training (Figure 6.6), we assessed individual variability among the subjects in those two groups. (A-M) CS-evoked concentration response functions from 1 day before (pre), 1 day after (1d post), and 1 month after (1m post) each individual subject underwent paired (A-H) or shock-alone (I-M) training. The mean \pm SEM normalized response amplitude ($\Delta F/F$) was averaged across

glomeruli for each imaging preparation in each subject and was plotted relative to the overall max across concentrations during pre-training imaging. Boxed regions on the concentration curves (**A-H**) indicate the training concentration. Most paired subjects (7 out of 8) exhibited enhanced sensitivity to the CS the day after training, and in a subset of those subjects (5 of 7) the altered sensitivity was still present to some extent 1 month later. By contrast, shock-alone exposure (**I-M**) decreased PG cell sensitivity to MV in about half of those subjects (3 out of 5), with the other half exhibiting no change in sensitivity (2 out of 5).

Supplementary Figure S6.15



Supplementary Figure S6.15. The enhanced sensitivity generalizes to PG interneuron activity that is evoked by unexposed odors. (A-F) Pseudocolored activity maps (A-C) and corresponding response amplitudes ($\Delta F/F$ s; D-F) from representative subjects that underwent either paired (A,D), shock-alone (B,E), or odor-alone (C,F) training. These examples illustrate activity that was evoked by the first inhalation of each of 3 concentrations of BA during individual trials that were presented 1 day before (pre), 1 day after (1d post), and 1 month after (1m post) conditioning. Boxed regions in D-F note the frames that were used for activity maps (A-C) and concentrations analyses (G-I). Traces from each individual subject (D-F) are scaled relative to the overall max of pre-training

across concentrations (scale bars: horizontal, 200 ms; vertical, 25% max $\Delta F/F$ of pre). **(G)** BA-evoked concentration response functions were calculated across the population of glomeruli that responded to BA (indicated by *Ns*) in the example paired (left), shock-alone (middle), and odor-alone (right) subjects. PG interneuron activity that was evoked by all 3 concentrations of BA was enhanced the day after fear conditioning, but returned to baseline levels 1 month later in this example paired subject (left, SFM022). The reverse effect occurred in this example shock-alone subject (middle, SFM053), because PG interneuron activity exhibited a decrease in sensitivity to BA the day after shock exposure, but returned to baseline levels 1 month later. This example odor-alone mouse (right, SFM021) did not exhibit a consistent shift in sensitivity to BA after training. **(H-I)** The mean \pm SEM response amplitudes **(H)** and number of glomerular responses **(I)** that were evoked by 2 unexposed esters (EV and BA) are pooled across all subjects in the paired (left), shock-alone (middle), and odor-alone (right) groups. Data are plotted relative to the overall max of pre-training and shown as a function of concentration for each imaging preparation. On average for the paired group, the number of glomerular responses, and the amplitudes of those responses, increased across a 4-fold range of unexposed ester concentrations after fear conditioning. Unexposed ester-evoked response amplitudes tended to decrease slightly across concentrations after shock-alone training, though the number of glomerular responses stayed relatively constant. In contrast with the paired and shock-alone groups, the odor-alone group exhibited relatively stable unexposed ester-evoked PG cell activity across imaging sessions.

CHAPTER 7

Differences in peripheral sensory input to the olfactory bulb between male and female mice

The results from this chapter are reported in Kass MD, Czarnecki LA, Moberly AH, McGann JP (2016) Differences in peripheral sensory input to the olfactory bulb between male and female mice. *Sci Rep* 7:45851.

Abstract

Female mammals generally have a superior sense of smell than males, but the biological basis of this difference is unknown. Here, we demonstrate sexually dimorphic neural coding of odorants by olfactory sensory neurons (OSNs), primary sensory neurons that physically contact odor molecules in the nose and provide the initial sensory input to the brain's olfactory bulb. We performed *in vivo* optical neurophysiology to visualize odorant-evoked OSN synaptic output into olfactory bulb glomeruli in unmanipulated (gonad-intact) adult mice from both sexes, and found that in females odorant presentation evoked more rapid OSN signaling over a broader range of OSNs than in males. These spatiotemporal differences enhanced the contrast between the neural representations of chemically related odorants in females compared to males during stimulus presentation. Removing circulating sex hormones makes these signals slower and less discriminable in females, while in males they become faster and more discriminable, suggesting opposite roles for gonadal hormones in influencing male and female olfactory function. These results demonstrate that the famous sex difference in olfactory abilities likely originates in the primary sensory neurons, and suggest that hormonal modulation of the peripheral olfactory system could underlie differences in how males and females experience the olfactory world.

Introduction

Though sex differences in olfaction can be complicated by factors like sensory experience (Dalton et al., 2002; Xu et al., 2016), age (Dorries et al., 1989; Segal et al., 1995; Hummel et al., 2007), and stimulus identity (Koelega and Koster, 1974; Segal et al., 1995; Wesson et al., 2006; Ohla and Lundstrom, 2013), the female olfactory system is generally more effective than the male olfactory system (Doty and Cameron, 2009). Females tend to exhibit enhanced sensitivity to odors (Koelega and Koster, 1974; Kobal et al., 2001; Baum and Keverne, 2002; Pierman et al., 2006; Cometto-Muniz and Abraham, 2008; Sorwell et al., 2008) as well as better discrimination and identification abilities (Doty et al., 1984; Doty et al., 1985) than males.

The biological basis of these sensory differences could be partly related to differences in endocrine status. Experimentally-induced alterations in hormonal status can influence odor detection thresholds in males (Doty and Ferguson-Segall, 1989; Pierman et al., 2006), and olfactory sensitivity in females can also vary with fluctuations in sex hormones (Koster, 1968; Pietras and Moulton, 1974; Good et al., 1976; Mair et al., 1978). Olfactory dysfunction can develop in women during menopause, and these deficits can be ameliorated by sex hormone therapy (Deems et al., 1991; Caruso et al., 2008). Analogously, 17 β -estradiol treatment in gonadectomized mice enhances the retention of an odor memory (Dillon et al., 2013) and also ameliorates olfactotoxicant-induced discrimination deficits (Dhong et al., 1999).

Despite the clear linkage between sex hormones and olfaction, it has been difficult to determine where in the olfactory system these hormones are acting. A growing body of work shows that peripheral chemosensory signaling can be modified by experience and

internal state (Kass et al., 2013b; Dias and Ressler, 2014; Stowers and Liberles, 2016; Xu et al., 2016), as well as by the activity of structures that process multisensory information (Fast and McGann, 2017a). The main olfactory epithelium expresses α - and β -type estrogen receptors (Barni et al., 1999), and estrogen replacement can protect against olfactory sensory neuron (OSN) loss in gonadectomized mice (Nathan et al., 2010, 2012), suggesting that sex and hormone effects could have a peripheral locus. Similarly, the vomeronasal organ undergoes state-dependent filtering in which sex hormones influence the responses of peripheral sensory neurons to specific chemical cues and consequently also behavioral responses to those cues (Cherian et al., 2014; Dey et al., 2015). We thus hypothesized that sex differences in olfaction could be at least partly mediated by sexually dimorphic sensory processing in the peripheral olfactory system.

Olfactory transduction occurs in the olfactory epithelium, where odorant molecules stimulate neural activity by binding to G protein-coupled odor receptors in the cilia of OSNs. The OSNs project their axons to the brain's olfactory bulb, where they segregate by receptor type, such that all the OSNs expressing a given receptor converge into one or two glomeruli on the surface of the olfactory bulb. Because each OSN expresses only one out of a large repertoire of odor receptors, a given odorant activates only a small subset of OSNs and thus drives neural input to a corresponding subset of glomeruli in the olfactory bulb. The brain's initial neural code for the identity of an odorant in the nose is thus the spatiotemporal pattern of olfactory bulb glomeruli receiving synaptic input from OSNs. These patterns of odorant-evoked neurotransmitter release from OSN axon terminals in the olfactory bulb can be visualized in a line of gene-targeted mice that express the fluorescent exocytosis indicator synaptopHluorin (spH) under the control of the olfactory marker

protein (OMP) promoter (Bozza et al., 2004). We performed *in vivo* optical neurophysiology to visualize these spatiotemporal patterns in gonad-intact, adult OMP-spH mice of both sexes to see if there was a sex difference in odor representations at the initial sensory input to the brain. We then tested whether circulating sex hormones influenced these initial neural representations of odors by performing the same *in vivo* optical imaging procedures in control and gonadectomized mice of both sexes.

Methods

Subjects.

The present experiments used a total of 62 mice that express the synaptobHluorin (spH) exocytosis indicator under the control of the olfactory marker protein (OMP) promoter (Bozza et al., 2004; Czarnecki et al., 2011; Kass et al., 2013d). The data that are summarized by Figures 7.1-7.3 came from 8 unmanipulated (gonad-intact) males and 11 unmanipulated (gonad-intact) females. The data that are shown in Figures 7.4-7.6 came from an additional 22 males and 21 females that underwent gonadectomy (or sham-control) surgical procedures 2 weeks prior to *in vivo* optical imaging (Supplementary Figure S7.2). All subjects were sexually-naïve adults (8-11 months old) that were still of reproductive age. Normal estrous cycles were observed in the sham-operated females (Supplementary Figure S7.2). All experiments were performed in accordance with protocols approved by the Rutgers University Institutional Animal Care and Use Committee.

Gonadectomy surgical procedures.

The data shown in Figures 7.4-7.6 came from 43 subjects that underwent either bilateral gonadectomy (Gnx) procedures (Gnx-male, $N = 10$; Gnx-female, $N = 10$) or sham-

control (Sham) surgical procedures (Sham-male, $N = 12$; Sham-female, $N = 11$) 2 weeks prior to *in vivo* epifluorescence imaging (Supplementary Figure S7.2).

For orchiectomies, a suprapubic midline incision was made along the lower abdomen, the skin was retracted, the linea alba was incised, and the testis, epididymis, and surrounding fat pad was exteriorized. The vas deferens and blood vessels were ligated, the testis and epididymis were excised, the remaining content was replaced through the abdominal incision, and then the process was repeated for the second gonad. For ovariectomies, a midline dorsal incision was made on the back directly below the rib cage, the skin was retracted, and the peritoneal cavity was accessed through a small incision in the muscle layer. The cranial portion of the uterine horn and vessels was ligated, the ovary and oviduct were severed, the uterus was gently replaced into the abdominal cavity, and the process was then repeated on the contralateral side. The same procedures were carried out for Sham surgeries, except that the gonads were exteriorized and then placed back into the abdominal cavity. After GnX or Sham surgeries all subjects were singly-housed for the duration of the study. To confirm the efficacy of ovariectomy in GNX females, all subjects underwent daily cytological procedures (Caligioni, 2009) that began 1 week after Sham or GnX surgeries (Supplementary Figure S7.2). Note that males underwent a daily “sham-smear” procedure to maintain equal treatment across all groups.

In vivo optical neurophysiology recordings.

Optical neurophysiology procedures are detailed in the General Methods section. Briefly, cranial windows were surgically implanted (examples in Figures 7.1A-B, 7.2A-B, and 7.4A-D), and odorant-evoked spH signals were visualized in freely-breathing, anesthetized subjects (Czarnecki et al., 2011; Czarnecki et al., 2012; Moberly et al., 2012;

Kass et al., 2013a; Kass et al., 2013d; Kass et al., 2013c; Kass et al., 2013b; Kass et al., 2016). Respiration was monitored in a subset of subjects ($N = 41$) by a force-transducing piezosensor strip positioned just below the diaphragm (Kass et al., 2013b).

Vapor dilution olfactometry was used to present subjects with a panel of 4 monomolecular odorants that included *n*-butyl acetate (BA), methyl valerate (MV), 2-hexanone (2HEX), and *trans*-2-methyl 2-butenal (2M2B). Odorant concentrations were standardized prior to all imaging sessions via a photoionization detector (PID; ppbRAE300, RAE Systems). Both the liquid dilution of odorant in mineral oil and the dilution of the nitrogen carrier were increased or decreased as needed to achieve 3 target concentrations on the PID for each odorant. These measurements are reported here in arbitrary units (au), because they have relative validity within odorants but uncertain absolute molar concentration. For example, the 3 reported concentrations of MV, which were 7.5 au, 15 au, and 30 au, were achieved by preparing a liquid dilution of MV that ranged from 1:1 to 1:4 and then diluting MV saturated vapor to $0.75 \pm 0.12\%$, $1.66 \pm 0.26\%$, and $3.13 \pm 0.41\%$, respectively. .

During all imaging preparations, 12 blocks of odorant trials (4 odorants \times 3 concentrations) were presented to each subject via a manifold that was positioned ~ 1 cm in front of the nose. Each odor block consisted of 4, 16-sec trials that were presented at 60 sec inter-trial intervals (ITIs). Several blocks of blank (no odorant) trials (2-4 trials/block, 16 sec/trial, 60 sec ITIs) were also presented, and were then averaged together offline and subtracted from each odorant trial to correct for photobleaching.

Quantification and analysis of odorant-evoked optical signals.

Imaging data were extracted and quantified as detailed in the General Methods section. Briefly, peak odorant-evoked response maps were generated by subtracting the average of 7 frames that were collected immediately prior to stimulus onset from the average of 7 frames that were approximately centered on the peak trace inflection. spH provides a relatively slow, cumulative signal, causing the peak response across most glomeruli to occur around the time of odorant offset, so frames 78-84 were used for this subtraction (see Figure 7.1D-E and 7.1I for examples of peak subtractions). We then performed 3 more subtractions and generated a time course of pre-peak response maps that were evoked throughout each odorant presentation (see Figure 7.2A-B for stimulus diagrams showing all subtractions). Specifically, we subtracted the average of 7 pre-odorant baseline frames from the average of frames 1) 36-42, 2) 50-56, and 3) 64-70. All difference maps were spatially filtered to separate discrete odorant-evoked spH signals from broad changes in tissue reflectance.

Putative glomerular regions of interest (ROIs) were first identified in the peak, spatially high-pass filtered difference maps, and were then confirmed through a statistical thresholding criterion (Czarnecki et al., 2011; Kass et al., 2013c). The raw data set for the results that are summarized by Figures 7.1-7.3 included 369 glomerular ROIs from 8 unmanipulated males and 679 glomerular ROIs from 11 unmanipulated females. The raw data set for the results that are summarized by Figures 7.4-7.6 included 718 ROIs from 12 Sham-males, 783 ROIs from 10 GnX-males, 852 ROIs from 11 Sham-females, and 604 ROIs from 10 GnX-females.

The average number of glomerular responses contributing to each odor representation during each response time bin were quantified in all 12 spatially high-pass-filtered odor maps from each subject. We also calculated peak odorant-evoked ΔF s for all glomerular ROIs in each subject. Parametric tests, including factorial ANOVAs and *t* tests, were used to evaluate group differences in central tendencies based on means from individual subjects. In these analyses, odorant (BA, MV, 2HEX, and 2M2B), concentration (7.5 au, 15 au, and 30 au), and response time bin (frames 36-42, 50-56, 64-70, and 78-84) were used as within-subjects factors and sex (male and female) and surgical treatment (Sham and GnX) were used as between-subjects factors.

To perform odorant response selectivity analyses, each individual glomerulus was identified as receiving input from OSNs that were stimulated by 1, 2, 3, or 4 odorants in the panel (Kass et al., 2013c), with lower numbers indicating relatively high odorant response selectivity and higher numbers indicating relatively low odorant response selectivity. These data were pooled across glomeruli and analyzed via ANOVAs and *t* tests that included sex and surgical treatment as between-groups factors.

To evaluate the time course of odorant-evoked nerve output, particularly during the relatively early, pre-peak part of the responses, traces from all glomerular ROIs were exported through custom software in Matlab. These data were extracted from trials corresponding to the moderate concentration (15 au) of all 4 odorants in the panel. Each individual trace, which represented a single glomerulus' fluorescence throughout the length of an entire trial, was normalized relative to its own minimum and maximum values. We used the normalized traces to quantify the amount of time that it took for each glomerulus to reach its peak response magnitude. The latency to peak onset was calculated

as time in sec and was constrained to the frame range corresponding to 2-9 sec after odorant onset. The mean latency to peak onset across each odor map was separately calculated for each mouse by averaging peak onset latencies across glomeruli within each odorant. These data were analyzed via ANOVAs that included sex and surgical treatment as between-subjects factors and odorant as a within-subjects factor. Additional non-parametric tests, including Kolmogorov-Smirnov (K-S) and Mann-Whitney (M-W) tests, were used to evaluate differences in latencies that were pooled across distributions of glomeruli.

To quantify differences in overall odor representations for each individual mouse, the pairwise Euclidean distances (EDs) between BA-, MV-, 2HEX-, and 2M2B-evoked glomerular response maps were calculated on a frame-by-frame basis. Differences among odorant-evoked glomerular response maps were quantified as EDs in N -dimensional vector space, where N was equivalent to the total number of glomerular ROIs identified across all 4 odorants in each mouse (Kass et al., 2013b). Each mouse's ROI array consisted of all ROIs ($\text{ROI}_1\text{-ROI}_N$) that were identified as glomeruli receiving synaptic input across all 4 odorants in our test panel. For example, a hypothetical array might have included 80 ROIs that were identified across both olfactory bulbs and all 4 odorants, but maybe only 20 of those ROIs were identified as glomeruli receiving 2HEX-evoked input while the remaining 60 were identified as receiving input that was evoked by 1 or more of the 3 remaining odorants in the panel. 2HEX would then be represented by an array of ROIs that includes 20 "active" glomeruli that are receiving odorant-evoked OSN input and 80 "inactive" (response of zero) glomeruli that are not receiving odorant-evoked OSN input. ED calculations for each odor pair were performed on normalized data in which the fluorescence values were normalized relative to the maximum fluorescence value across

all frames, ROIs, and both odorants within each odor pair. These data were analyzed via factorial ANOVAs that included sex and surgical treatment as between-subjects factors and also included odor pair (6; BA-MV, BA-2HEX, BA-2M2B, MV-2HEX, MV-2M2B, & 2HEX-2M2B) and frame number (64; frames 28-91, which correspond to 0-9 sec relative to odorant onset) as within-subjects factors. Additionally, a subset of subjects in the gonadectomy-imaging experiment ($N = 18$) were presented with 15 au ethyl valerate (EV), which is an ester that differs in functional group, but is highly similar to MV (another ester that was included in our 4×3 odor panel). The ED between EV- and MV-evoked odor maps was also quantified in this subset of mice and analyzed accordingly.

Results

Odors evoke OSN input to more olfactory bulb glomeruli in females than in males.

Gonad-intact male ($N = 8$) and female ($N = 11$) OMP-spH mice were each implanted with a bilateral cranial window overlying the dorsal surface of the olfactory bulbs. Subjects remained anesthetized while the synaptic output of OSNs was visualized by fluorescence microscopy during 4 6-sec presentations of each stimulus in the odor panel, which consisted of 3 separate concentrations of 4 monomolecular odorants. Because spH is a cumulative measure of exocytosis from OSNs, these long presentations permit odor-evoked responses to be detected even in weakly activated OSN populations (Bozza et al., 2004). The number of olfactory bulb glomeruli exhibiting a measurable odorant-evoked fluorescence response was quantified for each odorant in the panel in each mouse. These numbers of odorant-evoked glomerular responses were then analyzed via a mixed, 3-way

ANOVA to evaluate potential sex differences in the number of olfactory bulb glomeruli receiving OSN input.

As shown by the representative MV-evoked difference maps in Figure 7.1A-B and the dot plot in Supplementary Figure S7.1, the overall number of odorant-evoked glomerular responses observed in these unmanipulated female subjects was significantly greater than that observed in unmanipulated male subjects (Figure 7.1C, inset, main effect of sex, $F_{(1, 17)} = 11.199$, $p = 0.004$, $\eta_p^2 = 0.397$). Additionally, the observed difference between sexes was larger at higher odorant concentrations (Figure 7.1C; sex \times concentration interaction, $F_{(2, 34)} = 3.876$, $p = 0.030$, $\eta_p^2 = 0.186$). *Post hoc* analyses evaluating the 2-way interaction confirmed that there was an effect of concentration in both sexes, as expected. However, this effect was larger in females ($F_{(2, 20)} = 21.172$, $p < 0.001$, $\eta_p^2 = 0.679$) than in males ($F_{(2, 14)} = 10.997$, $p = 0.001$, $\eta_p^2 = 0.611$), indicating that concentration-dependent glomerular recruitment (Spors and Grinvald, 2002) is augmented in females.

The sex difference in the number of glomeruli receiving measurable odorant-evoked OSN input (Figure 7.1A-C) could be caused by a difference in odorant response selectivity, such that the OSNs projecting to each glomerulus respond to more odorants in females than in males. To test this possibility, we assessed the odor tuning of each responsive glomerulus by quantifying the number of odorants in the panel that evoked a measurable response in that glomerulus. For example, the two sample glomeruli in Figure 7.1D-E only received input from OSNs that were stimulated by a single odorant from the 4-odor panel. On average, glomeruli from females responded to slightly (8.6%) but significantly more odorants than glomeruli from males (Figure 7.1F; $t_{(df = 632.9)} = -2.855$, p

= 0.004). Even a slight shift in tuning would be sufficient to cause a robust difference in the number of odorant-evoked glomerular responses because certain glomeruli might exhibit no response to our odor panel in more narrowly tuned male OSNs, but might respond to just one of the odors in more broadly tuned female OSNs. We employed four structurally- and perceptually-disparate odors in our main odorant test panel, but we note that a much larger number of odorants would need to be screened to determine if the sex-dependent tuning of OSN output might differ depending on odor identity.

An alternative explanation would be that the sex difference in the number of glomerular inputs is an artifact of our optical detection threshold, which might arise if, for instance, females exhibited larger spH responses that were easier to detect optically. To evaluate this possibility, we measured total odorant-evoked OSN synaptic output into each olfactory bulb glomerulus by subtracting 1 sec of pre-odor baseline frames from 1 sec of frames centered on the approximate peak of the spH signal (Figure 7.1G-I). The average odorant-evoked ΔF was calculated across all glomeruli per odor map for each subject, and then the resulting data were analyzed via mixed-model ANOVA. On average, there was no difference between sexes in the peak odorant-evoked ΔF (Figure 7.1J, inset; main effect of sex, $F_{(1, 17)} = 0.119$, $p = 0.734$, $\eta_p^2 = 0.007$). Increasing the odorant concentration resulted in a corresponding increase in peak odorant-evoked response amplitudes ($F_{(2, 34)} = 56.891$, $p < 0.001$, $\eta_p^2 = 0.770$), as expected. However, this concentration-dependent increase in peak odorant-evoked ΔF s was comparable between sexes (Figure 7.1J, main; non-significant sex \times concentration interaction, $F_{(2, 34)} = 0.965$, $p = 0.391$, $\eta_p^2 = 0.054$). This result suggests that the noticeably different patterns of OSN synaptic input to the brain (Figures 7.1A-B and 7.1G-H) are not attributable to differences in response magnitudes,

and, perhaps more importantly, that the magnitude of OSN input to olfactory bulb glomeruli is similar in individual male and female subjects (Supplementary Figure S7.1) despite the difference in the number of glomeruli receiving input.

Odor-evoked OSN output is faster in females than in males.

Odor information is not only encoded by the static pattern of activity that is mapped across the glomerular layer of the bulb, but also by the temporal dynamics of that activity (Spors and Grinvald, 2002; Spors et al., 2006; Smear et al., 2011). To test whether the degree of the female-specific enhancement (Figure 7.1A-C) varies across the duration of the odorant presentation we separated the spH signals into 4 1-sec time bins (Figure 7.2A-B), and then analyzed the data via a mixed, 4-way ANOVA and additional planned *post hoc* tests. There were a larger number of glomeruli receiving OSN input in females, not only at the peak of the spH response (Figure 7.1A-C and time 4 in Figure 7.2A-B), but also during all earlier response times (Figure 7.2A-C; time 1, $F_{(1, 17)} = 8.985$, $p = 0.008$, $\eta_p^2 = 0.346$; time 2, $F_{(1, 17)} = 9.763$, $p = 0.006$, $\eta_p^2 = 0.365$; time 3, $F_{(1, 17)} = 10.242$, $p = 0.005$, $\eta_p^2 = 0.376$).

As illustrated by Figure 7.2A-C, the number of glomeruli receiving measurable OSN input increases with the time elapsed since odorant onset (main effect of time bin, $F_{(3, 51)} = 110.030$, $p < 0.001$, $\eta_p^2 = 0.866$). This likely reflects the gradual increase in spH fluorescence as OSNs release neurotransmitter over time, which rapidly exceeds our optical detection threshold for strongly activated glomeruli and more slowly exceeds our optical detection threshold for very weakly activated glomeruli. However, there was also a significant sex \times time bin interaction (Figure 7.2C; $F_{(3, 51)} = 7.428$, $p < 0.001$, $\eta_p^2 = 0.304$), showing that the number of responsive glomeruli increased faster in females than in males

(which cannot be the result of an optical detection threshold). To test whether the increased number of responsive glomeruli in females developed over time, we calculated the ratio of odorant-evoked glomerular responses in females relative to that in males for each response time bin. This qualitative analysis shows that even though the number of glomeruli receiving measurable OSN input increased throughout the odor presentation, this number was proportionately larger for females than males during all 4 measured time points (Figure 7.2D), averaging $48\% \pm 0.1\%$ more responsive glomeruli overall (Figure 7.2E).

Even though the magnitude of the peak spH responses was the same between sexes (Figure 7.1J), the time course-dependent sex differences in static spatial maps (Figure 7.2A-E) suggested that there might be subtle differences in the temporal dynamics of those signals. There is precedent in this, where odorant-evoked spH signals in OMP knockout mice eventually reach comparable peak magnitudes to that in OMP-expressing mice (Kass et al., 2013d), despite having relatively slowed OSN response kinetics and decreased sensitivity (Lee et al., 2011). Careful inspection of the fluorescence records in Figure 7.1I suggests that similar differences in response time course might exist between sexes because the peak amplitudes (boxed portion of traces) are comparable, but the slopes of the signals appear to differ during earlier (pre-peak) response times. While spH does not clearly illustrate the dynamics of individual inhalations, it does usefully report on the cumulative total odorant-evoked OSN output within each glomerulus over the course of an odorant presentation. To further evaluate potential sex differences in the time course of odorant-evoked nerve output, particularly during the relatively early, pre-peak part of the responses, fluorescence traces from all glomerular ROIs were normalized to their individual minima and maxima. To visualize the timing of odorant-evoked spH signals, the normalized traces

were separately pooled across glomeruli per odorant within a mouse, and the average odorant-evoked spH waveforms that were evoked by a given odorant in individual mice were plotted together for qualitative evaluation (as in Figure 7.2F).

Odorant-evoked OSN output appeared to increase slightly faster in females than in males (Figure 7.2F), reaching the plateau of the response slightly earlier. We quantified the latency (in sec) to onset of the peak response plateaus (which are relatively prolonged; e.g., Figures 7.1I & 7.2F) and looked for group differences between individual animals (Figure 7.2G; $N_{\text{Male}} = 8$, $N_{\text{Female}} = 11$) as well as between distributions of latency values pooled across glomerular fluorescence records from all animals (Figure 7.2H). On average, the onset of peak odorant-evoked response magnitudes occurred ~ 0.31 sec earlier in females than in males (Figure 7.2G; $F_{(1, 17)} = 9.861$, $p = 0.006$, $\eta_p^2 = 0.367$). This subtle difference in timing exceeds behaviorally-relevant timescales because sensory processing that is sufficient to support odor detection and discrimination occurs in under 200 ms (Uchida and Mainen, 2003; Wesson et al., 2008b; Cury and Uchida, 2010).

Higher contrast between odorants in the primary sensory odor representations of females than males.

What could be the functional significance of the spatiotemporal sex differences in odorant-evoked OSN activity that were observed here (Figures 7.1 and 7.2)? Fundamentally, the spatial pattern of OSN input across glomeruli is the initial representation of odor identity in the brain. The degree of difference between these spatial patterns of glomerular activity predicts the perceptual differences between odors (Linster et al., 2001; Youngentob et al., 2006), so we quantified the differences between the representations of different odor pairs within male and female mice.

Differences between odorant-evoked glomerular response maps were quantified as Euclidean distances (EDs) in N -dimensional vector space, where N was equivalent to the number of glomerular ROIs identified in each mouse. Smaller EDs indicate that neural representations of stimuli within a pair are more similar to each other, whereas larger EDs indicate that the stimulus representations are more dissimilar. We calculated the pairwise ED for all 4 odors in our panel, yielding 6 possible odor pairs: BA-MV, BA-2HEX, BA-2M2B, MV-2HEX, MV-2M2B, and 2HEX-2M2B. Figure 7.3A-B shows BA-, MV-, 2HEX-, and 2M2B-evoked response maps that were generated for time bin 1 (the first rising phase of the odor response – see Figure 7.2A-B) from representative male and female subjects. Pairwise comparisons across odor maps within each subject show that all pairs are discriminable by this time point (Figure 7.3C; EDs greater than 0), but that the maps are more easily distinguished in the female mouse than in the male mouse (Figure 7.3C; F11 has larger EDs for all 6 odor pairs). We analyzed the 6 pairwise EDs for all subjects during time bin 1 with a sex \times odor pair ANOVA and confirmed that, on average, odor maps were more dissimilar in females than in males during this relatively early response time bin (mean \pm SEM ED between odor maps; female group = 0.707 ± 0.015 , male group = 0.637 ± 0.019 , main effect of sex $F_{(1, 16)} = 7.942$, $p = 0.012$, $\eta_p^2 = 0.332$).

Because individual maps for a given odorant evolve over time throughout the duration of a stimulus presentation (e.g., Figure 7.2A-B), we extended this analysis and calculated EDs between odor pairs over 64 consecutive frames that began at time = 0 sec relative to stimulus onset (Figure 7.3D). While the ED between odor pairs got larger over time for all subjects (main effect of frame number; $F_{(63, 1008)} = 389.539$, $p < 0.001$, $\eta_p^2 = 0.961$), overall the odor representations were more dissimilar in females than they were in

males (Figure 7.3F; group means \pm SEMs pooled across 64 frames, $F_{(1, 16)} = 8.844$, $p = 0.009$, $\eta_p^2 = 0.356$). Additionally, the enhanced contrast between sensory maps that was observed in females occurred relatively early in the trial and became larger over time (Figure 7.3D; sex \times frame interaction, $F_{(63, 1008)} = 7.200$, $p < 0.001$, $\eta_p^2 = 0.310$). In fact, this frame-by-frame analysis reveals that the sex difference was detectable in these data as early as ~ 0.75 sec after odorant onset (Figure 7.3E). The more numerous, faster OSN outputs in females thus enhance the differences between odor representations.

The number of glomeruli receiving odorant-evoked OSN input is influenced by circulating gonadal hormones in males and females.

The sexually dimorphic odor-evoked activation of olfactory bulb glomeruli that we observed in unmanipulated males and females could be the result of organizational differences that are differentiated early in life, or it could alternatively be attributed to activational effects of circulating sex hormones on the peripheral olfactory system. To test these possibilities, we performed the same *in vivo* optical imaging procedures on an additional 43 mice 2 weeks after those subjects underwent bilateral gonadectomy or sham-control surgical procedures (Supplementary Figure S7.2). If the observed sex differences (Figures 7.1-7.3) are attributable to structural differences in the organization of this olfactory pathway, then the removal of circulating sex hormones through gonadectomy should have no effect on odorant-evoked glomerular response maps. Conversely, if odorant-evoked OSN neurotransmitter release is susceptible to hormonal modulation, then gonadectomy should induce changes in odor-evoked OSN activity between sham-manipulated and gonadectomized mice of each sex. If circulating sex hormones are the

only cause of the difference between male and female OSN responses, then gonadectomy should make the response maps in male and female mice equivalent.

The number of glomeruli receiving measurable OSN input was quantified for each odorant and concentration per mouse and analyzed via a mixed, 4-way ANOVA and additional *post-hoc* tests. Comparison of Sham-manipulated females and Sham-manipulated males replicated our initial findings (Figure 7.1A-C), revealing a greater number of glomeruli receiving odorant-evoked nerve input in Sham-females than in Sham-males (compare Figure 7.4A and 7.4B; $F_{(1, 21)} = 16.104$, $p \leq 0.001$, $\eta_p^2 = 0.434$). Critically, we also observed an interaction between sex and surgical treatment (Figure 7.4I, $F_{(1, 39)} = 23.250$, $p < 0.001$, $\eta_p^2 = 0.373$; and see Supplementary Figure S7.3). Regardless of the odorant being presented (Supplementary Figure S7.4), in females the removal of the ovaries resulted in a significant reduction in the number of glomeruli receiving measurable odorant-evoked OSN input (Figure 7.4I and also compare Figure 7.4B and 7.4D; $F_{(1, 19)} = 15.577$, $p \leq 0.001$, $\eta_p^2 = 0.451$), causing the GnX-females to have odor maps that were similar to those observed in the Sham-manipulated males (Figure 7.4I and also compare Figure 7.4A and 7.4D; non-significant difference in odorant-evoked glomerular responses, $F_{(1, 20)} = 0.222$, $p = 0.642$, $\eta_p^2 = 0.011$). Interestingly, orchiectomy had the opposite effect on males, such that GnX-males had a greater number of odorant-evoked glomerular responses than Sham-manipulated males (Figure 7.4I and also compare Figure 7.4A and 7.4C; $F_{(1, 20)} = 8.744$, $p = 0.008$, $\eta_p^2 = 0.304$), and were thus more similar to Sham-females (Figure 7.4I and also compare Figure 7.4B and 7.4C; non-significant difference in odorant-evoked glomerular responses, $F_{(1, 19)} = 0.019$, $p = 0.892$, $\eta_p^2 = 0.001$).

When we pooled across odorants and looked at odorant-evoked glomerular response maps over a range of concentrations we found that higher odorant concentrations tended to recruit more glomeruli than lower concentrations (effect of concentration, $F_{(2, 78)} = 75.476$, $p < 0.001$, $\eta_p^2 = 0.659$). However, we identified a sex \times group \times concentration interaction (Figure 7.4A-D and 7.4J; $F_{(2, 78)} = 5.655$, $p = 0.005$, $\eta_p^2 = 0.127$) that suggested concentration-dependent glomerular recruitment was not equivalent among sex \times surgical treatment groups. The largest effects of increasing concentration on glomerular recruitment were observed in Sham-female and GnX-male groups (which were equivalent to each other; non-significant 2-way interaction, $F_{(2, 38)} = 0.040$, $p = 0.961$, $\eta_p^2 = 0.002$), whereas concentration-dependent glomerular recruitment was relatively less-robust in both Sham-male and GnX-female groups (which were equivalent to each other; non-significant 2-way interaction, $F_{(2, 40)} = 0.760$, $p = 0.474$, $\eta_p^2 = 0.037$). Gonadectomy thus appears to attenuate concentration-dependent glomerular recruitment in females, but enhance it in males (Figure 7.4J).

We next separated the spH signals into 4 1-sec time bins (Supplementary Figure S7.5) and analyzed the data via a 5-way ANOVA, which yielded sex \times surgical treatment ($F_{(1, 39)} = 19.058$, $p < 0.001$, $\eta_p^2 = 0.328$) and sex \times surgical treatment \times time bin interactions (Figure 7.4K; $F_{(3, 117)} = 40.888$, $p < 0.001$, $\eta_p^2 = 0.512$). After performing additional *post-hoc* factorials, we once again confirmed that there were a larger number of odorant-evoked glomerular responses in intact females relative to intact males not only at the peak of spH response (Figure 7.4I and 7.4K, time = 7-8 sec), but also during all earlier response times (Figure 7.4K; time = 1-2 sec, $F_{(1, 21)} = 5.614$, $p = 0.027$, $\eta_p^2 = 0.211$; time = 3-4 sec, $F_{(1, 21)} = 14.178$, $p \leq 0.001$, $\eta_p^2 = 0.403$; time = 5-6 sec, $F_{(1, 21)} = 15.837$, $p \leq 0.001$, $\eta_p^2 = 0.376$).

Notably, this difference was reversed by gonadectomy (Supplementary Figure S7.5) because the number of odorant-evoked glomerular responses was proportionately reduced in GnX-females relative to Sham-manipulated females throughout the duration of the trial (Figure 7.4K; time = 1-2 sec, $F_{(1, 19)} = 8.724$, $p = 0.008$, $\eta_p^2 = 0.315$; time = 3-4 sec, $F_{(1, 19)} = 12.037$, $p = 0.003$, $\eta_p^2 = 0.388$; time = 5-6 sec, $F_{(1, 19)} = 13.685$, $p = 0.002$, $\eta_p^2 = 0.419$), whereas a proportional enhancement was observed throughout the trial in GnX-males relative to Sham-manipulated males (Figure 7.4K; time = 1-2 sec, $F_{(1, 20)} = 3.818$, $p = 0.065$, $\eta_p^2 = 0.160$; time = 3-4 sec, $F_{(1, 20)} = 7.791$, $p = 0.011$, $\eta_p^2 = 0.280$; time = 5-6 sec, $F_{(1, 20)} = 9.001$, $p = 0.007$, $\eta_p^2 = 0.310$).

Consistent with findings from the first experiment (Figure 7.1F), the differences between groups in the spatial arrangement of glomerular odor representations may be related to slight changes in odor tuning of individual glomeruli. We observed a small but significant interaction of sex and surgical treatment on the number of odorants that evoked a response in each glomerulus (Figure 7.4L; $F_{(1, 2817)} = 7.644$, $p = 0.006$, $\eta_p^2 = 0.043$). The interaction suggested that glomerular selectivity was increased by gonadectomy in females since glomeruli from GnX-females tended to respond to slightly fewer odorants than Sham-females (Figure 7.4L). By contrast, glomeruli from GnX-males responded to slightly more odorants than from Sham-males (Figure 7.4L), suggesting that gonadectomy in males may have broadened the tuning of individual glomeruli.

Similar to the first experiment (Figure 7.1G-J), there were no overall differences between groups in peak response magnitudes (Figure 7.4E-H, boxed portion of traces; Figure 7.4M, non-significant sex \times surgical treatment interaction, $F_{(1, 39)} = 1.768$, $p = 0.191$, $\eta_p^2 = 0.043$; Supplementary Figure S7.3). Additionally, the effects reported here cannot be

attributed to differences in respiration because they were identified in anesthetized imaging preparations in which depth of anesthesia and respiration frequency were constant throughout the duration of the experiment and did not differ between any groups (see sample respiration traces in Figure 7.4E-H and group means in Figure 7.4N; non-significant sex \times surgical treatment interaction, $F_{(1, 37)} = 0.802$, $p = 0.376$, $\eta_p^2 = 0.021$).

These data demonstrate that OSN physiology may normally be modulated by circulating sex hormones in both female and male mice. It is possible that this modulation could fluctuate in females in correlation with the fluctuating levels of sex hormones that are associated with different phases of the estrous cycle. Although Sham-manipulated females exhibited normal 4 day estrous cycles (Supplementary Figure S7.2), we saw no obvious relationship between estrous cycle phase and the number of odorant-evoked glomerular responses (Supplementary Figure S7.3). However, we note that the small number of animals in each phase of the cycle does not permit definitive conclusions.

Gonadal hormones modulate the timing and discriminability of odorant-evoked OSN activity.

To assess the potential influence of circulating gonadal hormones on OSN response timing and the contrast between odorant-evoked glomerular response maps, we repeated the analyses shown in Figures 7.2 and 7.3 with the data from sham-manipulated and gonadectomized mice.

The timing of odorant-evoked OSN neurotransmitter release was compared between Sham-male and GnX-male subjects (Figure 7.5A) as well as between Sham-female and GnX-female subjects (Figure 7.5B) (also see Figure 7.4E-H and compare slopes of traces). Intriguingly, the removal of circulating gonadal hormones resulted in opposite

effects on temporal properties of OSN physiology in males and females (Figure 7.5C; sex \times surgical treatment interaction, $F_{(1, 39)} = 6.092$, $p = 0.018$, $\eta_p^2 = 0.135$). Regardless of which odorant was presented (non-significant odorant \times sex \times surgical treatment interaction, $F_{(3, 117)} = 1.447$, $p = 0.233$, $\eta_p^2 = 0.036$), the onset of peak responses in Gnxfemales was ~ 0.18 sec delayed relative Sham-females, whereas the onset of peak responses in Gnxfemales was ~ 0.18 sec earlier than that in Sham-males. Though individual latency values from Gnxfemales tended to be slightly larger (i.e., slower responses) than those from Sham-females (Figure 7.5D, right panel; K-S, $Z = 1.428$, $p = 0.034$), they were equivalent to latency values in Sham-males (K-S, $Z = 0.960$, $p = 0.315$), which were also larger than those in Sham-females (K-S, $Z = 2.125$, $p < 0.001$). Conversely, individual latency values from Gnxfemales were smaller (i.e., faster responses) than those from Sham-males (Figure 7.5D, left panel; K-S, $Z = 1.992$, $p \leq 0.001$), but equivalent to those from Sham-females (K-S, $Z = 0.565$, $p = 0.906$). Importantly, these effects were not attributable to differences in respiration (Figure 7.4N).

When we quantified the ED between pairs of odor maps as above, we found that odor pairs tended to be further apart in Euclidean space (i.e., more dissimilar) in Sham-manipulated females than in Sham-manipulated males (Figure 7.6A, left panel), replicating our previous results (Figure 7.3). However, the reverse pattern was observed between Gnxfemales and Gnxfemales (Figure 7.6A, right panel), which suggests that while coarse odor discrimination between glomerular activity maps that are evoked by different odorants may be better in the gonad-intact female than in the gonad-intact male (e.g., Figure 7.3A-C), coarse discrimination between glomerular odor maps may be poorer in Gnxfemales than in Gnxfemales. The interactions between sex and surgical treatment ($F_{(1, 39)} = 5.891$, $p =$

0.020 $\eta_p^2 = 0.131$) and between sex, surgical treatment, and frame number ($F_{(63, 2457)} = 3.689$, $p < 0.001$ $\eta_p^2 = 0.086$) suggested that this was because odor pairs tended to be slightly more similar to each other in Gnxfemales than they were in Sham-females (Supplementary Figure S7.6), whereas those same odor pairs tended to be slightly more dissimilar from each other in Gnxfemales than they were in Sham-females (Supplementary Figure S7.6). To illustrate this point, we divided the overall ED between all 6 odor pairs across all 64 frames from each Gnxfemale group by the overall ED from their corresponding Sham-control group (Figure 7.6B). These ratios were plotted as the percent change in ED between odor pairs relative to that in Sham-controls, and they show that gonadectomy resulted in increased odor map discriminability in males and decreased odor map discriminability in females (Figure 7.6B).

In a subset of subjects the odor panel was expanded to include the odorant ethyl valerate (EV) to provide a close comparison to the odorant methyl valerate (MV) during *in vivo* optical imaging. In these subjects there was a significant interaction in the effects of sex and surgical treatment on the discriminability between primary sensory representations of MV and EV (Figure 7.6C-G; $F_{(1, 14)} = 6.784$, $p = 0.021$, $\eta_p^2 = 0.326$), as well as on the number of glomerular responses that were evoked by these 2 chemically-similar odorants (Supplementary Figure S7.7). Specifically, MV- and EV-evoked glomerular response maps tended to be more similar to each other (i.e., harder to discriminate) in Sham-males than they were in Sham-females (Figure 7.6G). By contrast, MV- and EV-evoked glomerular response maps tended to be more dissimilar from each other (i.e., easier to discriminate) in Gnxfemales than they were in Gnxfemales (Figure 7.6G). This result demonstrates that neuroendocrine factors can influence the representation of odor identity

at the input to the brain, such that circulating gonadal hormones likely help females in making challenging olfactory discriminations but may make such discriminations more difficult for males.

Discussion

In the present experiments we observed a sex difference in odorant-evoked signaling from the OSNs in the olfactory epithelium to the brain's olfactory bulb. Odorant presentation in unmanipulated female mice elicited OSN input into a broader range of olfactory bulb glomeruli than in males. Though responsive glomeruli received the same magnitude of OSN input on average between males and females, in females this input occurred earlier in the odor presentation. As a result, different odorants evoked more different spatial patterns of OSN input to the brain in females than males, even within the first second of odor presentation. Gonadectomy experiments revealed that circulating sex hormones may influence these responses. Gonadectomized females exhibited slower OSN responses in fewer glomeruli than control females, while gonadectomized males exhibited faster OSN responses in more glomeruli than control males. These results suggest that gonadal hormones may facilitate odor detection and discrimination of similar odorants in females but impair it in males.

Gonadectomy did not eliminate the sex difference between males and females but in fact reversed it, suggesting that the functional neuronal circuits underlying the sex-specific peripheral olfactory input to the brain exist in both males and females (Kimchi et al., 2007). Sexually dimorphic activation of sensory pathways presumably underlies many of the obvious differences in male and female behavior (Stowers and Logan, 2010; Stowers

and Liberles, 2016), and if both sexes are developmentally programmed with the same underlying circuitry then they may also be capable of displaying the same sex-specific behaviors in response to sensory stimuli (Kimchi et al., 2007). The reversal of sex-specific olfactory coding after gonadectomy implies a role for hormones in dynamically shaping the activity of sexually dimorphic sensory circuitry in the olfactory bulb. The functioning of these olfactory pathways could be further modulated by experiential factors (Oliva et al., 2010; Xu et al., 2016) since the within-cage olfactory environments of same-sex-housed males and females are different, as are the cage environments of mice with different endocrine statuses (Stowers and Logan, 2010; Stowers and Liberles, 2016) (i.e., sham-operated versus gonadectomized).

It is suggestive that these results parallel the common observation that females exhibit superior olfactory capabilities than males (Kobal et al., 2001; Baum and Keverne, 2002; Dalton et al., 2002; Pierman et al., 2006; Hummel et al., 2007; Cometto-Muniz and Abraham, 2008; Sorwell et al., 2008; Doty and Cameron, 2009). Sensory performance in a noisy environment is typically modeled as information accumulation over time, as demonstrated by the speed-accuracy tradeoff for odor detection and discrimination (Uchida and Mainen, 2003; Rinberg et al., 2006). The larger number of glomeruli receiving input in females (Figure 7.1) means that females receive more total olfactory sensory input to the brain, while the more rapid OSN response (Figure 7.2) gets that information to the brain earlier in females than in males. How would the larger number of glomerular responses in females affect odor discrimination performance? In principle the modest broadening of glomerular odor tuning could impair discrimination by increasing overlap in response maps, but conversely the greatly increased number of responding glomeruli in females

provides a much richer set of inputs for the brain to interpret. The utility of the Euclidean distance metrics reported here is that they quantify the actual difference in neural odorant representations, taking both the number of glomeruli and overlap of responses into account, and the larger EDs in females demonstrates that the neural response patterns are more different across odorants in females than they are in males. The finding that ovariectomy reduces these computational advantages in females is consistent with previous reports that estrogen replacement therapy protects against olfactory impairment in post-menopausal women (Deems et al., 1991; Caruso et al., 2008) and also in ovariectomized rats with lesions to the olfactory epithelium (Dhong et al., 1999).

What is the mechanism of the difference in OSN coding between males and females? Male and female mice have the same number of OSNs in the olfactory epithelium (Kawagishi et al., 2014), so the difference presumably arises physiologically, potentially from differences in the odor selectivity of OSNs (Figure 7.1F) or differences in OSN response kinetics (Figure 7.2F-H). The results from the gonadectomy-imaging experiment suggest that circulating gonadal hormones could influence those aspects of OSN odor processing, albeit in different directions in males and females. Notably, in these mice *spH* is expressed under the OMP promoter and the odor tuning, temporal properties, and sensitivity of OSNs are known to be influenced by OMP expression (Buiakova et al., 1996; Lee et al., 2011; Kass et al., 2013d). OMP expression might be susceptible to hormonal modulation (Tsim et al., 2004) that could conceivably result in sex-specific activation of OSNs. Regardless of potential interactions with OMP, a neuroendocrine mechanism could only be confirmed through the restoration of individual hormones such as estradiol or dihydrotestosterone. Without performing such a hormone replacement experiment we do

not know for certain if gonadal hormones cause the differences in olfactory sensory processing that were observed here, nor can we rule out the possibility of contributions from other endocrine effects because the gonadectomy surgical procedure can also result in several side effects, such as increased secretion of gonadotropins and alterations to the hypothalamic-pituitary system (Labhsetwar, 1969; Yen and Tsai, 1971). Nonetheless, the locus of these putative neuroendocrine interactions could be peripheral. Higher levels of odorant-binding protein genes have been observed in olfactory epithelia from female mice than from male mice (Shiao et al., 2012), which is consistent with the decreased OSN response latencies that we observed in unmanipulated females relative to males and suggests that gonad-intact females may have a more efficient odorant-transport system. Such differences may be dynamically regulated by varying levels of sex steroids that are synthesized locally in the epithelium (Lupo et al., 1986) or that are present in other structures in the mucosa. For example, in male mice, relatively high levels of testosterone have been found in the lateral nasal gland (Zhou et al., 2009), a structure that secretes odorant-binding proteins into the epithelium. There could also be an indirect effect of gonadal hormones on olfactory transduction via modifications to the anatomy of the olfactory mucosa (Mair et al., 1978; Caruso et al., 2008).

Alternatively, the observed effects of gonadal hormones on OSNs could be mediated in the glomerular layer of the olfactory bulb, where populations of periglomerular (PG) interneurons and short axon cells (SACs) influence primary sensory odor coding. PG interneurons directly mediate local gain control on OSN output via GABA-mediated presynaptic inhibition of OSN synaptic terminals (McGann, 2013). The activity of this intraglomerular inhibitory circuitry is in turn shaped by extensive interglomerular

connections that arise from SACs, which co-express GABA and TH (Kosaka and Kosaka, 2008; Kiyokage et al., 2010), and GABAergic (Li and Wu, 1964; Saad, 1970; Wallis and Luttge, 1980; Maggi and Perez, 1986; Weiland, 1992) and dopaminergic (Gao and Dluzen, 2001; Dluzen et al., 2002) signaling in the brain are subject to modulation by gonadal steroids.

Neuroendocrine effects in the glomerular layer could, for example, be mediated through estrogen receptors (Mitra et al., 2003; Merchenthaler et al., 2004). Aromatase, which is the enzyme necessary for the conversion of androgens to estrogens, is also expressed throughout the olfactory bulb (Horvath and Wikler, 1999; Hoyk et al., 2014), indicating that synthesis of estradiol occurs locally in the bulb. Notably, aromatase is broadly expressed in SACs in the glomerular layer (Hoyk et al., 2014), suggesting that the discriminability of different odor maps may indeed be related to estrogen-dependent regulation of interglomerular processing. Consistent with this, male olfactory bulbs contain a greater number of TH-positive neurons than female olfactory bulbs in both rodents (Gomez et al., 2007) and humans (Alizadeh et al., 2015). Additionally, TH mRNA in the olfactory bulb is increased by ovariectomy in female mice, and this effect can be reversed when ovariectomized mice are treated with estradiol (Dluzen et al., 2002). We thus speculate that gonadal hormones may play a role in tuning olfactory bulb circuitry by modulating SACs, which could potentially include direct effects on OSN synaptic terminals via dopamine receptors (Ennis et al., 2001) as well as indirect effects on OSN signaling via connections with PG cells. It might also be possible for neuroendocrine effects to directly influence PG cell-mediated GABAergic presynaptic inhibition of OSNs. Gonadectomy in females results in an increase in GABA content in the rat brain (Saad,

1970), whereas GABA content is decreased by gonadectomy in males (Li and Wu, 1964). This seems consistent with a system that exhibits relatively decreased presynaptic inhibition in gonad-intact females relative to gonad-intact males.

In rodents, there are notable sex differences in the accessory olfactory system that are essential for processing pheromone cues that are used to guide normal social and reproductive behaviors (Guillamon and Segovia, 1997; Stowers and Logan, 2010). It is increasingly understood that the main olfactory system is also involved in processing biologically relevant odors (Schaefer et al., 2001; Kang et al., 2009; Veyrac et al., 2011), though few studies have examined sex differences in processing such stimuli (Woodley and Baum, 2004; Waters et al., 2005). The present work demonstrates that OSN responses to odorants can differ between males and females even in the main olfactory bulb and even for non-social odorants, which could influence the interpretation of results from olfactory research and potentially the design of flavors and fragrances.

Regardless of the exact mechanisms by which sexually dimorphic OSN signaling emerges, these data are the first to demonstrate *in vivo* sex differences in primary sensory odor coding. These results further demonstrate that OSN function may normally be influenced by circulating gonadal hormones in both sexes, suggesting that sex hormones might underlie some of the differences in how males and females perceive their olfactory environments (Dey et al., 2015; Stowers and Liberles, 2016).

Acknowledgements

I thank Lindsey Czarnecki and Andrew Moberly for surgically implanting cranial windows. I also thank Michael Baum and Tracey Shors for helpful discussion on the project.

Chapter 7 Figures

Figure 7.1

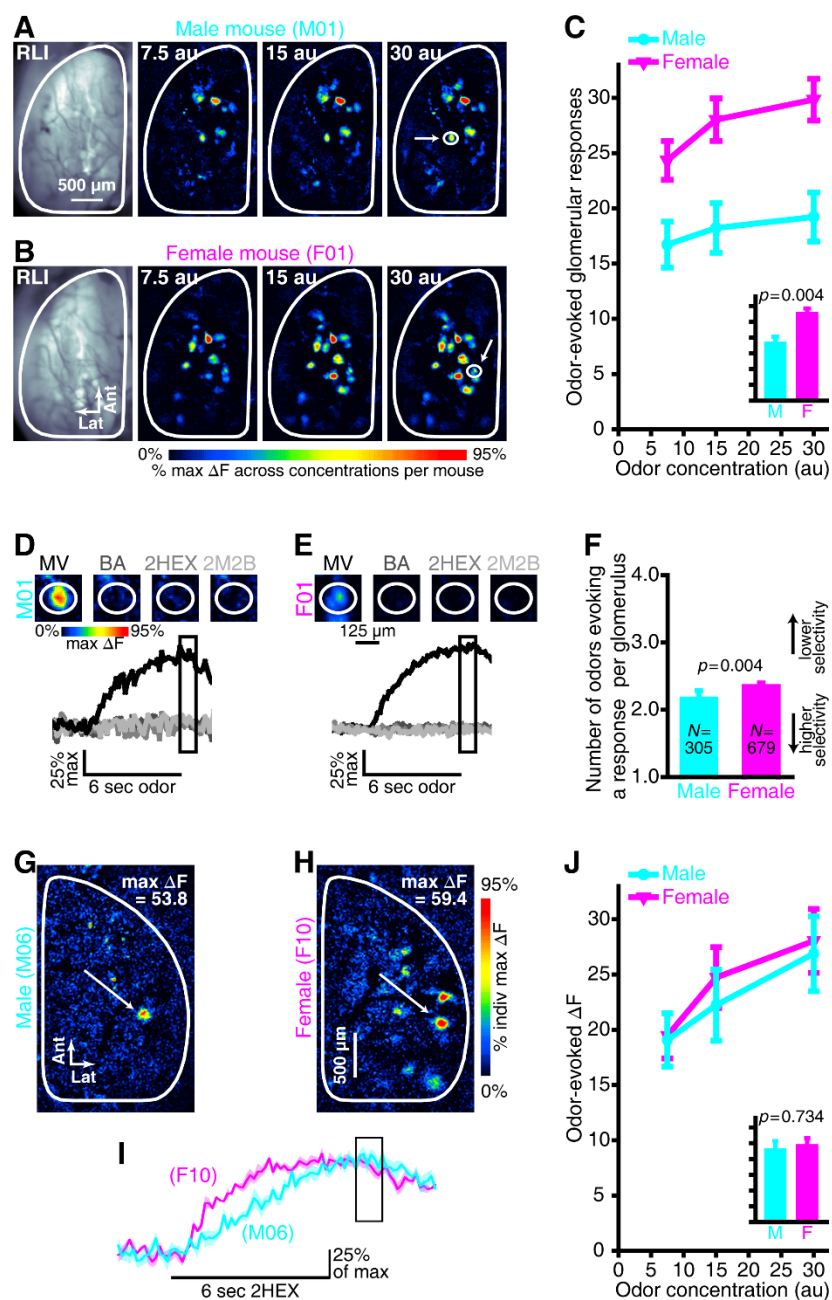


Figure 7.1. Odorant-evoked glomerular response maps contain a greater number of glomeruli receiving synaptic input in unmanipulated females than in unmanipulated males. (A-B) Resting light intensity (RLI) images through the cranial window and

pseudocolored difference maps showing the peak responses evoked by 3 concentrations of MV from representative male (**A**, M01) and female (**B**, F01) subjects. The circled callouts indicate the example glomeruli in **D-E**. (**C**) Mean \pm SEM number of odorant-evoked glomerular responses plotted as a function of odorant concentration. The inset shows the main effect of group pooled across concentrations and is scaled to the same y-axis as **C**. (**D-E**) Individual male (**D**, M01) and female (**E**, F01) glomeruli showing sample odorant response selectivity patterns. The pseudocolored difference maps that were evoked by MV, BA, 2HEX, and 2M2B are shown (top) with all 4 corresponding fluorescent records superimposed per glomerulus (bottom). Individual traces represent 4-trial averages per odorant and the boxed portion of the traces indicates the frames that were used to generate the response maps in **A-B** and **D-E** and the analyses in **C** and **F**. (**F**) The mean \pm SEM number of odorants that evoked a measurable response in each glomerulus are plotted for male and female glomerular populations. *N*s indicate the number of glomeruli per group. The y-axis ranges from 1-4 because each individual glomerulus was categorized as responding to 1-4 odorants in the panel. (**G-H**) Glomerular response maps that were evoked by 15 au 2HEX in a representative male mouse (**G**, M06) and a representative female mouse (**H**, F10). (**I**) Fluorescent records that correspond to the glomerular callouts in **G-H**. The boxed portion of the fluorescent records indicates the frames that were used to generate the peak response maps in **G-H** and the analyses that are summarized in **J**. Solid lines \pm shaded regions represent the mean \pm SEM fluorescent record across 4 repeated trials for each glomerulus. Each trace is scaled relative to its individual maximum. (**J**) Mean \pm SEM odorant-evoked change in fluorescence (ΔF) plotted as a function of odorant concentration. The inset shows the main effect of group pooled across concentrations and is scaled to the same y-axis as **J**.

Figure 7.2

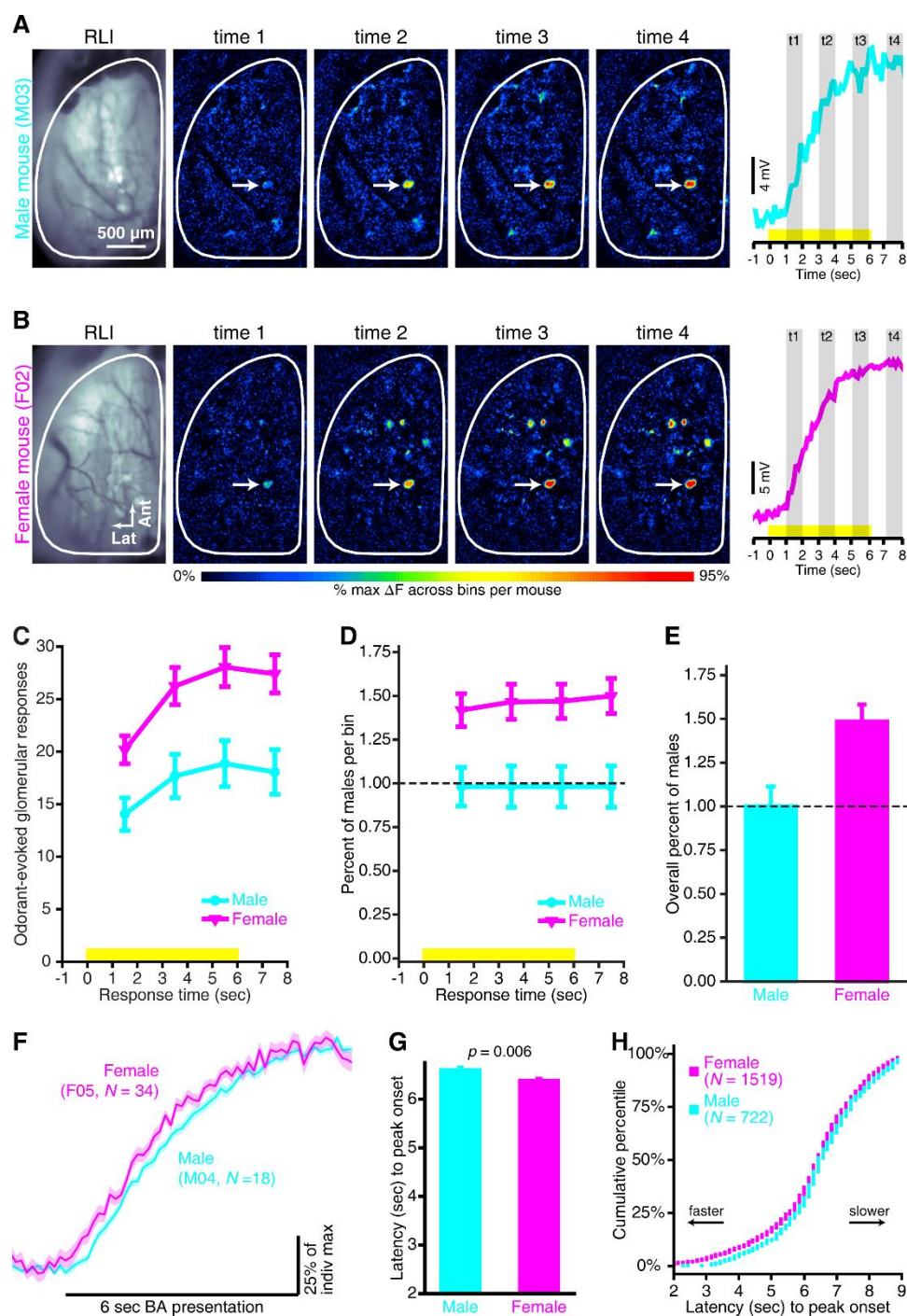


Figure 7.2. Temporal evolution of odorant-evoked OSN activity in unmanipulated females compared to unmanipulated males. (A-E) Sex-dependent differences in the temporal evolution of spatial odor maps. (A-B) RLIs and odorant-evoked difference maps

that were measured during 4, 1-sec time bins from a representative male mouse (**A**, M03) and a representative female mouse (**B**, F02). Timelines illustrating the 4, 1-sec time bins (shaded regions; t1-t4, response times 1-4) relative to stimulus presentation (yellow stimulus bar) are shown to the right. Example traces are superimposed on each timeline and correspond to the glomerular callouts (white arrows) in **A-B**. Each trace represents the average fluorescent record for that glomerulus across 4 trials of 15 au 2M2B. (**C**) Odorant-evoked glomerular responses plotted as a function of time relative to stimulus presentations (yellow bar). Times are plotted to correspond with the middle of each 1-sec bin. For example, data corresponding to time 1 (which was an average of 7 frames acquired during 1-2 sec after odorant onset) is plotted at 1.5 sec. These data are calculated across all concentrations (7.5 au, 15 au, and 30 au) of all odors (BA, MV, 2HEX, and 2M2B). (**D**) To show proportional differences in the number of odorant-evoked glomerular responses throughout the stimulus presentation, the data in **C** were normalized relative to the male group within each bin and are plotted as the percent of males as a function of response time. (**E**) Overall ratio of glomerular responses relative to males, pooled across all 4 time bins. Dashed lines in **D-E** indicate 100% of male activity. (**F-H**) Odorant-evoked spH signals reach maximum response magnitudes slightly faster in intact-females than in intact-males. (**F**) BA-evoked spH signals compared between representative male (M04, cyan) and female (F05, magenta) subjects. Solid lines \pm shaded regions, mean \pm SEM BA-evoked response across glomerular responses per subject; *N*s, number of BA-responsive glomeruli per subject. (**G**) Overall, when averaged across odorants and between sexes the mean \pm SEM latency to peak onset is \sim 0.31 sec faster in intact-females than in intact-males. (**H**) Cumulative probability plot showing the male and female distributions of peak latency values pooled across individual fluorescent records.

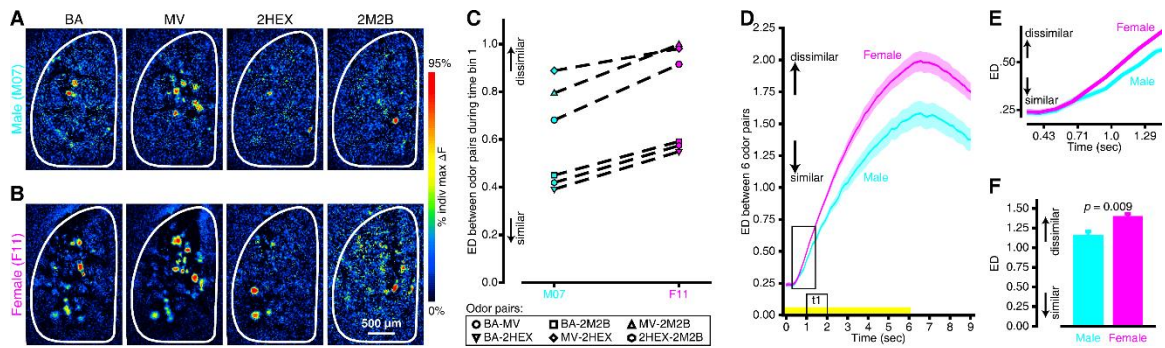
Figure 7.3

Figure 7.3. Sex differences in the contrast between the primary sensory representations of different odors. (A-B) BA-, MV-, 2HEX-, and 2M2B-evoked difference maps from representative male (A, M07) and female (B, F11) mice. (C) Euclidean distance (ED) between 6 pairwise odor map comparisons for the static maps that are shown in A and B. (D) Mean \pm SEM ED between all 6 odor pairs from all male (cyan) and female (magenta) subjects across 64 frames that correspond to 0-9 sec relative to odorant onset. The yellow stimulus bar indicates the time of odorant presentations and the boxed region of the stimulus bar (t1, time bin 1) notes the frames that were used to generate the difference maps in A-B and the corresponding ED comparisons shown in C. (E) Enlargement of the boxed region of the frame-by-frame ED analysis in D shows that odor maps are more dissimilar in females than in males by as early as 1 sec into the odorant presentations. (F) Overall mean \pm SEM ED between odor representations pooled across 6 odor pairs and 64 frames.

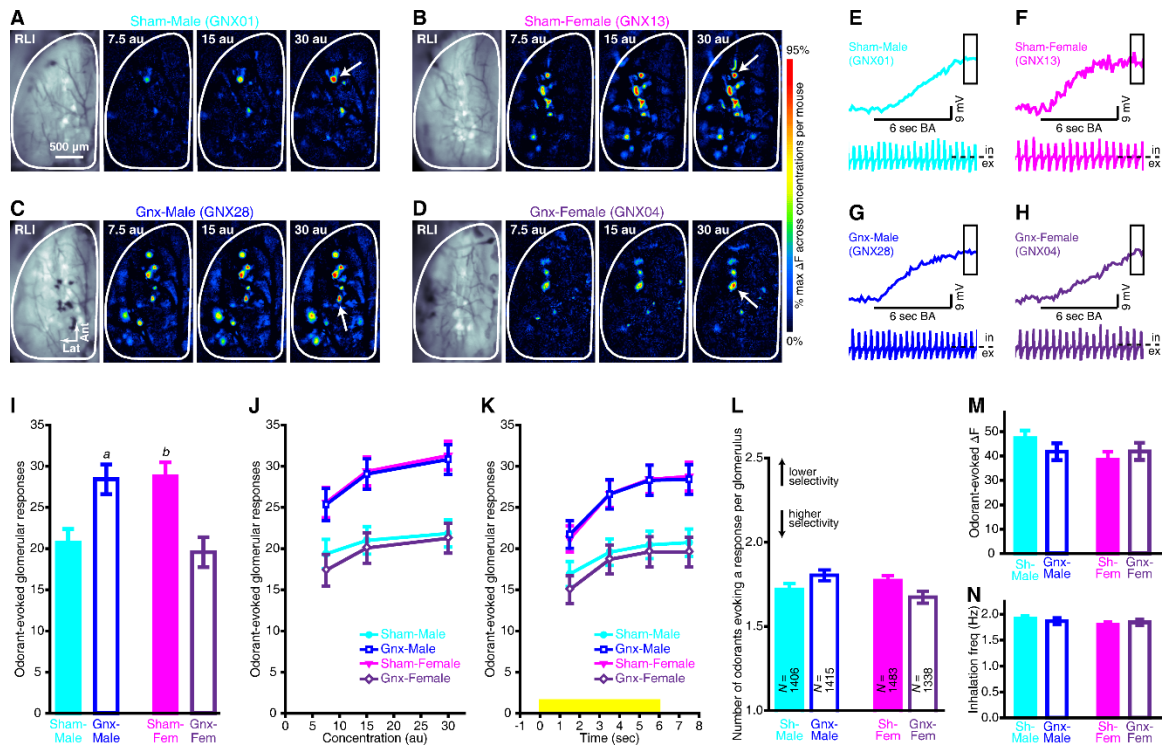
Figure 7.4

Figure 7.4. Sexually dimorphic activation of olfactory bulb glomeruli is dependent upon circulating gonadal hormones. (A-D) RLI images through the cranial window and pseudocolored difference maps showing the peak responses evoked by 3 concentrations of BA from a Sham-male (A, GNX01), a Sham-female (B, GNX13), a GnX-male (C, GNX28), and a GnX-female (D, GNX04). (E-H) Fluorescent records from individual trials that correspond to the glomerular callouts that are noted by white arrows on the 30 au BA-evoked maps in A-D. The boxed portion of the fluorescent records indicates the frames that were used to generate response maps in A-D and analyses summarized in I, J, L, and M. The example piezosensor recordings that are shown below each response amplitude are from a single trial of 30 au BA. Positive and negative portions of each respiration trace respectively correspond to inhalation (in) and exhalation (ex) phases of the respiratory cycle. (I) Odorant-evoked glomerular responses during the peak response phase are pooled across all odorants and concentrations and plotted separately for each group. *a* indicates $p = 0.008$ when compared with Sham-male and GnX-female groups; *b* indicates $p = 0.001$ when compared with Sham-male and GnX-female groups. (J) Odorant-evoked glomerular

responses are pooled across odorants and plotted as a function of concentration for each group. **(K)** Odorant-evoked glomerular responses are plotted as a function of time relative to stimulus presentation (yellow stimulus bar). **(L)** The number of odorants that evoked a measurable response in each glomerulus are plotted for sex \times surgical treatment glomerular populations. *Ns* indicate the number of glomeruli per group. Note that each individual glomerulus was categorized as responding to 1, 2, 3, or 4 odorants in the panel, but the y-axis is truncated at 2.5 to display an appropriate range for the group means. **(M)** Peak odorant-evoked change in fluorescence (ΔF) pooled across all odorants and concentrations for each group. **(N)** Inhalation frequency during 6 sec odorant presentations for each group. Data are pooled across respiration measurements that were recorded during trials from each concentration of each odorant. The data shown in **I-N** are plotted as the mean \pm SEM.

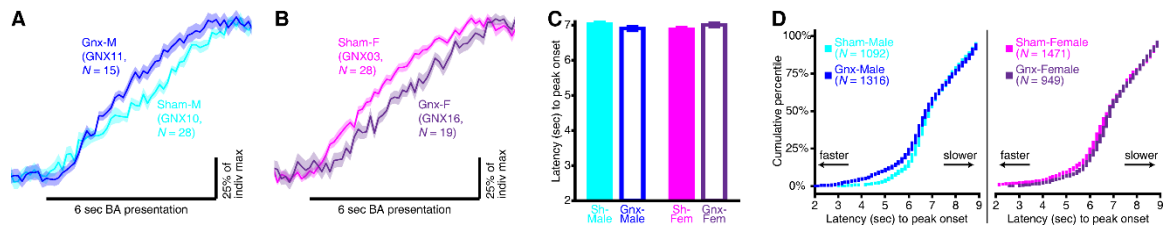
Figure 7.5

Figure 7.5. Odorant-evoked spH signals are accelerated by gonadectomy in males, but slowed by gonadectomy in females. (A-B) BA-evoked spH signals compared between representative Sham-male (GNX11) and GnX-male (GNX10) subjects (A) and also between representative Sham-female (GNX03) and GnX-female (GNX16) subjects (B). The solid lines \pm shaded regions represent the mean \pm SEM fluorescent record across all BA-evoked glomerular responses per subject, and the *N*s indicate the number of glomeruli that are contributing to each subject's mean BA-evoked spH signal. (C) Mean \pm SEM latency to onset of peak spH signal from sex \times surgical treatment groups. (D) Cumulative probability plots showing the distributions of peak latency values pooled across individual fluorescent records. The *N*s indicate the number of odorant-evoked spH signals pooled across odorants.

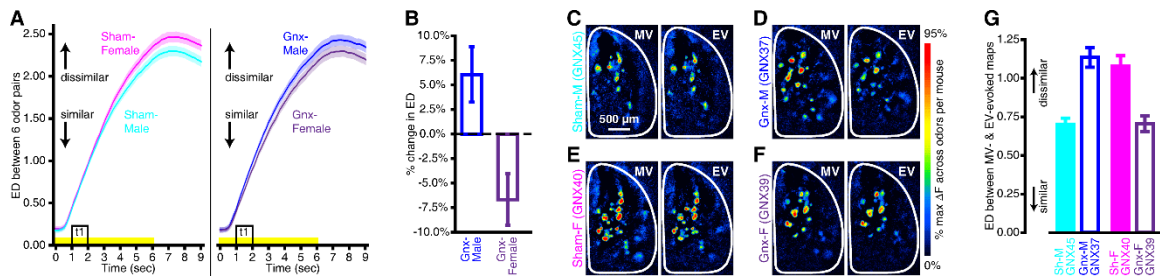
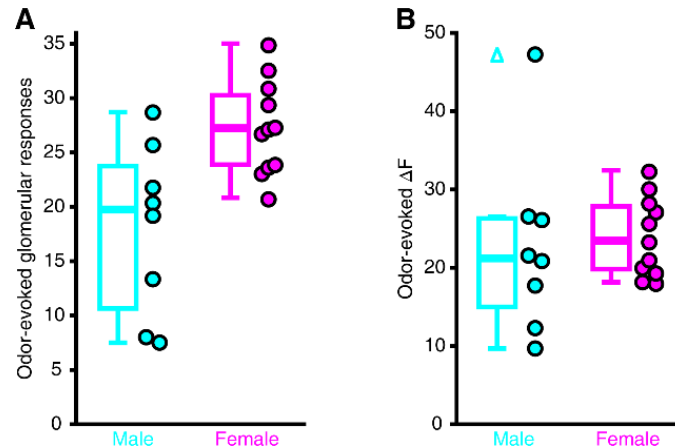
Figure 7.6

Figure 7.6. Odor maps become relatively more discriminable after gonadectomy in males, but relatively less discriminable after gonadectomy in females. (A) Odor pairs tended to be further apart in Euclidean space (i.e., more dissimilar) in Sham-females than in Sham-males (left panel), and this difference was reversed by gonadectomy (right panel). The mean \pm SEM ED between all 6 odor pairs is plotted across 64 frames that correspond to 0-9 sec relative to odorant onset. The yellow stimulus bar indicates the time of odorant presentations and the boxed region of the stimulus bar (t1, time bin 1) notes the frames that were used to generate the difference maps in C-F. (B) The effects of gonadectomy on primary sensory odor representations are plotted as the percent change in ED relative to Sham-control groups. The dashed line indicates no change relative to Sham-controls. Values above and below the dashed line respectively note relative increases and decreases in odor map discriminability. (C-F) Pairs of MV- vs EV-evoked difference maps from a representative Sham-male (C, GNX45), Gnx-male (D, GNX37), Sham-female (E, GNX40), and Gnx-female (F, GNX39). (G) Mean \pm SEM ED between MV- and EV-evoked maps across all 64 frames for each subject shown in C-F.

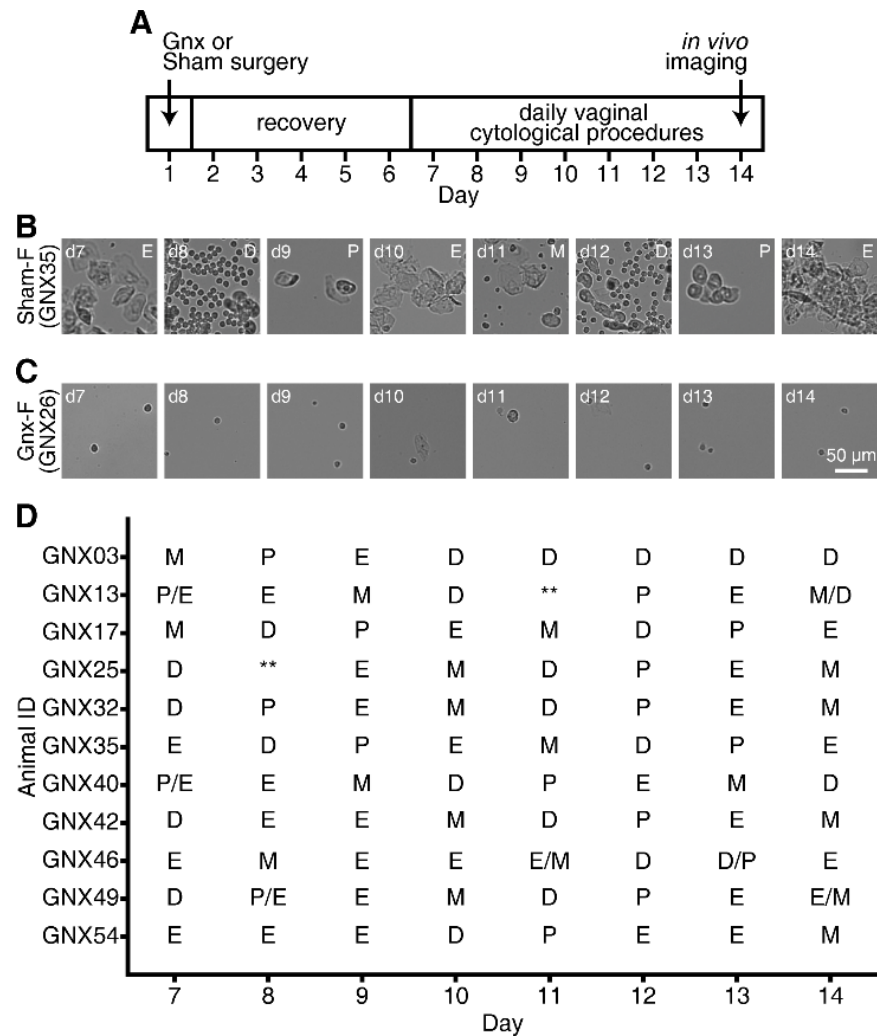
Chapter 7 Supplementary Information

Supplementary Figure S7.1



Supplementary Figure S7.1. Individual variability in the number of glomeruli receiving odorant-evoked OSN input and peak response amplitudes in unmanipulated males and females. (A-B) Box plots showing the distributions of odorant-evoked glomerular responses (A) and odorant-evoked response amplitudes (ΔF s, B) for male and female subjects. Box, 25th-75th percentile; thick, solid line, median; whiskers, minimum and maximum; open triangles, outliers 1.5 \times the interquartile range. Individual subjects are represented by circles that are plotted immediately to the right of each distribution. (A) Odorant-evoked glomerular responses are plotted for the individual male ($N = 8$) and female ($N = 11$) subjects that contributed to the analyses summarized in Figure 7.1C. Each individual subject is represented here by the average number of odorant-evoked glomerular responses that was observed across all 3 concentrations of all 4 odorants; Mann-Whitney U test, $Z = -2.642$, $p = 0.008$. (B) Odorant-evoked ΔF s from the individual male ($N = 8$) and female ($N = 11$) subjects that contributed to the analyses summarized in Figure 7.1J. Each individual subject is represented here by the average odorant-evoked ΔF calculated across all 3 concentrations of all 4 odorants; Mann-Whitney U test, $Z = -0.826$, $p = 0.409$.

Supplementary Figure S7.2



Supplementary Figure S7.2. Procedure summary for the gonadectomy-imaging experiment. (A) Experimental timeline showing gonadectomy (Gnx) or sham-control (Sham) procedures (day 1), followed by daily vaginal cytological procedures (days 7-14), and finally *in vivo* optical imaging procedures (day 14). (B-C) Example images of unstained vaginal secretion from a Sham-female (B, GNX35) and a Gnx-female (C, GNX26) across 8 consecutive days (d7-d14). P, proestrus; E, estrus; M, metestrus; D, diestrus. (D) The estrous cycle of all 11 Sham-females is plotted across 8 consecutive days leading up to the optical imaging experiment. **unable to determine from sample. Note that subjects in the gonadectomy (GNX)-imaging experiment were identified in sequence as GNX₀₁ through GNX_{NN}, regardless of sex or surgical group assignment.

Vaginal smear cytology (Caligioni, 2009) was used to determine the estrous cycle phases in Sham-females and to confirm the efficacy of ovariectomy in GnX-females. Females were gently restrained, the vulva was cleaned with gauze soaked in saline, and the vagina was then gently flushed 5-7 times with a sterile saline solution. The final flush was collected back into the pipette and then dispensed on a glass slide for cytological analysis via brightfield microscopy. Photographs of vaginal secretion were taken at a magnification of 10× with a Jenoptik MFcool Peltier-cooled CCD camera mounted on an Olympus BX41 microscope. Note that males underwent a similar “sham-smear” procedure to maintain equal treatment across all experimental groups. For the sham-smear procedure, males were gently restrained and the genital area was cleaned with saline solution and delicately prodded with a pipette.

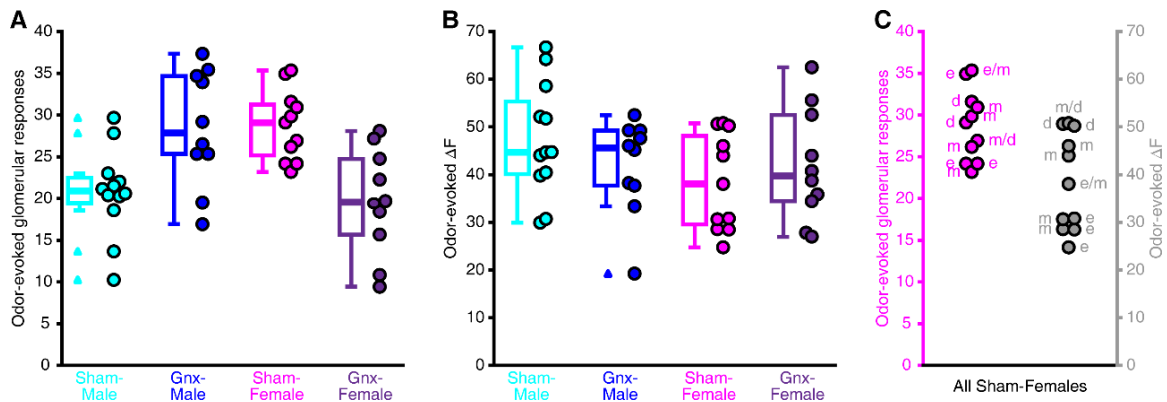
The estrous cycle stages were identified in Sham-females based on the proportion of cell types that were observed in the vaginal secretion (Supplementary Figure S7.2B). Overall, we observed approximately normal, 4-day cycles in Sham-females (Supplementary Figure S7.2B and S7.2D). Macroanatomic manifestations of the estrous cycle (Champlin et al., 1973; Byers et al., 2012) were also observed in Sham-females through visual inspection that was performed during the restraint that occurred immediately prior to performing vaginal smear procedures.

The density of cells in samples that were collected from GnX-females was notably lower than that observed in samples from Sham-females (compare Supplementary Figures S7.2B and S7.2C), and there was no change in the relative proportion of different cell types from day to day. In fact, very few cells were present in many of the GnX-female samples (Supplementary Figure S7.2C), which is consistent with observations from other groups (Ng et al., 2010). While there were no day to day changes in the appearance of the vagina in GnX-females, there was a striking difference in the appearance of the vaginal opening in GnX-females relative to Sham-females. Consistent with other reports (Ng et al., 2010), the vaginal opening in GnX-females was pale in coloration, very dry, and extremely narrow/closed.

The differences across days in the vaginal opening and vaginal smears that were observed in Sham-females, and the lack of such differences in GnX-females, suggests that

circulating gonadal hormones were relatively unaffected by the sham-surgical procedures but successfully eliminated by gonadectomy.

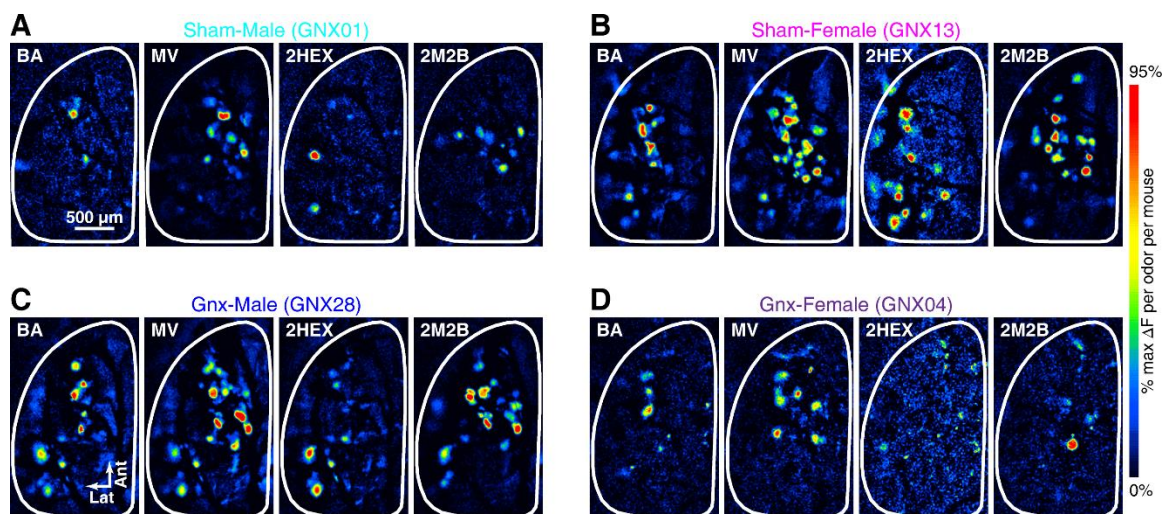
Supplementary Figure S7.3



Supplementary Figure S7.3. Odorant-evoked glomerular responses and response amplitudes from all individual subjects from sex \times surgical treatment groups. (A-B) Box plots showing the distributions of odorant-evoked glomerular responses (**A**) and odorant-evoked response amplitudes (ΔF s, **B**) from sex \times surgical treatment groups. Box, 25th-75th percentile; thick, solid line, median; whiskers, minimum and maximum; closed triangles, outliers 1.5 \times the interquartile range. Individual subjects are represented by circles plotted immediately to the right of each distribution. (**A**) Odorant-evoked glomerular responses are plotted for the individual Sham-male ($N = 12$), GnX-male ($N = 10$), Sham-female ($N = 11$), and GnX-female ($N = 10$) subjects that contributed to the analyses summarized in Figure 7.4I-J. Each individual subject is represented here by the average number of odorant-evoked glomerular responses that was observed across all 3 concentrations of all 4 odorants; Kruskal-Wallis test across 4 groups, $\chi^2_{(df=3)} = 15.915$, $p = 0.001$. *Post hoc* Mann-Whitney tests between pairwise group comparisons: Sham-male versus GnX-male, $Z = -2.243$, $p = 0.025$; Sham-male versus Sham-female, $Z = -3.386$, $p < 0.001$; Sham-male versus GnX-female, non-significant, $Z = -0.593$, $p = 0.582$; Sham-female versus GnX-female, $Z = -2.959$, $p = 0.002$; Sham-female versus GnX-male, non-significant, $Z = -0.070$, $p = 0.973$; GnX-female versus GnX-male, $Z = -2.420$, $p = 0.015$. (**B**) Odorant-evoked ΔF from the individual subjects that contributed to the analyses summarized in Figure 7.4M. Each individual subject is represented here by the average odorant-evoked ΔF calculated across all 3 concentrations of all 4 odorants; non-significant Kruskal-Wallis test across 4 groups, $\chi^2_{(df=3)} = 3.143$, $p = 0.370$. (**C**) The data that are plotted for the Sham-Female group in panels **A** and **B** are replotted with lettering to indicate the phase of the

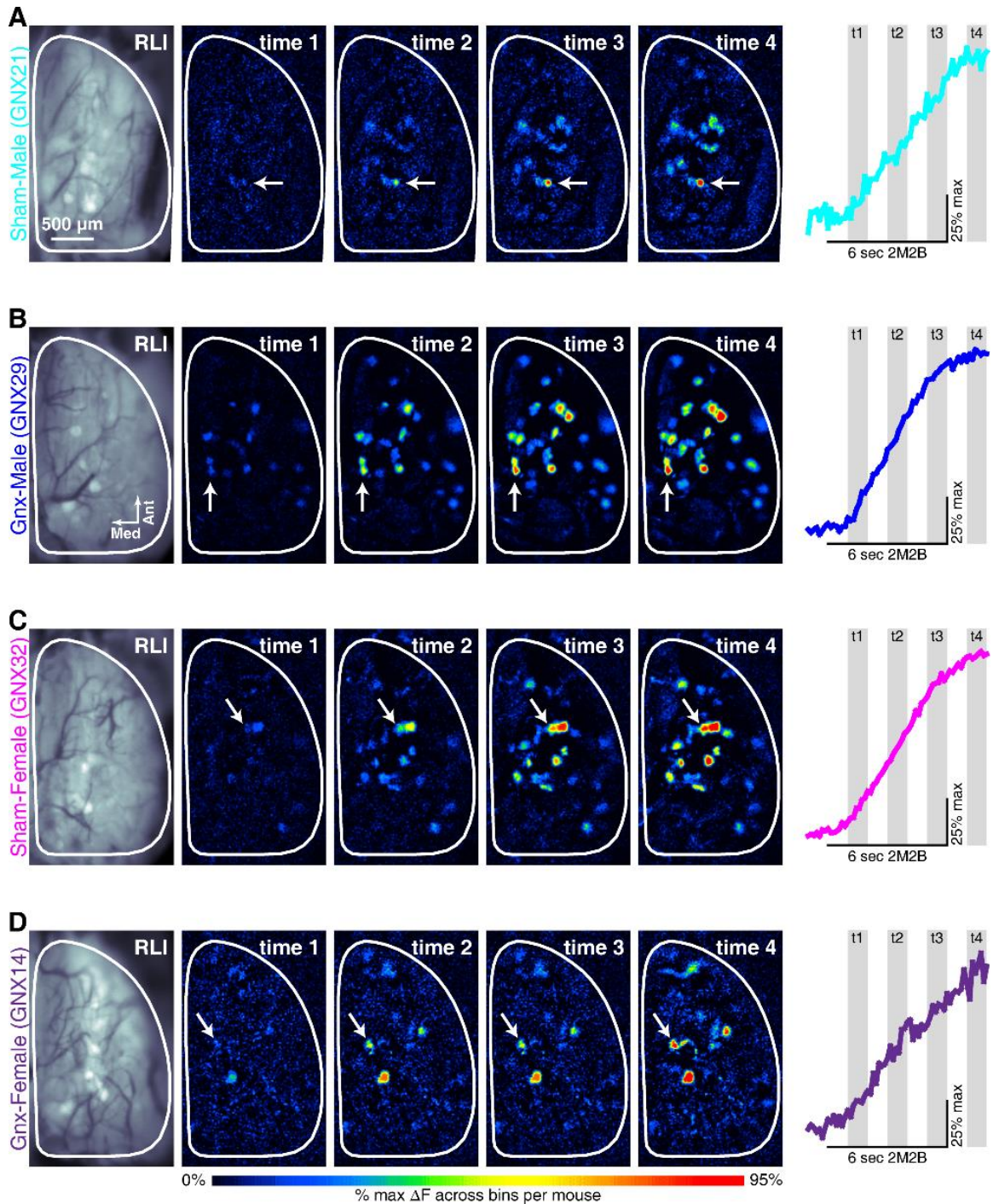
estrous cycle for each subject. The left y-axis is shown in magenta and corresponds with the mean number of odorant-evoked glomerular responses per subject, and the right y-axis is shown in grey and corresponds with the mean odorant-evoked ΔF per subject. p, proestrus; e, estrus; m, metestrus; d, diestrus.

Supplementary Figure S7.4



Supplementary Figure S7.4. Glomerular response maps that were evoked by two esters, a ketone, and an aldehyde. (A-D) Additional pseudocolored difference maps from the representative Sham-male (A, GNX01), Sham-female (B, GNX13), GnX-male (C, GNX28), and GnX-female (D, GNX04) subjects that are shown in Figure 7.4A-D. The maps that are shown in Figure 7.4A-D were evoked across a 4-fold range of BA concentrations, and thus illustrate the interactive effects of sex and surgical treatment on concentration-dependent glomerular recruitment. To further demonstrate that the interactive effects of sex and surgical treatment were observed in response to all of the odorants that we tested, the peak odorant-evoked glomerular response maps that were evoked by the 15 au concentration of two esters (BA and MV), a ketone (2HEX), and an aldehyde (2M2B) are shown here for each subject. Regardless of the odorant (or concentration, Figure 7.4A-D) that was being presented, a larger number of olfactory bulb glomeruli received OSN synaptic input in Sham-females than in Sham-males (compare panels A and B). Interestingly, this sexually dimorphic activation of olfactory bulb glomeruli seemed to be reversed by gonadectomy because there were a larger number of odorant-evoked glomerular responses in GnX-males than in GnX-females (compare panels C and D). Thus, patterns of glomeruli receiving odorant-evoked synaptic input in gonadectomized males and females are more similar to opposite-sex control animals than they are to same-sex control animals.

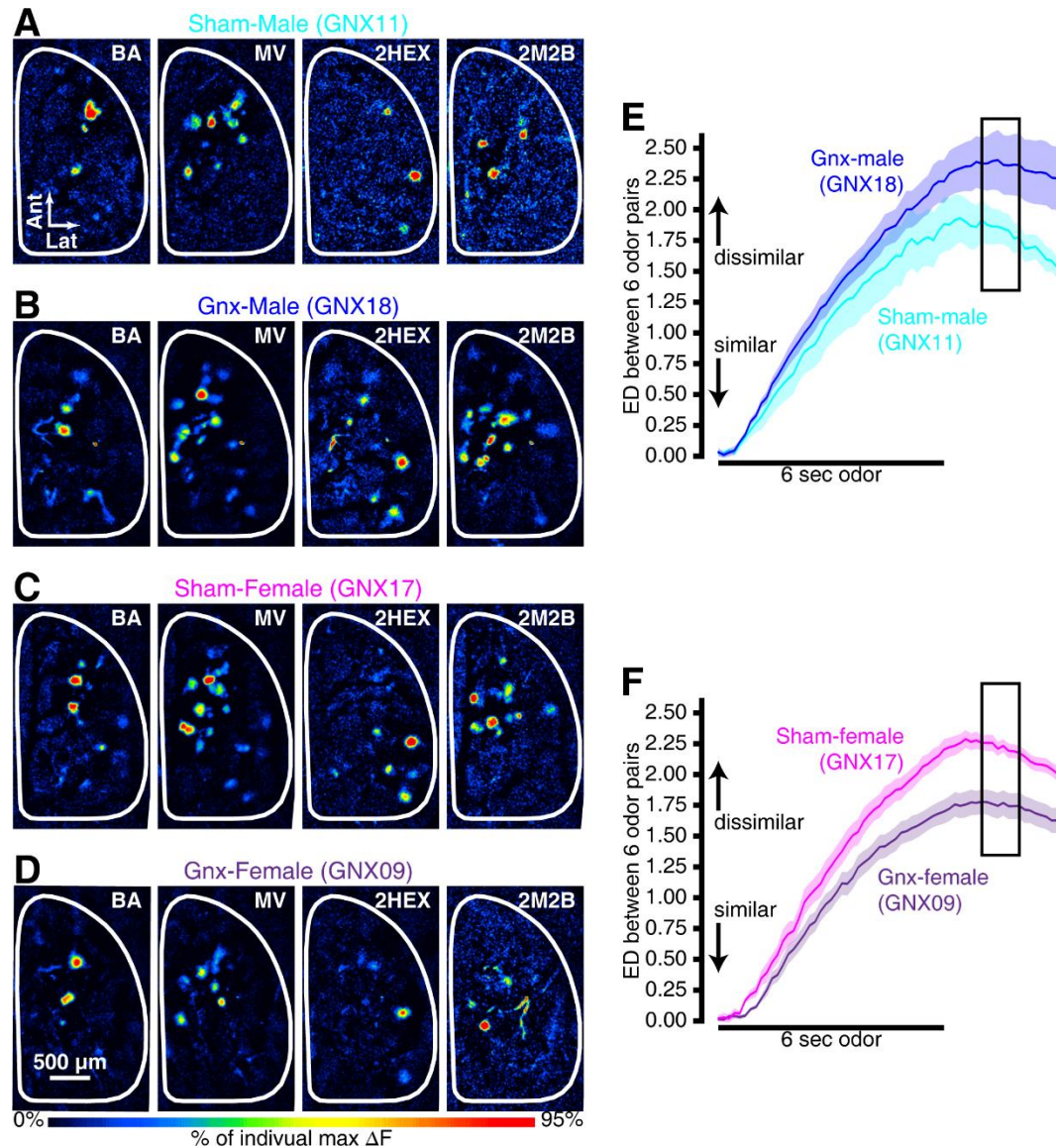
Supplementary Figure S7.5



Supplementary Figure S7.5. Time course of odorant-evoked glomerular response maps. (A-D) Each panel shows a resting light intensity (RLI) image through the cranial window along with pseudocolored difference maps that were measured during 4, sequential 1-sec time bins (time 1-4), from representative Sham-male (A, GNX21), GnX-male (B,

GNX29), Sham-female (**C**, GNX32), and Gnx-female (**D**, GNX14) subjects. A timeline is shown in the right of each panel to illustrate the 4, 1-sec time bins (shaded regions; t1-t4, response times 1-4) that were used to generate the example glomerular response maps in **A-D** and the analyses that are summarized in Figure 7.4K. The example fluorescent records that are superimposed on each timeline correspond to the glomerular callouts (white arrows) on the difference maps in **A-D**, which are 4-trial block averages of 15 au 2M2B.

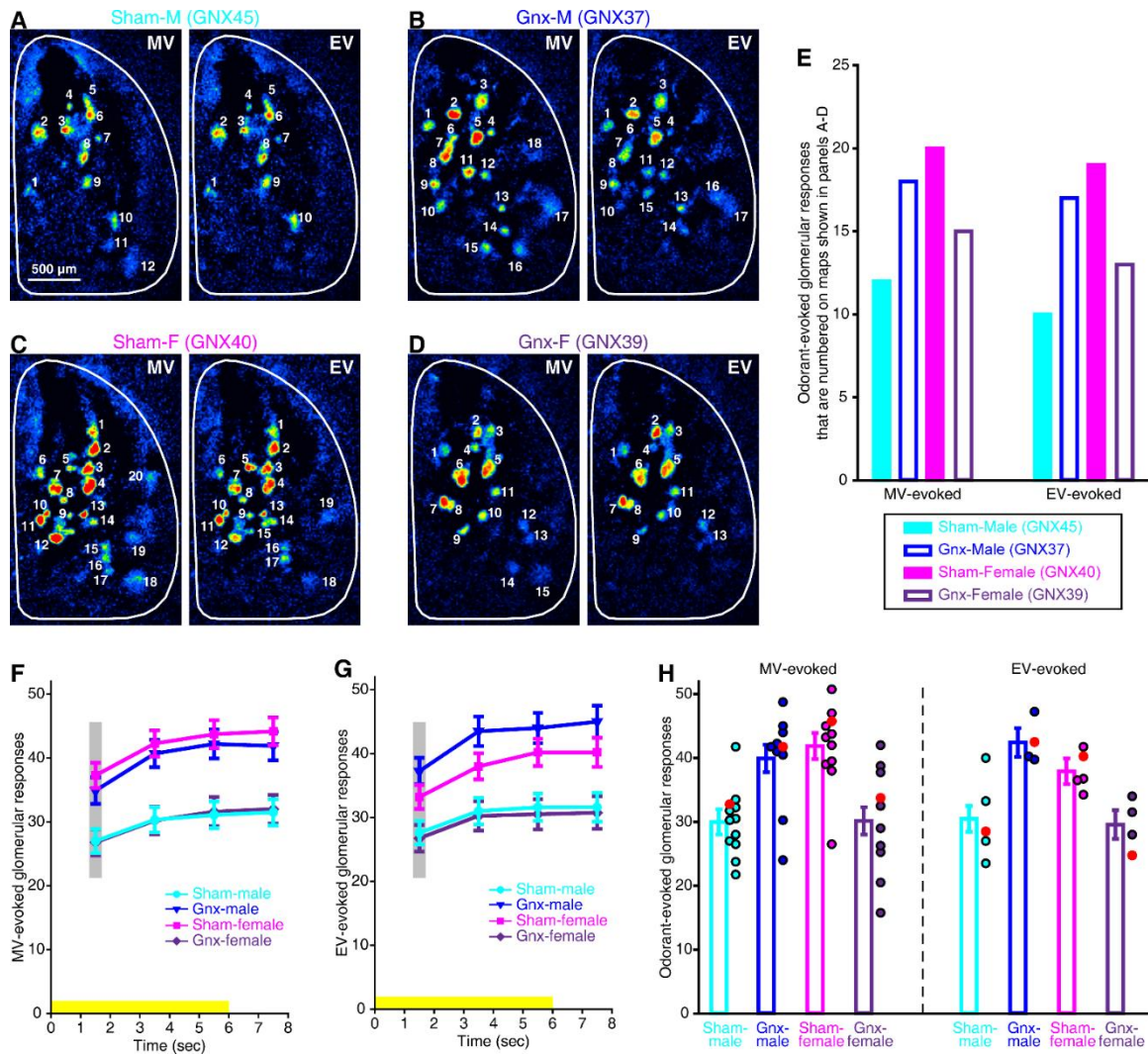
Supplementary Figure S7.6



Supplementary Figure S7.6. Pairs of odor maps become closer together in Euclidean space after gonadectomy in females, but further apart after gonadectomy in males. (A-D) BA-, MV-, 2HEX-, and 2M2B-evoked difference maps from representative Sham-male (A, GNX11), GnX-male (B, GNX18), Sham-female (C, GNX17), and GnX-female (D, GNX09) subjects. (E-F) The mean \pm SEM Euclidean distance (ED) is calculated between all 6 odor pairs (BA-MV, BA-2HEX, BA-2M2B, MV-2HEX, MV-2M2B, AND 2HEX-2M2B) and across 64 consecutive frames (from time = 0-9 sec relative to odorant onset) for each representative subject shown in A-D. The yellow stimulus bar indicates

the time of odorant presentations and the boxed region of the mean \pm SEM EDs notes the frames that were used to generate the difference maps in **A-D**. Odor maps were more dissimilar from each other (i.e., further apart in Euclidean space) in the example Gn_x-male than in the example Sham-male (**E**). By contrast, odor maps were more similar to each other (i.e., closer together in Euclidean space) in the example Gn_x-female than in the example Sham-female (**F**).

Supplementary Figure S7.7



Supplementary Figure S7.7. The interactive effects of sex and surgical treatment on the number of glomeruli receiving OSN synaptic input are observed in response to the presentation of chemically similar odorants. (A-D) The pairs of MV- and EV-evoked difference maps that are shown in Figure 7.6C-F are enlarged here and are shown for the same Sham-male (A, GNX45), GnX-male (B, GNX37), Sham-female (C, GNX40), and GnX-female (D, GNX39) subjects. Each pair of maps is scaled relative to the overall maximum across odorants, as specified in Figure 7.6C-F. All glomerular regions of interest (ROIs) that are receiving odorant-evoked OSN input are numbered separately (from ROI₁-ROI_N) for each individual difference map. (E) The glomerular ROIs that are numbered in A-D are separated by odorant and plotted for each individual subject. Note that these

values are only used for demonstration purposes because they only reflect the number of odorant-evoked glomerular responses that are visible on the olfactory bulb that is being displayed, while the data were actually analyzed across both olfactory bulbs as shown in **F-H**. (**F-G**) The number of glomerular responses that was evoked by MV (**F**) and EV (**G**) is plotted as a function of time for each group. The difference maps that are shown in **A-D** correspond to the shaded response time bin, which occurred 1-2 sec into the stimulus presentation. The time of stimulus presentation is noted by the yellow bar. (**H**) The number of glomerular responses that was evoked by MV (left) and EV (right) is collapsed across all 4 response time bins for each group. Individual subjects are represented by circles that are plotted immediately to the right of each group mean. Red circles indicate the subjects whose difference maps are shown in **A-D**. The data shown in **F-H** are plotted as the mean \pm SEM.

The MV-evoked data that is shown here was included in the analyses that are summarized in Figure 7.4 because it came from the entire study sample; Sham-male, $N = 12$, GnX-male, $N = 10$, Sham-female, $N = 11$, and GnX-female, $N = 10$. The EV-evoked data that is shown here was analyzed separately because only a subset of the subjects from that sample were presented with EV during their imaging preparations; Sham-male, $N = 5$, GnX-male, $N = 4$, Sham-female, $N = 5$, and GnX-female, $N = 4$. EV-evoked glomerular responses were analyzed via a sex (Male, Female) \times surgical treatment (Sham, GnX) \times response time bin (time 1, time 2, time 3, time 4) mixed ANOVA, with sex and surgical treatment as between-subjects factors and response time bin as a within-subjects factor. There was a significant interaction between sex and surgical treatment (Supplementary Figure S7.7H, right panel; $F_{(3, 42)} = 5.452$, $p = 0.003$, $\eta_p^2 = 0.618$) such that Sham-females exhibited more EV-evoked glomerular responses than Sham-males ($F_{(1, 8)} = 5.550$, $p = 0.046$, $\eta_p^2 = 0.410$), while GnX-females exhibited fewer glomerular responses than GnX-males ($F_{(1, 6)} = 23.619$, $p = 0.003$, $\eta_p^2 = 0.797$). Gonadectomy thus resulted in opposite effects on EV-evoked glomerular responses in males and females, with the number of EV-evoked glomerular responses being reduced in GnX-females relative to Sham-females ($F_{(1, 7)} = 12.574$, $p = 0.009$, $\eta_p^2 = 0.642$), but increased in GnX-males relative to Sham-males ($F_{(1, 7)} = 11.277$, $p = 0.012$, $\eta_p^2 = 0.617$). The results from this analysis 1) replicate the findings from the analyses that were performed on the main data set (Figure 7.4), which

included 4 structurally- and perceptually-disparate odorants, and 2) extend those findings to a pair of structurally-similar odorants (which could potentially be relatively more challenging to discriminate).

REFERENCES

- Ahs F, Miller SS, Gordon AR, Lundstrom JN (2013) Aversive learning increases sensory detection sensitivity. *Biol Psychol* 92:135-141.
- Aizenberg M, Geffen MN (2013) Bidirectional effects of aversive learning on perceptual acuity are mediated by the sensory cortex. *Nat Neurosci* 16:994-996.
- Alizadeh R, Hassanzadeh G, Soleimani M, Joghataei MT, Siavashi V, Khorgami Z, Hadjighassem M (2015) Gender and age related changes in number of dopaminergic neurons in adult human olfactory bulb. *J Chem Neuroanat* 69:1-6.
- Altundag A, Cayonu M, Kayabasoglu G, Salihoglu M, Tekeli H, Saglam O, Hummel T (2015) Modified olfactory training in patients with postinfectious olfactory loss. *Laryngoscope* 125:1763-1766.
- Aston-Jones G, Rajkowski J, Kubiak P, Valentino RJ, Shipley MT (1996) Role of the locus coeruleus in emotional activation. *Prog Brain Res* 107:379-402.
- Aungst JL, Heyward PM, Puche AC, Karnup SV, Hayar A, Szabo G, Shipley MT (2003) Centre-surround inhibition among olfactory bulb glomeruli. *Nature* 426:623-629.
- Baker H, Grillo M, Margolis FL (1989) Biochemical and immunocytochemical characterization of olfactory marker protein in the rodent central nervous system. *J Comp Neurol* 285:246-261.
- Baker H, Morel K, Stone DM, Maruniak JA (1993) Adult naris closure profoundly reduces tyrosine hydroxylase expression in mouse olfactory bulb. *Brain Res* 614:109-116.
- Bakin JS, Weinberger NM (1990) Classical conditioning induces CS-specific receptive field plasticity in the auditory cortex of the guinea pig. *Brain Res* 536:271-286.
- Baldi E, Lorenzini CA, Bucherelli C (2004) Footshock intensity and generalization in contextual and auditory-cued fear conditioning in the rat. *Neurobiol Learn Mem* 81:162-166.
- Baldisseri DM, Margolis JW, Weber DJ, Koo JH, Margolis FL (2002) Olfactory marker protein (OMP) exhibits a beta-clam fold in solution: implications for target peptide interaction and olfactory signal transduction. *J Mol Biol* 319:823-837.
- Bar-Haim Y, Lamy D, Pergamin L, Bakermans-Kranenburg MJ, van IJZENDIJK IMH (2007) Threat-related attentional bias in anxious and nonanxious individuals: a meta-analytic study. *Psychol Bull* 133:1-24.
- Barnes DC, Chapuis J, Chaudhury D, Wilson DA (2011) Odor fear conditioning modifies piriform cortex local field potentials both during conditioning and during post-conditioning sleep. *PLoS One* 6:e18130.
- Barni T, Maggi M, Fantoni G, Granchi S, Mancina R, Gulisano M, Marra F, Macorsini E, Luconi M, Rotella C, Serio M, Balboni GC, Vannelli GB (1999) Sex steroids and odorants modulate gonadotropin-releasing hormone secretion in primary cultures of human olfactory cells. *J Clin Endocrinol Metab* 84:4266-4273.
- Baroncelli L, Sale A, Viegi A, Maya Vetencourt JF, De Pasquale R, Baldini S, Maffei L (2010) Experience-dependent reactivation of ocular dominance plasticity in the adult visual cortex. *Exp Neurol* 226:100-109.
- Barrett LF, Bar M (2009) See it with feeling: affective predictions during object perception. *Philos Trans R Soc Lond B Biol Sci* 364:1325-1334.
- Baum MJ, Keverne EB (2002) Sex difference in attraction thresholds for volatile odors from male and estrous female mouse urine. *Horm Behav* 41:213-219.

- Beck AT, Clark DA (1997) An information processing model of anxiety: automatic and strategic processes. *Behav Res Ther* 35:49-58.
- Blumhagen F, Zhu P, Shum J, Scharer YP, Yaksi E, Deisseroth K, Friedrich RW (2011) Neuronal filtering of multiplexed odour representations. *Nature* 479:493-498.
- Boccaccio A, Lagostena L, Hagen V, Menini A (2006) Fast adaptation in mouse olfactory sensory neurons does not require the activity of phosphodiesterase. *J Gen Physiol* 128:171-184.
- Bonzano S, Bovetti S, Fasolo A, Peretto P, De Marchis S (2014) Odour enrichment increases adult-born dopaminergic neurons in the mouse olfactory bulb. *Eur J Neurosci* 40:3450-3457.
- Bovetti S, Veyrac A, Peretto P, Fasolo A, De Marchis S (2009) Olfactory enrichment influences adult neurogenesis modulating GAD67 and plasticity-related molecules expression in newborn cells of the olfactory bulb. *PLoS One* 4:e6359.
- Boyd AM, Sturgill JF, Poo C, Isaacson JS (2012) Cortical feedback control of olfactory bulb circuits. *Neuron* 76:1161-1174.
- Bozza T, McGann JP, Mombaerts P, Wachowiak M (2004) In vivo imaging of neuronal activity by targeted expression of a genetically encoded probe in the mouse. *Neuron* 42:9-21.
- Brenner N, Bialek W, de Ruyter van Steveninck R (2000) Adaptive rescaling maximizes information transmission. *Neuron* 26:695-702.
- Brunjes PC (1985) Unilateral odor deprivation: time course of changes in laminar volume. *Brain Res Bull* 14:233-237.
- Brunjes PC, Smith-Crafts LK, McCarty R (1985) Unilateral odor deprivation: effects on the development of olfactory bulb catecholamines and behavior. *Brain Res* 354:1-6.
- Bryant RA, Felmingham KL, Kemp AH, Barton M, Peduto AS, Rennie C, Gordon E, Williams LM (2005) Neural networks of information processing in posttraumatic stress disorder: a functional magnetic resonance imaging study. *Biol Psychiatry* 58:111-118.
- Buck L, Axel R (1991) A novel multigene family may encode odorant receptors: a molecular basis for odor recognition. *Cell* 65:175-187.
- Buiakova OI, Krishna NS, Getchell TV, Margolis FL (1994) Human and rodent OMP genes: conservation of structural and regulatory motifs and cellular localization. *Genomics* 20:452-462.
- Buiakova OI, Baker H, Scott JW, Farbman A, Kream R, Grillo M, Franzen L, Richman M, Davis LM, Abbondanzo S, Stewart CL, Margolis FL (1996) Olfactory marker protein (OMP) gene deletion causes altered physiological activity of olfactory sensory neurons. *Proc Natl Acad Sci U S A* 93:9858-9863.
- Buonviso N, Chaput M (2000) Olfactory experience decreases responsiveness of the olfactory bulb in the adult rat. *Neuroscience* 95:325-332.
- Buonviso N, Gervais R, Chalansonnet M, Chaput M (1998) Short-lasting exposure to one odour decreases general reactivity in the olfactory bulb of adult rats. *Eur J Neurosci* 10:2472-2475.
- Byers SL, Wiles MV, Dunn SL, Taft RA (2012) Mouse estrous cycle identification tool and images. *PLoS One* 7:e35538.

- Cadiou H, Aoude I, Tazir B, Molinas A, Fenech C, Meunier N, Grosmaître X (2014) Postnatal odorant exposure induces peripheral olfactory plasticity at the cellular level. *J Neurosci* 34:4857-4870.
- Caligioni CS (2009) Assessing reproductive status/stages in mice. *Curr Protoc Neurosci* Appendix 4:Appendix 4I.
- Carmichael ST, Clugnet MC, Price JL (1994) Central olfactory connections in the macaque monkey. *J Comp Neurol* 346:403-434.
- Carr VM, Farbman AI (1993) The dynamics of cell death in the olfactory epithelium. *Exp Neurol* 124:308-314.
- Caruso S, Serra A, Grillo C, De Leo V, Maiolino L, Agnello C, Cianci A (2008) Prospective study evaluating olfactometric and rhinomanometric outcomes in postmenopausal women on 1 mg 17beta-estradiol and 2 mg drospirenone HT. *Menopause* 15:967-972.
- Cavallin MA, Powell K, Biju KC, Fadool DA (2010) State-dependent sculpting of olfactory sensory neurons is attributed to sensory enrichment, odor deprivation, and aging. *Neurosci Lett* 483:90-95.
- Champlin AK, Dorr DL, Gates AH (1973) Determining the stage of the estrous cycle in the mouse by the appearance of the vagina. *Biol Reprod* 8:491-494.
- Chang EF, Merzenich MM (2003) Environmental noise retards auditory cortical development. *Science* 300:498-502.
- Chapuis J, Wilson DA (2012) Bidirectional plasticity of cortical pattern recognition and behavioral sensory acuity. *Nat Neurosci* 15:155-U194.
- Chen CF, Barnes DC, Wilson DA (2011) Generalized vs. stimulus-specific learned fear differentially modifies stimulus encoding in primary sensory cortex of awake rats. *J Neurophysiol* 106:3136-3144.
- Chen TW, Wardill TJ, Sun Y, Pulver SR, Renninger SL, Baohua A, Schreier ER, Kerr RA, Orger MB, Jayaraman V, Looger LL, Svoboda K, Kim DS (2013) Ultrasensitive fluorescent proteins for imaging neuronal activity. *Nature* 499:295-300.
- Cherian S, Wai Lam Y, McDaniels I, Struziak M, Delay RJ (2014) Estradiol rapidly modulates odor responses in mouse vomeronasal sensory neurons. *Neuroscience* 269:43-58.
- Cho JY, Min N, Franzen L, Baker H (1996) Rapid down-regulation of tyrosine hydroxylase expression in the olfactory bulb of naris-occluded adult rats. *J Comp Neurol* 369:264-276.
- Ciocchi S, Herry C, Grenier F, Wolff SB, Letzkus JJ, Vlachos I, Ehrlich I, Sprengel R, Deisseroth K, Stadler MB, Müller C, Luthi A (2010) Encoding of conditioned fear in central amygdala inhibitory circuits. *Nature* 468:277-282.
- Clancy K, Ding M, Bernat E, Schmidt NB, Li W (2017) Restless 'rest': intrinsic sensory hyperactivity and disinhibition in post-traumatic stress disorder. *Brain* 140:2041-2050.
- Clark CR, Galletly CA, Ash DJ, Moores KA, Penrose RA, McFarlane AC (2009) Evidence-based medicine evaluation of electrophysiological studies of the anxiety disorders. *Clin EEG Neurosci* 40:84-112.
- Cleland TA, Johnson BA, Leon M, Linster C (2007) Relational representation in the olfactory system. *Proc Natl Acad Sci U S A* 104:1953-1958.

- Cohen-Cory S (2002) The developing synapse: construction and modulation of synaptic structures and circuits. *Science* 298:770-776.
- Cometto-Muniz JE, Abraham MH (2008) Human olfactory detection of homologous n-alcohols measured via concentration-response functions. *Pharmacol Biochem Behav* 89:279-291.
- Coppola DM (2012) Studies of olfactory system neural plasticity: the contribution of the unilateral naris occlusion technique. *Neural Plast* 2012:351752.
- Coppola DM, Waggener CT (2012) The effects of unilateral naris occlusion on gene expression profiles in mouse olfactory mucosa. *J Mol Neurosci* 47:604-618.
- Coppola DM, Waguespack AM, Reems MR, Butman ML, Cherry JA (2006) Naris occlusion alters transducing protein immunoreactivity in olfactory epithelium. *Histol Histopathol* 21:487-501.
- Cortese BM, Leslie K, Uhde TW (2015) Differential odor sensitivity in PTSD: Implications for treatment and future research. *J Affect Disord* 179:23-30.
- Cummings DM, Brunjes PC (1997) The effects of variable periods of functional deprivation on olfactory bulb development in rats. *Exp Neurol* 148:360-366.
- Cummings DM, Belluscio L (2010) Continuous neural plasticity in the olfactory intrabulbar circuitry. *J Neurosci* 30:9172-9180.
- Cummings DM, Henning HE, Brunjes PC (1997) Olfactory bulb recovery after early sensory deprivation. *J Neurosci* 17:7433-7440.
- Cury KM, Uchida N (2010) Robust odor coding via inhalation-coupled transient activity in the mammalian olfactory bulb. *Neuron* 68:570-585.
- Czarnecki LA, Moberly AH, Rubinstein T, Turkel DJ, Pottackal J, McGann JP (2011) In vivo visualization of olfactory pathophysiology induced by intranasal cadmium instillation in mice. *Neurotoxicology* 32:441-449.
- Czarnecki LA, Moberly AH, Turkel DJ, Rubinstein T, Pottackal J, Rosenthal MC, McCandlish EF, Buckley B, McGann JP (2012) Functional rehabilitation of cadmium-induced neurotoxicity despite persistent peripheral pathophysiology in the olfactory system. *Toxicol Sci* 126:534-544.
- Dahmen JC, King AJ (2007) Learning to hear: plasticity of auditory cortical processing. *Curr Opin Neurobiol* 17:456-464.
- Dalton P, Wysocki CJ (1996) The nature and duration of adaptation following long-term odor exposure. *Percept Psychophys* 58:781-792.
- Dalton P, Doolittle N, Breslin PAS (2002) Gender-specific induction of enhanced sensitivity to odors. *Nat Neurosci* 5:199-200.
- Damm M, Pikart LK, Reimann H, Burkert S, Goktas O, Haxel B, Frey S, Charalampakis I, Beule A, Renner B, Hummel T, Huttenbrink KB (2014) Olfactory training is helpful in postinfectious olfactory loss: a randomized, controlled, multicenter study. *Laryngoscope* 124:826-831.
- Danciger E, Mettling C, Vidal M, Morris R, Margolis F (1989) Olfactory marker protein gene: its structure and olfactory neuron-specific expression in transgenic mice. *Proc Natl Acad Sci U S A* 86:8565-8569.
- de Olmos J, Hardy H, Heimer L (1978) The afferent connections of the main and the accessory olfactory bulb formations in the rat: an experimental HRP-study. *J Comp Neurol* 181:213-244.

- de Villers-Sidani E, Simpson KL, Lu YF, Lin RC, Merzenich MM (2008) Manipulating critical period closure across different sectors of the primary auditory cortex. *Nat Neurosci* 11:957-965.
- Deems DA, Doty RL, Settle RG, Moore-Gillon V, Shaman P, Mester AF, Kimmelman CP, Brightman VJ, Snow JB, Jr. (1991) Smell and taste disorders, a study of 750 patients from the University of Pennsylvania Smell and Taste Center. *Arch Otolaryngol Head Neck Surg* 117:519-528.
- Dey S, Chamero P, Pru JK, Chien MS, Ibarra-Soria X, Spencer KR, Logan DW, Matsunami H, Peluso JJ, Stowers L (2015) Cyclic Regulation of Sensory Perception by a Female Hormone Alters Behavior. *Cell* 161:1334-1344.
- Dhawale AK, Hagiwara A, Bhalla US, Murthy VN, Albeanu DF (2010) Non-redundant odor coding by sister mitral cells revealed by light addressable glomeruli in the mouse. *Nat Neurosci* 13:1404-1412.
- Dhong HJ, Chung SK, Doty RL (1999) Estrogen protects against 3-methylindole-induced olfactory loss. *Brain Res* 824:312-315.
- Dias BG, Ressler KJ (2014) Parental olfactory experience influences behavior and neural structure in subsequent generations. *Nat Neurosci* 17:89-96.
- Dillon TS, Fox LC, Han C, Linster C (2013) 17 β -estradiol enhances memory duration in the main olfactory bulb in CD-1 mice. *Behav Neurosci* 127:923-931.
- Dluzen DE, Park JH, Kim K (2002) Modulation of olfactory bulb tyrosine hydroxylase and catecholamine transporter mRNA by estrogen. *Brain Res Mol Brain Res* 108:121-128.
- Dorries KM, Schmidt HJ, Beauchamp GK, Wysocki CJ (1989) Changes in sensitivity to the odor of androstene during adolescence. *Dev Psychobiol* 22:423-435.
- Doty RL, Ferguson-Segall M (1989) Influence of adult castration on the olfactory sensitivity of the male rat: a signal detection analysis. *Behav Neurosci* 103:691-694.
- Doty RL, Cameron EL (2009) Sex differences and reproductive hormone influences on human odor perception. *Physiol Behav* 97:213-228.
- Doty RL, Applebaum S, Zusho H, Settle RG (1985) Sex differences in odor identification ability: a cross-cultural analysis. *Neuropsychologia* 23:667-672.
- Doty RL, Shaman P, Applebaum SL, Giberson R, Siksorski L, Rosenberg L (1984) Smell identification ability: changes with age. *Science* 226:1441-1443.
- Doucette W, Gire DH, Whitesell J, Carmean V, Lucero MT, Restrepo D (2011) Associative cortex features in the first olfactory brain relay station. *Neuron* 69:1176-1187.
- Dowd EW, Mitroff SR, LaBar KS (2016) Fear generalization gradients in visuospatial attention. *Emotion* 16:1011-1018.
- Dunsmoor JE, Murphy GL (2015) Categories, concepts, and conditioning: how humans generalize fear. *Trends Cogn Sci* 19:73-77.
- Dunsmoor JE, Paz R (2015) Fear Generalization and Anxiety: Behavioral and Neural Mechanisms. *Biol Psychiatry* 78:336-343.
- Dunsmoor JE, Mitroff SR, LaBar KS (2009) Generalization of conditioned fear along a dimension of increasing fear intensity. *Learn Mem* 16:460-469.
- Dunsmoor JE, White AJ, LaBar KS (2011a) Conceptual similarity promotes generalization of higher order fear learning. *Learn Mem* 18:156-160.

- Dunsmoor JE, Prince SE, Murty VP, Kragel PA, LaBar KS (2011b) Neurobehavioral mechanisms of human fear generalization. *Neuroimage* 55:1878-1888.
- Eckmeier D, Shea SD (2014) Noradrenergic plasticity of olfactory sensory neuron inputs to the main olfactory bulb. *J Neurosci* 34:15234-15243.
- Eldar S, Yankelevitch R, Lamy D, Bar-Haim Y (2010) Enhanced neural reactivity and selective attention to threat in anxiety. *Biol Psychol* 85:252-257.
- Ennis M, Zhou FM, Ciombor KJ, Aroniadou-Anderjaska V, Hayar A, Borrelli E, Zimmer LA, Margolis F, Shipley MT (2001) Dopamine D2 receptor-mediated presynaptic inhibition of olfactory nerve terminals. *J Neurophysiol* 86:2986-2997.
- Escanilla O, Arrellanos A, Karnow A, Ennis M, Linster C (2010) Noradrenergic modulation of behavioral odor detection and discrimination thresholds in the olfactory bulb. *Eur J Neurosci* 32:458-468.
- Fanselow MS (1980) Conditioned and unconditional components of post-shock freezing. *Pavlov J Biol Sci* 15:177-182.
- Farbman AI, Margolis FL (1980) Olfactory marker protein during ontogeny: immunohistochemical localization. *Dev Biol* 74:205-215.
- Farbman AI, Buchholz JA, Walters E, Margolis FL (1998) Does olfactory marker protein participate in olfactory neurogenesis? *Ann N Y Acad Sci* 855:248-251.
- Fast CD, McGann JP (2017a) Amygdalar gating of early sensory processing through interactions with locus coeruleus. *J Neurosci* In Press.
- Fast CD, McGann JP (2017b) Amygdalar Gating of Early Sensory Processing through Interactions with Locus Coeruleus. *J Neurosci* 37:3085-3101.
- Felmingham KL, Rennie C, Gordon E, Bryant RA (2012) Autonomic and cortical reactivity in acute and chronic posttraumatic stress. *Biol Psychol* 90:224-227.
- Finnerty GT, Roberts LS, Connors BW (1999) Sensory experience modifies the short-term dynamics of neocortical synapses. *Nature* 400:367-371.
- Fletcher ML (2012) Olfactory aversive conditioning alters olfactory bulb mitral/tufted cell glomerular odor responses. *Front Syst Neurosci* 6:16.
- Fletcher ML, Wilson DA (2002) Experience modifies olfactory acuity: acetylcholine-dependent learning decreases behavioral generalization between similar odorants. *J Neurosci* 22:RC201.
- Fletcher ML, Wilson DA (2003) Olfactory bulb mitral-tufted cell plasticity: odorant-specific tuning reflects previous odorant exposure. *J Neurosci* 23:6946-6955.
- Franks KM, Isaacson JS (2005) Synapse-specific downregulation of NMDA receptors by early experience: a critical period for plasticity of sensory input to olfactory cortex. *Neuron* 47:101-114.
- Gao X, Dluzen DE (2001) Tamoxifen abolishes estrogen's neuroprotective effect upon methamphetamine neurotoxicity of the nigrostriatal dopaminergic system. *Neuroscience* 103:385-394.
- Gdalyahu A, Tring E, Polack PO, Gruver R, Golshani P, Fanselow MS, Silva AJ, Trachtenberg JT (2012) Associative fear learning enhances sparse network coding in primary sensory cortex. *Neuron* 75:121-132.
- Ghosh S, Chattarji S (2015) Neuronal encoding of the switch from specific to generalized fear. *Nat Neurosci* 18:112-120.
- Gilbert CD, Li W, Piech V (2009) Perceptual learning and adult cortical plasticity. *J Physiol* 587:2743-2751.

- Goel A, Lee HK (2007) Persistence of experience-induced homeostatic synaptic plasticity through adulthood in superficial layers of mouse visual cortex. *J Neurosci* 27:6692-6700.
- Gomez C, Brinon JG, Valero J, Recio JS, Murias AR, Curto GG, Orio L, Colado MI, Alonso JR (2007) Sex differences in catechol contents in the olfactory bulb of control and unilaterally deprived rats. *Eur J Neurosci* 25:1517-1528.
- Good PR, Geary N, Engen T (1976) The effect of estrogen on odor detection. *Chem Senses* 2:46-50.
- Graziadei GA, Stanley RS, Graziadei PP (1980) The olfactory marker protein in the olfactory system of the mouse during development. *Neuroscience* 5:1239-1252.
- Griff ER, Greer CA, Margolis F, Ennis M, Shipley MT (2000) Ultrastructural characteristics and conduction velocity of olfactory receptor neuron axons in the olfactory marker protein-null mouse. *Brain Res* 866:227-236.
- Grosmaître X, Vassalli A, Mombaerts P, Shepherd GM, Ma M (2006) Odorant responses of olfactory sensory neurons expressing the odorant receptor MOR23: a patch clamp analysis in gene-targeted mice. *Proc Natl Acad Sci U S A* 103:1970-1975.
- Grosmaître X, Santarelli LC, Tan J, Luo M, Ma M (2007) Dual functions of mammalian olfactory sensory neurons as odor detectors and mechanical sensors. *Nat Neurosci* 10:348-354.
- Grosmaître X, Fuss SH, Lee AC, Adipietro KA, Matsunami H, Mombaerts P, Ma M (2009) SR1, a mouse odorant receptor with an unusually broad response profile. *J Neurosci* 29:14545-14552.
- Guillamon A, Segovia S (1997) Sex differences in the vomeronasal system. *Brain Res Bull* 44:377-382.
- Guthrie KM, Wilson DA, Leon M (1990) Early unilateral deprivation modifies olfactory bulb function. *J Neurosci* 10:3402-3412.
- He J, Tian H, Lee AC, Ma M (2012) Postnatal experience modulates functional properties of mouse olfactory sensory neurons. *Eur J Neurosci* 36:2452-2460.
- Headley DB, Weinberger NM (2013) Fear conditioning enhances gamma oscillations and their entrainment of neurons representing the conditioned stimulus. *J Neurosci* 33:5705-5717.
- Homma R, Cohen LB, Kosmidis EK, Youngentob SL (2009) Perceptual stability during dramatic changes in olfactory bulb activation maps and dramatic declines in activation amplitudes. *Eur J Neurosci* 29:1027-1034.
- Horvath TL, Wikler KC (1999) Aromatase in developing sensory systems of the rat brain. *J Neuroendocrinol* 11:77-84.
- Hoyk Z, Csakvari E, Gyenes A, Siklos L, Harada N, Parducz A (2014) Aromatase and estrogen receptor beta expression in the rat olfactory bulb: Neuroestrogen action in the first relay station of the olfactory pathway? *Acta Neurobiol Exp (Wars)* 74:1-14.
- Hubel DH, Wiesel TN (1970) The period of susceptibility to the physiological effects of unilateral eye closure in kittens. *J Physiol* 206:419-436.
- Hummel T, Kobal G, Gudziol H, Mackay-Sim A (2007) Normative data for the "Sniffin' Sticks" including tests of odor identification, odor discrimination, and olfactory thresholds: an upgrade based on a group of more than 3,000 subjects. *Eur Arch Otorhinolaryngol* 264:237-243.

- Isaacson JS, Strowbridge BW (1998) Olfactory reciprocal synapses: dendritic signaling in the CNS. *Neuron* 20:749-761.
- Ivic L, Pyrski MM, Margolis JW, Richards LJ, Firestein S, Margolis FL (2000) Adenoviral vector-mediated rescue of the OMP-null phenotype in vivo. *Nat Neurosci* 3:1113-1120.
- Jiang M, Griff ER, Ennis M, Zimmer LA, Shipley MT (1996) Activation of locus coeruleus enhances the responses of olfactory bulb mitral cells to weak olfactory nerve input. *J Neurosci* 16:6319-6329.
- Johnson BA, Leon M (2000) Modular representations of odorants in the glomerular layer of the rat olfactory bulb and the effects of stimulus concentration. *J Comp Neurol* 422:496-509.
- Jones SV, Choi DC, Davis M, Ressler KJ (2008) Learning-dependent structural plasticity in the adult olfactory pathway. *J Neurosci* 28:13106-13111.
- Jovanovic T, Ressler KJ (2010) How the neurocircuitry and genetics of fear inhibition may inform our understanding of PTSD. *Am J Psychiatry* 167:648-662.
- Kaas JH (1991) Plasticity of sensory and motor maps in adult mammals. *Annu Rev Neurosci* 14:137-167.
- Kang N, Baum MJ, Cherry JA (2009) A direct main olfactory bulb projection to the 'vomeronasal' amygdala in female mice selectively responds to volatile pheromones from males. *Eur J Neurosci* 29:624-634.
- Karmarkar UR, Dan Y (2006) Experience-dependent plasticity in adult visual cortex. *Neuron* 52:577-585.
- Kass MD, Moberly AH, McGann JP (2013a) Spatiotemporal alterations in primary odorant representations in olfactory marker protein knockout mice. *PLoS One* 8:e61431.
- Kass MD, Rosenthal MC, Pottackal J, McGann JP (2013b) Fear learning enhances neural responses to threat-predictive sensory stimuli. *Science* 342:1389-1392.
- Kass MD, Pottackal J, Turkel DJ, McGann JP (2013c) Changes in the neural representation of odorants after olfactory deprivation in the adult mouse olfactory bulb. *Chem Senses* 38:77-89.
- Kass MD, Guang SA, Moberly AH, McGann JP (2016) Changes in Olfactory Sensory Neuron Physiology and Olfactory Perceptual Learning After Odorant Exposure in Adult Mice. *Chem Senses* 41:123-133.
- Kass MD, Czarnecki LA, Moberly AH, McGann JP (2017) Differences in peripheral sensory input to the olfactory bulb between male and female mice. *Sci Rep* 7:45851.
- Kass MD, Moberly AH, Rosenthal MC, Guang SA, McGann JP (2013d) Odor-specific, olfactory marker protein-mediated sparsening of primary olfactory input to the brain after odor exposure. *J Neurosci* 33:6594-6602.
- Kato HK, Gillet SN, Peters AJ, Isaacson JS, Komiyama T (2013) Parvalbumin-expressing interneurons linearly control olfactory bulb output. *Neuron* 80:1218-1231.
- Katz LC, Shatz CJ (1996) Synaptic activity and the construction of cortical circuits. *Science* 274:1133-1138.
- Kawagishi K, Ando M, Yokouchi K, Sumitomo N, Karasawa M, Fukushima N, Moriizumi T (2014) Stereological quantification of olfactory receptor neurons in mice. *Neuroscience* 272:29-33.
- Kay LM, Laurent G (1999) Odor- and context-dependent modulation of mitral cell activity in behaving rats. *Nat Neurosci* 2:1003-1009.

- Kerr MA, Belluscio L (2006) Olfactory experience accelerates glomerular refinement in the mammalian olfactory bulb. *Nat Neurosci* 9:484-486.
- Kim HH, Puche AC, Margolis FL (2006) Odorant deprivation reversibly modulates transsynaptic changes in the NR2B-mediated CREB pathway in mouse piriform cortex. *J Neurosci* 26:9548-9559.
- Kimchi T, Xu J, Dulac C (2007) A functional circuit underlying male sexual behaviour in the female mouse brain. *Nature* 448:1009-1014.
- Kirkwood A, Rioult MC, Bear MF (1996) Experience-dependent modification of synaptic plasticity in visual cortex. *Nature* 381:526-528.
- Kiyokage E, Pan YZ, Shao Z, Kobayashi K, Szabo G, Yanagawa Y, Obata K, Okano H, Toida K, Puche AC, Shipley MT (2010) Molecular identity of periglomerular and short axon cells. *J Neurosci* 30:1185-1196.
- Kobal G, Palisch K, Wolf SR, Meyer ED, Huttenbrink KB, Roscher S, Wagner R, Hummel T (2001) A threshold-like measure for the assessment of olfactory sensitivity: the "random" procedure. *Eur Arch Otorhinolaryngol* 258:168-172.
- Koelega HS, Koster EP (1974) Some experiments on sex differences in odor perception. *Annals of the New York Academy of Sciences* 237:234-246.
- Kosaka T, Kosaka K (2008) Tyrosine hydroxylase-positive GABAergic juxtaglomerular neurons are the main source of the interglomerular connections in the mouse main olfactory bulb. *Neurosci Res* 60:349-354.
- Koster EP (1968) Olfactory sensitivity and ovulatory cycle duration. *Olfactologia* 1:43-51.
- Krech D, Rosenzweig M, Bennett E (1962) Relations between brain chemistry and problem-solving among rats raised in enriched and impoverished environments. *J Comp Physiol Psychol* 55:801-807.
- Krishna NS, Getchell TV, Margolis FL, Getchell ML (1992) Amphibian olfactory receptor neurons express olfactory marker protein. *Brain Res* 593:295-298.
- Krusemark EA, Li W (2012) Enhanced Olfactory Sensory Perception of Threat in Anxiety: An Event-Related fMRI Study. *Chemosens Percept* 5:37-45.
- Krusemark EA, Li W (2013) From early sensory specialization to later perceptual generalization: dynamic temporal progression in perceiving individual threats. *J Neurosci* 33:587-594.
- Kwon HJ, Koo JH, Zufall F, Leinders-Zufall T, Margolis FL (2009) Ca extrusion by NCX is compromised in olfactory sensory neurons of OMP mice. *PLoS One* 4:e4260.
- Labhsetwar AP (1969) Pituitary levels of FSH and LH at various intervals after ovariectomy in the rat. *J Reprod Fertil* 18:531-533.
- Lau CG, Murthy VN (2012) Activity-dependent regulation of inhibition via GAD67. *J Neurosci* 32:8521-8531.
- Laxmi TR, Stork O, Pape HC (2003) Generalisation of conditioned fear and its behavioural expression in mice. *Behav Brain Res* 145:89-98.
- Lecoq J, Tiret P, Charpak S (2009) Peripheral adaptation codes for high odor concentration in glomeruli. *J Neurosci* 29:3067-3072.
- LeDoux JE (2000) Emotion circuits in the brain. *Annu Rev Neurosci* 23:155-184.
- Lee AC, He J, Ma M (2011) Olfactory marker protein is critical for functional maturation of olfactory sensory neurons and development of mother preference. *J Neurosci* 31:2974-2982.

- Lendvai B, Stern EA, Chen B, Svoboda K (2000) Experience-dependent plasticity of dendritic spines in the developing rat barrel cortex in vivo. *Nature* 404:876-881.
- Li TY, Wu CH (1964) [Changes in the Amount of Gamma-Aminobutyric Acid in the Male Rat Brain after Castration]. *Sheng Li Xue Bao* 27:1-4.
- Li W, Howard JD, Parrish TB, Gottfried JA (2008) Aversive learning enhances perceptual and cortical discrimination of indiscriminable odor cues. *Science* 319:1842-1845.
- Liberzon I, Taylor SF, Amdur R, Jung TD, Chamberlain KR, Minoshima S, Koeppe RA, Fig LM (1999) Brain activation in PTSD in response to trauma-related stimuli. *Biol Psychiatry* 45:817-826.
- Linster C, Cleland TA (2010) Decorrelation of Odor Representations via Spike Timing-Dependent Plasticity. *Front Comput Neurosci* 4:157.
- Linster C, Nai Q, Ennis M (2011) Nonlinear effects of noradrenergic modulation of olfactory bulb function in adult rodents. *J Neurophysiol* 105:1432-1443.
- Linster C, Johnson BA, Yue E, Morse A, Xu Z, Hingco EE, Choi Y, Choi M, Messiha A, Leon M (2001) Perceptual correlates of neural representations evoked by odorant enantiomers. *J Neurosci* 21:9837-9843.
- Lissek S, Kaczurkin AN, Rabin S, Geraci M, Pine DS, Grillon C (2014) Generalized anxiety disorder is associated with overgeneralization of classically conditioned fear. *Biol Psychiatry* 75:909-915.
- Lissek S, Biggs AL, Rabin SJ, Cornwell BR, Alvarez RP, Pine DS, Grillon C (2008) Generalization of conditioned fear-potentiated startle in humans: experimental validation and clinical relevance. *Behav Res Ther* 46:678-687.
- Lissek S, Rabin S, Heller RE, Lukenbaugh D, Geraci M, Pine DS, Grillon C (2010) Overgeneralization of conditioned fear as a pathogenic marker of panic disorder. *Am J Psychiatry* 167:47-55.
- Liu S, Plachez C, Shao Z, Puche A, Shipley MT (2013) Olfactory bulb short axon cell release of GABA and dopamine produces a temporally biphasic inhibition-excitation response in external tufted cells. *J Neurosci* 33:2916-2926.
- Liu S, Shao Z, Puche A, Wachowiak M, Rothermel M, Shipley MT (2015) Muscarinic receptors modulate dendrodendritic inhibitory synapses to sculpt glomerular output. *J Neurosci* 35:5680-5692.
- Lupo C, Lodi L, Canonaco M, Valenti A, Dessi-Fulgheri F (1986) Testosterone metabolism in the olfactory epithelium of intact and castrated male rats. *Neurosci Lett* 69:259-262.
- Ma M, Luo M (2012) Optogenetic activation of basal forebrain cholinergic neurons modulates neuronal excitability and sensory responses in the main olfactory bulb. *J Neurosci* 32:10105-10116.
- Maggi A, Perez J (1986) Estrogen-induced up-regulation of gamma-aminobutyric acid receptors in the CNS of rodents. *J Neurochem* 47:1793-1797.
- Mair RG, Bouffard JA, Engen T, Morton TH (1978) Olfactory sensitivity during the menstrual cycle. *Sens Processes* 2:90-98.
- Malnic B, Hirono J, Sato T, Buck LB (1999) Combinatorial receptor codes for odors. *Cell* 96:713-723.
- Mandairon N, Linster C (2009) Odor perception and olfactory bulb plasticity in adult mammals. *J Neurophysiol* 101:2204-2209.

- Mandaïron N, Stack C, Linster C (2006a) Olfactory enrichment improves the recognition of individual components in mixtures. *Physiol Behav* 89:379-384.
- Mandaïron N, Didier A, Linster C (2008a) Odor enrichment increases interneurons responsiveness in spatially defined regions of the olfactory bulb correlated with perception. *Neurobiol Learn Mem* 90:178-184.
- Mandaïron N, Stack C, Kiselycznyk C, Linster C (2006b) Enrichment to odors improves olfactory discrimination in adult rats. *Behav Neurosci* 120:173-179.
- Mandaïron N, Ferretti CJ, Stack CM, Rubin DB, Cleland TA, Linster C (2006c) Cholinergic modulation in the olfactory bulb influences spontaneous olfactory discrimination in adult rats. *Eur J Neurosci* 24:3234-3244.
- Mandaïron N, Peace S, Karnow A, Kim J, Ennis M, Linster C (2008b) Noradrenergic modulation in the olfactory bulb influences spontaneous and reward-motivated discrimination, but not the formation of habituation memory. *Eur J Neurosci* 27:1210-1219.
- Maren S, Quirk GJ (2004) Neuronal signalling of fear memory. *Nat Rev Neurosci* 5:844-852.
- Markopoulos F, Rokni D, Gire DH, Murthy VN (2012) Functional properties of cortical feedback projections to the olfactory bulb. *Neuron* 76:1175-1188.
- McGann JP (2013) Presynaptic inhibition of olfactory sensory neurons: new mechanisms and potential functions. *Chem Senses* 38:459-474.
- McGann JP (2015) Associative learning and sensory neuroplasticity: how does it happen and what is it good for? *Learn Mem* 22:567-576.
- McGann JP, Pirez N, Gainey MA, Muratore C, Elias AS, Wachowiak M (2005) Odorant representations are modulated by intra- but not interglomerular presynaptic inhibition of olfactory sensory neurons. *Neuron* 48:1039-1053.
- McNally RJ, Kaspi SP, Riemann BC, Zeitlin SB (1990) Selective processing of threat cues in posttraumatic stress disorder. *J Abnorm Psychol* 99:398-402.
- Meister M, Bonhoeffer T (2001) Tuning and topography in an odor map on the rat olfactory bulb. *J Neurosci* 21:1351-1360.
- Mendez P, Bacci A (2011) Assortment of GABAergic plasticity in the cortical interneuron melting pot. *Neural Plast* 2011:976856.
- Merchenthaler I, Lane MV, Numan S, Dellovade TL (2004) Distribution of estrogen receptor alpha and beta in the mouse central nervous system: in vivo autoradiographic and immunocytochemical analyses. *J Comp Neurol* 473:270-291.
- Miasnikov AA, Weinberger NM (2012) Detection of an inhibitory cortical gradient underlying peak shift in learning: a neural basis for a false memory. *Neurobiol Learn Mem* 98:368-379.
- Miragall F, Monti Graziadei GA (1982) Experimental studies on the olfactory marker protein. II. Appearance of the olfactory marker protein during differentiation of the olfactory sensory neurons of mouse: an immunohistochemical and autoradiographic study. *Brain Res* 239:245-250.
- Mitra SW, Hoskin E, Yudkovitz J, Pear L, Wilkinson HA, Hayashi S, Pfaff DW, Ogawa S, Rohrer SP, Schaeffer JM, McEwen BS, Alves SE (2003) Immunolocalization of estrogen receptor beta in the mouse brain: comparison with estrogen receptor alpha. *Endocrinology* 144:2055-2067.

- Moberly AH, Czarnecki LA, Pottackal J, Rubinstein T, Turkel DJ, Kass MD, McGann JP (2012) Intranasal exposure to manganese disrupts neurotransmitter release from glutamatergic synapses in the central nervous system in vivo. *Neurotoxicology* 33:996-1004.
- Mombaerts P (2006) Axonal wiring in the mouse olfactory system. *Annu Rev Cell Dev Biol* 22:713-737.
- Mombaerts P, Wang F, Dulac C, Chao SK, Nemes A, Mendelsohn M, Edmondson J, Axel R (1996) Visualizing an olfactory sensory map. *Cell* 87:675-686.
- Monti-Graziadei GA, Margolis FL, Harding JW, Graziadei PP (1977) Immunocytochemistry of the olfactory marker protein. *J Histochem Cytochem* 25:1311-1316.
- Moreno MM, Linster C, Escanilla O, Sacquet J, Didier A, Mandairon N (2009) Olfactory perceptual learning requires adult neurogenesis. *Proc Natl Acad Sci U S A* 106:17980-17985.
- Moreno MM, Bath K, Kuczewski N, Sacquet J, Didier A, Mandairon N (2012) Action of the noradrenergic system on adult-born cells is required for olfactory learning in mice. *J Neurosci* 32:3748-3758.
- Mueller-Pfeiffer C, Schick M, Schulte-Vels T, O'Gorman R, Michels L, Martin-Soelch C, Blair JR, Rufer M, Schnyder U, Zeffiro T, Hasler G (2013) Atypical visual processing in posttraumatic stress disorder. *Neuroimage Clin* 3:531-538.
- Murphy GJ, Darcy DP, Isaacson JS (2005) Intraglomerular inhibition: signaling mechanisms of an olfactory microcircuit. *Nat Neurosci* 8:354-364.
- Nagashima A, Touhara K (2010) Enzymatic conversion of odorants in nasal mucus affects olfactory glomerular activation patterns and odor perception. *J Neurosci* 30:16391-16398.
- Nathan BP, Tonsor M, Struble RG (2010) Acute responses to estradiol replacement in the olfactory system of apoE-deficient and wild-type mice. *Brain Res* 1343:66-74.
- Nathan BP, Tonsor M, Struble RG (2012) Long-term effects of estradiol replacement in the olfactory system. *Exp Neurol* 237:1-7.
- Ng KY, Yong J, Chakraborty TR (2010) Estrous cycle in ob/ob and ovariectomized female mice and its relation with estrogen and leptin. *Physiol Behav* 99:125-130.
- Nickell WT, Behbehani MM, Shipley MT (1994) Evidence for GABAB-mediated inhibition of transmission from the olfactory nerve to mitral cells in the rat olfactory bulb. *Brain Res Bull* 35:119-123.
- Notebaert L, Crombez G, Van Damme S, De Houwer J, Theeuwes J (2011) Signals of threat do not capture, but prioritize, attention: a conditioning approach. *Emotion* 11:81-89.
- Ohla K, Lundstrom JN (2013) Sex differences in chemosensation: sensory or emotional? *Front Hum Neurosci* 7:607.
- Olatunji BO, Armstrong T, McHugo M, Zald DH (2013) Heightened attentional capture by threat in veterans with PTSD. *J Abnorm Psychol* 122:397-405.
- Oliva AM, Jones KR, Restrepo D (2008) Sensory-dependent asymmetry for a urine-responsive olfactory bulb glomerulus. *J Comp Neurol* 510:475-483.
- Oliva AM, Salcedo E, Hellier JL, Ly X, Koka K, Tollin DJ, Restrepo D (2010) Toward a mouse neuroethology in the laboratory environment. *PLoS One* 5:e11359.

- Ottoni EB (2000) EthoLog 2.2: a tool for the transcription and timing of behavior observation sessions. *Behav Res Methods Instrum Comput* 32:446-449.
- Parma V, Ferraro S, Miller SS, Ahs F, Lundstrom JN (2015) Enhancement of Odor Sensitivity Following Repeated Odor and Visual Fear Conditioning. *Chem Senses* 40:497-506.
- Parrish-Aungst S, Shipley MT, Erdelyi F, Szabo G, Puche AC (2007) Quantitative analysis of neuronal diversity in the mouse olfactory bulb. *J Comp Neurol* 501:825-836.
- Parrish-Aungst S, Kiyokage E, Szabo G, Yanagawa Y, Shipley MT, Puche AC (2011) Sensory experience selectively regulates transmitter synthesis enzymes in interglomerular circuits. *Brain Res* 1382:70-76.
- Pavlov IP, Anrep GV (1927) Conditioned reflexes; an investigation of the physiological activity of the cerebral cortex. London: Oxford University Press: Humphrey Milford.
- Perez-Orive J, Mazor O, Turner GC, Cassenaer S, Wilson RI, Laurent G (2002) Oscillations and sparsening of odor representations in the mushroom body. *Science* 297:359-365.
- Phelps EA, LeDoux JE (2005) Contributions of the amygdala to emotion processing: from animal models to human behavior. *Neuron* 48:175-187.
- Pienkowski M, Eggermont JJ (2011) Cortical tonotopic map plasticity and behavior. *Neurosci Biobehav Rev* 35:2117-2128.
- Pierman S, Douhard Q, Balthazart J, Baum MJ, Bakker J (2006) Attraction thresholds and sex discrimination of urinary odorants in male and female aromatase knockout (ArKO) mice. *Horm Behav* 49:96-104.
- Pietras RJ, Moulton DG (1974) Hormonal influences on odor detection in rats: changes associated with the estrous cycle, pseudopregnancy, ovariectomy, and administration of testosterone propionate. *Physiol Behav* 12:475-491.
- Pirez N, Wachowiak M (2008) In vivo modulation of sensory input to the olfactory bulb by tonic and activity-dependent presynaptic inhibition of receptor neurons. *J Neurosci* 28:6360-6371.
- Potter SM, Zheng C, Koos DS, Feinstein P, Fraser SE, Mombaerts P (2001) Structure and emergence of specific olfactory glomeruli in the mouse. *J Neurosci* 21:9713-9723.
- Poulos AM, Mehta N, Lu B, Amir D, Livingston B, Santarelli A, Zhuravka I, Fanselow MS (2016) Conditioning- and time-dependent increases in context fear and generalization. *Learn Mem* 23:379-385.
- Protopopescu X, Pan H, Tuescher O, Cloitre M, Goldstein M, Engelien W, Epstein J, Yang Y, Gorman J, LeDoux J, Silbersweig D, Stern E (2005) Differential time courses and specificity of amygdala activity in posttraumatic stress disorder subjects and normal control subjects. *Biol Psychiatry* 57:464-473.
- Quirk GJ, Armony JL, LeDoux JE (1997) Fear conditioning enhances different temporal components of tone-evoked spike trains in auditory cortex and lateral amygdala. *Neuron* 19:613-624.
- Rajbhandari AK, Zhu R, Adling C, Fanselow MS, Waschek JA (2016) Graded fear generalization enhances the level of cfos-positive neurons specifically in the basolateral amygdala. *J Neurosci Res* 94:1393-1399.

- Rauch SL, Whalen PJ, Shin LM, McInerney SC, Macklin ML, Lasko NB, Orr SP, Pitman RK (2000) Exaggerated amygdala response to masked facial stimuli in posttraumatic stress disorder: a functional MRI study. *Biol Psychiatry* 47:769-776.
- Reisert J, Matthews HR (2001) Response properties of isolated mouse olfactory receptor cells. *J Physiol* 530:113-122.
- Reisert J, Yau KW, Margolis FL (2007) Olfactory marker protein modulates the cAMP kinetics of the odour-induced response in cilia of mouse olfactory receptor neurons. *J Physiol* 585:731-740.
- Resnik J, Paz R (2015) Fear generalization in the primate amygdala. *Nat Neurosci* 18:188-190.
- Resnik J, Sobel N, Paz R (2011) Auditory aversive learning increases discrimination thresholds. *Nat Neurosci* 14:791-796.
- Rinberg D, Koulakov A, Gelperin A (2006) Speed-accuracy tradeoff in olfaction. *Neuron* 51:351-358.
- Rubin BD, Katz LC (1999) Optical imaging of odorant representations in the mammalian olfactory bulb. *Neuron* 23:499-511.
- Saad AF (1970) The effect of ovariectomy on the gamma-aminobutyric acid content in the cerebral hemispheres of young rats. *J Pharm Pharmacol* 22:307-308.
- Saghatelyan A, Roux P, Migliore M, Rochefort C, Desmaisons D, Charneau P, Shepherd GM, Lledo PM (2005) Activity-dependent adjustments of the inhibitory network in the olfactory bulb following early postnatal deprivation. *Neuron* 46:103-116.
- Sawada M, Kaneko N, Inada H, Wake H, Kato Y, Yanagawa Y, Kobayashi K, Nemoto T, Nabekura J, Sawamoto K (2011) Sensory input regulates spatial and subtype-specific patterns of neuronal turnover in the adult olfactory bulb. *J Neurosci* 31:11587-11596.
- Schaefer ML, Young DA, Restrepo D (2001) Olfactory fingerprints for major histocompatibility complex-determined body odors. *J Neurosci* 21:2481-2487.
- Schwarzkopf DS, Zhang J, Kourtzi Z (2009) Flexible learning of natural statistics in the human brain. *J Neurophysiol* 102:1854-1867.
- Segal NL, Topolski TD, Wilson SM, Brown KW, Araki L (1995) Twin Analysis of Odor Identification and Perception. *Physiol Behav* 57:605-609.
- Sevelinges Y, Moriceau S, Holman P, Miner C, Muzny K, Gervais R, Mouly AM, Sullivan RM (2007) Enduring effects of infant memories: infant odor-shock conditioning attenuates amygdala activity and adult fear conditioning. *Biol Psychiatry* 62:1070-1079.
- Shaban H, Humeau Y, Herry C, Cassasus G, Shigemoto R, Cioocchi S, Barbieri S, van der Putten H, Kaupmann K, Bettler B, Luthi A (2006) Generalization of amygdala LTP and conditioned fear in the absence of presynaptic inhibition. *Nat Neurosci* 9:1028-1035.
- Shao Z, Puche AC, Liu S, Shipley MT (2012) Intraglomerular inhibition shapes the strength and temporal structure of glomerular output. *J Neurophysiol* 108:782-793.
- Shao Z, Puche AC, Kiyokage E, Szabo G, Shipley MT (2009) Two GABAergic intraglomerular circuits differentially regulate tonic and phasic presynaptic inhibition of olfactory nerve terminals. *J Neurophysiol* 101:1988-2001.
- Shea SD, Katz LC, Mooney R (2008) Noradrenergic induction of odor-specific neural habituation and olfactory memories. *J Neurosci* 28:10711-10719.

- Shiao MS, Chang AY, Liao BY, Ching YH, Lu MY, Chen SM, Li WH (2012) Transcriptomes of mouse olfactory epithelium reveal sexual differences in odorant detection. *Genome Biol Evol* 4:703-712.
- Shipley MT, Ennis M (1996) Functional organization of olfactory system. *J Neurobiol* 30:123-176.
- Simoncelli EP, Olshausen BA (2001) Natural image statistics and neural representation. *Annu Rev Neurosci* 24:1193-1216.
- Smear M, Shusterman R, O'Connor R, Bozza T, Rinberg D (2011) Perception of sniff phase in mouse olfaction. *Nature* 479:397-400.
- Smear M, Resulaj A, Zhang J, Bozza T, Rinberg D (2013) Multiple perceptible signals from a single olfactory glomerulus. *Nat Neurosci* 16:1687-1691.
- Smith PC, Firestein S, Hunt JF (2002) The crystal structure of the olfactory marker protein at 2.3 Å resolution. *J Mol Biol* 319:807-821.
- Sorwell KG, Wesson DW, Baum MJ (2008) Sexually dimorphic enhancement by estradiol of male urinary odor detection thresholds in mice. *Behav Neurosci* 122:788-793.
- Soucy ER, Albeanu DF, Fantana AL, Murthy VN, Meister M (2009) Precision and diversity in an odor map on the olfactory bulb. *Nat Neurosci* 12:210-220.
- Spors H, Grinvald A (2002) Spatio-temporal dynamics of odor representations in the mammalian olfactory bulb. *Neuron* 34:301-315.
- Spors H, Wachowiak M, Cohen LB, Friedrich RW (2006) Temporal dynamics and latency patterns of receptor neuron input to the olfactory bulb. *J Neurosci* 26:1247-1259.
- St John JA, Key B (2005) Olfactory marker protein modulates primary olfactory axon overshooting in the olfactory bulb. *J Comp Neurol* 488:61-69.
- Stevens JS, Kim YJ, Galatzer-Levy IR, Reddy R, Ely TD, Nemeroff CB, Hudak LA, Jovanovic T, Rothbaum BO, Ressler KJ (2017) Amygdala Reactivity and Anterior Cingulate Habituation Predict Posttraumatic Stress Disorder Symptom Maintenance After Acute Civilian Trauma. *Biol Psychiatry* 81:1023-1029.
- Stewart LP, White PM (2008) Sensory filtering phenomenology in PTSD. *Depress Anxiety* 25:38-45.
- Stewart WB, Kauer JS, Shepherd GM (1979) Functional organization of rat olfactory bulb analysed by the 2-deoxyglucose method. *J Comp Neurol* 185:715-734.
- Stowers L, Logan DW (2010) Sexual dimorphism in olfactory signaling. *Curr Opin Neurobiol* 20:770-775.
- Stowers L, Liberles SD (2016) State-dependent responses to sex pheromones in mouse. *Curr Opin Neurobiol* 38:74-79.
- Suh KS, Kim SY, Bae YC, Ronnett GV, Moon C (2006) Effects of unilateral naris occlusion on the olfactory epithelium of adult mice. *Neuroreport* 17:1139-1142.
- Sullivan RM, Zyzak DR, Skierkowski P, Wilson DA (1992) The role of olfactory bulb norepinephrine in early olfactory learning. *Brain Res Dev Brain Res* 70:279-282.
- Sullivan RM, Stackenwalt G, Nasr F, Lemon C, Wilson DA (2000) Association of an odor with activation of olfactory bulb noradrenergic beta-receptors or locus coeruleus stimulation is sufficient to produce learned approach responses to that odor in neonatal rats. *Behav Neurosci* 114:957-962.
- Sydor W, Teitelbaum Z, Blacher R, Sun S, Benz W, Margolis FL (1986) Amino acid sequence of a unique neuronal protein: rat olfactory marker protein. *Arch Biochem Biophys* 249:351-362.

- Taniguchi H, He M, Wu P, Kim S, Paik R, Sugino K, Kvitsiani D, Fu Y, Lu J, Lin Y, Miyoshi G, Shima Y, Fishell G, Nelson SB, Huang ZJ (2011) A resource of Cre driver lines for genetic targeting of GABAergic neurons in cerebral cortex. *Neuron* 71:995-1013.
- Tian H, Ma M (2008) Activity plays a role in eliminating olfactory sensory neurons expressing multiple odorant receptors in the mouse septal organ. *Mol Cell Neurosci* 38:484-488.
- Tian N, Copenhagen DR (2001) Visual deprivation alters development of synaptic function in inner retina after eye opening. *Neuron* 32:439-449.
- Todd RM, MacDonald MJ, Sedge P, Robertson A, Jetly R, Taylor MJ, Pang EW (2015) Soldiers With Posttraumatic Stress Disorder See a World Full of Threat: Magnetoencephalography Reveals Enhanced Tuning to Combat-Related Cues. *Biol Psychiatry* 78:821-829.
- Tsim TY, Wong EY, Leung MS, Wong CC (2004) Expression of axon guidance molecules and their related genes during development and sexual differentiation of the olfactory bulb in rats. *Neuroscience* 123:951-965.
- Tyler WJ, Petzold GC, Pal SK, Murthy VN (2007) Experience-dependent modification of primary sensory synapses in the mammalian olfactory bulb. *J Neurosci* 27:9427-9438.
- Uchida N, Mainen ZF (2003) Speed and accuracy of olfactory discrimination in the rat. *Nat Neurosci* 6:1224-1229.
- Valle-Leija P, Blanco-Hernandez E, Drucker-Colin R, Gutierrez-Ospina G, Vidaltamayo R (2012) Supernumerary formation of olfactory glomeruli induced by chronic odorant exposure: a constructivist expression of neural plasticity. *PLoS One* 7:e35358.
- van Meurs B, Wiggert N, Wicker I, Lissek S (2014) Maladaptive behavioral consequences of conditioned fear-generalization: a pronounced, yet sparsely studied, feature of anxiety pathology. *Behav Res Ther* 57:29-37.
- Veyrac A, Wang G, Baum MJ, Bakker J (2011) The main and accessory olfactory systems of female mice are activated differentially by dominant versus subordinate male urinary odors. *Brain Res* 1402:20-29.
- Vinera J, Kermen F, Sacquet J, Didier A, Mandairon N, Richard M (2015) Olfactory perceptual learning requires action of noradrenaline in the olfactory bulb: comparison with olfactory associative learning. *Learn Mem* 22:192-196.
- Wachowiak M, Shipley MT (2006) Coding and synaptic processing of sensory information in the glomerular layer of the olfactory bulb. *Semin Cell Dev Biol* 17:411-423.
- Wachowiak M, McGann JP, Heyward PM, Shao Z, Puche AC, Shipley MT (2005) Inhibition [corrected] of olfactory receptor neuron input to olfactory bulb glomeruli mediated by suppression of presynaptic calcium influx. *J Neurophysiol* 94:2700-2712.
- Wachowiak M, Economo MN, Diaz-Quesada M, Brunert D, Wesson DW, White JA, Rothermel M (2013) Optical dissection of odor information processing in vivo using GCaMPs expressed in specified cell types of the olfactory bulb. *J Neurosci* 33:5285-5300.

- Waggener CT, Coppola DM (2007) Naris occlusion alters the electro-olfactogram: evidence for compensatory plasticity in the olfactory system. *Neurosci Lett* 427:112-116.
- Wallis CJ, Luttge WG (1980) Influence of estrogen and progesterone on glutamic acid decarboxylase activity in discrete regions of rat brain. *J Neurochem* 34:609-613.
- Wang HW, Wysocki CJ, Gold GH (1993) Induction of olfactory receptor sensitivity in mice. *Science* 260:998-1000.
- Waters P, Woodley SK, Baum MJ (2005) Sex difference in the distribution and size of glomeruli in the ferret's main olfactory bulb. *Neurosci Lett* 381:237-241.
- Watt WC, Sakano H, Lee ZY, Reusch JE, Trinh K, Storm DR (2004) Odorant stimulation enhances survival of olfactory sensory neurons via MAPK and CREB. *Neuron* 41:955-967.
- Weiland NG (1992) Glutamic acid decarboxylase messenger ribonucleic acid is regulated by estradiol and progesterone in the hippocampus. *Endocrinology* 131:2697-2702.
- Weinberger NM (2004) Specific long-term memory traces in primary auditory cortex. *Nat Rev Neurosci* 5:279-290.
- Weinberger NM (2007) Associative representational plasticity in the auditory cortex: a synthesis of two disciplines. *Learn Mem* 14:1-16.
- Wesson DW, Donahou TN, Johnson MO, Wachowiak M (2008a) Sniffing behavior of mice during performance in odor-guided tasks. *Chem Senses* 33:581-596.
- Wesson DW, Carey RM, Verhagen JV, Wachowiak M (2008b) Rapid encoding and perception of novel odors in the rat. *PLoS Biol* 6:e82.
- Wesson DW, Keller M, Douhard Q, Baum MJ, Bakker J (2006) Enhanced urinary odor discrimination in female aromatase knockout (ArKO) mice. *Horm Behav* 49:580-586.
- Wiesel TN, Hubel DH (1965) Comparison of the effects of unilateral and bilateral eye closure on cortical unit responses in kittens. *J Neurophysiol* 28:1029-1040.
- Wilbrecht L, Holtmaat A, Wright N, Fox K, Svoboda K (2010) Structural plasticity underlies experience-dependent functional plasticity of cortical circuits. *J Neurosci* 30:4927-4932.
- Willmore B, Tolhurst DJ (2001) Characterizing the sparseness of neural codes. *Network* 12:255-270.
- Wilson DA, Sullivan RM (1995) The D2 antagonist spiperone mimics the effects of olfactory deprivation on mitral/tufted cell odor response patterns. *J Neurosci* 15:5574-5581.
- Wilson DA, Fletcher ML, Sullivan RM (2004) Acetylcholine and olfactory perceptual learning. *Learn Mem* 11:28-34.
- Woo CC, Leon M (1995) Early olfactory enrichment and deprivation both decrease beta-adrenergic receptor density in the main olfactory bulb of the rat. *J Comp Neurol* 360:634-642.
- Woo CC, Hingco EE, Taylor GE, Leon M (2006) Exposure to a broad range of odorants decreases cell mortality in the olfactory bulb. *Neuroreport* 17:817-821.
- Woo CC, Hingco EE, Johnson BA, Leon M (2007) Broad activation of the glomerular layer enhances subsequent olfactory responses. *Chem Senses* 32:51-55.

- Woodley SK, Baum MJ (2004) Differential activation of glomeruli in the ferret's main olfactory bulb by anal scent gland odours from males and females: an early step in mate identification. *Eur J Neurosci* 20:1025-1032.
- Wright NT, Margolis JW, Margolis FL, Weber DJ (2005) Refinement of the solution structure of rat olfactory marker protein (OMP). *J Biomol NMR* 33:63-68.
- Xu F, Liu N, Kida I, Rothman DL, Hyder F, Shepherd GM (2003) Odor maps of aldehydes and esters revealed by functional MRI in the glomerular layer of the mouse olfactory bulb. *Proc Natl Acad Sci U S A* 100:11029-11034.
- Xu PS, Lee D, Holy TE (2016) Experience-Dependent Plasticity Drives Individual Differences in Pheromone-Sensing Neurons. *Neuron* 91:878-892.
- Yen SS, Tsai CC (1971) The effect of ovariectomy on gonadotropin release. *J Clin Invest* 50:1149-1153.
- Yokoi M, Mori K, Nakanishi S (1995) Refinement of odor molecule tuning by dendrodendritic synaptic inhibition in the olfactory bulb. *Proc Natl Acad Sci U S A* 92:3371-3375.
- Youngentob SL, Margolis FL (1999) OMP gene deletion causes an elevation in behavioral threshold sensitivity. *Neuroreport* 10:15-19.
- Youngentob SL, Margolis FL, Youngentob LM (2001) OMP gene deletion results in an alteration in odorant quality perception. *Behav Neurosci* 115:626-631.
- Youngentob SL, Kent PF, Margolis FL (2003) OMP gene deletion results in an alteration in odorant-induced mucosal activity patterns. *J Neurophysiol* 90:3864-3873.
- Youngentob SL, Pyrski MM, Margolis FL (2004) Adenoviral vector-mediated rescue of the OMP-null behavioral phenotype: enhancement of odorant threshold sensitivity. *Behav Neurosci* 118:636-642.
- Youngentob SL, Johnson BA, Leon M, Sheehe PR, Kent PF (2006) Predicting odorant quality perceptions from multidimensional scaling of olfactory bulb glomerular activity patterns. *Behav Neurosci* 120:1337-1345.
- Zaborszky L, Carlsen J, Brashear HR, Heimer L (1986) Cholinergic and GABAergic afferents to the olfactory bulb in the rat with special emphasis on the projection neurons in the nucleus of the horizontal limb of the diagonal band. *J Comp Neurol* 243:488-509.
- Zariwala HA, Borghuis BG, Hoogland TM, Madisen L, Tian L, De Zeeuw CI, Zeng H, Looger LL, Svoboda K, Chen TW (2012) A Cre-dependent GCaMP3 reporter mouse for neuronal imaging in vivo. *J Neurosci* 32:3131-3141.
- Zhao H, Ivic L, Otaki JM, Hashimoto M, Mikoshiba K, Firestein S (1998) Functional expression of a mammalian odorant receptor. *Science* 279:237-242.
- Zhou X, Merzenich MM (2007) Intensive training in adults refines A1 representations degraded in an early postnatal critical period. *Proc Natl Acad Sci U S A* 104:15935-15940.
- Zhou X, Zhang X, Weng Y, Fang C, Kaminsky L, Ding X (2009) High abundance of testosterone and salivary androgen-binding protein in the lateral nasal gland of male mice. *J Steroid Biochem Mol Biol* 117:81-86.
- Zinchenko A, Al-Amin MM, Alam MM, Mahmud W, Kabir N, Reza HM, Burne THJ (2017) Content specificity of attentional bias to threat in post-traumatic stress disorder. *J Anxiety Disord* 50:33-39.

Zou DJ, Feinstein P, Rivers AL, Mathews GA, Kim A, Greer CA, Mombaerts P, Firestein S (2004) Postnatal refinement of peripheral olfactory projections. *Science* 304:1976-1979.